Investigating the Fluorous Effect to Direct DNA Origami Assembly

Jiajia Zou

Submitted in fulfilment of the requirements for the
Degree of Philosophy

School of Engineering
College of Science and Engineering
University of Glasgow

January 2022

Abstract

DNA origami is a robust method for the creation of nanostructures with arbitrary shapes, whereby a long single strand is folded into extended patterns with the aid of hundreds of short stands. DNA origami has been shown as an ideal technique to control and organise individual molecules with nanoscale accuracy, which is of great importance in the fields like bio-sensing and nano-engineering. Assembly of DNA origami sheets into higher-ordered structures is desirable for the fabrication of new materials and devices that are currently beyond the reach of top-down fabrication techniques. However, there are major constraints when attempting to create origami super-structures larger than one micron, including the inefficiency of attachment reactions between individual origami tiles, the complexity of the design, and the number of unique DNA sequences required.

The primary focus of this thesis is to explore the fluorous-effect as a new method to promote DNA origami dimerization. Firstly, affecting factors to origami dimerization using sticky-ends strategy was explored. This work showed that changing the number and length of sticky-ends largely affect the dimer yield. Bridging strands work cooperatively when in proximity, when they were placed in distance, however, the binding of one doesn't help the binding of another, thus they work independently.

The fluorous effect was then introduced as a novel strategy to join distinct origami tiles together. Fluorous-fluorous interactions differ from conventional base-pairing interactions in that they are relatively strong and non-specific. This work showed that fluorous-tagged origami can be used as a mean to direct origami dimerization. Among all of the fluorous species that were explored, branched-RF8 tags were most efficient at directing origami dimerization.

A hybrid linker system containing both fluorous strands and sticky-ends was then explored. It was found that the hybrid system significantly improves the dimer yield when compared to the equivalent DNA-only system. The fact that double extension sticky-ends are more efficient than single extensions may suggest that a more stable, higher-yield dimer could form with the use of double-extended RF-oligos.

The final experimental chapter demonstrates the construction of an origami-based FRET system comprising quantum dots and organic fluorophores. This works explored several dye patterns including linear, checkerboard and a quantum dot - dye complex to obtain an

optimized energy transfer network. This is the first time that quantum dots have been used as a FRET donor in an origami platform. It is thought that this work has potential application in multiplex assays as quantum dots can, unlike fluorophores, serve as multiple acceptors.

Table of Content

List of Tables

List of Figures

Acknowledgement

I express sincere gratitude to my supervisor Dr Alasdair Clark. Thank you for your trust, encouragement and patience throughout the years. I would also like to thank Dr Julien Reboud, my second supervisor, who always been helpful and considerate. It was a great pleasure to work with both of you. Thank China Scholarship Council for supporting my study in UK.

I extend my appreciation to Dr Ashley Stammers for his continued input and guidance on this work. He generously shared his knowledge and has provided some of the AFM results included in this thesis. I benefited a lot from his interest in DNA nanotechnology and expertise in Atomic Force Microscopy. Thank you for always being around whenever I encountered difficulties.

Thank you to the other members of the Clark group, Dr Marina Vega, Dr Justin Sperling, Iain Christie, Sara Angelucci, Hammed Onilude, Greig Govenlock, for being great company. For our collaborators, Dr Glenn Burley, Dr Andrea Sender, Dr Jamie Withers and Dr William Peveler, thank you for your input into this project.

I would like to thank my best friend, Yuxin Xie. You have always been up for chat whenever I need you, especially during the pandemic. Without you the past few years would have been lonely and dull. My thanks also go to Yumeng Liu, for all the good time spent together.

The biggest thank you goes to my family back in China, for the continued supports throughout the PhD. Mum and Dad, your love has always been around with me even being so far away. Thank you for your unconditional love and support.

Author’s Declaration

'I declare that, except where explicit reference is made to the contribution of others, this thesis is the result of my own work and has not been submitted for any other degree at the University of Glasgow or any other institution**.** '

Jiajia Zou

Definitions/Abbreviations

A	Adenine
AFM	Atomic Force Microscopy
AGE	Agarose Gel Electrophoresis
bp	Base pair
C	Cytosine
CAD	Computer-Aided Design
DI water	Deionised Water
DNA	Deoxyribonucleic Acid
EDTA	Ethylenediaminetetraacetic Acid
FRET	Förster Resonance Energy Transfer
G	Guanine
HJ	Holiday Junction
HPLC	High-performance Liquid Chromatography
nt	Nucleotides
SE	Sticky-ends
SPM	Scanning Probe Microscopy
STM	Scanning Tunnelling Microscopy
T	Thymine

TAE	Tris-Acetate EDTA
TEM	Transmission Electron Microscope
Qdot	Quantum Dot
RT	Room Temperature

Chapter 1 Introduction

1.1 General introduction

This work is set to provide solutions on how to efficiently scale up DNA constructs, by utilising the fluorous effect as a mean of attaching origami tiles. Fluorous effect can be incorporated on to DNA origami system through modifying fluorous compounds on to one end of DNA oligos. As such, the main objects of this thesis were categorised into four sections: 1) to study the interfacial design of the origami interface, understand the traditional sticky-ends directed origami dimerization mechanism (Chapter 3). 2) to determine if the fluorous effect can be employed as a novel attachment strategy to direct the dimerization of origami (Chapter 4). 3) to investigate if adding fluorous tags into the DNA system would stabilise and improve the dimer yield (Chapter 5). 4) Attempting to build a Qdots-directed FRET multi-chromophores system on DNA origami (Chapter 6).

Each objective aligns with one results chapter, which overall provide a novel solution of efficient dimerization of origami tiles, took one step further toward the stable micron-scale DNA assembly. As such, this chapter intends to give a broader introduction to the field of structural DNA technology, fluorous effect and the FRET.

1.2 Deoxyribonucleic Acid

Deoxyribonucleic Acid (DNA) is the hereditary basis of most living organisms. A long sequence of DNA carries the complete set of genetic information, and its specific structure allows the storage and transfer of genetic information. DNA is normally stored inside the cell nucleus in of the eukaryotic organisms, in a form of chromosomes. The process of gene expression has two key stages: one is transcription, where DNA converts to small, messenger RNA; subsequently RNA translates to proteins. These two processes, along with the DNA replication, where the old DNA makes new DNA, forms the central dogma, which states the most frequently occurred information pattern in our cells [1]. DNA is vitally important in biology as it partakes replication and transcription process, any mutation of DNA would introduce downstream changes. Therefore, DNA always appears in a duplex conformation exhibits the best stability. This section focuses on the basic structural and chemical properties of DNA, as pertinent for the subsequent sections of DNA nanotechnology.

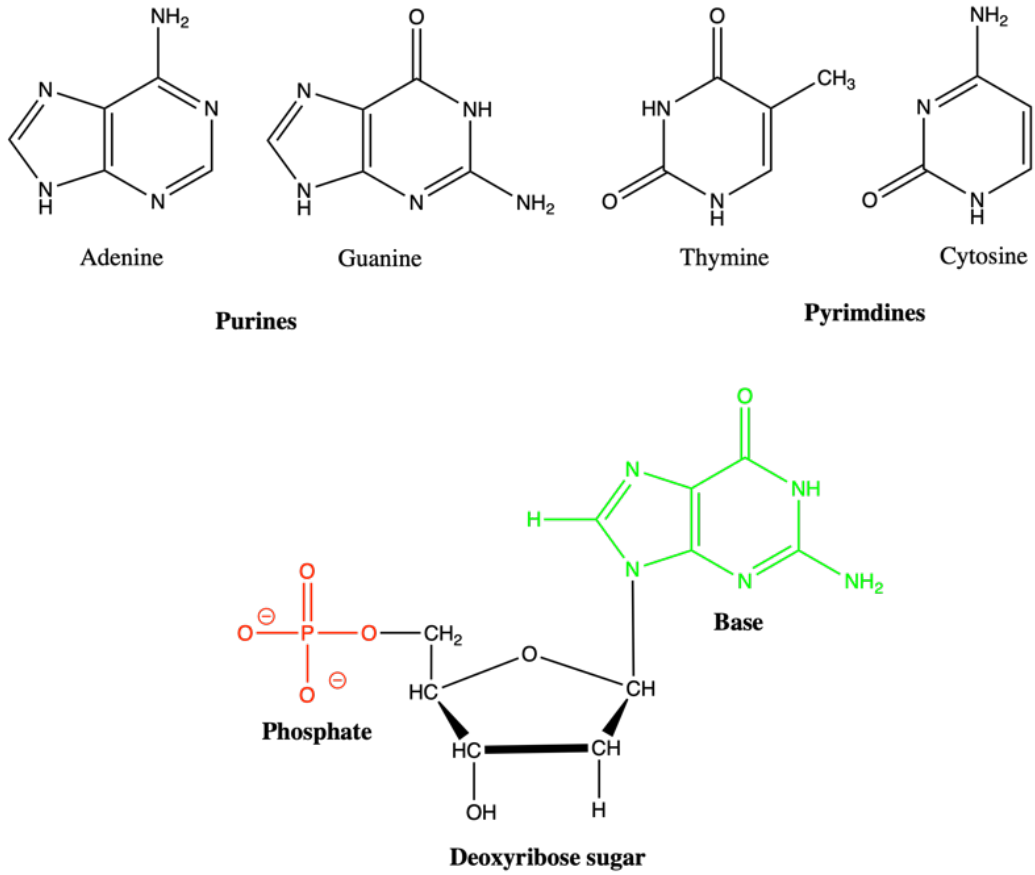

Figure 1-1 Chemical structure of four types of bases (upper) and the nucleotide (bottom). One nucleotide contains three elements: a phosphate group, a five-carbon sugar, and a base, either a purine or pyrimidine.

DNA is composed of subunits called nucleotides. One nucleotide contains three elements: a sugar ring, a phosphate group and one of four bases: adenine(A), thymine(T), cytosine(C) and guanine(G). (Figure 1-1) Although nucleotides derive their names from the nitrogen-

containing bases, the key part of this molecule is the five-carbon ring, also called 2'-deoxyribose, where an oxygen atom on the 2' carbon is missed. The phosphate group attaches to the 5' carbon site of one nucleotide forming a phosphodiester bond with the 3' carbon in the sugar ring of an adjacent nucleotide. This asymmetric covalent bond is what gives each single-stranded DNA chain directionality and chirality.

DNA can exist as single-stranded (ssDNA), whilst it is more stable when two ssDNA strands hybridise to form a double helix (Figure 1-2). Watson and Crick has proposed the duplex structure of DNA based the image of DNA using X-ray crystallography [2], [3]. Both polynucleotide chains store the same biological information, but their backbone chains run in opposite directions such that one runs from 5' to 3' with the other running 3' to 5'. The double helix is held together through hydrogen bonds between complementary base pairs strictly following the Watson-Crick base-pairing rules [2], [4]. Base A binds to T with two hydrogen bonds and G binds to C with three hydrogen bonds, so the A-T interaction is inherently weaker than the G-C [5]. Those hydrophobic bases stack on the inside perpendicularly to the helix axis; while the hydrophilic sugar-phosphate backbone is on the exterior of the helix [6]. There are two main factors responsible for the stability of DNA double helical structures: the hydrogen bond and the base stacking force between nucleic acid bases [7]. The π–π stacking between aromatic bases accumulated and formed a hydrophobic core inside the DNA molecules, which benefic the formation of hydrogen bond between complementary bases [8].

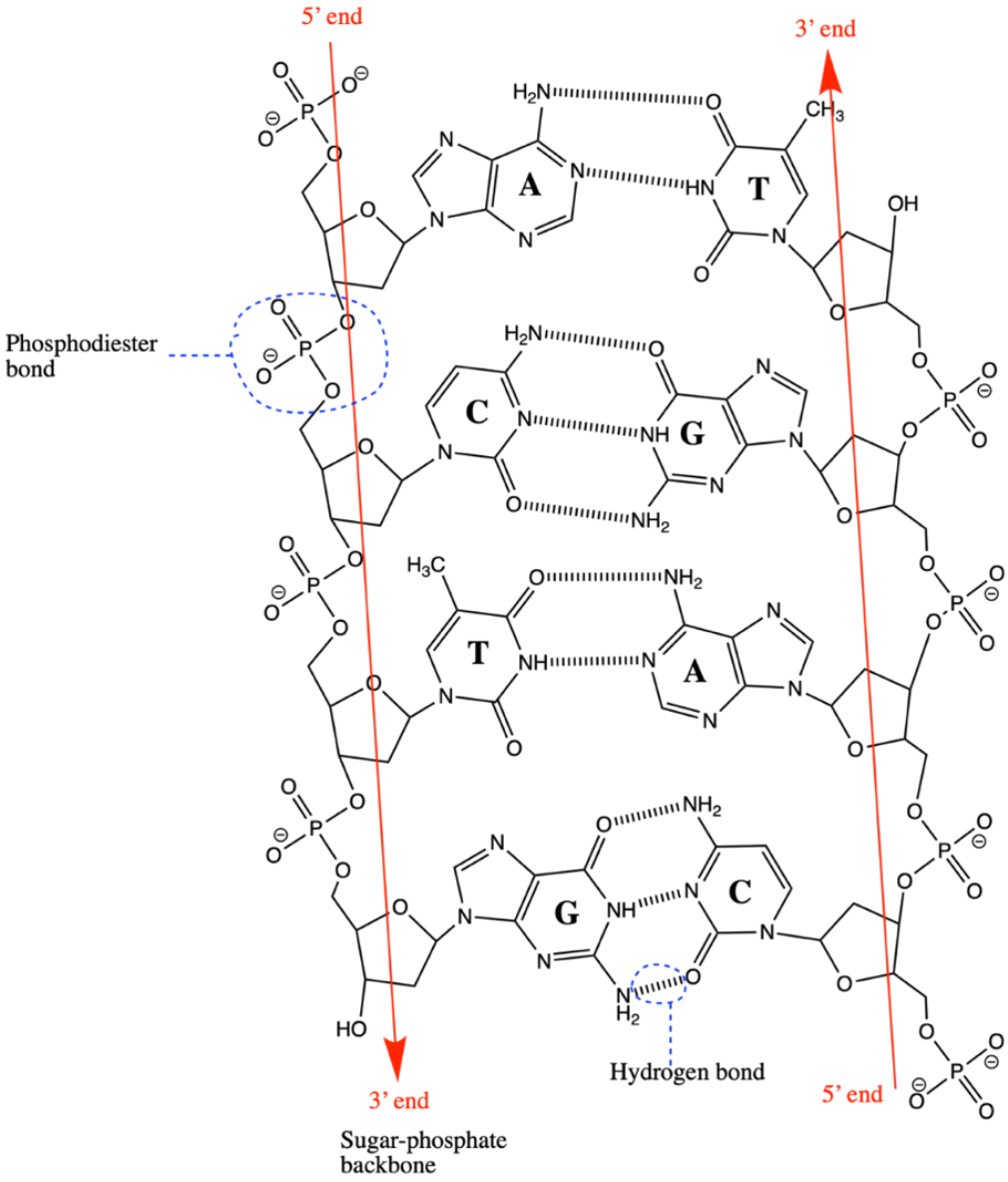

Figure 1-2 Double helical structure: base pairing and base stacking. In this polynucleotide chain, nucleotides are connected though a phosphodiester bond. The double-stranded structure is held via hydrogen bond between the base (two between A-T, three between G-C), and the sugar phosphate backbone with directionality of strands are indicated.

Double-stranded DNA can exist as different helical forms but exists predominantly as B-form in native environment (Figure 1-3). B-form DNA is a right-handed helix with a diameter of 2 nm [9]–[11]. The double-helical structure of DNA has a diameter of 2 nm and roughly 3.57 nm long for one helical turn in aqueous solutions. Helical pitch is defined as the distance that parallels to the helical axis between consecutive bases for each full turn, the average helical pitch in B-DNA often equates to 10.5 nt. Also, there are two grooves in the helical structure of DNA where proteins can bind to. As presented in Figure 1-3C, the major groove is where the backbone far apart, wider than the minor groove.

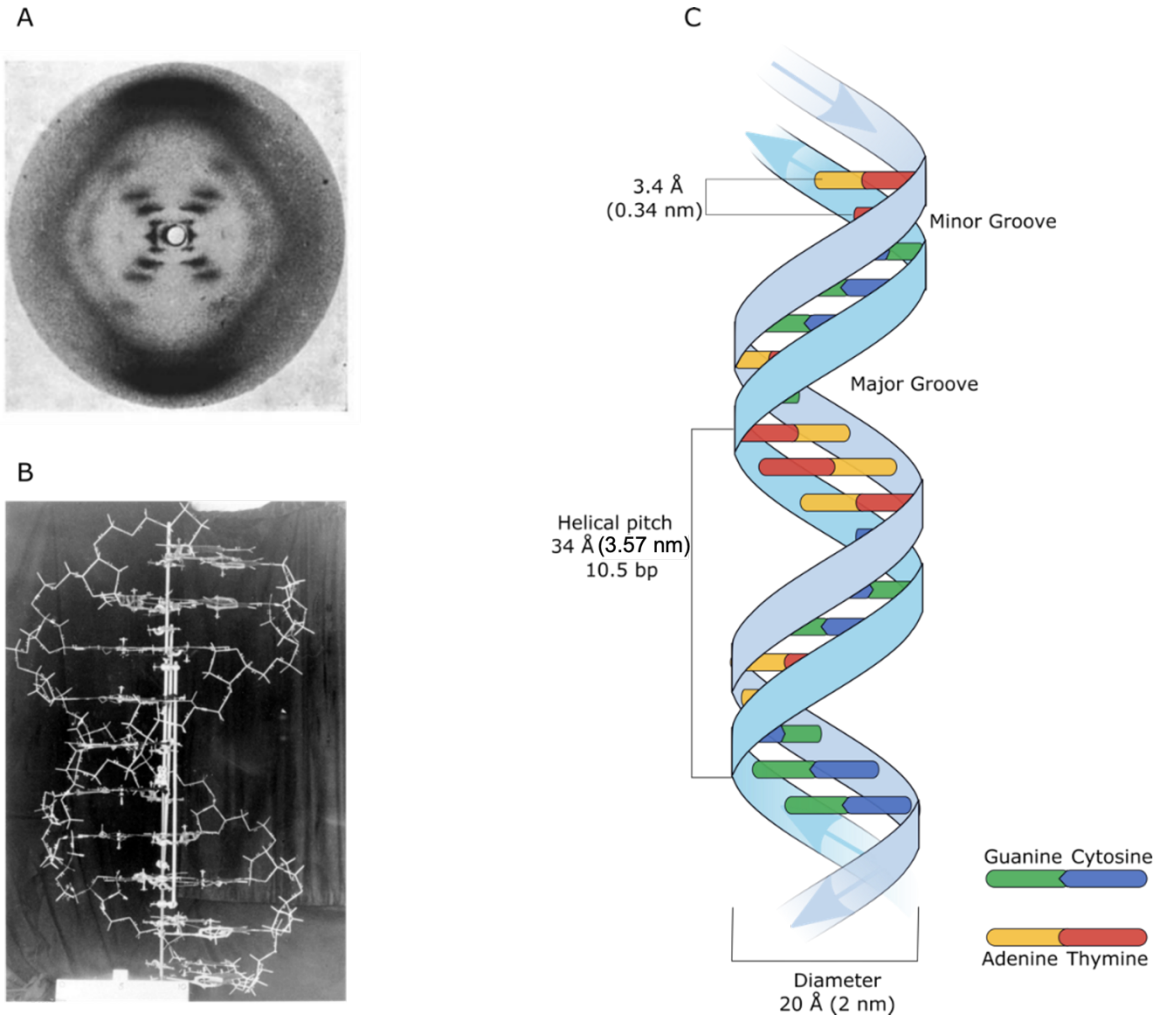

Figure 1-3 A) Rosalind Franklin's X-ray: the diffraction of DNA. B) Original model of Watson-Crick's DNA structures. C) Schematic of B-form DNA structure with helical pitch of 3.4 nm, diameter of 2 nm, minor groove and major groove are indicated. Image in figure A is taken from[2], image in figure B is taken from [3].

Under certain conditions, B-DNA can transition to other forms: with the most common being A-DNA and Z-DNA [12]. (Figure 1-4) In A-form DNA, the major groove becomes narrower and deeper, while the minor groove becomes wider and shallower. A-form DNA commonly occurs in dehydrated conditions [13]. It has a similar right-handed double-helical structure but is broader and more compressed along the helical axis. Double-stranded DNA with the sequence (CG)n can flip to a Z-DNA [14]. This transition is favoured by purine-pyrimidine repeats, high salt concentrations and low temperatures [15]. Unlike A- and B-form DNA, Z-DNA adopts a left-handed conformation [16]. Though DNA is modelled as double-helical structures, it naturally serves roles in its secondary structure. One example is a four-arm DNA crossover structure now known as the " Holliday junction" [17], [18], which is a type of DNA secondary structures appears during genetic recombination. It is an intermediate thus mobile due to its symmetric sequences. In biology, Holliday junctions usually have symmetric sequences and are thus mobile. In DNA nanotechnology, the immobile junctions usually have asymmetric sequences thus they can bind together and build large lattices.

There are various branched structures found as intermediates during replication, recombination and gene expression like hairpin loops [19], H-DNA(triplex) [20], G-quadruplexes (tetraplex) [21].

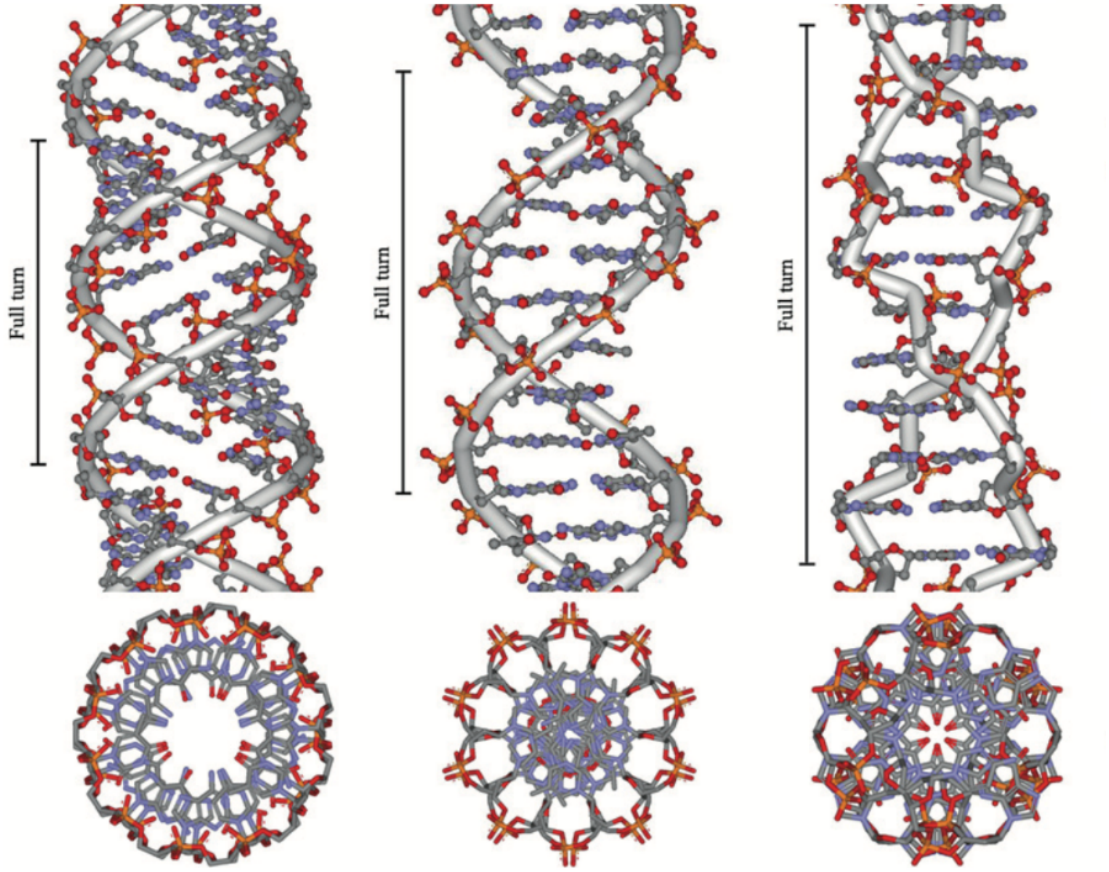

Figure 1-4 Conformations adopted by DNA. A-form DNA and B-form adopt right-handed, and Z-form is left-handed. Images taken from [16].

1.3 DNA as building materials

Whilst typically considered as the carrier of genetic information, many features of DNA such as the defined nanoscale, stiff structural repeats and persistence length (around 50 nm in 1 M NaCl [22]) in combined with the predictable base-pairing patterns, has been exploited for the self-assembly to create rational materials with nanoscale features [23]–[25]. This section introduces the earliest establishments of DNA nanotechnology and the two general approaches to create nanostructures: tile assembly and scaffold-based assembly.

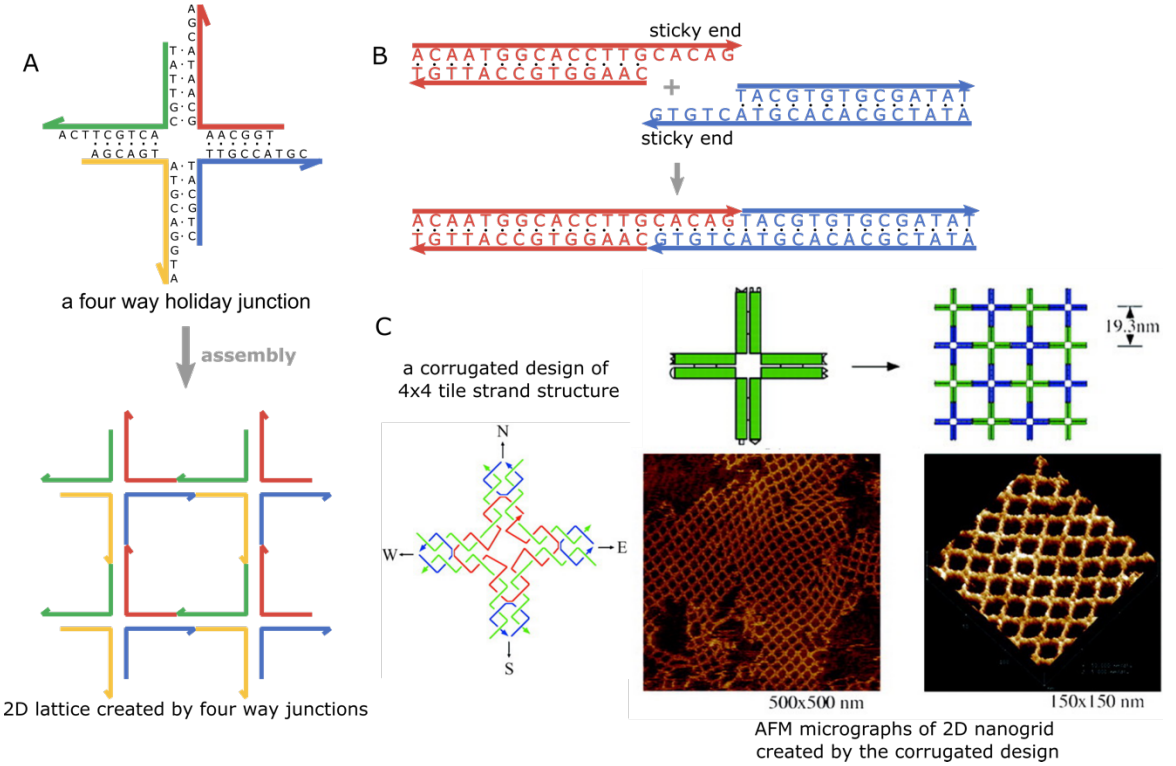

Figure 1-5 The beginning of DNA as building blocks. A) a four-way Holiday-Junction structure formed four DNA strands, the assembly of 2D lattices through sticky-ends hybridisation; B) illustration of sticky-end cohesion led the hybridisation of two DNA duplexes. C) Schematic of a corrugated cross shape design, and AFM micrographs of 2D nano-gird created by the design. Images in figure C are taken from [26].

The field of DNA nanotechnology was first laid out by Nadrian Seeman, who developed immobile junctions by mimicking the naturally occurred Holiday Junction (HJ) structures [25] (Figure 1-5A). In 1982, Seeman generated a larger scale of junctions assembles through omitting the sequence symmetry and the sticky-end hybridisation method [27] (Figure 1-5B). Sticky-end is a short single-stranded overhang protruding from the end of double-stranded DNA that is complementary to another protruding end. It is naturally a product of restriction enzyme cleaving a duplex and now an efficient tool used to program the interface between distinct DNA subjects. The idea of joining branched DNA structures to form crystalline lattices has become fundamental in DNA nanotechnology, with sticky-ends base-pairing being the efficient tool to link DNA junctions with each other. Another important steppingstone is the development of double crossovers (DX) motifs (Figure 1-6). A DX motif consists of two adjacent Holliday junction, forcing the HJ to adapt a side-by-side conformation. It remains the central motif in DNA nanotechnology still as rigidity and stability are needed for constructing large 2D DNA arrays and 3D structures of arbitrary shape.

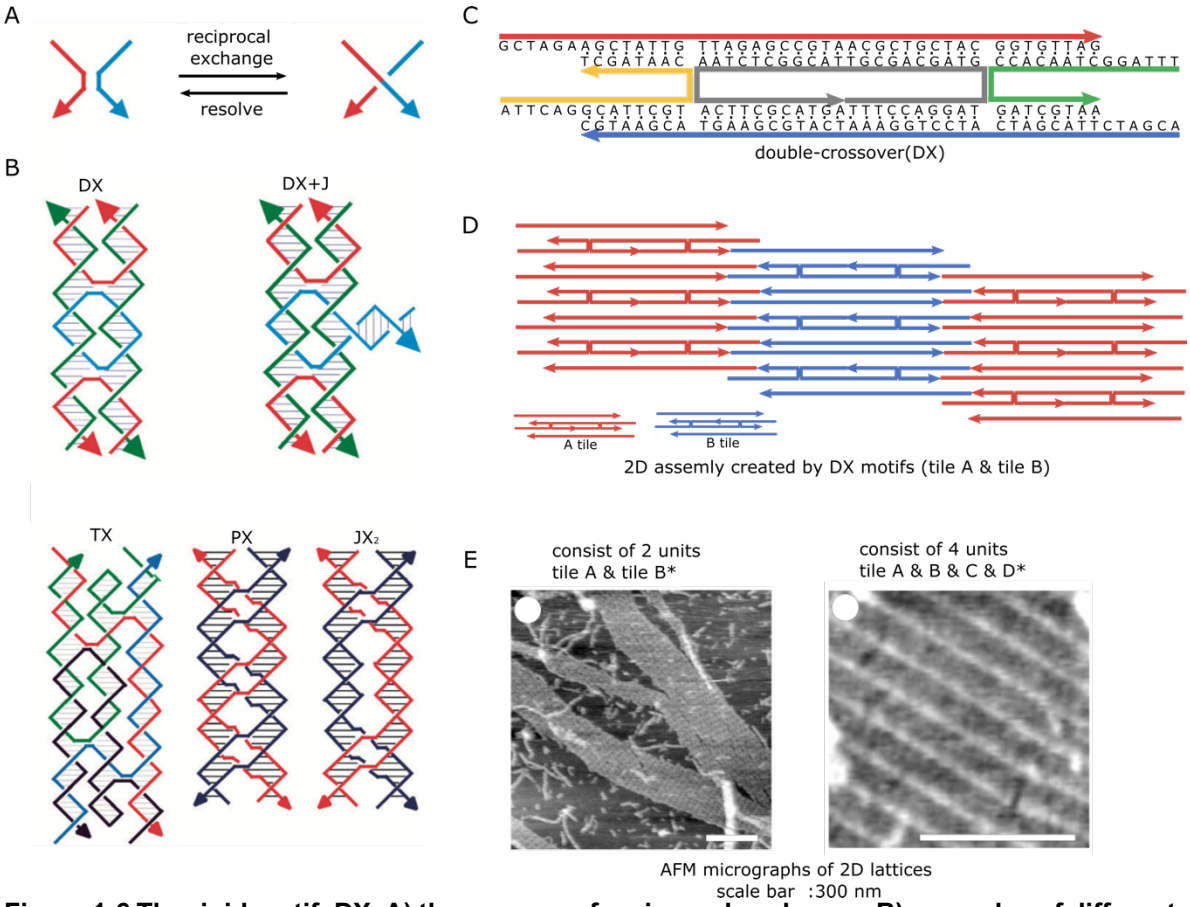

Figure 1-6 The rigid motif- DX. A) the process of reciprocal exchange; B) examples of different motifs that can result from reciprocal exchange; C) A double-crossover motif with sticky-ends results from reciprocal exchange of two holiday junctions. D) Schematic of two-dimension lattice containing two type of DX tiles. E) AFM micrographs of DNA lattices composed of two types of DX tiles and four types of DX tiles. Tile. B* and D* has a hairpin marker to differentiate from other tiles. Images in figure A are taken from [25], Images in figure E are taken from [26].

Early DNA structures were constructed from multiple short ssDNA strands [28], [29]. The fact that DNA tiles are non-uniformed in shape and size, also lack aperiodic control at large scales has led the methods with infinite theoretical boundaries. This system is very sensitive and requires exact stoichiometric control of a great number of short strands, stepwise protocols including purification steps to create a relatively large addressable array, thus always resulting in low yield [30]. Now tile-based multistranded approaches are still one of the main assembly methods to form small structures. More recent 'single-stranded tile' (SST) and "DNA bricks" strategies can construct 2D and 3D nanostructures in one-step annealing reactions [31], [32]. Alternatively, Yan and Shih have subsequently developed a scaffold-based approach (Figure 1-7) to construct an aperiodic lattice and an octahedron structure [33], [34]. Unlike the tiles approach which involves N to N interactions among ssDNA, thus requires precise stoichiometric concentrations [35] and lengthy filtration, the scaffold-based approach proceeds simple and quick by mixing the scaffold with an excess of staples strands in a tube, which is then annealed from a high temperature to room temperature. The most promising scaffold-based technology is named "DNA origami". It was introduced by Paul

Rothemund in 2006, can easily synthesize high-yield discrete structures with defined shapes through a simple temperature-controlled process [36]. The products are often in high yields and with neglectable misfolds.

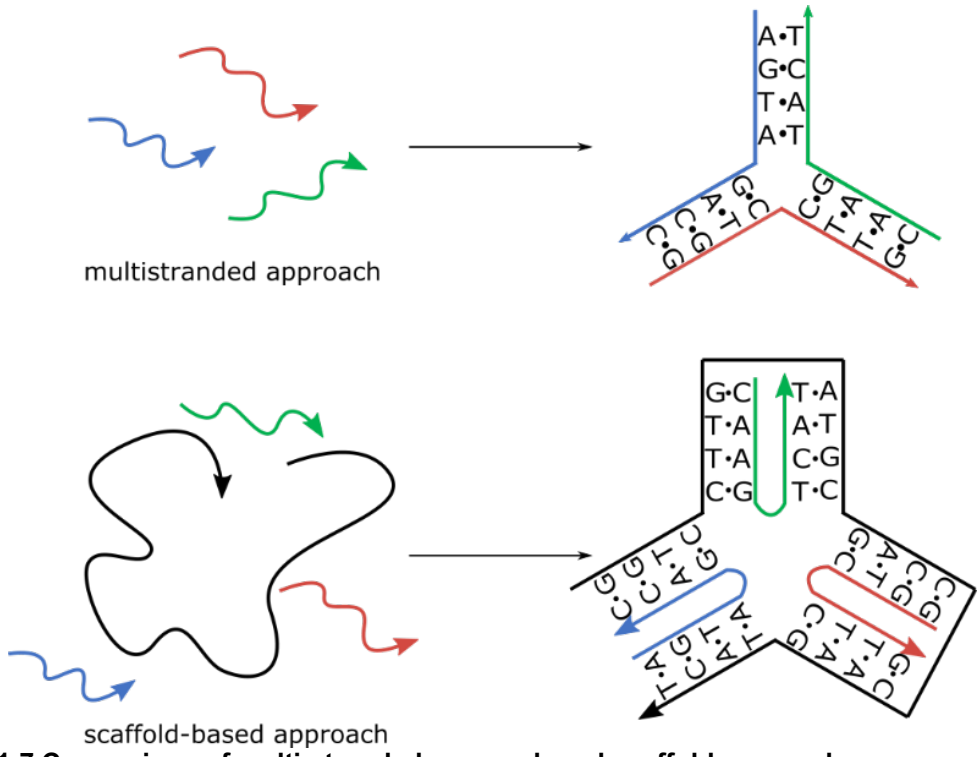

Figure 1-7 Comparison of multi-stranded approach and scaffold approach.

1.4 DNA origami

DNA origami is a method that can create many 2D or 3D nanoscale objects in a one-step reaction. It was introduced to structural DNA nanotechnology in 2006 by Paul Rothemund [36] and has transformed this field for the potential it can bring and its desirable properties. DNA origami is a fast and simple process that can produce complex structures in high yields. The ability to spatially organise functional materials has a large impact on a wide range of fields from biomedical applications [37]–[40] to nanoelectronics and optical devices [41]–[44]. To fully harness the potential of DNA origami as a universal pegboard, it is important to establish systematic understanding including designing consideration and downstream applications. This section includes basic knowledge of DNA origami technology. Planar DNA nanostructures are heavily stated here as their applications were the main body of the thesis.

1.4.1 Designing considerations

Existing computer-aided design (CAD) software like caDNAno or Tiamat has largely simplified the design process [45], [46]. Fast manufacture of sophisticated shapes has become friendly to new users although some considerations are still required. Of most importance is that a fine DNA nanostructure lies on the natural geometry of B-DNA. The double helices in origami are made of both scaffold and staple strands, such that staple strands should be arranged in a way to match the idealised spacing. As described above, a typical B-DNA exhibit a right-handed double-helix structure (2 nm diameter) with a periodical helical turn of 3.6 nm, composed of 10.5 bases. The offset between helices determines the length of crossovers with attention to minimizing structure deformations. On the other hand, the success of the self-assembly origami method lies in the cooperation of staple incorporation. Across the structure, every staple strand has two or more subsections (usually three) that hybridize to different fragments of the scaffold. The initial attachment of correct staples would help the subsequent binding of remaining ones during the folding, with strands invasion displacing staples that have bound incorrectly. The sufficient strength of each binding segment supports this cooperation, which means that the staple strands should be in a suitable length, typically 15-60 nt.

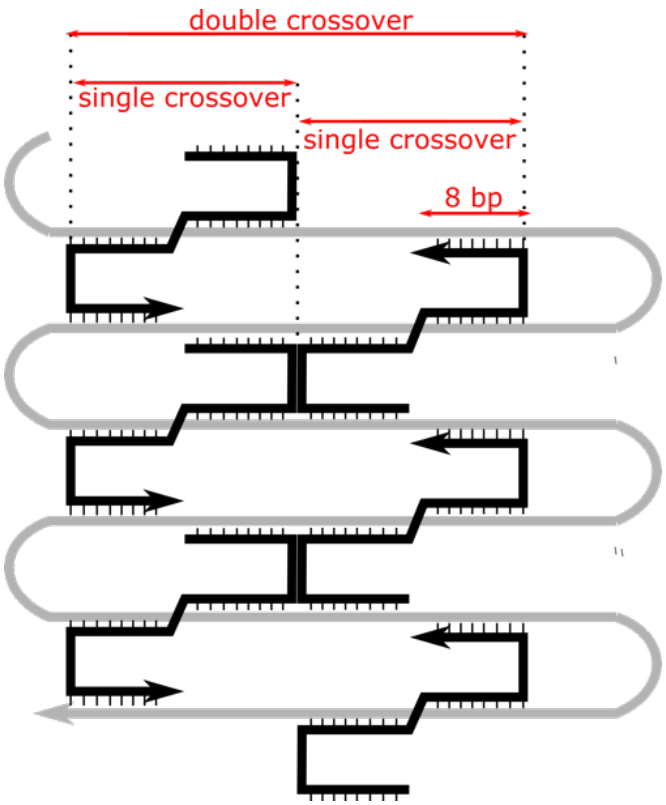

Figure 1-8 Simplified schematic illustrates how staple binds to different domains of scaffold, showing the definition of single and double crossover spacing. Blacks are staples strands adapt to an 8-16-8 pattern; grey is the scaffold strand.

Taking the example of Rothemund's single layer origami, which has been classified as square-based design, the offset between helices is 180°, meaning that the ideal single crossover (SX) spacing is an odd number of half helical turn. Therefore, the length of an SX should be close to 5.25 bp, 15.75 bp or 26.15 bp, correlating to 0.5, 1.5, 3 turns of B-form DNA. 1.5 turns of SX spacing is a more reasonable choice, but as it's not possible to get a non-integer number of bases, most single-layer square-based origami designs adapt to 8-16-8 patterns to staples (Figure 1-8) [47]. This results in non-planar structures with inherent twist and curvature, although methods have been developed to *correct* this mismatch (alternating between 31 and 32 DX). Another lattice-based design, honeycomb, fortunately, needs no compromise to the spacing as the offset between helices here is 120°. Each double helical strand rotates by 240° about the helical axis exactly every 7 bp so the spacing requires an integer. The crossover spacing can be used to adjust the structural twist and curvature of origami, leading to more complicated patterns. Another design strategy beyond packing helixes in parallel in these lattice conformations, is the wireframe method [48], in which four-arm junctions was used as the basic structural unit (Figure 1-9A). This wireframe design strategy was first introduced in 2013 and more complex objects with multi-arm junctions appeared [49]–[51]. Here the scaffold strand goes through a set of vertices as lines, staple strands surrounding the vertex have T loops to adjust the angle between arms [52], and there can be a range of arms meeting at each vertex, from three to eight. This method allows assembly for complex structures [49], such as a pen-rose tiling, an eight-fold quasi-crystalline pattern, and even a flower-and-bird pattern. From the aspect of practicability, it also gets rid of dense packing DNA helices and geometric constraints, making the wireframe structures greater promise in biomedical applications as they have enhanced resistance to cation depletion under physiological environment [53].

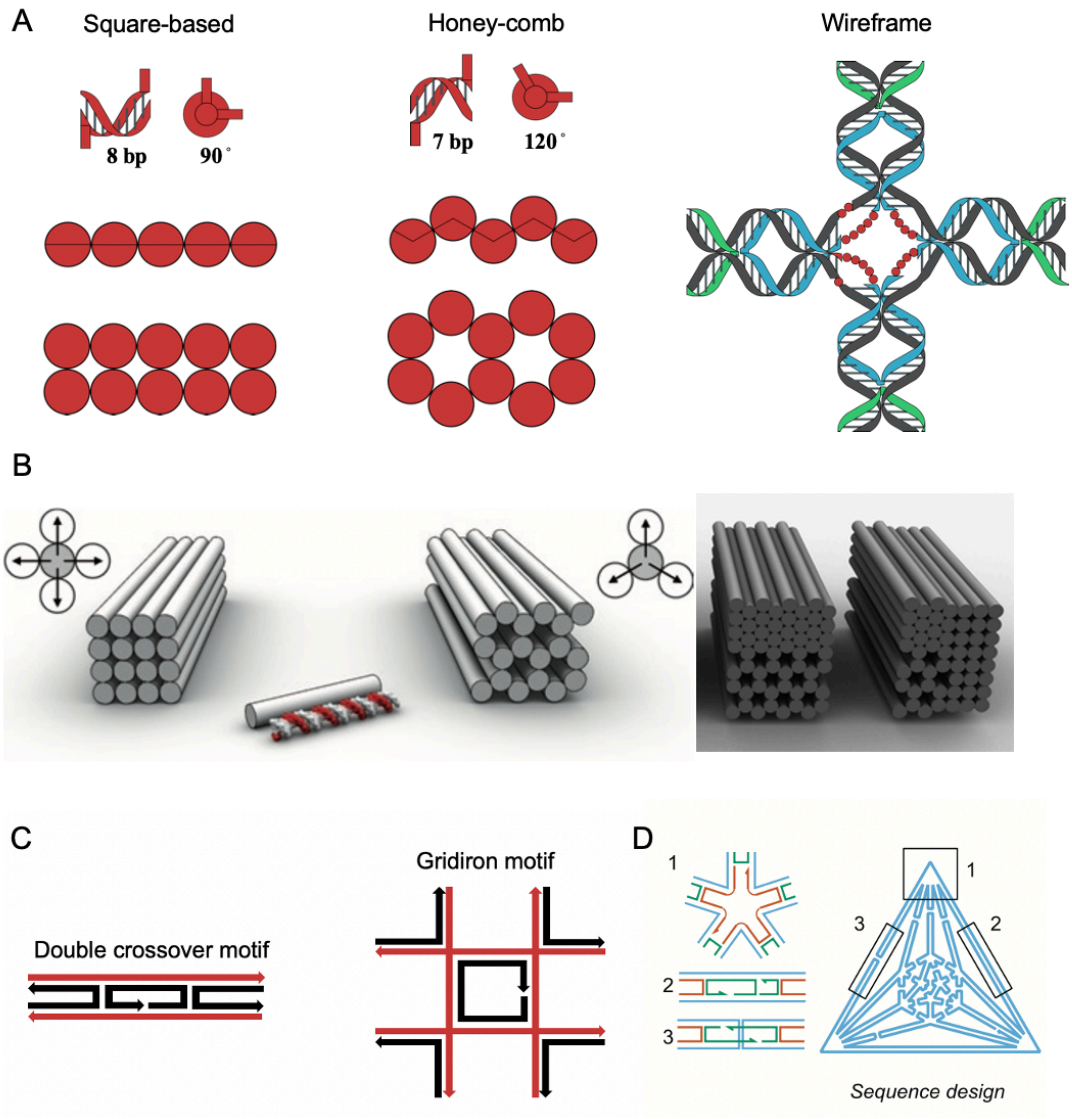

Figure 1-9 A) Schematics showing the packing rules of DNA origami including square-based, honeycomb, wireframe assembly. In square-based design, the offsets between adjacent helices are 90° or 180°, while in honeycomb the offsets are 120° or 240°. B) Square lattice, honeycomb and hybrid assembly combined. C) The basic units of tightly packed design and wireframe assembly; D) A polyhedron design utilises both DX and gridiron motifs. Images in figure B are taken from [54]**, images in figure D are taken from** [50]**.**

The three packing rules mentioned above do not conflict with each other thus one can combine either two or more depends on custom demands. For examples, the DAEDALUS introduced by Veneziano et al. [50] is a software with fully automatic DNA origami sequence design algorithm, in which the DX-based wireframe motif was chosen to render the arbitrary geometries as in it combines both the flexibility of wireframe and the rigidity of DX tiles, as each interconnected edges consists of duplexes joined by antiparallel DX (Figure 1-9D). By means of this approach, any 3D shape input model is allowed.

1.4.2 Artisan creations of DNA origami

Rothemund through his paper demonstrated the generality of DNA origami strategy to form a variety of planar nanostructures with different geometries including rectangle, square, triangle, star, and a three-hole disk (Figure 1-10). These can be easily achieved through adjusting the scaffold routing. Inspire by this work, more fascinating creations have followed up and they were not limited in two dimensions. Soon after, with the development of CAD software such as caDNAno and Tiamat, solid 3D constructs have been brought out and more designing concepts were demonstrated including honeycomb, square and wireframe lattices. Creations of DNA origami structures ranging from single-layered lattices like simple hollow containers [55] to solid bundled helices, from traditional flat lattice model to concentric rings with certain features including controllable twist and curvatures, from steady wireframe bunny [51] to mobile robots[56] that reacts to cation concentrations. Up to now, a wide variety of 2D or 3D constructures have been created [48], [49], [52]. Functions arise from structures. DNA origami-based applications have experienced rapid growth over the past decades. DNA origami devices are suitable to perform complex tasks at the molecular level due to 1) the ability to precisely arranging multiple functional molecules through different conjugation approaches, and 2) the introduction of DNA nanomachines [40], [57] adds reversibility/dynamics to the system.

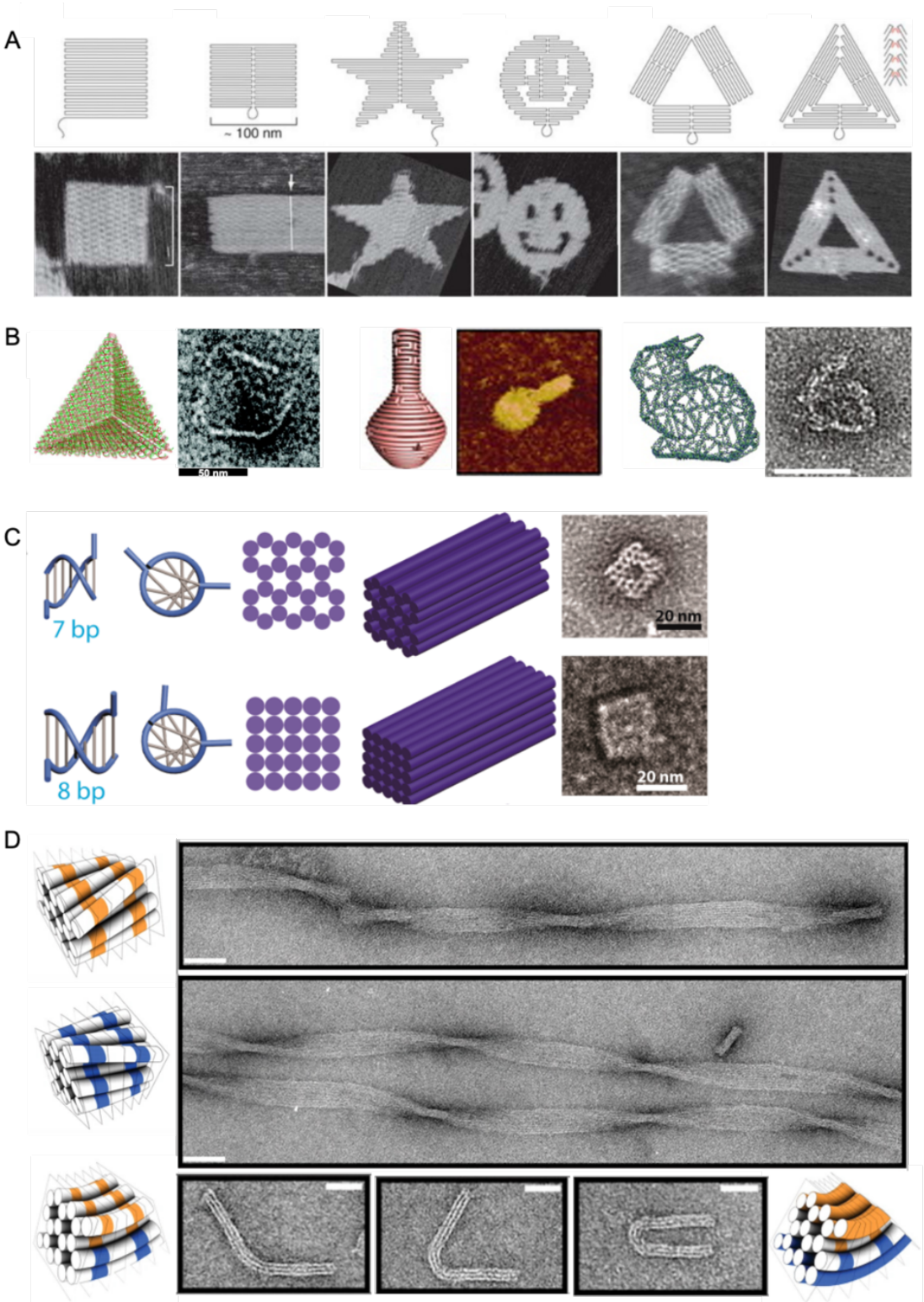

Figure 1-10 Creations of different origami nanostructures. A) Single-layered 2D nanostructures presented in Rothemund's first paper. B) Single-layered 3D DNA origami structures. From left to right, they are a compact tetrahedron [58]**, a nanoscale flask** [49]**, a wireframe rabbit** [51]**. C) Multi-layered DNA origami structures with hexagonal honeycomb, square packing of parallel DNA helices** [59]–[62]**. D) DNA origami with tuneable global bending and twists** [63]**.**

1.4.3 Decorated origami structures

Many complex tasks can be achieved through advanced 2D/3D origami constructs. The very first demonstration was achieved through functionalising oligos with dumbbell hairpin

structures. Rothemund used DNA to write the word “DNA”, created a map of America. (Figure 1-11A) They can be visualised with AFM since the height difference would result in bright pixels. Combined with toehold strands displacement, Seeman and co-workers [64] has developed an efficient device to detect single nucleotide polymorphisms (SNPs). The rectangular origami chips were equipped with DNA helices consisting of removable strands. One strand from each duplex formed a hairpin structure which was displayed for four alphabets. (Figure 1-11B) This method can detect invading strands with one mutation, adding target strands that perfectly matches, can cause the disappearance of the alphabetic. One system used chemical conjugations including CCP-Halo, mSTV and mKate-Snap to achieve orthogonal decoration of proteins. (Figure 1-11C) They use chemical coupling of amino-modified DNA staple strands with benzylguanine or chlorohexane groups, thereby multiple proteins with halo-tag or snap-tag can be captured by these modified staples onto human-face shaped origami specifically on three sites: eyes, nose and mouth [65]. The incorporation of small molecules is usually achieved through directly modifying the staple strands with, for example, dye molecules. Origami structures allow the arrangement of fluorescent dyes within 10 nm precisely, which can be fabricated as the light-harvesting or sensing application. (Figure 1-11D&E) Hemmig et al. programmed Förster resonance energy transfer efficiency using DNA origami. They drastically enhanced the FRET emission from one acceptor to multiple donors in an antenna array [66]. Subsequently, Choi et al. demonstrated a ratio metric sensor by constructing various FRET nanoarrays of different sizes and patterns [67]. The sensitivity of the sensor was improved by arranging dyes into a 3x4 checkboard pattern. With the incorporation of metallic materials, DNA origami has been demonstrated as a plasmonic structure, where the proximity of gold nanoparticles can increase plasmonic resonance, making functional nanoelectronics devices. For example, DNA functionalized AuNRs were immobilised onto triangular origami with certain angles (180°, 60°, 0°, 90°) [68]. The author demonstrated that scaffold precisely orienting can interrupt the spatial symmetry of metallic nanoparticles. Using the same strategy, one had amplified the surface-enhanced Raman spectroscopy (SERS) by arranging two gold nanoparticles with a distance of 25 nm [42]. They further demonstrated it is possible to detect TAMRA molecules since the dye can be excited by the electromagnetic field enhancement in the hot spots.

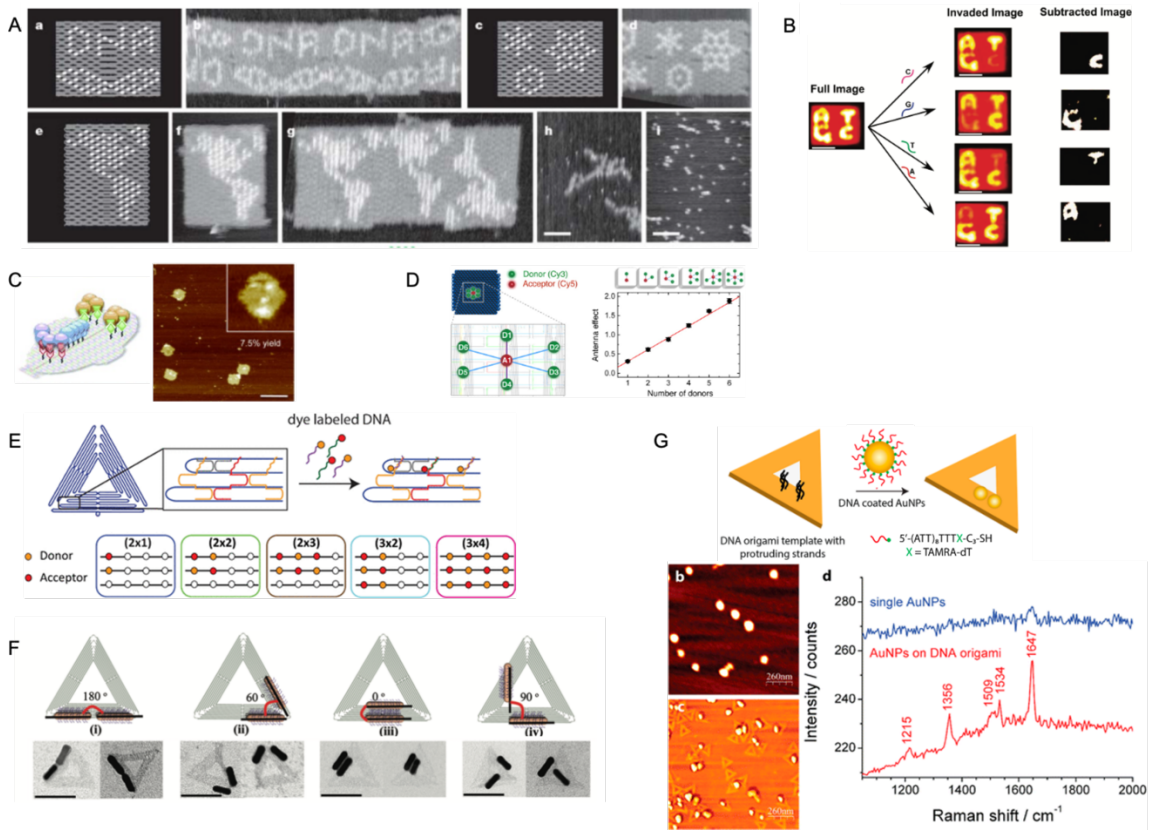

Figure 1-11 Applications based on single-sheet origami design. A) AFM images showing patterned DNA origami tiles, rendered with the use of hairpin. B) A DNA origami chip built for SNPs detection mediated by controlled strands displacement reaction. C) Multi-protein decoration of DNA origami structures resembling a human face. D) An efficient antenna system that achieved energy from multiple donors to one acceptor. E) A 4x3 array on DNA origami that can precisely arrange dye molecules. F) AuNRs were immobilized in arbitrary directions on DNA origami; G) Plasmonic hotspots for the surface-enhanced Raman scattering on DNA origami. Images imported from [36], [42], [64]–[68].

1.4.4 Dynamic structures

Dynamic DNA nanostructures often make use of a simple toe-hold strands displacement reaction. This process involves three strands, one strand (called invader strand) which fully complementary to the target strand can displace a shorter incumbent strand [69]. As shown in Figure 1-12A, in the initial state the unpaired sequences behave as a toehold which the invader binds first. Toehold strand displacement is slow to reverse since the invader-target duplex is more stable than the incumbent-target. Toehold strand displacement makes use of branch migration in biology and was introduced to the field of DNA nanotechnology in 2000 by Yurker and co-workers who developed a molecular tweezer structure (Figure 1-12B) with open and close states[70]. Douglas and co-workers have developed this concept into a drug delivery system by using a aptamer based locks that allows to control the open and close state of the delivery barrel [71] (Figure 1-12C). This kind of reactions can be linked to a cascade when the output strand of one reaction can initiate another displacement reactions elsewhere. Cascades of strands displacement can be used to make molecular logic gates and DNA circuitry for DNA computing [72], [73].

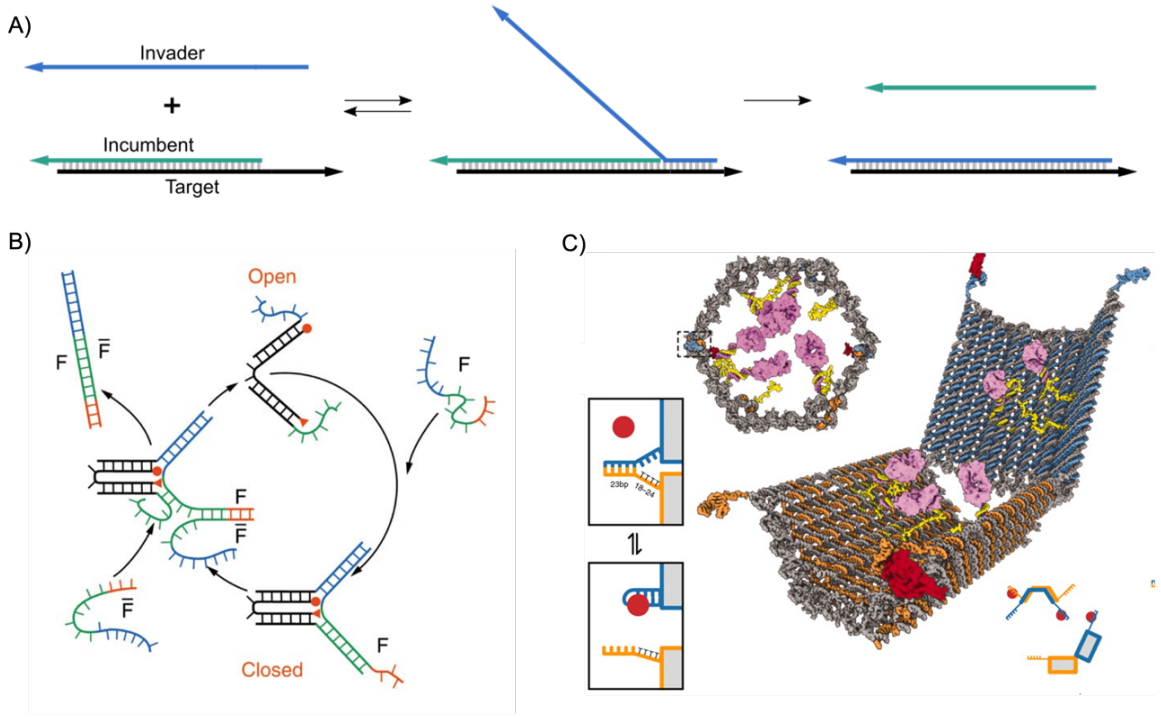

Figure 1-12 A) Illustration of toe-hold strands displacement; B) Molecular tweezer structure with close and open state; C) A DNA origami barrel for the drug delivery.

1.5 Toward large origami

Although origami has demonstrated powerful applications in many fields, micron-scale origami structures are highly desired because they can perform more complex tasks. However, the size of origami is limited by the length of the scaffold strand. A typical scaffold would be an M13mp18 in a length of 7249 nt, which normally results in origami structures with a scale of ~100 nm. To open complexity and utility, scaling up of origami constructs is desirable, especially for device fabrication.

1.5.1 Pure DNA methods

To address this concern, the most straightforward way is to use a larger scaffold template as it is what limits the scale of the final origami constructs. Increasing the length of the scaffold has been attempted using many molecular biology methods (Figure 1-13). For example, Zhang et al. has amplified a 26k-nt scaffold using polymerase chain reaction (PCR), created an origami with the dimensions of 238 x 108 nm[74]. Subsequently, Marchi et al. have produced a 51k-nt long ssDNA as the scaffold, which is so far the largest scaffold [75]. Whilst this increases the size of monomeric origami, there is also an associated increase in cost, due to the larger amount of staple strands needed to fold the scaffold. This problem persists with the use of multiple scaffolds [76]. The alternative approach includes

hierarchical assembly, using bridging strands to connect individual origami. These are often achieved by using base pairing of sticky-ends [77], base stacking of blunt-ends [44], shape complementarity of DNA structures [78], or a combination of all.

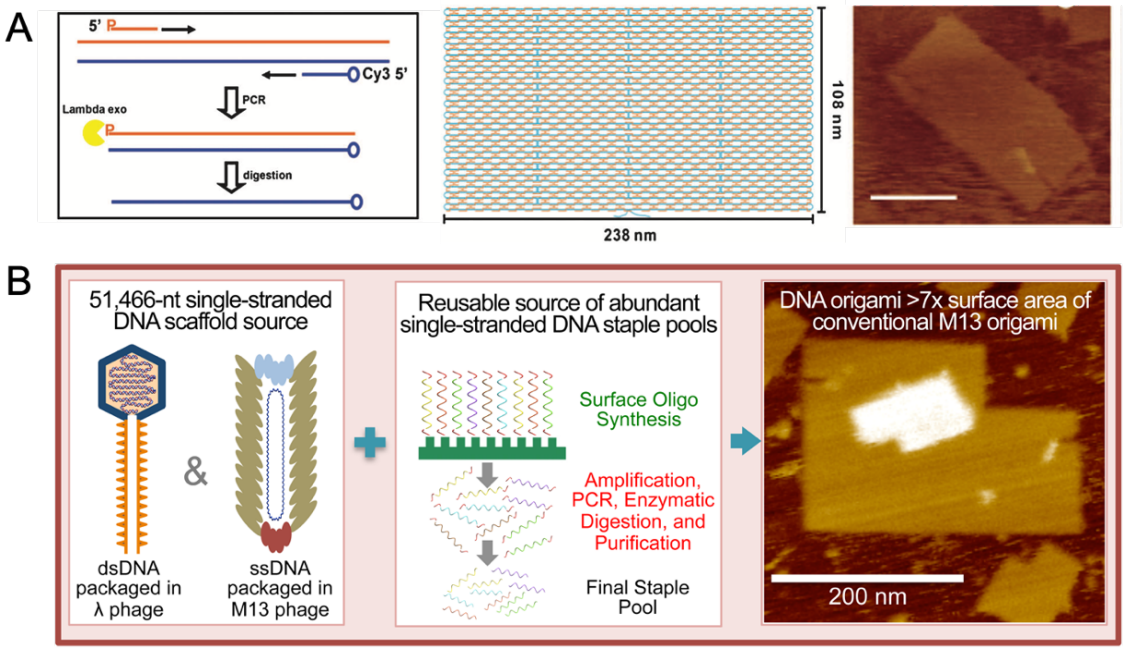

Figure 1-13 Create larger origami through extending the scaffold template. A) A 26 kb single strand DNA that can fold into a rectangle with the dimension of 108 x 238 nm, requires ~800 staple strands to help. B) A 52 kb super long DNA scaffold produced using a λ/M13 hybrid virus, can fold origami whose surface area is over 7 times than the origami fold with the M13mp18. This scaffold requires ~1600 staple strand to fold. Images exported from[74], [75]

Identical origami tiles have been polymerised with sticky-ends hybridisation, resulting in 2D crystalline assemblies with hundreds of tiles [79]–[81]. One of the earliest attempts was achieved by Liu et al [79], who used cross-like shaped DNA origami whose helix axes propagate in two perpendicular directions for avoiding nonspecific binding. As shown in Figure 1-14A, this design allowed a large periodic 2D lattice with dimensions up to 2 x 3 μm^2. Although this strategy has been applied to discrete architectures, it brought us close to the point where bottom-up technology can meet the limits of top-down technology. Instead of forming infinite structures, finite structures are more desired for their controllable full addressability. Like the recent half microscale construct, an 8 x 8 origami array was assembled through blunt-end stacking and 2-nt base pairing [82]. With the four-fold rotational symmetry of individual DNA motifs, Tikhomirov et al. produced a 0.5 μm^2 assembly composed of 64 motifs using a constant set of unique edge strands. This way is termed as fractal assembly results in large arrays in a multi-stage fashion, while the dimer yield was 95% and the yield of the final construct was 1.8% (Figure 1-14B).

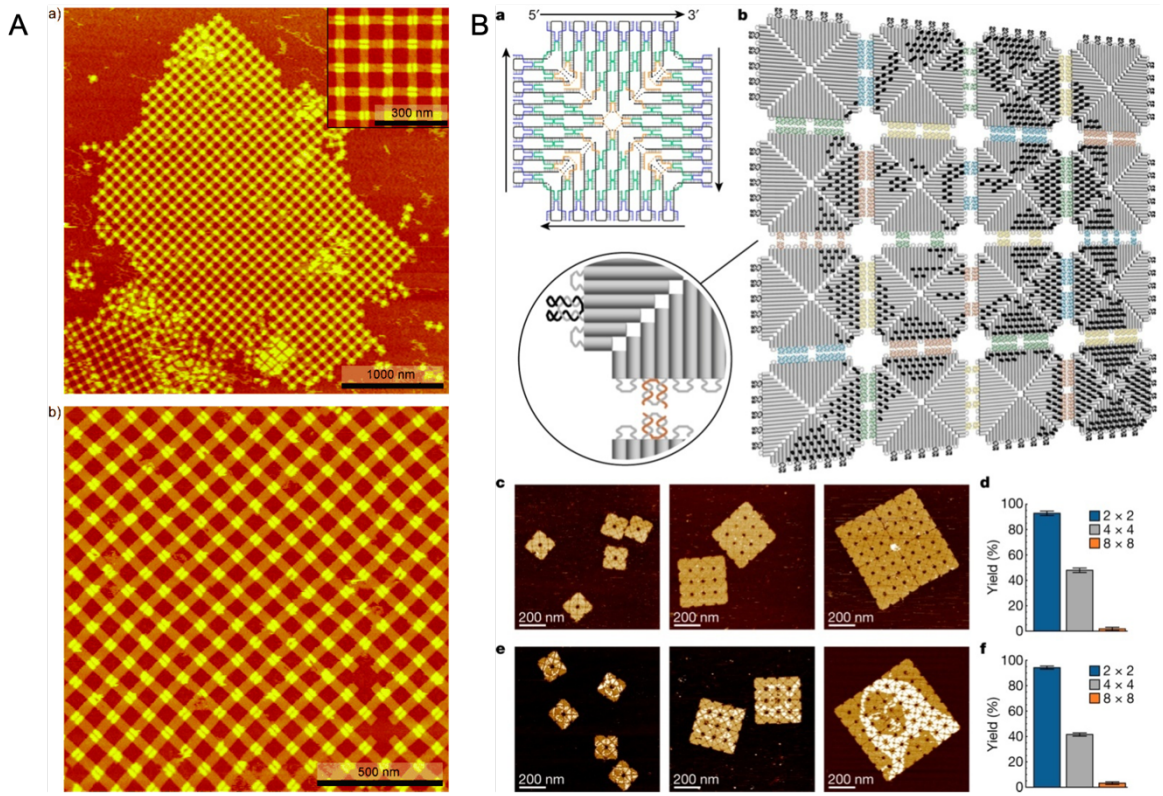

Figure 1-14 A) AFM image of a two-dimensional origami array with a dimension of about 2 x 3 μm^2. B) A 0.5 μm^2 Mona-Lisa composed of 64 tiles assembled in multi-stage fashion. Images exported from [79], [82]

Pure-DNA strategy, mainly the sticky-ends dominated connection method has its own simplicity and limitations. Theoretically, those approaches should allow desired architectures of any size. Practically, however, the assembly yield of origami tiles by means of hybridisation methods are typically low, largely restricting the scale of the final assembly and their downstream utility for device applications. It is clear that the increased number of distinct origami tiles complicates the assembly process including the incubating, purifying, and concentrating, and therefore lower the yield. It is not clear why assembly consisting of a small number of origami tiles were not typically high yielding. Normally, sticky-end dominated dimer yield is about 85% to 95%, and this lost can be amplified exponentially with multiple purifications, which however is unavoidable if to hierarchical assemble addressable origami constructs. Liber et al. mentioned that the highest dimerization yield to obtain is about 86%, which emphasizes the importance to explore the impact factors of origami assembly and improving the assembly strategy [83]. Although they have discovered that the structural imperfections and the dimer thermodynamic instability are less likely to limit the dimer yield, how to properly improve dimerization efficiency has not been well-studied yet. If to create a micron-scale or larger architecture for reliable devices based on origami strategy in a more efficient way, more understanding of the mechanism of

dimerization is one prerequisite. Furthermore, although highly programmable, above pure DNA methods often come with the excessive cost of massive sets of unique DNA sequences and low yield of final products. Novel strategies to expand the repertoire of interactions available for large-area origami construction are much desired.

1.5.2 Chemical strategies

One avenue of interest is chemical strategies of origami attachment. There exist many ways to attach molecules to origami through chemical strategies [68], [84]–[86], researchers have only begun to explore the use of chemical groups to attach origami tile together for the purpose of hierarchical assembly [87], [88]. One impediment is that the chemical interaction is often used for the aggregation or polymerization of DNA nanostructures. Ohmann and co-workers has demonstrated that it is possible to control the aggregation of cholesterol-modified DNA nanostructures [89]. 3D origami bricks have been polymerized via a host/guest interaction between adamantane (Adm) or beta-cyclodextrin (βCD), the degree of polymerization can be tuned though adjusting the number of connecting strands at the interface[87]. It is possible to introduce new connection mode to assembly DNA nanostructures rather than classic DNA hybridisation. If to preserve the controllable addressability of the final construct, however, it is necessary to combine the specific DNA base-pairing with a relative strong chemical interaction, thus, to have both to complement each other. For example, to date the largest assemble of 8 x 8 origami arrays used a combination of 2-nt sticky-ends base-pairing and blunt ends stacking, where sticky-ends dominate the specific binding, and the latter stabilise the constructs. Therefore, it is ideal to have a chemical interaction that can complement the sticky-end hybridisation. This way to improve the strength of tile attachment without the loss of specificity.

1.6 Brief introduction of fluorous effect

The fluorous effect is often considered as an extreme example of hydrophobicity, whereby fluorine-rich molecules seek to exclude themselves from non-fluorous media. This affinity is so strong that the fluorous effect can be employed as a reversible, non-covalent binding technique; an attribute commonly used in organic synthesis to separate small molecules, and, more recently, as a means to immobilise small molecules such as proteins, carbohydrates, or ssDNA oligos onto patterned perfluorinated substrates [90]–[92].

The fluorous effect has attracted our interest for three reasons. First, fluorous introduce no defect in the function of DNA oligos [91]. Previous work has demonstrated that the fluorous effect could be used for the immobilisation of DNA onto patterned surfaces, whilst at the same time allowing hybridization to its complements. Second, akin to how the strength of sticky-ends can be altered, the strength of the fluorous effect is adjustable and highly dependent on the fluorine content of fluorous molecules which can be varied through changes in the ponytail length and the number of branch points. Last but not least, fluorous molecules is a noncovalent interaction such that the fluorous ponytails may slide over one another without separating them. Thus, the fluorous effect might be able to strengthen the site-specific interaction of base-pairing and at the same time allow the base-pair interaction to correct mismatch led by its non-specificity, providing added stability when mixed with ssDNA sticky-end systems. Overall, the fluorous effect may have high potential to play a role in the assembly of origami tiles, e.g., act as an auxiliary molecular recognition mode to complement base-pairing, but the utility of this interaction remains unexplored in the field of structural DNA nanotechnology.

1.7 Fluorescence and energy transfer

1.7.1 Fluorescence and FRET

The fluorescence emission can be described a process that some molecules (called fluorophores) emit a photon to deal with the energy received from photons [93]. When absorb an excitation photon, the fluorophore transits from the ground singlet state (S_0) to the higher excited level of either first singlet state (S_1) or second singlet state (S_2), then return to the S_0 by emitting another photon. As depicted in Figure 1-15, prior to the emission process, molecules in condensed phases would rapidly relax to the lowest vibrational level of S_1 by transferring to adjacent molecules [94], this energy lost results in the energy of the emission is always lower than that of absorption, thus fluorescence often occurs at longer wavelengths [95]. The phosphorescence phenomenon happens in a manner like fluorescence, only electrons convert from excited states to the first triplet state (T_1) by intersystem crossing, then return to S_0. Hence fluorescence has a much shorter excited lifetime than phosphorescence.

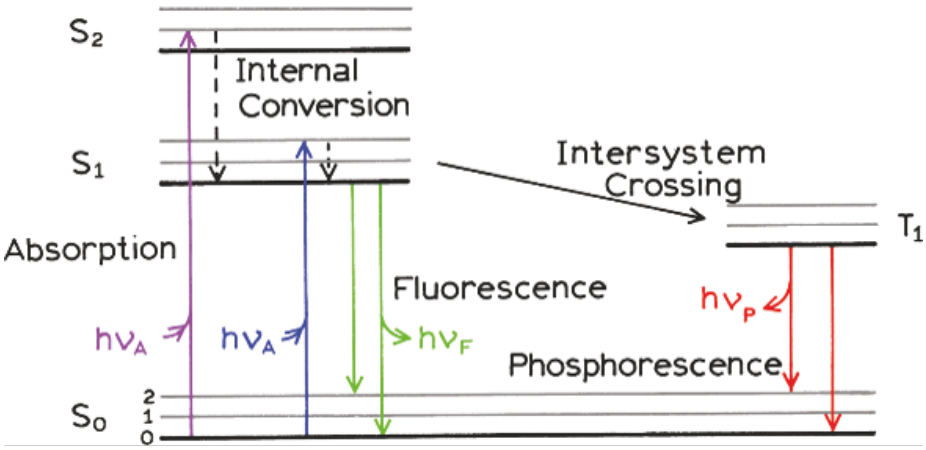

Figure 1-15 Jablonski diagrams illustrating fluorescence and phosphorescence. Images extracted from [93]**.**

Förster resonance energy transfer (FRET) is a nonradiative energy transfer process that occurs between two chromophores in proximity (typically within 10 nm) [96]. The principle of FRET was well developed by Theodor Förster [97]. As illustrated in Figure 1-16, this process involves a donor fluorophore is excited by a photon and then relaxes through transferring energy to nearby acceptor fluorophores, thus associated with the quenching of the donor emission, the acceptor emits a fluorescent photon. The energy transfers from the donor in S_1 to the acceptor in S_0 via dipole-dipole interaction.

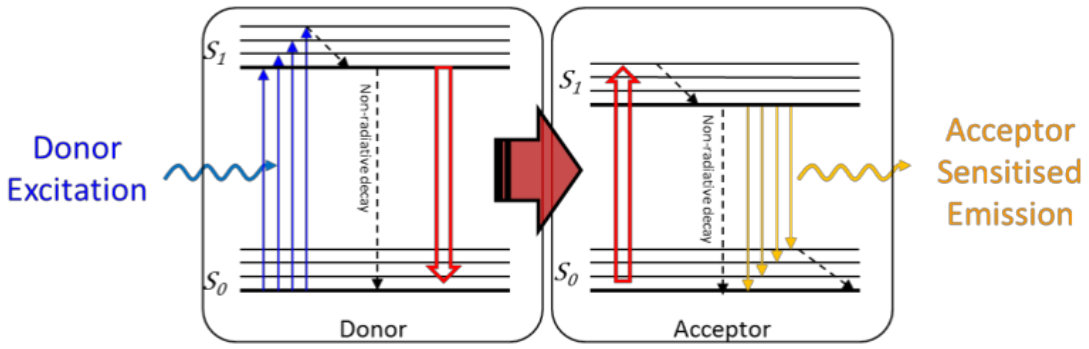

Figure 1-16 Jablonski diagrams illustrating the of FRET process. Image extracted from [94]**.**

1.7.2 Factors that influence FRET

The transfer rate from a donor to an acceptor (k_{FRET}) is given by

$$k_{FRET} = \frac{1}{\tau_D}\left(\frac{R_0}{r}\right)^6$$

where τ_D is the decay time of the donor without the presence of the acceptor, R_0 is the Förster distance with 50% transfer efficiency, r is the distance between donor and acceptor.

The efficiency of energy transfer (E) is defined as the proportion of donor fluorophore in excited state has transferred energy to acceptors [98], the followed equation showed that the FRET efficiency is highly dependent on the donor-acceptor distance.

$$E = \frac{k_{FRET}}{{\tau_D}^{-1} + k_{FRET}} = \frac{1}{1 + \left(\frac{r}{R_0}\right)6}$$

Other factors that determine the occurrence of FRET includes the emission spectrum of the donor fluorophore overlaps with the excitation spectrum of the acceptor fluorophore [99]; and that the FRET pairs are properly orientated according to the dipole-dipole coupling system.

1.7.3 FRET on origami

The sensitive distance-dependence of FRET makes it a powerful tool for characterizing the feature of DNA nanostructures. For example, DNA origami blocks have been realized as single-molecule FRET ruler to measure distance in nanometre scale [100].This work suggests that the FRET probes could be used as a mean to characterize the folding of more complex origami construct with the improved local resolution. Urban et al., designed a system to have FRET signal correlated to the sliding effect of duplet DNA origami tiles [101]. A single-molecule force spectroscopy based on DNA origami has been demonstrated that can elucidates the stability of the RNA Polymerase III pre-initiation complex [102]. The binding of TBP could lead a 90° bending of DNA, which can be linked with the change in FRET efficiency through careful design of DNA origami.

Vice versa, DNA origami construct with high rigidity has been demonstrated as versatile platform to place molecules with nanometre precision. Many solutions have been realized toward enhanced FRET. Energy transfer among two or three fluorophores of the same kind (homo-FRET) has formed an energy cascade thus can lead to the overall enhanced FRET [103]. A study has shown that placing a gold nanoparticle close to the donor can promote the FRET process and improve the efficiency [104]. To summarize, DNA origami is a good platform to investigate the distance-dependence of FRET, to optimize the pair of donor and acceptors and to improve the FRET efficiency in general.

1.8 Motivations and Objectives

DNA origami constructs are often treated as a pegboard that has over 200 sites that can be modified. Due to the versatility of DNA chemistry [105], [106], ssDNA oligos can be modified with various functional materials including proteins, peptides, fluorophores and inorganic metal nanoparticles, etc [35], [68], [107]–[110]. The beauty of the DNA origami is that it can serve as a linker platform and conjugate materials with different functions together with nanoscale control. The applications of DNA origami have found in many fields such as drug delivery, biosensing, diagnostics, nanoelectronics and nanophononics. With its prosperous development in science, several challenges need to be overcome before DNA origami nanostructures can be applied in real-world devices. One of the issues is the size of the origami is limited by the length of the scaffold, with the use of m13mp18, the scale of the single origami tiles is often within 100 nm. Hierarchical assembly has been one effective strategy to scale up DNA origami. Tikhomirov et.al has created a 0.5 micron-scale Mona-Lisa and this is so far the largest distinct origami constructs [111]. However, the yield of the final construct was only 2-3%, as the yield drop as the assembly size increases using the sticky-ends hybridisation method. Therefore, novel strategies that can assist and complement the sticky-ends hybridisation is desired for the creation of micron-scale DNA assembly with satisfying yield.

As an adjustable, reversible non-covalent interactions, fluorous effect works orthogonal to DNA base-pairing, has potential to address the limitation of pure DNA methods [91], [112]. It is believed that fine control of the non-specific fluorous interaction would provide a strong yet mobile binding solution to sticky-ends strategy, has potential to deliver added stability to the system. Majority work presented in this thesis was to investigate if the fluorous could direct efficient dimerization of high yield, take one step further toward the stable micron-scale DNA assembly. The last result chapter was an application-vise exploration to determine if Qdots could directed FRET on origami.

Chapter 2 Materials and Methods

2.1 Materials

This chapter provides an overview of the analytical and general experimental techniques that have been used in thesis.

2.1.1 DNA strands

2.1.1.1 Strands for DNA origami

DNA origami is made of a M13mp18 (7249 nt, Tilibt nanosystem) scaffold strand and hundreds of short staple strands, mixed in the presence of Tris-acerate-EDTA buffer and magnesium salt. All staple strands (with the exception of the modified DNA oligos) were purchased from Integrated DNA Technologies, Inc. (IDT). Normal staple strands were purified through standard desalting. The M13mp18 purchased from IDT was produced by Tilibit nanosystems.

2.1.1.2 Modified DNA strands

The fluorous modifications used throughout this thesis were achieved via modifying specific staple strands. Staple strands with modifications were purified via high performance liquid chromatography (HPLC) to ensure accurate attachment of functional groups. Other modified staple strands were purchase from IDT. Modifications such as (i) extended sticky-ends, (ii) fluorescent molecules, (iii) biotinylated tags were also obtained from IDT. Fluorous-tagged strands were obtained from University of Strathclyde (UK), synthesised in Dr Glenn Burley's group using standard solid-phase methods[113] on an applied biosystems 392 DNA synthesiser.

2.1.2 Buffer solutions

Stock buffers were made using DI water. All buffers and solutions can be found in Table 2-1.

Table 2-1 List of buffer solutions and their composition

Buffer Name	Composition	Source
10 X Tris Acetate-EDTA (TAE)	0.4 M Tris, 0.4 M acetate, and 10 mM EDTA, pH 8.3.	Sigma-Aldrich
Magnesium acetate solution	~1 M in H2O	Sigma-Aldrich
1 X Tris Acetate-EDTA (TAE)	40 mM Tris, 40 mM acetate, 1 mM EDTA, and 12.5 mM magnesium	Freshly made in lab
TE buffer	10 mM Tris, 10 mM EDTA, pH 8.0	Invitrogen
Direct Load 1 kb DNA Ladder	2.5% Ficoll (Type 400), 0.0125% bromophenol blue, and 0.00625% xylene cyanol	Sigma-Aldrich
DNA Gel Loading Dye (6X)	10 mM Tris-HCl (pH 7.6) 0.03 % bromophenol blue, 0.03 % xylene cyanol FF, 60 % glycerol 60 mM EDTA	Thermo Scientific
SYBER Safe DNA gel stain	10000 X concentrate in DMSO	Invitrogen
Deionized (DI) Millipore water	resistivity of 18 MΩcm	

2.2 Preparation of DNA origami

This section introduces general protocols of DNA origami technology. Specific implementation of the protocols is introduced in the relevant experimental chapters.

2.2.1 Designs

Research in this thesis has used three origami designs (Figure 2-1): a wireframe square [49], a normal rectangle [114], and an asymmetric rectangle. Sequences of the wireframe and the normal rectangles were obtained from the literature, the asymmetric rectangle was modified using caDNAno, the sequences were shown in Appendices.

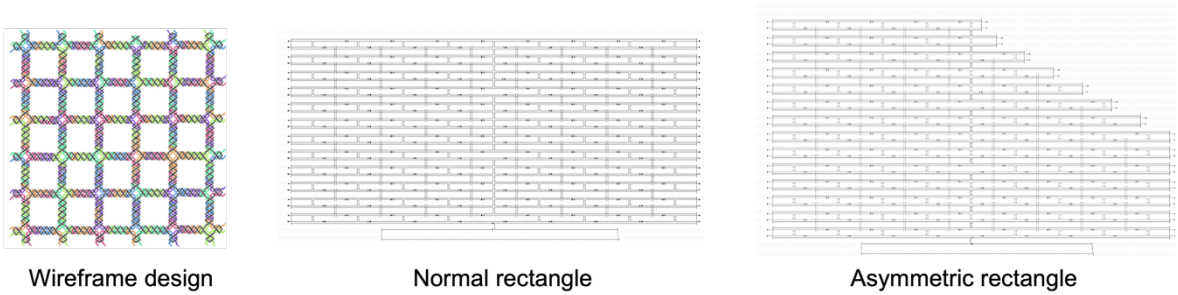

Figure 2-1 Schematics of the three origami-designs used in this thesis

2.2.2 Preparation and storage of oligonucleotides

Based on the manufacturer's instructions, all DNA strands were resuspended with nuclease-free water (Sigma Aldrich) to a final concentration of 100 μM. The mixture of strands was mixed in autoclaved Eppendorf tubes to a final concentration of 1 μM. All solutions were stored at -20 ˚C.

2.2.3 Annealing of DNA nanostructures

All DNA origami nanostructures were synthesised as described below. The annealing mixtures contain 10x excess complementary staple strands to M13mp18, were prepared in the presence of 1x TAE (Tris, 40 mM; Acetic acid, 20 mM; EDTA, 1 mM) and 12.5 mM magnesium salt by heating to 95 ˚C and cooling to 20 ˚C in a thermal cycler at a rate of 1˚C/minute in 1˚C steps. An appropriate quantity of ions, such as magnesium here or sodium in the DNA hybridization approach, were required to equilibrate the electrostatic repulsion between highly negatively charged DNA molecules. Based on different demands, the final concentration of the scaffold ssDNA was at a range of 1-10 nM with an equivalent ratio of other components. The mixing and folding normally takes only a few hours [115].

Table 2-2 An example of an annealing system for a RF-origami

Solution	Volume (μL)
M13mp18 (100 nM)	5
Mixed staple strands (1 μM)	5
Mixed Fluorous strands (500 nM)	10
10 x TAE buffer	10
10 x Mg^{2+} buffer	10
Water	Up to 100

2.2.4 Centrifugal purification

Purification of DNA nanostructures generally refers to the removal of free staple strands. Excess staple strands were removed using a 100 kDa Amicon Ultra-0.5 mL spin column. The column was rinsed with 500 μL of 1xTAE-Mg^{2+} buffer and spun at 10,000 g for 5 mins before samples were added. Then 100 μL of the unfiltered origami and 370 μL of buffer were added and spun at 5,000 g for 7 min. Samples was rinsed by centrifuging at 5000 g for 7 minutes for three times and each time topping up with buffer and repeating. The resident sample (origami without excess staple strands) was then collected into a fresh 0.5 mL tube after being spun at 13,000 g for 2 min.

2.2.5 Determining the concentration of DNA/ DNA origami

The concentration of annealed and/or filtered origami was determined by a spectrophotomer (NanoDropTM Lite Spectrophotometer, Thermo Scientific, USA). Beer-Lambert Law was used to estimate the DNA/DNA origami concentration by measuring the absorbance at OD 260 nm:

$$A_{260} = \varepsilon \, c_{DNA} \, l$$

where A_{260} is the absorbance at 260 nm, ε is the molar extinction coefficient (M^{-1} cm^{-1}), l is the length of the light patch (cm). Here a constant extinction coefficient (ε = 91886000 M^{-1} cm^{-1}) was obtained through calculating the base pairs in origami [116]. Each measurement was carried out on 2 μL of sample.

2.3 Gel electrophoresis

2.3.1 Introduction

Electrophoresis is a technique to separate molecules in a sample mixture under an applied electric field. The migration rate is determined by the molecules' shape, sizes, and charge. For linear dsDNA molecules, AGE typically separates based on mass [117]. The secondary structure of origami has a large effect on migration, with designs running fast/slower than the M13, despite the change in mass of the folded origami. When electrophoresis is performed in a gel, the size of samples becomes a factor. The gel is commonly made of agarose, polyacrylamide which contains intricate networks of pores where molecules can migrate through under applied electric field.

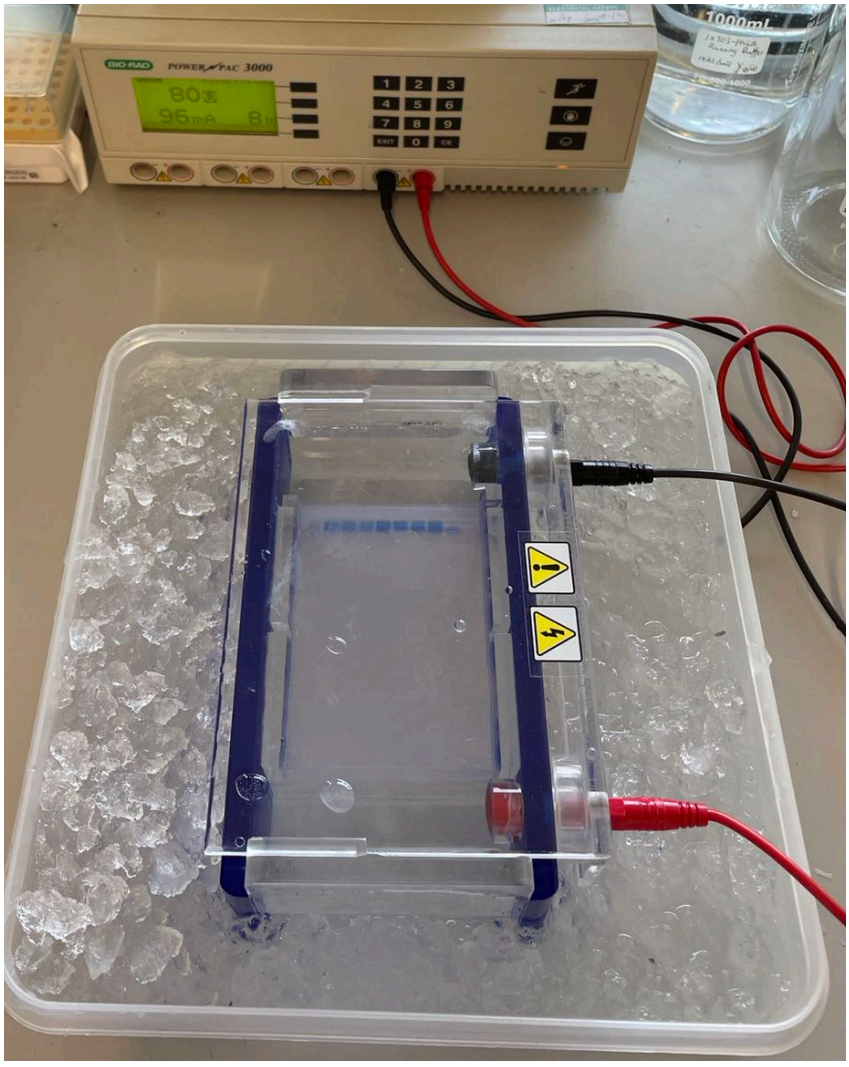

Figure 2-2 Pictures of a running gel in ice bath.

Gel electrophoresis is an effective tool for DNA origami, in terms of purification and characterisation. The process involves placing the folded DNA origami into wells of gel matrix and applying electric field along the matrix. DNA is negatively charged, so it runs from negative to positive terminal. AGE allows us to distinguish structures which migrate at a different rate when a voltage is applied, where the migrating distance depends on the size of DNA molecules. Large DNA structures such as origami tiles, always run slower than short staples strands. In general, the folded DNA origami is more compact than unfolded scaffold strands. It is suitable for the separation of DNA origami tiles from excess short staple strands and therefore effective for purification. Visualisation of DNA in gel is always achieved by using a syber safe gel stain containing DNA dye which revels distinct DNA bands. Gel electrophoresis is often used as an initial characterisation step to indicate successful folding before more complicated and detailed analysis like direct visualisation via AFM or TEM was carried out. It is possible to determine the yield of samples with different mobilities; and to observe the distribution of structures with fluorophore-labelled strands [118].

The standard agarose gel used in this thesis is a 1% gel consisting of 1% agarose in 1 x TAE Mg^{2+} buffer. It was made by adding 5 g of agarose powder (Invitrogen) into 50 mL 1 x TAE Mg^{2+} buffer. 5 µL of SYBR™ safe gel stain was added to pre-stain the gel. 4 µL of 6 x loading buffer was added in to 20 µL of sample. 4 µL of DirectLoad™ 1 kb ladder was used a reference. The gel was set to run 90 min in ice bath under a voltage of 80 V. Samples can be extracted from the gel with the use of Freezen' Squeeze DNA Gel Extraction Spin Column (Bio-Rad Laboratories Ltd.). Gel contains DNA samples were cut out and the chopped pieces were placed into the spin column. After staying in -20 °C for 5 min, sample were collected after being spun at 13000 g for 3 min at room temperature.

2.3.2 Quantifying the gel band with densitometry

Before mixing, origami monomers were annealed and purified through spin column, concentrations were measured using Nanodrop (Thermo Fisher Scientific). Samples were incubated with equivalent monomer-A and monomer-B (A and B are complementary tiles that can bind together) in 1x TAE Mg^{2+} buffer for over 12h. The outcome was determined using gel electrophoresis and AFM of hybridised origami tiles without further filtration. The quantification of products was estimated by ImageJ, through measuring the mean-grey value, which is defined by the number of pixels in selected area. Such that the brightness of bands in agarose gel provides an approximate prediction of dimer/monomer distribution. Figure 2-3 gives an example of how quantified data was obtained from gel images.

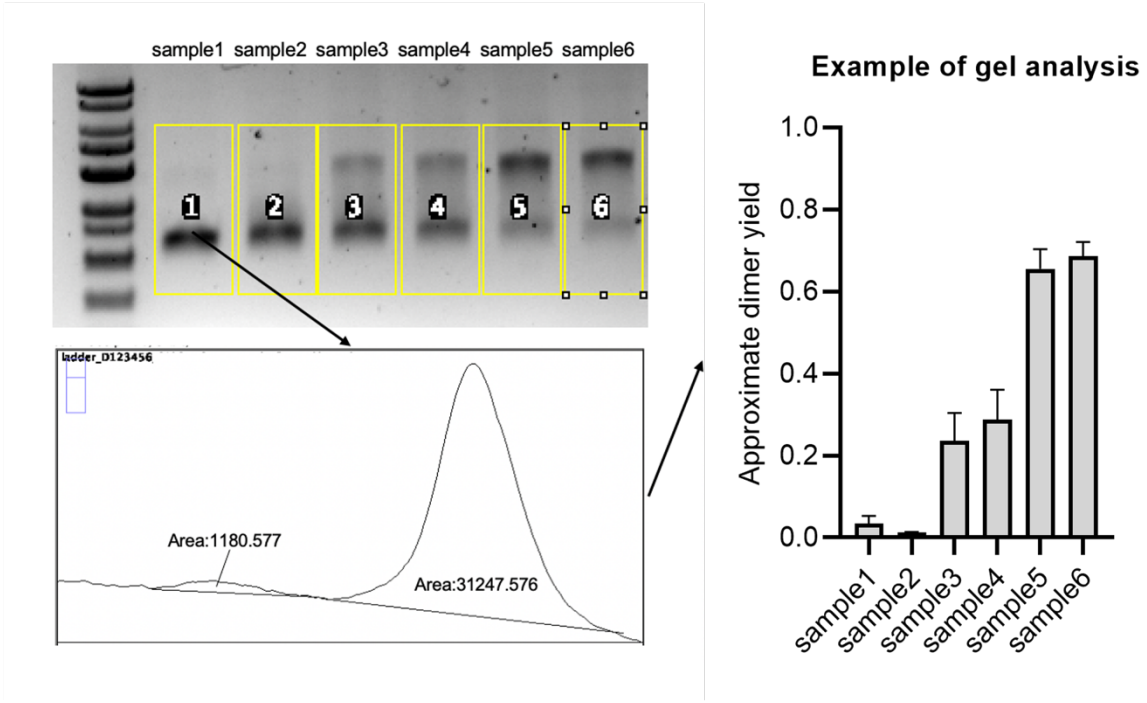

Figure 2-3 Gel analysis through ImageJ, quantifying the band with densitometry, providing an approximate value of the dimer yield. Molecular weight difference results in two distant bands in agarose gel of dimers and monomers.

2.4 Atomic Force Microscopy

2.4.1 Introduction

Atomic force microscopy (AFM) is a form of scanning probe microscopy (SPM) that utilises the tip-sample interactions to obtain data range of measurements, such as magnetic forces, adhesion strength, and mechanical properties, most notably however is the topographical feature - sample height [119]. The first SPM in world is a scanning tunnelling microscopy (STM) [120], which was invented by G. Binnig and H. Rohrer in 1982. It is the first instrument that can reflect information of sample surface in atomic level. Binnig and Rohrer won Nobel Prize in 1986. That same year they developed the first AFM [121], further expanding the toolbox available for the investigation of materials in nanoscale.

The basic working principle of SPM is to measure the change of a parameter, which is a sharp and single-valued dependence P=P(z) of tip-sample distance (Table 2-3), then the parameter can be used to control tip-sample distance in a feedback system. For example, STM relies on the tunnelling current between a conductive tip and sample which in fact is exponentially dependent on their separation. Therefore, this technique is typically limited to conductive/ semiconducting surface. One of the key reasons that led to the development of AFM - the desire to image non-conductive samples.

Table 2-3 Parameters measured under different working mode of SPM

P=P(z)	**Woking mode**
Tunnelling current i	Scanning tunnelling microscopy
Cantilever Amplitude A	Contact mode AFM
Cantilever deflection D	Tapping mode AFM
Tip-sample Peak Force F	Peak Force Tapping AFM

AFM was designed to provide topographical information based on the force between the tip and the sample surface. In the simplest mode of AFM, contact mode, the P(z) is the deflection of a flexible cantilever, which is measured when the sharp tip (which is attached on the end of the cantilever) contacts with the sample's surface. The bending of the cantilever caused by the contact force is monitored by a feedback system. A basic AFM setup (Figure 2-4) includes the cantilever, a laser beam, a position sensitive photodiode and a piezo actuator. A laser beam is focused and reflected from the topside of the cantilever [122] to a position sensitive four-sectional photodiode, which can amplify the sub-nanometre deflections of the cantilever and covert this signal into electrical signal. The tubular piezo actuator controls the movement of the tip to keep the bending of cantilever constant based on the feedback system. Thus, when the probe scans along the sample, the (x, y) position information and Z position details can be calculated from piezo movement and combined to generate the topographic image of the sample.

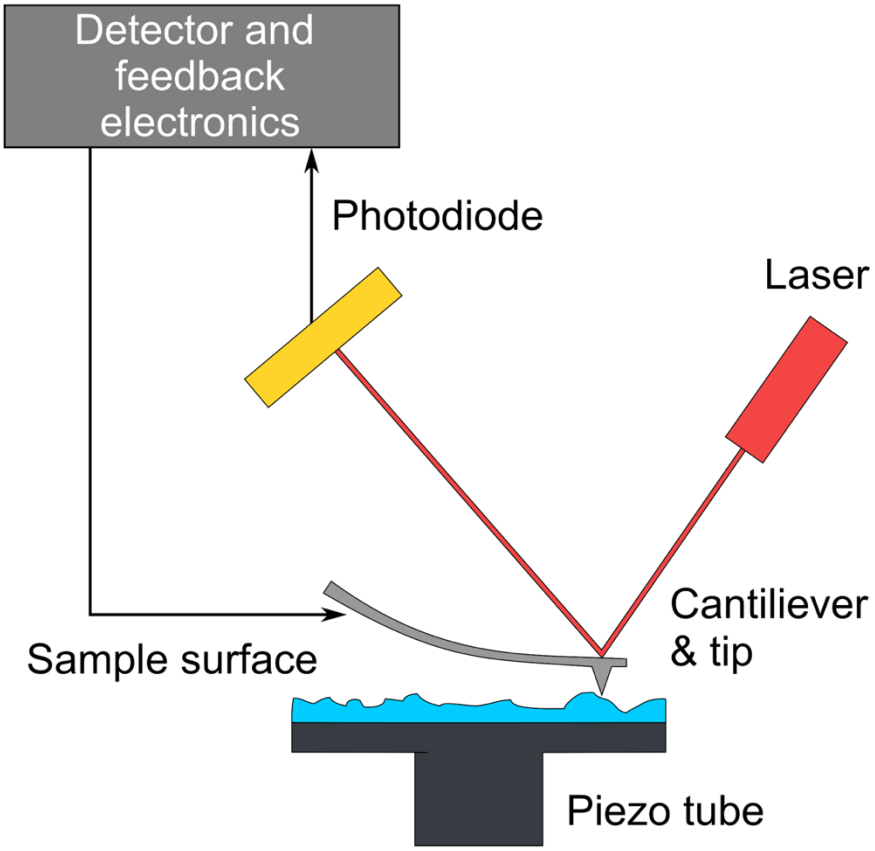

Figure 2-4 Working principles of AFM. Images obtained. Image obtained from OverlordQ and has been re-adjusted.

When the probe moves across the samples, the force between them can be modelled by Hooke's law.

$$F = -kz$$

Where F is the force, k is the spring constant, and z is the cantilever deflection. The force between the tip and the sample is mainly the Van Der Waals attractive forces and the repulsive short range coulomb interactions [123]. The force and tip-sample distance can be approximated by the Lennard-Jones potential as shown in Figure 2-5.

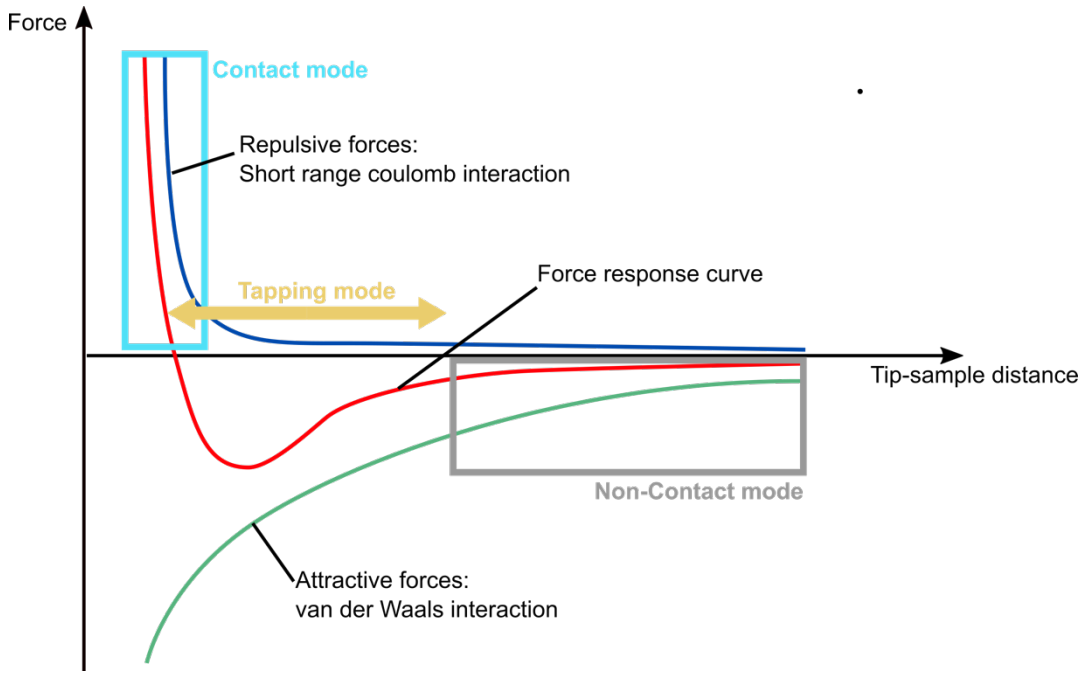

Figure 2-5 Force and distance curve based on the Lennard-Jones potential.

The tip experiences an attractive force as it approaches the surface, when tip moves closer, the force changes to repulsive thus bending the cantilever and lead the tip in contact with sample. In contact mode, the AFM maintains a constant cantilever deflection and operates in the repulsive regime. In tapping mode, the tip moves into and out of contact with sample surface, as it intends to maintain a constant oscillation amplitude. The non-contact (NC) mode operates in the attractive regime at a larger tip-sample distance.

2.4.2 Imaging DNA origami with AFM

Direct visualization of DNA origami is the most conclusive method to ascertain their structures, however they cannot be imaged by optical microscopy as they are smaller than the wavelength of visible light. Individual DNA origami tiles range from 10 to 100 nm. As AFM relies on a physical interaction between the sample and the probe, there is no requirement for samples to be conductive (as like for STM, or TEM). AFM allows for imaging in ambient/liquid conditions, such that the B-form of DNA is maintained. AFM is the standard imaging technique used for 2D DNA origami structures, while TEM is often used for imaging 3D DNA constructs. Figure 2-6 shows the Bruker's Dimension Icon AFM in cleanroom, which imaged all origami samples mentioned in this thesis.

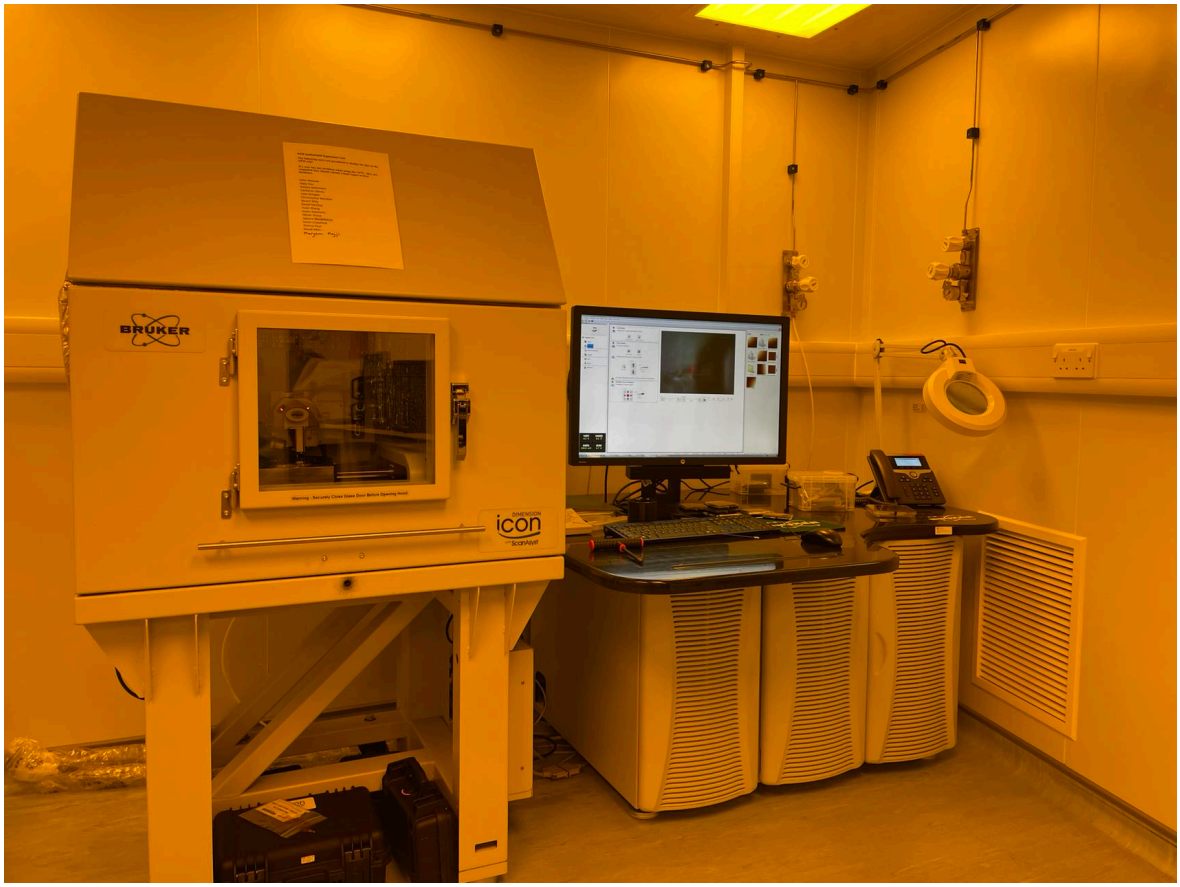

Figure 2-6 Bruker's Dimension Icon AFM system in cleanroom.

As AFM is a surface-based technique, a substrate is required to mount the sample on. In the case of DNA origami, the most common choice is mica. There are two advantages to use mica. First, it is an atomically flat surface so the difference between DNA sample and mica surface is easy to distinguish. Second, freshly cleaved mica layer and DNA are both negatively charged. Mica contains K^+ which can be displaced by the Mg^{2+} in origami solution. Thus, the Mg^{2+} can form an ion charged bridge between DNA and mica, help to immobilise DNA on mica surface. Magnetism ions are often excess in DNA origami solution as to neutralise sugar-phosphate backbone. Although mica is ideal for imaging DNA origami in both air and liquid conditions. In this thesis the imaging of DNA origami was operated in air condition. As shown in Figure 2-7, samples that was incomplete dried often presents irregular shapes and undesired features. Therefore, it was necessary to ensure that the surface was dried completely.

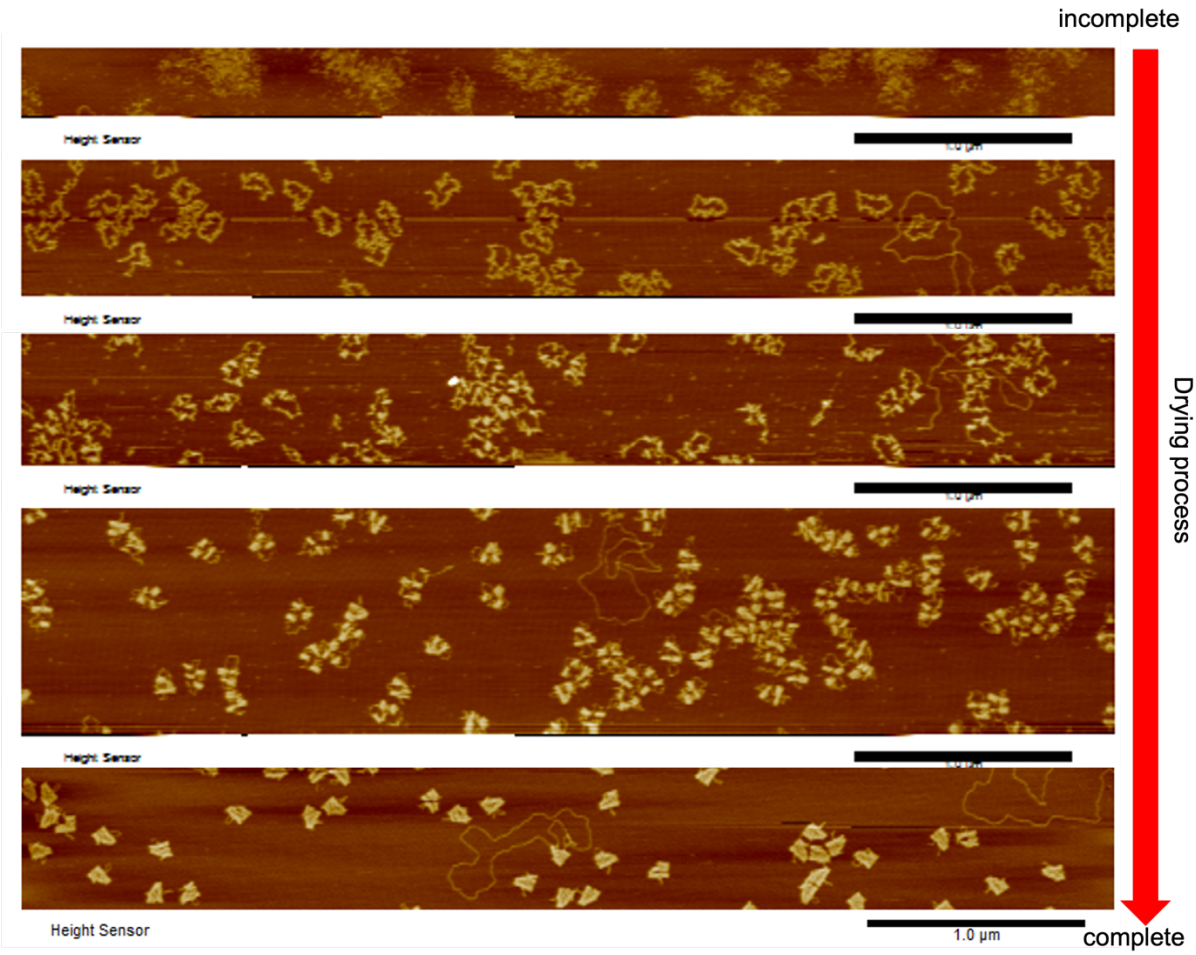

Figure 2-7 Comparison of the AFM images of incomplete and complete drying process. Samples were from the same batch.

2.4.3 Sample preparation

The DNA origami solution was diluted to 1 nM with 1 x TAE.Mg^{2+} buffer for a good separation on a surface. Mica is the most used substrate for DNA origami. 10 µL of each DNA origami solutions was deposited onto freshly cleaved mica and left on the substrate for absorption for 3 min. Then the substrate was rinsed by DI water to remove non-absorbed DNA structures and reduce the formation of salt crystal before being dried under a flux of N_2.

AFM images were taken in Tapping Mode in air on a Dimension Icon ScanAsyst (Bruker, USA). A FESPA-V2 probes with a cantilever radius of 8 nm was used for imaging.

2.5.3 Sample analysis

Images were analysed using Nanoscope Analysis 1.9 software and Gwyddion scanning probe microscopy analysis software. The quantification of the dimer rate was achieved by counting the number of tiles in AFM images using Fiji ImageJ with the counting plugins.

Chapter 3 Preliminary Experiments

3.1 Introduction

To break the current limitation on assembling micron-scale DNA constructs, there is a desire for a novel attachment strategy – the "fluorous effect", to substitute/ complement the traditional DNA-based attachment method (sticky-end hybridisation). This will be the first attempt to incorporate the fluorous effect on DNA origami as a connection strategy, therefore it is necessary to understand impact factors to the dimerization reaction before starting the fluorous study.

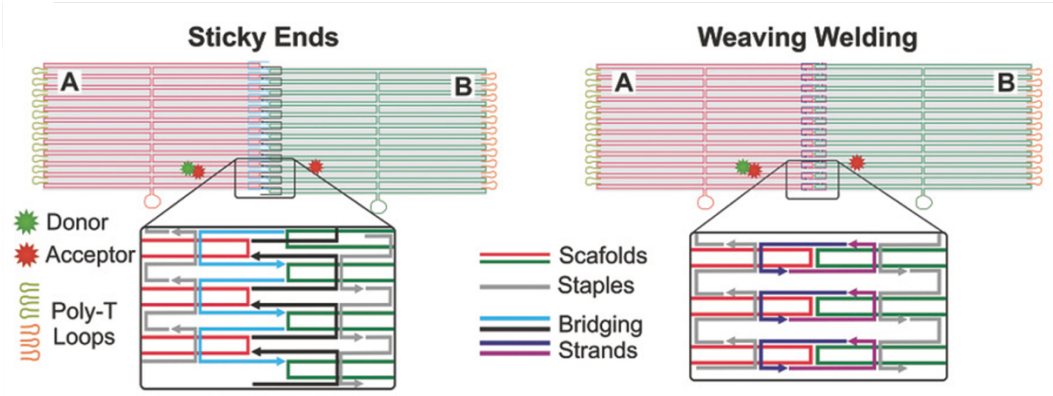

Figure 3-1 Two strategies for the attachment of origami tiles: sticky-ends and weaving welding. Images exported from[83].

Ongoing studies have explored two different attachment techniques: "sticky-ends" and "weaving welding" [77], [80], [81], [124]. Bridging strands are often those staple strands on the interfacial domain that have been extended with unpaired sequences. As presented in Figure 3-1, bridging strands in the sticky-ends technique would hybridize to the scaffold during the folding process, leaving two overhangs protruding towards one side. Origami tile-A binds to origami tile-B through sticky-ends with a certain length of sequences that are complementary to each other. In the weaving welding technique, the dimerization reaction happens between the overhangs on bridging strands of one tile and the scaffold segments of another. The weave-welding on the other hand can be likened to a continuous origami since the binding of staples replicates what you see in the seam (where the direction of the scaffold reverses halfway). Both techniques allow us to modify the bridging strands of both tiles whilst the weaving welding technique might introduce interference between the fluorous tag and un-paired ssDNA if we consider incorporating fluorous tags onto the origami interface.

For the sticky-ends strategy, the number of overhangs, the length of the sticky-ends is often considered as the major impact factors to dimerization yield. However, when it comes to hierarchical assembly**,** maximum occupancy of bridging strands was often chosen since it is considered to guarantee optimal efficiency which however is not true for two reasons: firstly, the binding kinetics would cause dimer dissociation [83], losses which accumulate with the assembly process, leading to a small yield of final products [82]; secondly, the dimer yield increases and remains the same when reaching a certain number of overhangs [125]. Therefore, a proper interfacial design is necessary for efficient dimerization assembly.

3.1.1 Context and aim of this results chapter

Fluorous effect has never been utilised as a linker to connect origami tiles. Before introducing a novel bridging regime to sticky-ends hybridisation system, it is important to understand the dimerization mechanism of DNA origami. Therefore, this chapter is set to explore the affecting factors to the origami dimerization. Work presented in this chapter hopes to:

1) Determine the effect of changing length and the number of the sticky-ends on dimerization yield.

2) Determine the effect of changing the position of the overhangs on dimerization yield.

3) Explore the dimerization mechanism of wireframe square and square-based rectangle, determine which is a better platform for fluorous study.

3.2 Results and Discussions

Although current dimer studies were mainly focused on the square-based origami tiles, e.g., rectangular origami, this study was first carried out on a wireframe origami design since there are three advantages: 1) wireframe designs have a larger surface area compared to square-based designs using the same scaffold template - the wireframe square is about 112 x 112 nm whilst a rectangular design is about 90 x 70 nm; 2) the cavities inside the structures allow the arrangement of functional materials inside the structure, benefits the transaction from origami to solid surfaces, e.g., fabricating the array of nanoparticles on to silicon pattern through the cavities rather than having origami structures underneath the information; 3) the wireframe can be expanded from both x and y directions through easily sticky-ends strategy as the edge staples extending away vertically from the structures inherently.

3.2.1 Interfacial design

A wireframe square design was used as a monomeric motif in this chapter [49]. This wireframe square (with 5 x 5 cavities) is 112 x 112 nm (as measured by AFM), with six protruding arms on each side. Each arm contains two overhangs allowing to be extended in 5’ and 3’ directions, which leaves a maximum of twelve overhangs on one side. The twelve strands can be divided into 6 groups and each group contains two overhangs. The calculated distance between two arms is about 17.68 nm based on the length of a 52 bp B-DNA helical structure. As presented in in Table 3-1&Table 3-2, the homogeneous interfacial domain was designed to make two complementary monomeric motifs share the same sequences of the scaffold. This way to reuse the monomeric origami motif and use the unique sticky ends to direct the interactions.

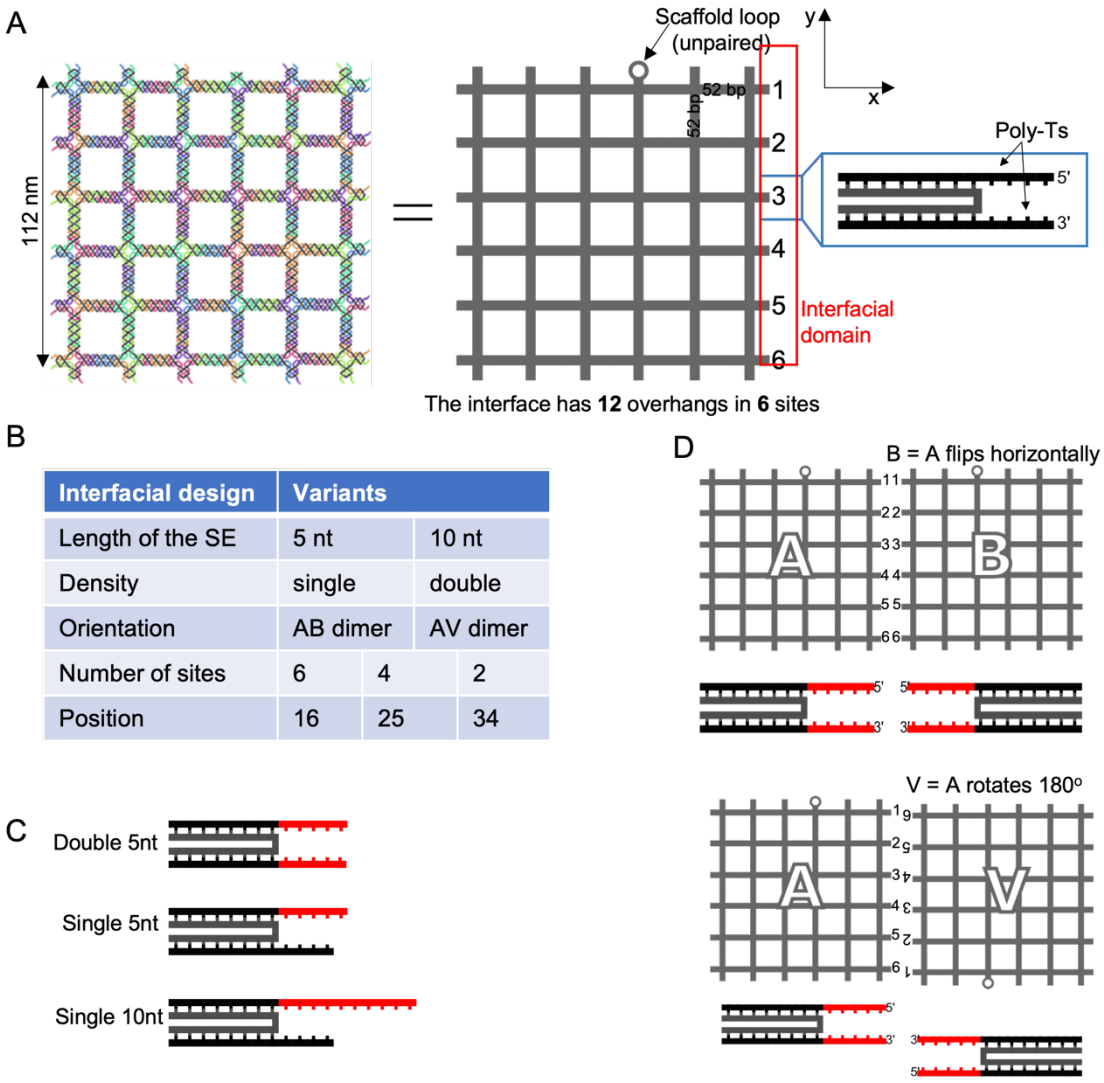

Interfacial design	Variants		
Length of the SE	5 nt	10 nt	
Density	single	double	
Orientation	AB dimer	AV dimer	
Number of sites	6	4	2
Position	16	25	34

Figure 3-2 A) Schematics of wireframe square design, a top view from Tiamat (left) and a simplified version(right). The scaffold loop was left unpaired in one vertex. Four Ts are added into the ends to prevent non-specific blunt-end stacking. The wireframe square origami in a scale of 112 x 112 nm. B) An overview of the interfacial design, variants include the length of the SE, double or single overhangs, the number of sites, position variants and the monomer orientation. C) Bridging strategies used throughout this chapter, strands were modified with sticky-ends on 5' or 3' end of the overhang. For single SEs, the other one is with poly-Ts. D) Two orientations of the monomer for dimerization: AB dimer and AV dimer.

To systematically access how the interfacial structure determines the assembly efficiency, we altered five variables: the length, number, density, position of the SEs, and the orientation of monomers (Figure 3-2). The length of the SE overhangs used in this work were 5 and 10 nt. For 5-nt SEs, they were arranged in single/double extensions; 10-nt SEs were arranged in single extensions only. SEs were placed in 6, 4, 2 sites in the interfacial domain, and for the 2-site set-up, SEs were altered from centre to the side with the position number being: 34, 25, 16.As shown in

Figure 3-2D, monomer-B is flipped horizontally from monomer-A, and monomer-V is rotated 180° in-plane relative to monomer-A in the dimer. The interface for binding contains

bridging edge strands to connect two motifs through Watson-Crick base pairing and blocker edge stands (4-polyTs) to prevent nonspecific interactions such as blunt-end stacking. Monomer-A and monomer-B/V were each prepared with bridging and non-bridging strands incorporated into the interface.

3.2.2 5-nt SEs

Table 3-1 Sequences of the bridging strands for double 5nt design, with the extended sticky-ends highlighted.

position of the staple	number of the staple	TileA-double5nt
site1	201A-5nt	**TCAAC**TTTTGATAAGAGGTCATTTTTTTTTGCGGATGGCTTTTT
	202A-5nt	ACCGAGATTAGAGAGTTTTTACCTTTAATTGCTCC**AACTT**
site2	203A-5nt	**AAGGA**GCGTTTTAATTCGAGCTTTTTTCAAAGCGAAACTG
	204A-5nt	GCCCGATTTTAAGACTTCAAATATC**GTCAT**
site3	205A-5nt	**GATAA**GTCTTTACCCTGACTATTTTTTATAGTCAGAAGTT
	206A-5nt	TGACCATTTTTAAATCAAAAATCAG**GGTGA**
site4	207A-5nt	**TTCGT**GAATCGTCATAAATATTTTTTCATTGAATCTAGCA
	208A-5nt	TGGATATTTTGCGTCCAATACTGCG**AGACT**
site5	209A-5nt	**ATCGC**AATAGCGAGAGGCTTTTTTTTGCAAAAGAAACGAT
	210A-5nt	CCAGACTTTTGACGATAAAAACCAA**TACAG**
site6	211A-5nt	**CTGTC**TACATAACGCCAAAAGTTTTGAATTACGAGTTGGG
	212A-5nt	TTTTATTTAGGAATACCACATTTTTTCAACTAATGCAGA**ATAAT**
position of the staple	**number of the staple**	**TileB-double5nt**
site1	201B-5nt	**GTTGA**TTTTGATAAGAGGTCATTTTTTTTTGCGGATGGCTTTTT
	202B-5nt	ACCGAGATTAGAGAGTTTTTACCTTTAATTGCTCC**AAGTT**
site2	203B-5nt	**TCCTT**GCGTTTTAATTCGAGCTTTTTTCAAAGCGAAACTG
	204B-5nt	GCCCGATTTTAAGACTTCAAATATC**ATGAC**
site3	205B-5nt	**TTATC**GTCTTTACCCTGACTATTTTTTATAGTCAGAAGTT
	206B-5nt	TGACCATTTTTAAATCAAAAATCAG**TCACC**
site4	207B-5nt	**ACGAA**GAATCGTCATAAATATTTTTTCATTGAATCTAGCA
	208B-5nt	TGGATATTTTGCGTCCAATACTGCG**AGTCT**
site5	209B-5nt	**GCGAT**AATAGCGAGAGGCTTTTTTTTGCAAAAGAAACGAT
	210B-5nt	CCAGACTTTTGACGATAAAAACCAA**CTGTA**
site6	211B-5nt	**GACAG**TACATAACGCCAAAAGTTTTGAATTACGAGTTGGG
	212B-5nt	TTTTATTTAGGAATACCACATTTTTTCAACTAATGCAGA**ATTAT**

Double 5-nt SEs were employed in 6, 4, 2 sites of the origami, the AFM results in Figure 3-3 showed that monomers with the full set of bridging strands form more dimers (90.2% for 12 bridging strands in 6 sites). With decreased number of bridging strands, the dimer

yields are significantly lower (75.6% for 8 bridging strands in 4 sites, 23.5% for 4 bridging strands in 2 sites). A positive correlation is in existence between the yield and the number of bridging strands but is not simply linear, indicating that each SEs overhang works non-independently therefore there is an accumulation effect. It's noteworthy that clumps that appeared in AFM images were neglected when counting dimer yields. The clumps were reasoned as 1) higher-ordered structures lead by nonspecific binding and crosstalk between tile and tile, staples and scaffold, staples and staples; 2) sample preparation issue as it was observed that the drying process during the sample preparation would affect the characterisation of origami structures (as presented in 2.4.2). Moreover, the gel gives few higher-ordered assemblies, suggesting that electrophoresis may accelerate the tile dissociation. In addition, analysis based on agarose gel images gives approximate measurement which agrees to the tendency of AFM results, however, the overall dimer yield is 14.7 %.

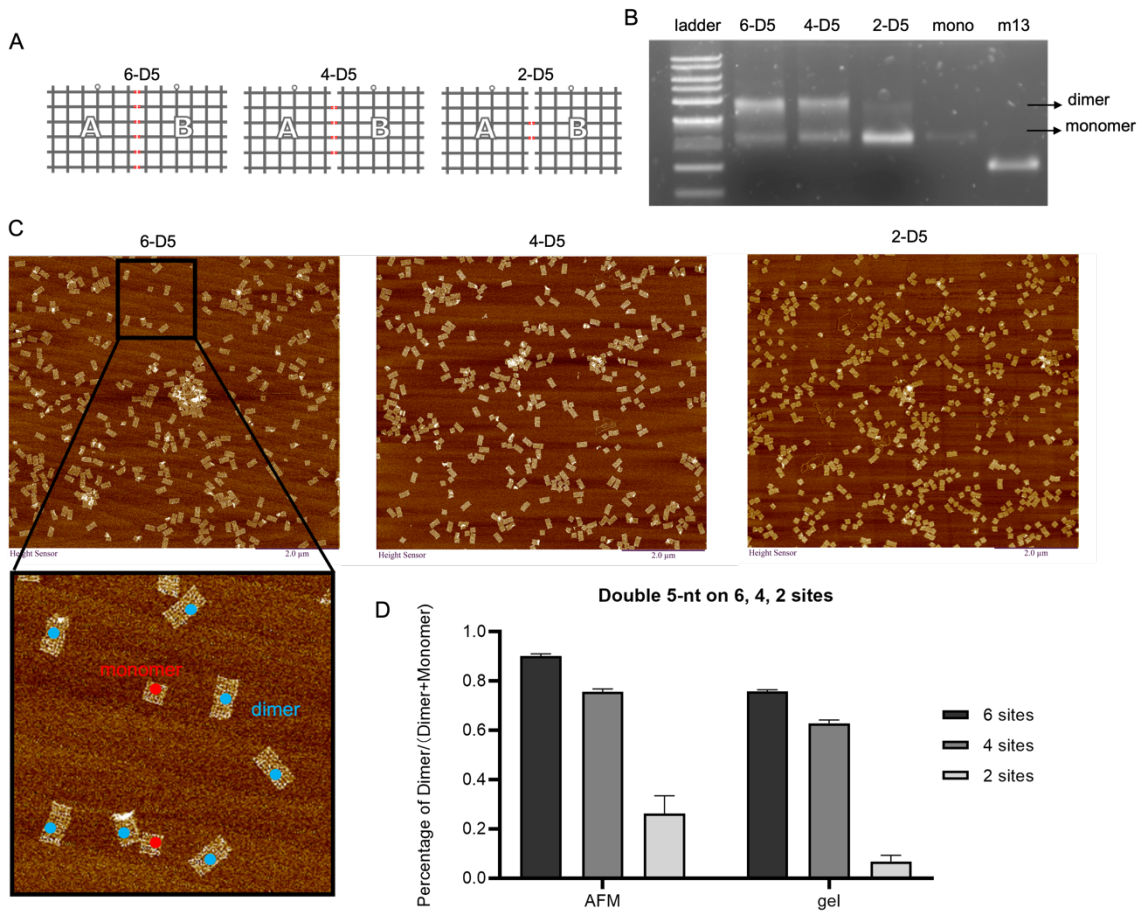

Figure 3-3 Measurements of dimer yield. A) Schematics of dimer employs monomers with double 5-nt SEs in 6, 4, 2 sites, containing 12, 8, 4 SE overhangs separately. B) Agarose gel electrophoresis images, samples are ladder, double 5-nt 6 sites, 4 sites, 2 sites, monomer and m13mp18 scaffold (from left to right); C) AFM images of 6-D5, 4-D5, 2-D5, and illustration of how dimer fraction was measured; D) diagrams of double 5-nt analysis comparing AFM and gel results.

Single extension of 5-nt sticky-ends was then studied on the wireframe origami, where on position of the SE overhangs was presented in Figure 3-2, showing the monomer-V was rotated 180° from monomer A. The adjacent strand was shortened from four Ts to one T to avoid poly-T interfering with SEs from hybridising to its complement. Compared to 2-D5 (23.6% in AFM, 7.5% in gel), although monomer with single 5-nt in 6 sites employs more bridging overhangs (6-S5), it doesn't yield any dimer (Figure 3-4). It seems that two SEs in proximity work highly cooperatively, thus the hybridization of one of the SEs with its complement benefits the binding of neighbouring SE with its complement by bringing them closer, and one can hold the tiles together when dissociation occurs to another. SEs in distance, has a spacing of 52 bp, equals to 17.68 nm, work independently as they are too far to align the interface for one and the other. The structural limitation of this wireframe design restricts further exploration to SEs spacing, as the distance between each protruding point is fixed.

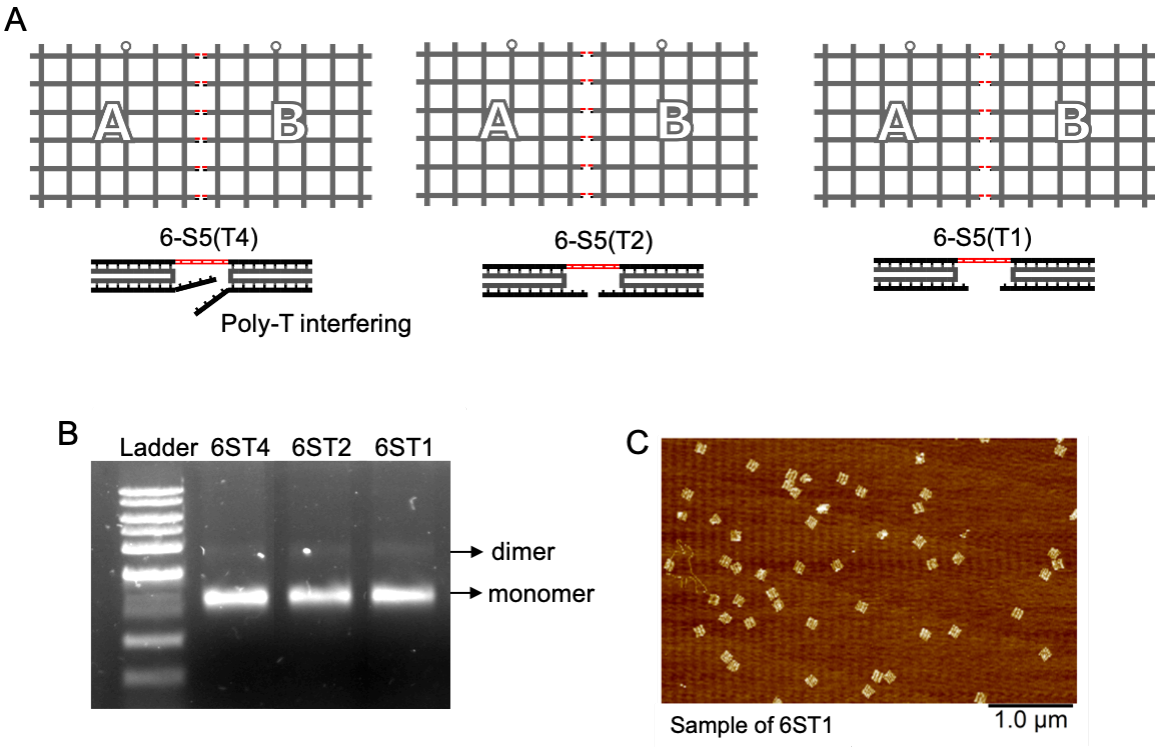

Figure 3-4 Schematics and measurement of dimer yield employing single 5-nt SEs overhangs. A) schematics of monomers with 6 single 5-nt SE overhangs, the adjacent poly-T strands in each site varying in 1,2,4 of thymine, to ensure if potential poly-T interfering hinder dimer formation. B) Agarose gel images of three samples, all suggest no dimer formation. D) AFM images of 6ST1, all monomers.

3.2.3 10-nt SE

To obtain a more quantitative comparison of single and double SE binding, also to overcome the structural limitation of the wireframe design, dimerization using single 10-nt SE was studied. Here, each vertex on the interface displays a single 10-nt SE, with equivalent base pairs of double 5-nt. The sequences of the single and double SEs have equal GC content to ensure that any difference is solely from the arrangement of SE overhangs. The image of agarose gel electrophoresis is shown in Figure 3-5. Monomers with single 10-nt SEs showed distinctly higher yield than those with double 5nt-SEs in one to all sites, indicating that the yield of origami dimerization can be enhanced efficiently by combing two 5-nt SEs to a single 10-nt SE. The previous study for small tiles has shown, however, the association between two DX tiles via double 5-nt SEs is beneficial compared to single 10-nt [126]. In the ideal case, the interface can be considered as 6 of DX tile connected by the scaffold.

Table 3-2 Sequences of the bridging strands for single 10nt design, with the extended sticky-ends highlighted.

Position of the staple	Number of the staple	TileA-single10nt
site1	202-10BP-A	ACCGAGATTAGAGAGTTTTTACCTTTAATTGCTCC**TAACGACACC**
site2	204-10BP-A	GCCCGATTTTAAGACTTCAAATATC**TCCTCCGTAA**
site3	206-10BP-A	TGACCATTTTTAAATCAAAAATCAG**TGGTGGTTCT**
site4	208-10BP-A	TGGATATTTTGCGTCCAATACTGCG**ATGCCAAACC**
site5	210-10BP-A	CCAGACTTTTGACGATAAAAACCAA**TCTGCTCACA**
site6	212-10BP-A	TTTTATTTAGGAATACCACATTTTTTCAACTAATGCAGA**ATGAGGGCAA**
Position of the staple	**Number of the staple**	**TileV-single10nt**
site1	202-10BP-B	ACCGAGATTAGAGAGTTTTTACCTTTAATTGCTCC**GGTGTCGTTA**
site2	204-10BP-B	GCCCGATTTTAAGACTTCAAATATCT**TACGGAGGA**
site3	206-10BP-B	TGACCATTTTTAAATCAAAAATCAG**AGAACCACCA**
site4	208-10BP-B	TGGATATTTTGCGTCCAATACTGCG**GGTTTGGCAT**
site5	210-10BP-B	CCAGACTTTTGACGATAAAAACCAA**TGTGAGCAGA**
site6	212-10BP-B	TTTTATTTAGGAATACCACATTTTTTCAACTAATGCAGA**TTGCCCTCAT**

The yield tendency based on double 5-nt is a gradual increasing with an increasing number of overhangs, for single 10-nt, on the other hand, there is a yield jump from S2 to S3, then it reaches the equilibrium afterwards. Compared to single 5-nt, the strength of single 10-nt is significantly higher to direct the dimer reaction, without the support from adjacent SE. 10-nt SE has a higher melting temperature, therefore it's less likely to fully dissociate once associate with its complement. It seems that the strength of a single bridging strand is more

dominant compared to the double bridging with equivalent bases when it comes to large constructs like DNA origami.

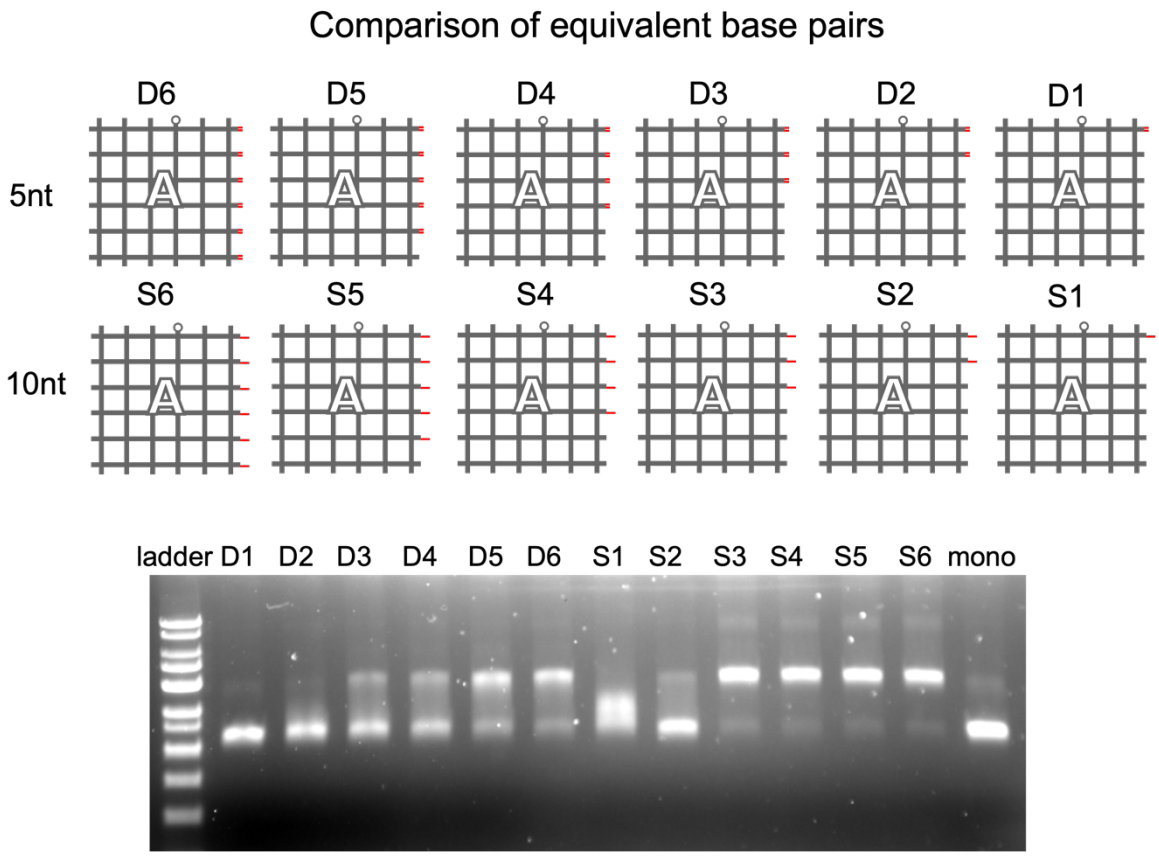

Figure 3-5 Gel comparison of how single and double SEs using equivalent bases works in dimerization of DNA origami, with from 1 to 6 sites on the interfaces occupied subsequently. Schematics showing only monomer-A.

3.2.4 Position variations and monomer orientations

As mentioned before, Han et.al observed the inherent bias with their wireframe designs (a waving gird and a flower-and-bird design [49]), suggesting there are curvature and twist in existence. In order to investigate whether the solution shape affects the dimerization process; we firstly designed a protruding tag composed of three oligonucleotides was used to extend the unused scaffold as labelled in Figure 3-6, such that allows the distinguishment of the orientation of face1 and face2 depositing onto mica surfaces.

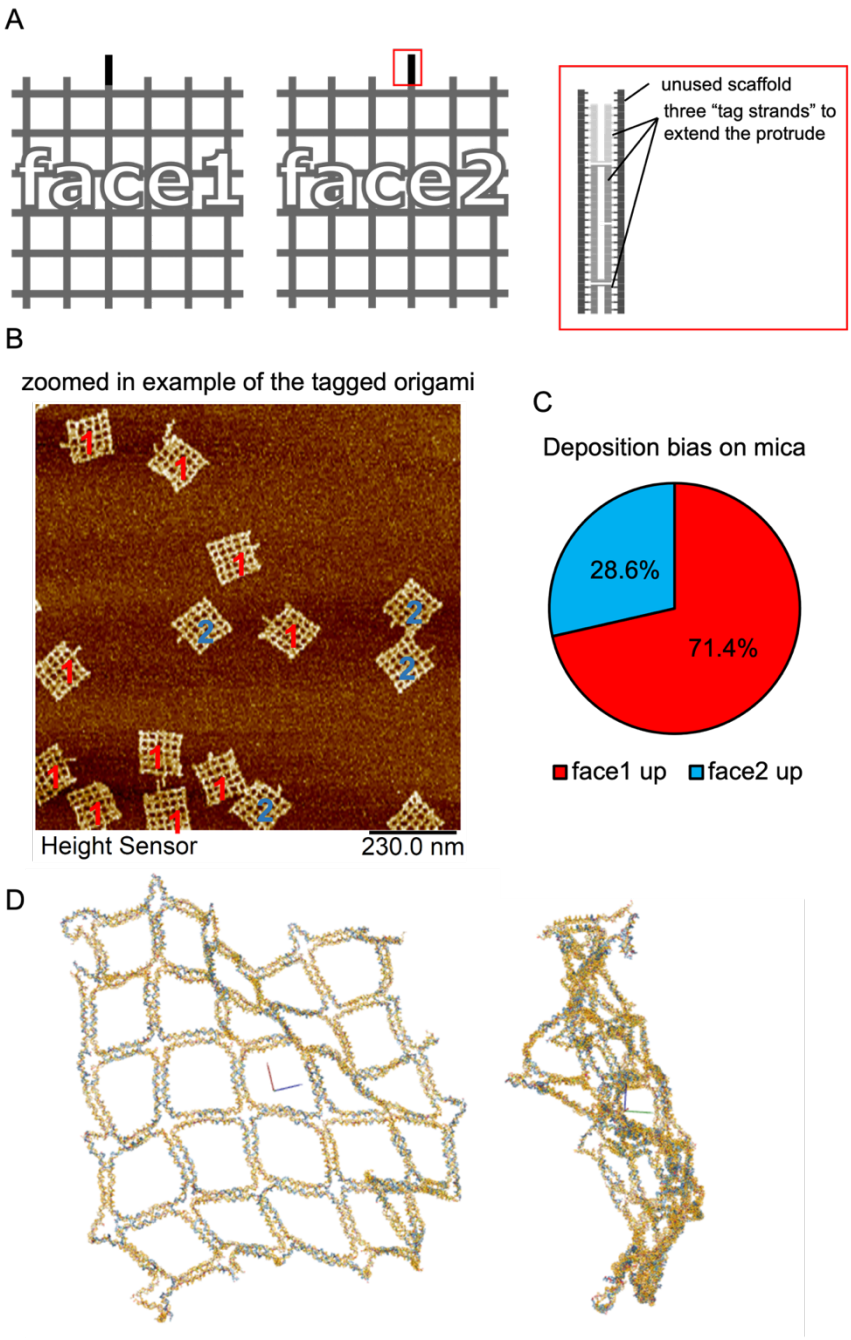

Figure 3-6 Deposition bias of the origami tiles on mica surfaces. A) Schematics illustrated the tag on wireframe square. B) a zoomed in example of the tagged origami showing the two orientations: face1 and face2 up. C) the deposition bias of origami onto mica surface. Total number of analysed nanostructures = 203. D) The modelling of wireframe square.

As the oxDNA modelling showing that the wireframe origami is not flat, meaning the edge where origamis contact has a curvature. Here AV dimer was arranged as a way that the interface aligns optimally to reduce the physical mismatch along the edges of the origami tiles (to maximize the chance of interacting), where AB dimer is assembled to have alternative faces of the monomeric tiles. Additionally, one downside of AV dimers is that they can have only single overhangs aligned, while AB dimer allows the double sticky-ends. Only single 10-nt bridging was equipped with AV dimers. Based on the modelling and the

deposition bias face1: face2 = 71.4%: 28.6%, it is believed that the wireframe square origami is in a relatively flexible bowl shape due to the constraint across the structures (Figure 3-6D). This modelling was predicted through oxDNA coarse-grained model[69], [127]–[129], which treats DNA as a string of rigid nucleotides with many potential interactions including sugar-phosphate backbone connectivity, hydrogen bonding, cross-stacking, etc.

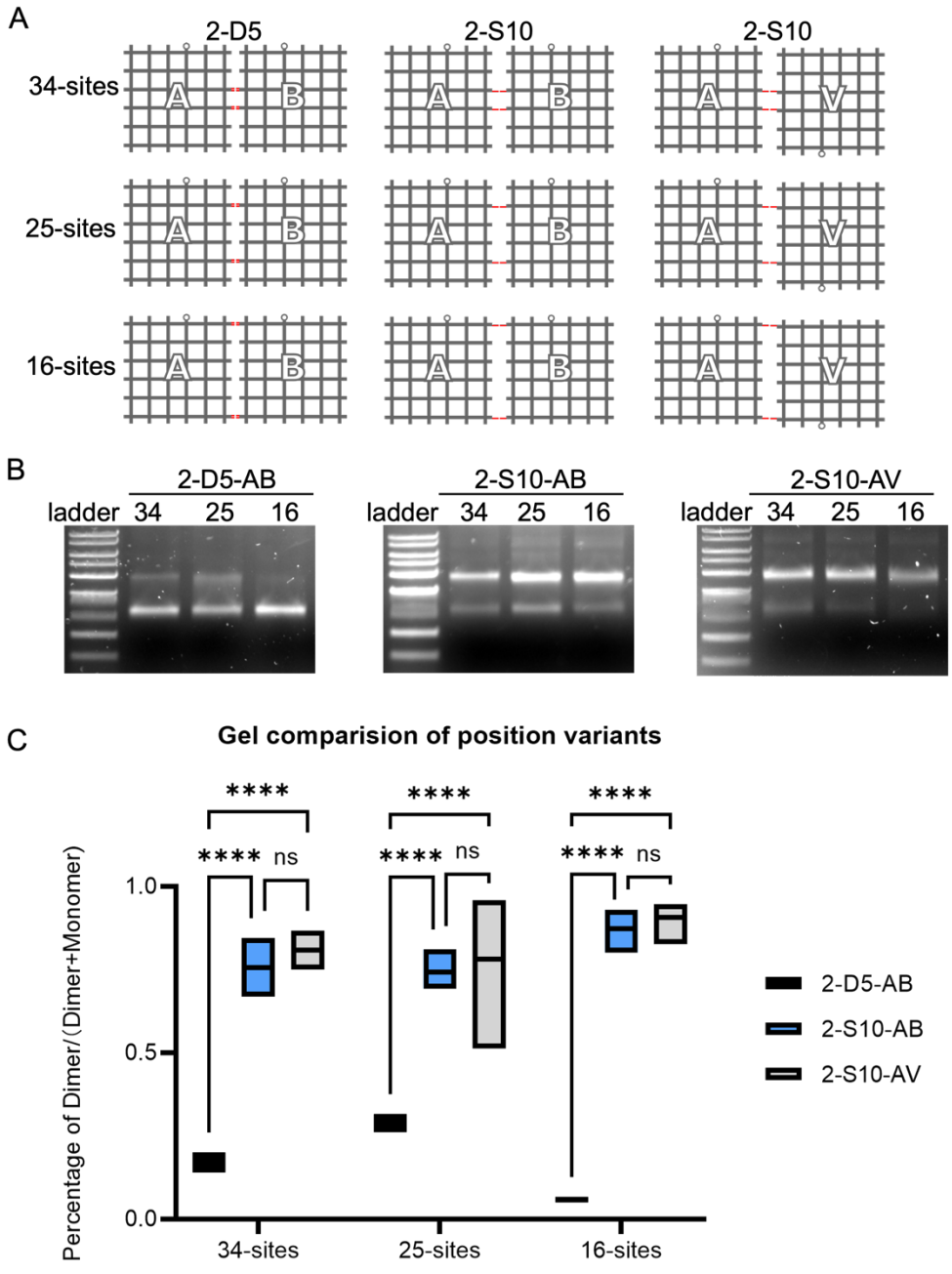

Figure 3-7 Position variants with monomers employing 2 sites. A) schematics of A-B, A-V dimer joined by double 5-nt, single 10-nt in three positions: site34, 25, 16. B) &C) Gel images and analysis of above samples. One-way ANOVA was used for the statistical analysis of the data, ns p>0.1 (from left to right, ns p= 0.7834, 0.8675, 0.9013), ****p<0.0001.

To explore how the mismatch of the interface affects the dimer formation, it's studied from not just the monomer orientations but also the position variations, using only 2 sites to arrange SEs. Based on the gel data in Figure 3-7B, the relative brightness was visualised into dimer proportions. It is showing that monomer A&B with 2 of single 10-nt SEs can result from a major dimerization (above 80%) while tile with 2 of double 5-nt SEs largely remains monomeric (about 20%) in three-position variations. Among that, 2,5-5-nt SEs have the highest dimer yield (~25%), followed by 3,4-5-nt SEs (20%), 1,6-5-nt SEs are the least dimerized (5%), it is considered that the connection on site1/6 is mostly likely to have monomer-A and monomer-B flips while it's yet strong enough to hold the distinct structures and make it flip over before breaking up.

When using single 10nt base pairing as the bridge, the effect from monomer orientations is less impacting, and the yields are quite similar, modelling outcome proves that the solution structure of the wireframe square is rather flexible and loose, therefore the interface misalignment can be neglected as factors affecting dimer formation (Figure 3-7C). It is noteworthy that monomers with 2-S10 obtain the yield at ~80%, similar to dimer yield driven by 6-D5. Longer and fewer bridging strands are preferable to achieve efficient assembly as well as simplify the sequence and cost.

3.2.5 Linker study

The effects of the flexibility of SEs were also tested by introducing poly-T linkers between the origami structures and the complementary region of the overhangs. To have the assembly protocol that would stay close to equilibrium, two monomers were mixed at equal concentrations and incubated at 25 °C for 12h and 36h. Both indicated that binding between SEs with linkers from T0 to T5 produced a decreased dimer yield (Figure 3-8). The interfaces with 5nt extended linkers produce the smallest yield, which is likely because 1) the interactions between these sticky ends are not strong enough to maintain a bond between origami motifs; 2) linkers may interfere with adjacent SEs preventing the hybridisation to its complement on another distinct motif; 3) the distance between every two SEs breaks the overall cooperativity of SEs like how they behave on helical packed rectangle design.

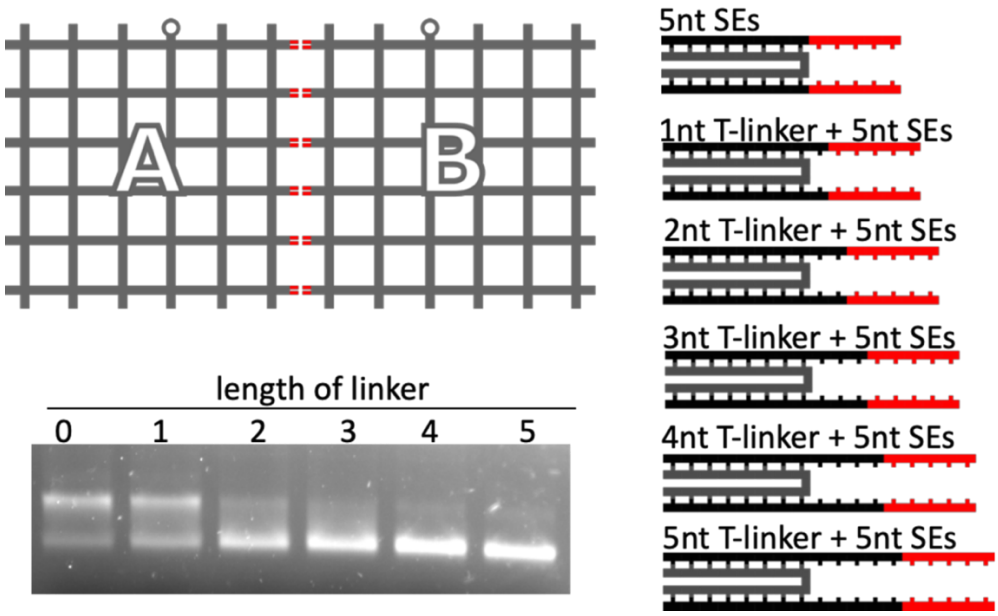

Figure 3-8 Schematics of linker study conducted with 6-D5 with a linker length from 0 to 5.

3.2.6 Dimerization on square-based rectangular origami

The inherent spacing between vertices in the wireframe design somehow overlays the design on the interfacial domain. It is not an ideal platform if to explore a novel connection strategy like the fluorous effect, which itself exists many uncertainties. Although longer SE gives higher yields, but it also breaks the "uniformity" of the dimer/higher-order structure. Whilst for the square-based rectangle, where the helical bundles are lightly packed together, therefore all overhangs are adjacent to one and other, largely reduces the structural impacts.

3.2.6.1 Designing the asymmetric rectangular origami

Adjusting the aspect ratio of a rectangle origami can allow for a wider range of adjustment at the interface [125]. Rather than solely adjusting the aspect ratio in the new design, the symmetry was broken such that the two sides where protruding overhangs extend contain 14 (the long side) and 7 (the short side) helices respectively as shown in Figure 3-9. The asymmetric rectangle was modified from an existing rectangle design [114] (contains 12 helices, with a dimension of 60 x 90 nm). It was measured 70 x 90 nm with AFM and has 14 U-shaped staple strands along the longest edge. Each of these edge staples contains two overhangs (5' and 3') which can be modified or extended such that the modifications protrude from the main body of the origami. (Figure 3-9)

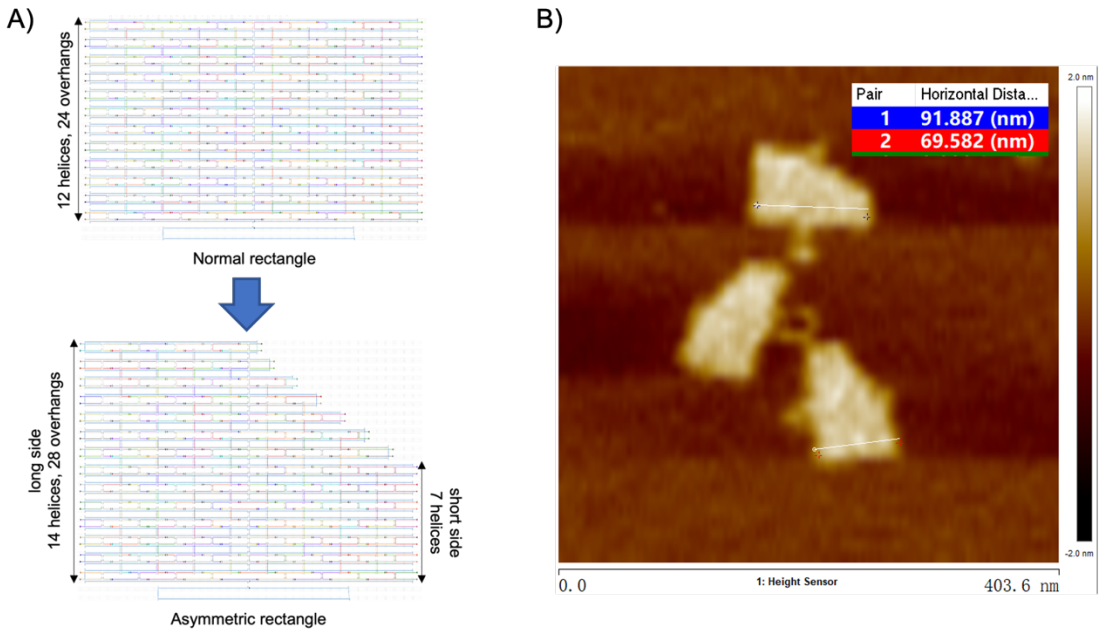

Figure 3-9 A) The design of the asymmetric rectangle, modified from a normal rectangle with 12 helices, in a dimension of 60x90 nm, the resulting asymmetric rectangle contains 14 helices in the long side, with a dimension of 70x90 nm. B) AFM measurement of the asymmetric rectangle with a dimension of 70x90 nm.

3.2.6.2 Number and spacing of overhangs

With rectangle dimers, 5-nt SE was chosen for varying the number and spacing of overhangs, to determine how they determine the dimer yield. Figure 3-10 displays the monomer and the dimer formation directed by the SE hybridisation (the SEs were set in a way that monomers orientated the same face up), as well as the layout of the SE overhangs. For in-series, overhangs were in the middle area (except one pair of SE was replaced with poly-Ts for shape symmetry), while the out-series overhangs were arranged on two sides. In- and out-series arrange to explore how the spacing affects the dimerization efficiency.

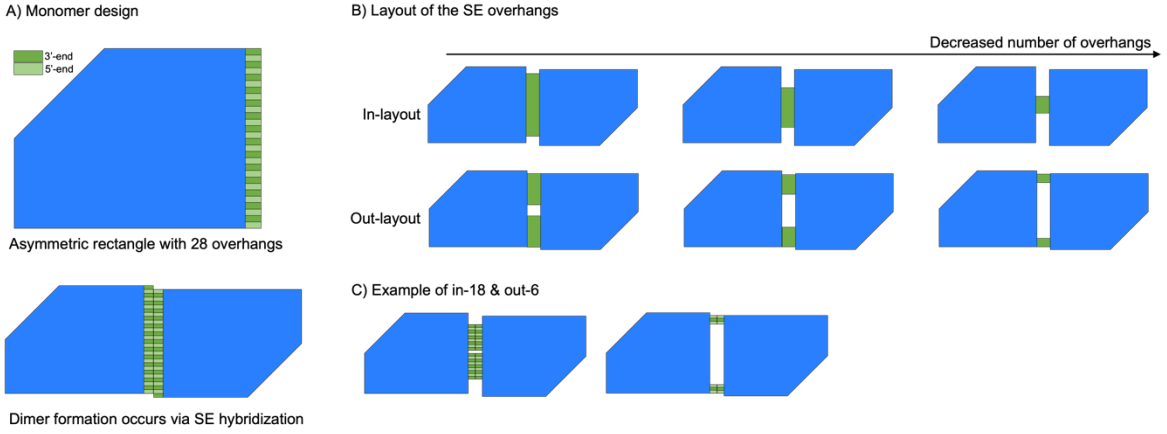

Figure 3-10 Monomer design and the SE layout in the interfacial area

Built upon the wireframe study, here the number of overhangs was decreased from maximum to minimum (26 to 2) with a resolution of 4 DNA overhangs. As presented in Figure 3-11A, the results agree with the wireframe work- the dimer yield decreases with a fewer number of overhangs. The gel indicates that the dimer barely forms with the use of 2 overhangs in the in- layout, while in out-layout it stops with the use of 10 overhangs. The data become more precise by narrowing down the resolution from 4 to 2, showing that monomers barely interact with the use of 6 overhangs in out-layout. The difference between in- and out- series shows that the spacing of overhangs does affect the dimer formation because multiple bridging overhangs works together can stabilize the dimerization reaction. The fact that the overhangs (helices) are evenly distributed throughout the square-based rectangle design makes it an ideal platform for dimerization study, as it does not introduce extra spacing or fixed position that may affect the arrangement of overhangs.

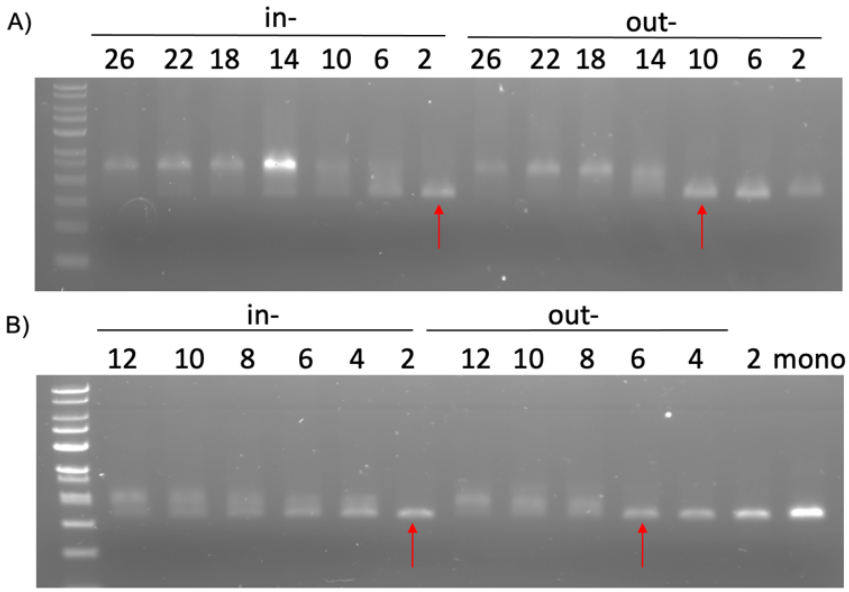

Figure 3-11 Gel data of decreasing number of overhangs in in- /out- patterns. *In-14 was considered as an error, results from adding too many samples accidently. Samples in A) and B) are decreasing the number of overhangs with a resolution of 4 and 2 respectively.

3.3 Conclusion

A wireframe square origami with six groups of overhangs along the edge was used to study how individual origami tiles interact with one and other. The dependence of origami dimerization on many structural factors including number, length and position of SE overhangs, construction of the SEs and the orientation of attached origami tiles. It is found that 1) yield generally increases with more bridging strands, they are in non-linear positive correlations; 2) adjacent SEs work cooperatively, such that the hybridization of one of the

SEs with its complement helps to bring the neighbouring SE with its complement closer together so that alignment occurs before dissociation; 3) outcomes largely rely on the binding strength of single bridging strand, as using single 10-nt SEs to attach origami tiles is more beneficial compare to double 5-nt SEs; 4) solution structure of origami tiles could affect the dimerization as the interface alignment determines the positions of corresponding bridging strands.

The effects of the flexibility of SEs were also tested by introducing poly-T linkers between the origami structures and the complementary region of the overhangs. To have the assembly protocol that would stay close to equilibrium, two monomers were mixed at equal concentrations and incubated at 25C for 12h and 36h. Both indicated that binding between SEs with linkers from T0 to T5 produced a decreased dimer yield (Figure 3-8). The interfaces with 5nt extended linkers produce the smallest yield, which is likely as 1) the interactions between these sticky ends are not strong enough to maintain a bond between origami motifs; 2) linkers may interfere with adjacent SEs preventing the hybridisation to its complement on another distinct motif; 3) the distance between every two SEs breaks the overall cooperativity of SEs like how they behave on helical packed rectangle design.

The dimer study on the square-based asymmetric rectangle involves the variants of the number and the spacing of sticky-ends bridging overhangs. The tendency of results follows the pattern of relationship between the number of overhangs and dimer yield [130]. Furthermore, it was shown that during dimerization reaction, the multiple overhangs work together and stabilise the interaction, meaning that the co-operative binding does not just happen between staple strands during the annealing origami [131]. More importantly, it is the spacing of overhangs should be close. This study suggests that the dimer yield increases with the number of bridging strands; the impact of the layout becomes more significant with fewer bridging strands, as the minor difference could switch the dimerization reaction.

Overall, the aim of this pure DNA study not only helped to understand the impact factors of dimerization but also inspired the author of how to access the fluorous directed dimerization in the following chapters.

Chapter 4 Fluorous directed origami attachment

4.1 Introduction

Nature uses a combination of non-covalent interactions to enable hierarchical assembly of complex systems out of basic building blocks. To achieve efficient assembly of larger origami constructions, the key is to control the yields dropping below single figure percentages. Novel chemical strategies like the fluorous effect have the potential to expand the repertoire of interactions available for origami assembly.

4.1.1 The adaptability of fluorous effect

The fluorous interaction can be considered complementary/orthogonal to the Watson-Crick base-pairing interactions and as such increase the utility of origami-based devices. The utility of this interaction remains unexplored in the field of structural DNA nanotechnology, where the size of a monomeric origami motif is magnitudes larger than surface-immobilised ssDNA strands. The only exploration of this interaction in the field of DNA origami was carried out in the author's group (unpublished work), which shows that a streptavidin-coated with fluorous-tagged biotinylated DNA can be immobilised on an origami nanostructure through fluorous interactions. It is strongly believed that the incorporation of fluorous effect can engender novel properties of DNA origami: the non-covalent nature of the fluorous-effect provides a strong yet mobile binding solution (the fluorous ponytails can slide over one another without separating) which may provide added stability when mixed with ssDNA sticky-end systems. Furthermore, akin to how the strength of sticky-ends base-pairing can be altered [125], the fluorine content of fluorous molecules can also be varied through changes in the ponytail length as well as the number of branch points, allowing one to adjust the strength of the fluorous-fluorous interaction.

In theory, the strength of the fluorous interactions can be enhanced by increasing the fluorine content until it meets the threshold of directing origami attachment. To test this concept, this work was set to explore the dimerization of origami as example components of a hierarchical assembly reaction. The tendency for fluorous molecules to exclude themselves from other molecules in solution can lead to micelle formation, especially in high fluorine oligos. This may lead to aggregation of ssDNA on origami, or even for fluorous-origami. Oligos with low-fluorine content might not exhibit sufficient fluorous effect to support origami dimerization. To enable the use of the fluorous-effect as a means for origami dimerization,

it is necessary to be able to control the strength of the fluorous effect. One to meet the threshold of dimer formation, another is to achieve clean dimerization by shifting it from micelle to the linear interactions as presented in Figure 4-1.

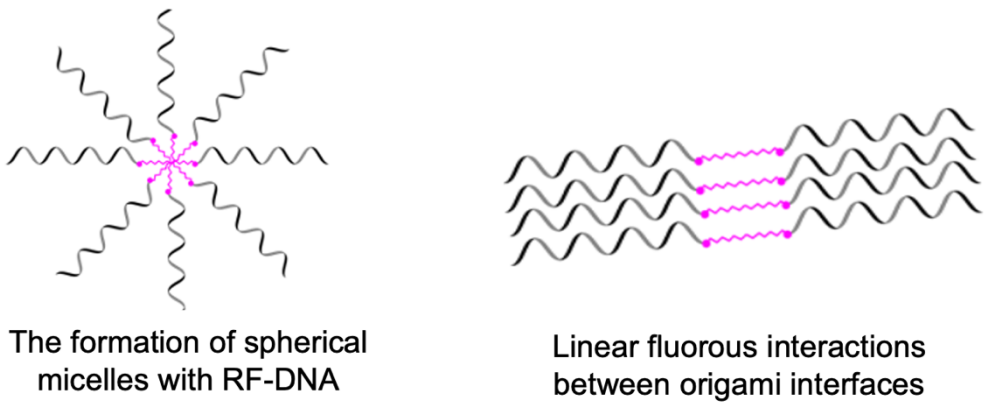

Figure 4-1 Illustration of the fluorous interactions. This work is sought to control the interaction by shifting it from micelle to linear interactions.

4.1.2 Context and aim of this chapter

It was discussed in the last chapter that the square based rectangle is a better candidate for fluorous study. Fluorous-fluorous has been used for directing the assembly of small molecules including carbohydrate, ssDNA oligos and proteins [90], [112], [132], neither is larger than DNA origami tiles. Work in this chapter is for the first time to use fluorous as a linker to connect origami tiles. Therefore, the work carried out in this chapter hopes to:

1) Use capture method to test fluorous variants, to explore the threshold strength of fluorous directed dimerization.

2) Reveal the optimal length of fluorous ponytails for origami dimerization.

3) Achieve fine assembly control using integrated method, determine the effect of changing the number of fluorous overhangs on the dimerization.

4.2 Results and discussions

4.2.1 The incorporation method and the choice of monomer

The incorporation of fluorous compounds onto origami structures was achieved by using per-fluorinated DNA oligonucleotides (RF-oligos). All RF-oligos used throughout this work were synthesized and HPLC purified in the University of Strathclyde [91]. Fluorous ponytails were functionalized onto the 5'- end of the ssDNA oligos using the standard solid-phase methods where the oligonucleotides were synthesized from 3'- to 5'- end [113]. RF-oligos were then attached to the origami structures through two methods, which are referred to as the captured method and the integrated method. In the capture method, edge staples were modified such that that the 3' end of the staple contained a 16-nt sequence which is complementary to the RF-oligos. After the folding of the origami had taken place, the RF-oligos were incubated for 12 hours with the modified origami motifs, after which excess staple strands were removed using spin-columns. Edge staples in the integrated method were directly modified with a fluorous ponytail tag on the 5' end. These integrated RF-oligos were mixed with the other staple strands before annealing and purification such that they hybridized directly onto the scaffold, leaving the fluorous tag pointing outwards from the edge of the rectangle (Figure 4-2).

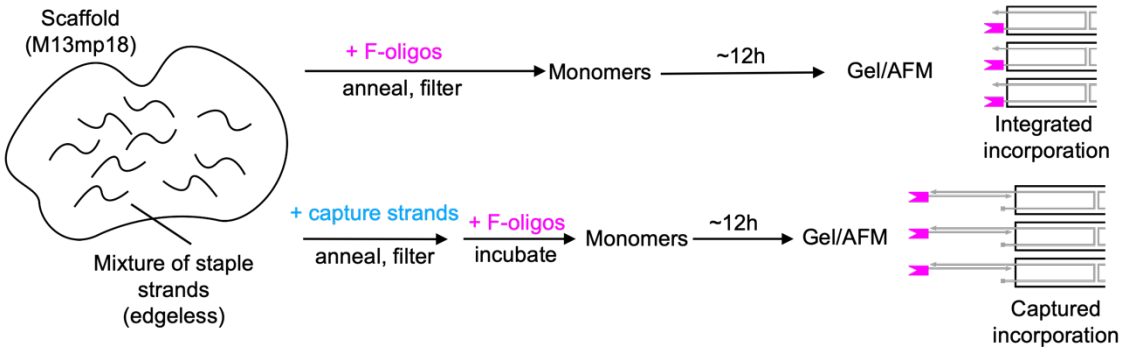

Figure 4-2 The protocol of two incorporation methods: the captured and the integrated method. RF-oligos in the captured method were attached indirectly to the extended 16-nt sequences of the edge staples, after the folding of origami. Rf-oligos in integrated method was attached directly to the scaffold, during the formation of origami

The monomeric origami used here was the asymmetric rectangle used in Chapter 3, on a scale of 70 x 90 nm and has 14 U-shaped staple strands along the long side (Figure 4-3). Each of these edge staples contains two overhangs (5'- and 3'-) which can be modified or extended such that the modifications protrude from the main body of the origami. Fluorous

groups are able to be added to each origami motif using the 5'- end of all 14 edge strands mentioned above.

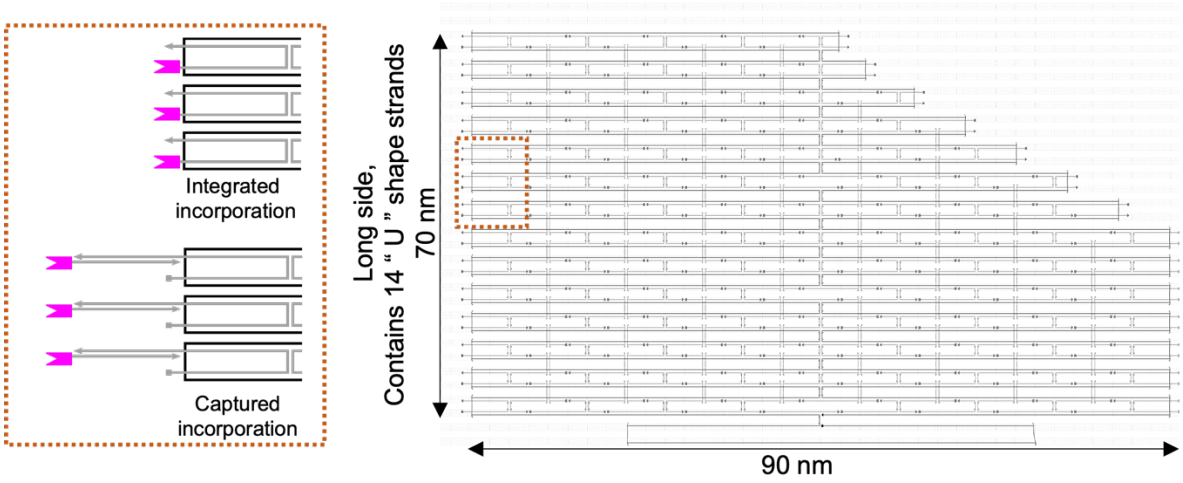

Figure 4-3 Design of the monomeric origami, the long side is where bridging strands are arranged and where origami tiles are attached through. Top: caDNAno design of the asymmetric rectangle; bottom: illustration of the captured and integrated incorporation. The fluorous tag was only arranged at one end of the U-shape edge staples.

4.2.2 Dimerization through the captured method

4.2.2.1 Optimizing RF-oligo size

First, to determine if fluorous effect can link origami tiles together, several RF-oligos with different fluorous tags were tested. As shown in Figure 4-4, the RF-oligos used in the captured method varied in their fluorine content depending on the length and density of the fluorous tag: C_4F_9, C_6F_{13}, C_8F_{17}, double branched $(C_8F_{17})_2$, quad-branched $(C_8F_{17})_4$, which will be referred to as RF4, RF6, RF8, $(RF8)_2$, $(RF8)_4$, respectively, in the following context.

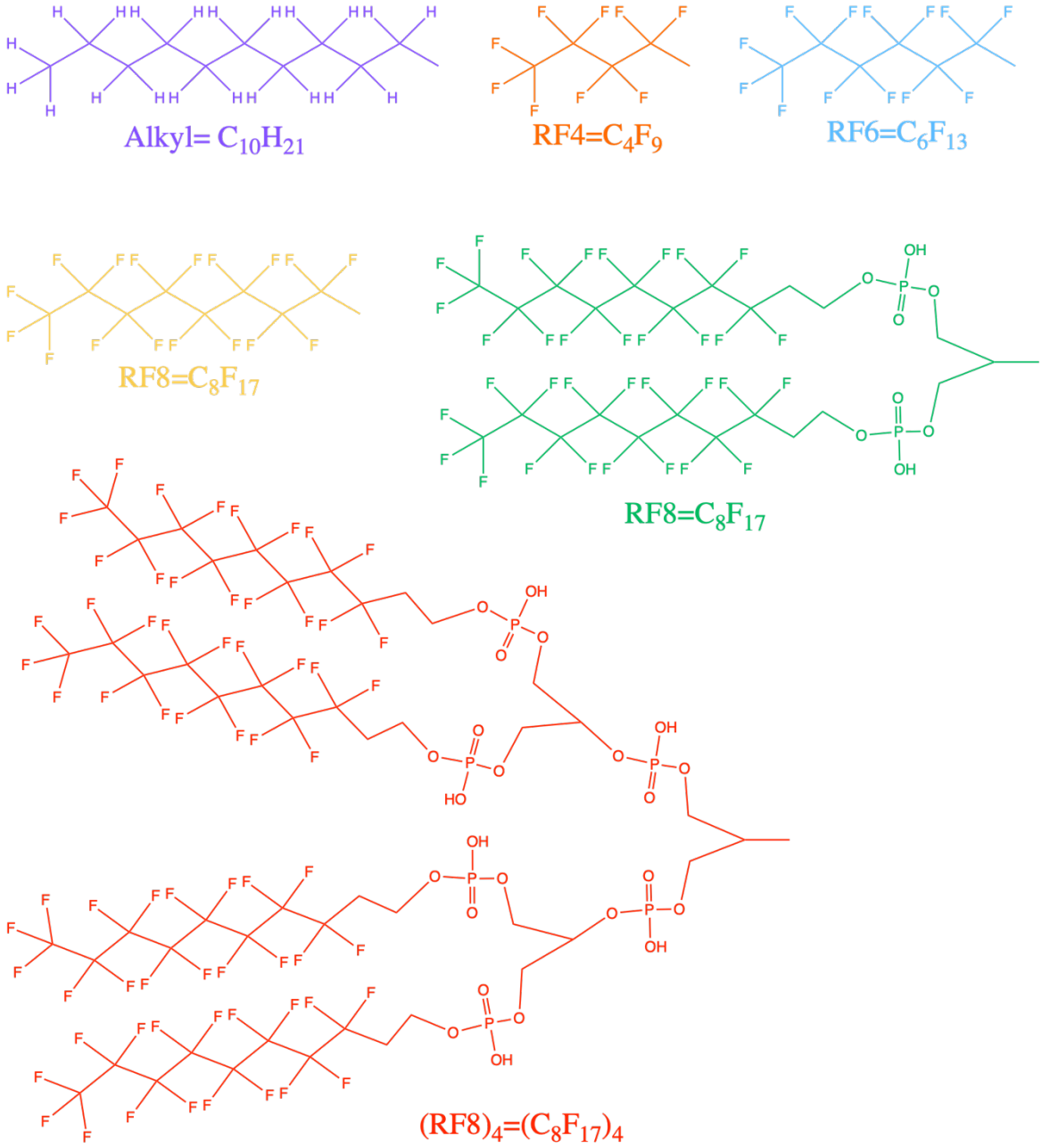

Figure 4-4 Chemical structures of fluorous tags.

Origami incorporated with RF-oligos was termed RF-origami. These initial experiments have used full occupancy to maximize the likelihood of showing the performance of fluorous. RF-origami were incubated at room temperature for 12 hours to initiate the dimerization reaction. Agarose gel electrophoresis (AGE) was performed to assess the dimer formation. In general, it was found that increasing the fluorine content (increased length in mono-fluorous ponytails and added branches), benefits the dimer formation, as well as the formation of more complex structures. AGE separates samples solely based on their molecular weight, normally DNA structures with lower molecule weight appear to be at the lower positions in the gel (starting from the top to the bottom of the gel). As such, it was concluded from the gel in Figure 4-5 that the origami tiles start to interact with the use of

RF8, as RF-origami with RF4 and RF6 appeared as a single band indicative of monomeric origami. The same monomeric band was also observed with the no-tag and alkyl control (no-tag is a negative control where the oligos contains complementary sequences only). The presence of a single monomer band in the alkyl ($C_{10}H_{12}$) modified origami suggests that the formation of *aggregates* is not driven by a simple hydrophobic interaction, but rather the dimerization is being driven by the fluorous-fluorous interaction. The lack of dimerization observed with lower-weight RF-oligos (RF4 and RF6, Lane 4&5 in Figure 4-5) suggest there were no interactions between origami tiles. Although these RF-oligos might still interact with each other and will be captured by origami tiles, their strength is not strong enough to drive the movement of origami tiles with such size and weight.

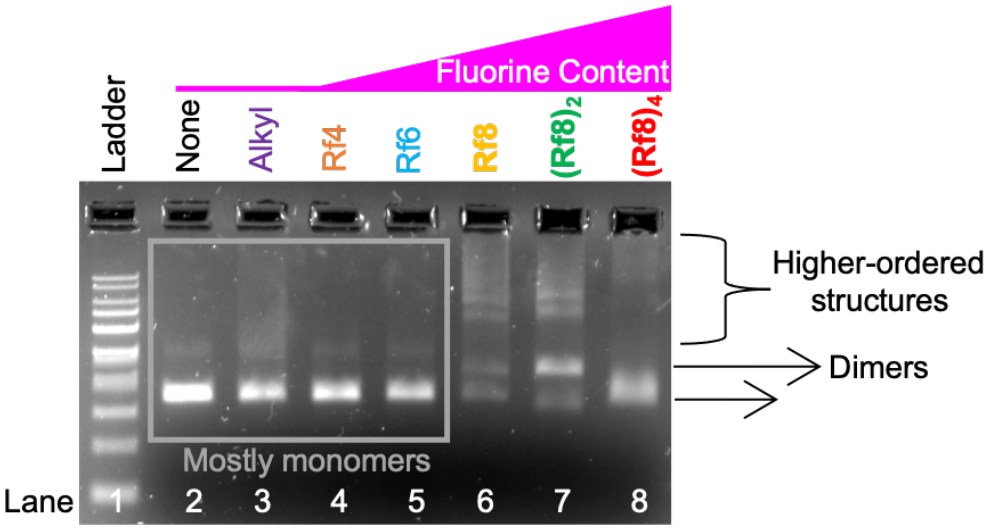

Figure 4-5 AGE (agarose gel electrophoresis) data of captured samples. Origami tiles in samples were loaded with maximum occupancy, thus all edge staples were in use.

RF-origami modified with higher fluorine content oligos: RF8, double-branched $(RF8)_2$ and quad-branched $(RF8)_4$, lead to a greater degree of dimerization, compared to lower-weight fluorine RF-oligos occurred with the use of the $(RF8)_2$ tag. The distinct jump from monomer to dimer band was far beyond the observation of either the RF8 or the $(RF8)_4$, both produced a mixture of dimers and monomers, as well as some higher-ordered structures. The upshift of the monomer band at $(RF8)_4$ was considered as the result of micelle structures adding weight on origami tiles. Because origami tiles can still capture RF-oligos in spherical structure via the exposed ssDNA sequences being outside of the micelles. This was also proven by AFM results presented in Figure 4-6. Overall, AFM images of RF8 and strands of higher fluorine suggest the degree of origami assembly was not limited at the dimer stage, with a number of polymers/concatemers containing 3 to 7 or even more origami motifs. Conformations of all products observed can be related into two types of fluorous-fluorous

interactions. (Figure 4-6B) Linear interactions often result in single-layered dimers and polymers. Micelle interactions often result in dimers and polymers with white spots appearing at where origamis connect, and sometimes multiple-layered polymers. The formation of micelles leads to a ball/spherical structure where the fluorous is contained on the inside. This creates a ball/sphere where the 16 nt capture-complementary sequences are exposed. As the capture sequences are the same along each edge strand and hence the same between each origami, there is a possibility that these exposed ssDNA strands can bind to several capture sties on the same origami, as well as between different monomeric origami, resulting in the observation of single-layered structures with white spots, or multiple-layered polymers where the micelle of fluorous strands led to the micelle formation of origamis.

Aggregations are undesirable but can be controlled as the degree of micelle formation is adjustable. For RF-oligos with low fluorine, there might be rare micelle formations, or the micelles are readily broken when they are captured by origami. Micelles are easy to form as they are smaller than origami. If RF-oligos are too weak to form stable micelles, they might also be too weak to join origami tiles together. For RF-oligos with high fluorine, the strength is too strong thus the micelles can form between RF-origami. From all variants, the $(RF8)_2$ appears to show the greatest promise in the formation of dimers, whilst the investigation of how to fine control the strength is still required.

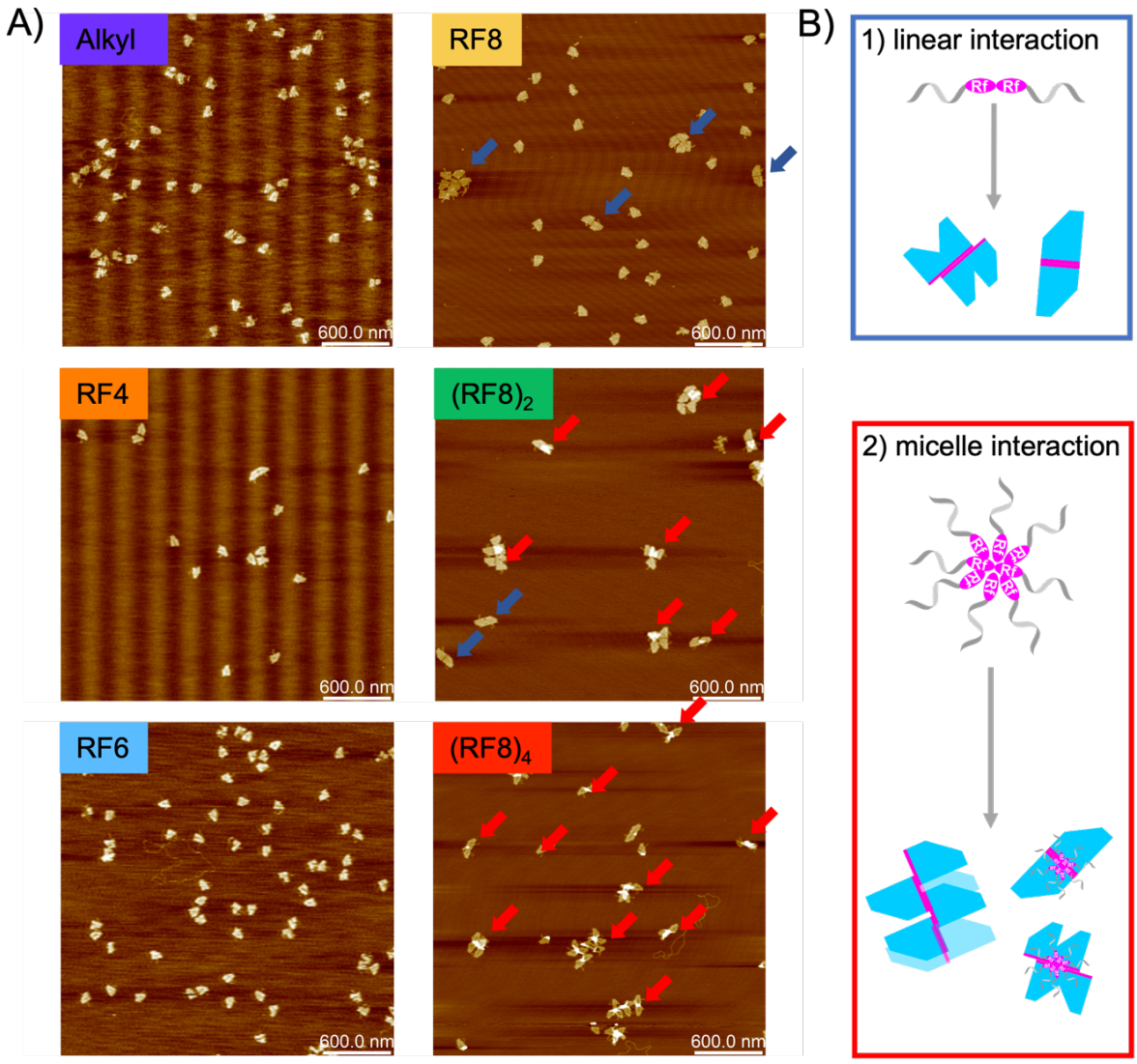

Figure 4-6 A) AFM images of captured samples. Samples on the left row were alkyl control and low fluorine tags (RF4 and RF6), resulting in mostly monomeric origamis; samples on the right row were high fluorine tags (RF8, $(RF8)_2$, $(RF8)_4$), dimers appeared in all samples, and more complex structures subsequently occurred from top to bottom. Blue arrows pointed to linear interactions that happened between origami tiles, red arrows pointed to micelle interactions. B) Description of how RF-oligos interact at the interface and the resulting structures.

4.2.2.2 Control the fluorous interaction by reducing the number of RF-oligos

Reducing the number of capture sites/oligos along the edge of the origami is another way to mediate the fluorous effect, with the hope of creating more desirable dimers, rather than concatemers. It was achieved through varying the number of capture sites incorporated into the origami from 14 to 2 as illustrated in Figure 4-7. These overhangs were centred about the midpoint of the long side of the origami tile. This method has been effectively demonstrated in chapter 3 that dimer yield decreases when reducing the number of sticky-ends overhangs. As before, origami motifs were then incubated with an excess of the RF-

oligos, with a certain ratio of capture sites to RF-oligos before excess staples being removed using spin-columns.

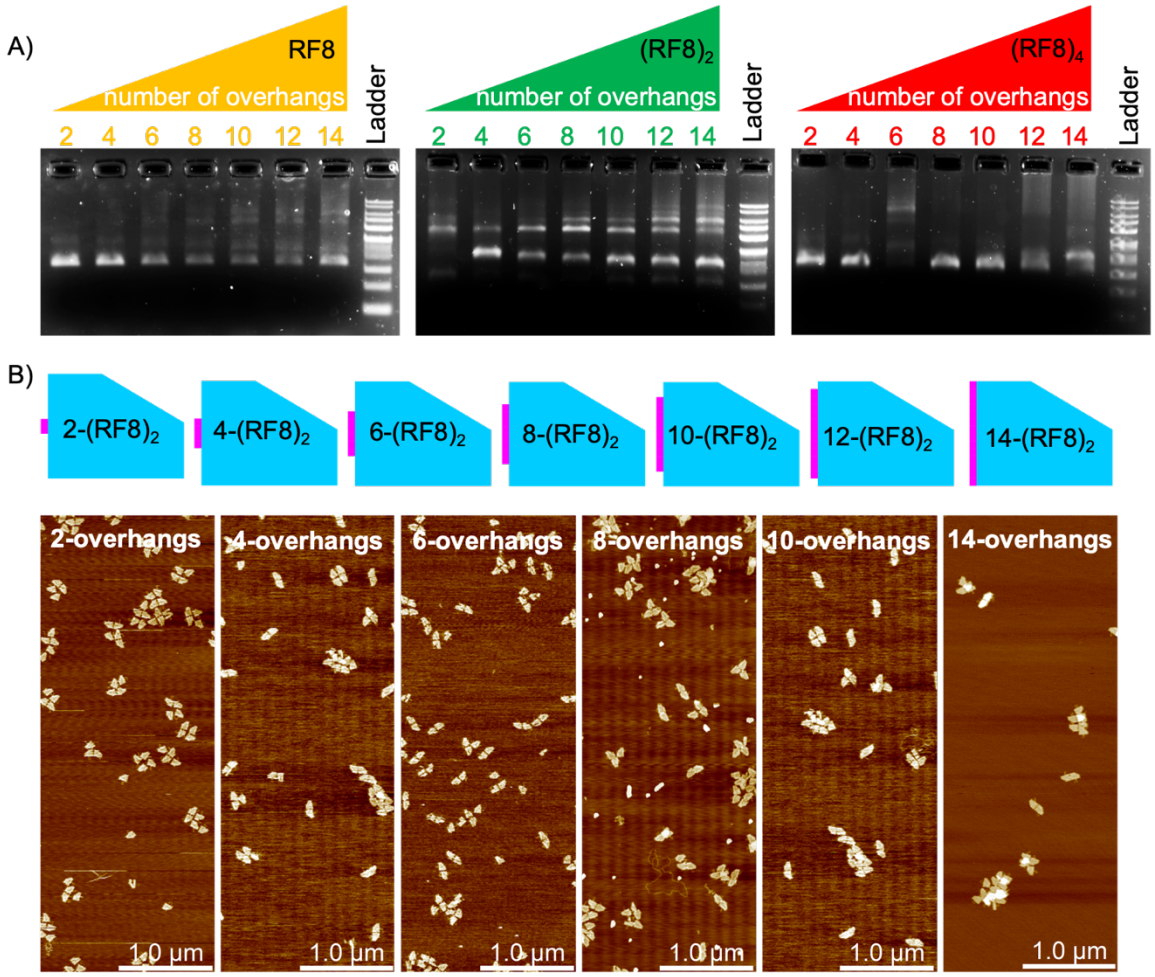

Figure 4-7 A) AGE data showing origami assembly with different number of fluorous overhangs. From left to right, they are RF8, $(RF8)_2$, $(RF8)_4$ overhangs. B) Top: Schematic showing the placement of the $(RF8)_2$ overhangs; bottom: AFM images of origami assemblies created with different numbers of $(RF8)_2$ overhangs.

Gel data overall suggests that reduced capture sites can limit the fluorous interactions between origami tiles. Again, for origamis with RF8 and $(RF8)_4$, there is no distinct dimer bands. For origami with $(RF8)_2$, with capture sites from 14 to 2, both AGE and AFM data presents the formation of dimers and other aggregations. It is evident that when decreasing the number of capture sites, whilst still existing, there are fewer higher-weight bands in AGE, indicating there is fewer aggregations form. Although chain-like aggregations (Figure 4-7B) were observed in most species including origami with 2 capture sites, again, this was attributed to the formation of micelles from the excess RF-oligos in solution, which can then mediate the linkage of monomeric origami motifs. Furthermore, the formation of dimers happens in all variants. This was attributed to the affinity between the $(RF8)_2$ ponytails, the connection was too stable to dissociate even with only two connected sites. As previously

described in Chapter3, bridging strands work together to promote an equilibrium from dissociation to association, stabilising the interactions between two origami tiles, which was called strands co-operativity. This might suggest that through the captured method, the dimerization reaction was not largely relied on strands co-operativity, as reducing the number of RF-oligos induce no significant impact on dimer formations.

4.2.2.3 Dimerization in the y-direction

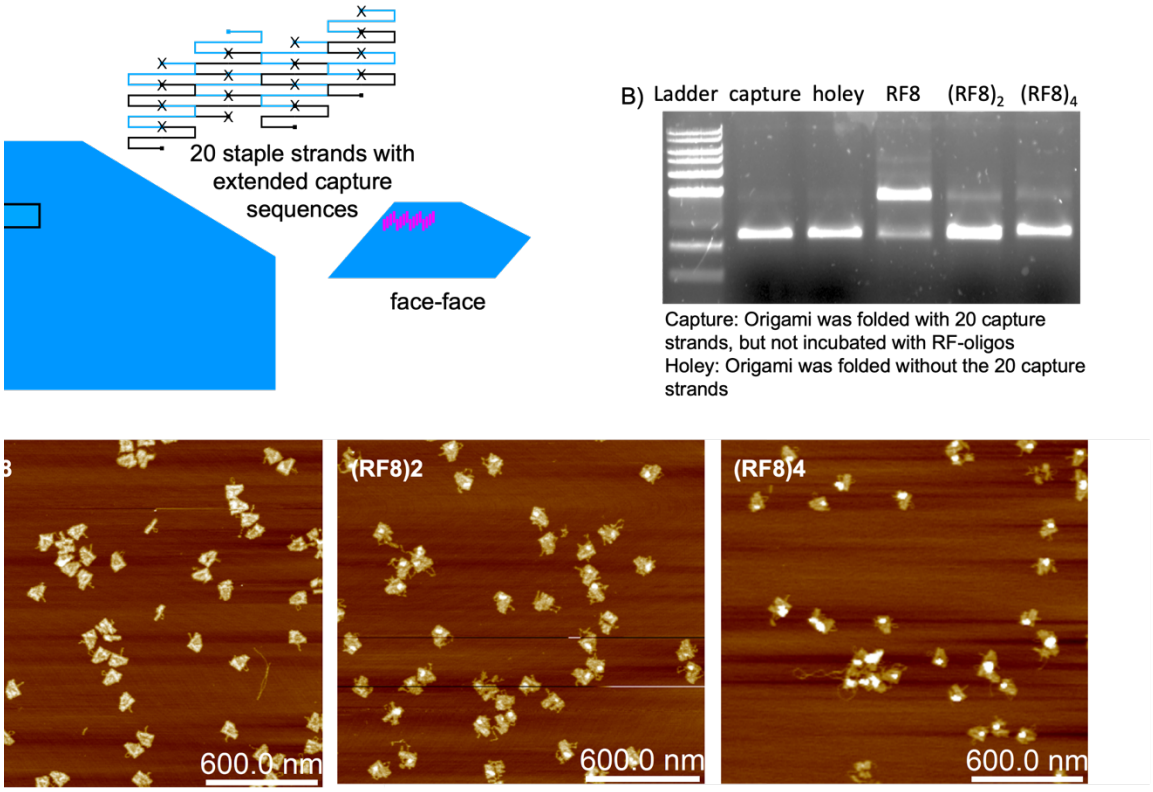

Figure 4-8 A) Illustration of how the RF-oligos were attached for face-face strategy. B) AGE of face-face samples; C) AFM images of RF8, $(RF8)_2$, $(RF8)_4$ face-face samples.

Work presented in Figure 4-8 was carried out on the same asymmetric rectangle design. Rather than modifying the edge staples (thus the interactions between two origami tiles was "edge-edge"), where fluorous ponytails protrude in-plane with the origami structures, here fluorous ponytails was arranged vertically, pointing away from one face (face-face). This was achieved by a capture domain containing 20 staple strands all with 16-nt ssDNA extensions that can capture RF-oligos with complementary sequences. As shown in Figure 4-8A, the RF-origami here contains a density fluorous domain. Following the above "edge-edge" work, three RF-oligos: RF8, $(RF8)_2$, $(RF8)_4$ that meet the threshold to drive the dimerization reactions were tested. Same as before, they were incubated for 12 hours and then AGE & AFM were characterised.

Unlike the results of edge-edge, the gel suggests that the mono-RF8 result in the highest amount of dimer, with some higher-ordered structures observed as bands in higher positions. (Figure 4-8B) Whereas origami with $(RF8)_2$ and $(RF8)_4$ tags appeared to have fewer/weaker dimer bands, with monomers being the most dominating products. Again, this was attributed to the non-specific interactions between excess RF-oligos in solution and those at the fluorous domain on origami thus blocking the interactions between origami tiles. This was shown by the white spherical spots observed in AFM, which was considered because of micelle formations at the fluorous domain, especially with the use of high fluorine tags. Also, most samples were observed to be monomeric. The disagreement between AFM and gel data suggest that the "sandwich" structures might dissociate during the depositing and drying process for sample preparation. (Figure 4-8C)

4.2.3 Dimerization through the integrated method

4.2.3.1 Reducing the number of fluorous-overhangs

To further investigate methods to modulate the fluorous effect, an "integrated method" was carried out to incorporate RF-oligos more efficiently onto origami. Rather than using ssDNA extension to capture RF-oligos, here the fluorous ponytails were directly modified at 5'- end of the edge staples. This way excess RF-oligos in solution were filtered out before mixing monomers thus creating a cleaner environment. Moreover, the number of integrated fluorous strands along the origami edge was also varied. Again, all the 3'- ends, and the 5'- ends which weren't modified to contain fluorous were terminated with poly-T_4 overhangs to prevent base-stacking interactions.

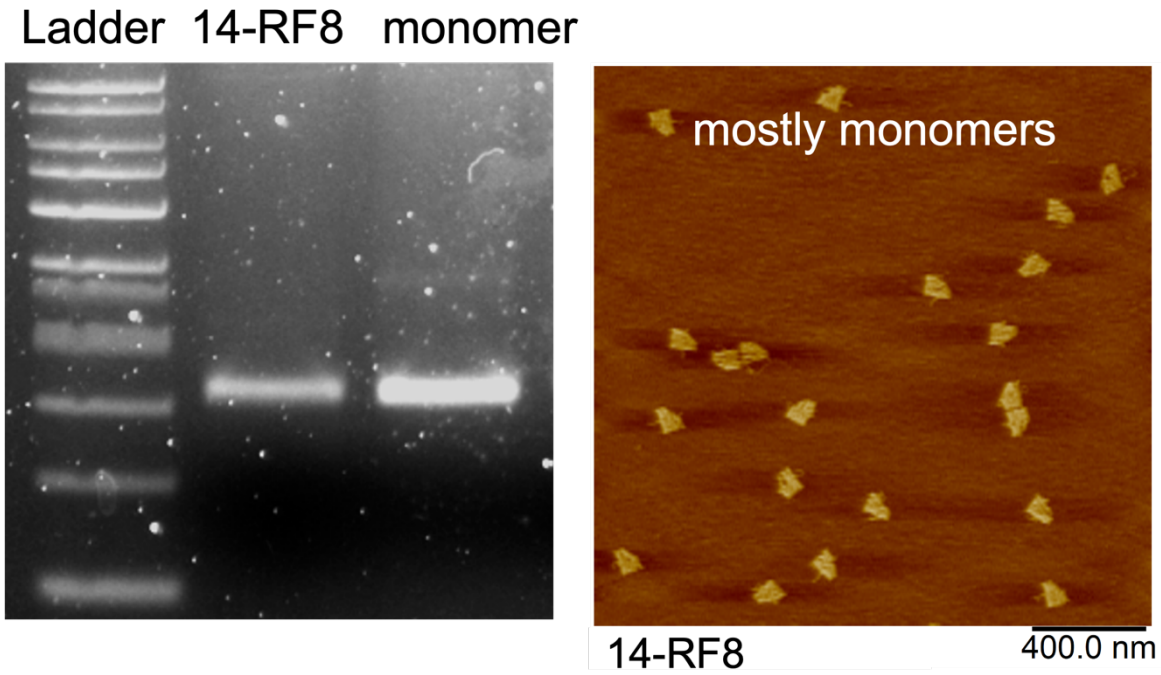

Figure 4-9 AGE and AFM data for integrated RF8.

A relatively weak interaction might be a better choice for better controlling this non-specific interaction. It has been observed that the branched $(RF8)_2$ has the greatest balance between the formation of dimer and aggregation among all variants. With cost of synthesis integrated $(RF8)_4$-oligos being one limiting factor, RF8 and $(RF8)_2$ were used for the integrated incorporation. As shown in Figure 4-9, with maximum occupancy, origami with integrated RF8 tag presents no dimer formations.

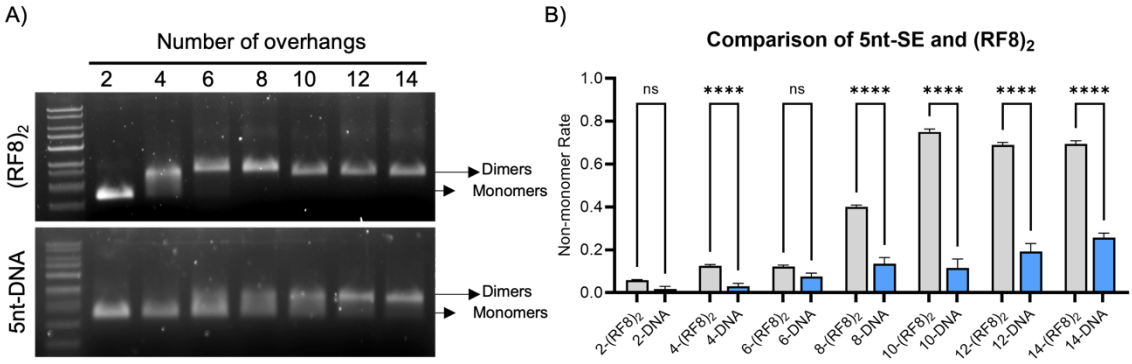

Figure 4-10 Results of origami with integrated $(RF8)_2$. A) AGE shows a comparison of $(RF8)_2$ and single-extended 5nt sticky-ends (control). B) Analysis of AFM data showing the assembly rate of using 2 to 14 overhangs. The non-monomer rates with the use of $(RF8)_2$ were 6.1%, 13.2%, 13%, 40.9%, 76.15, 70%, 70.7% (grey) respectively; the rates with 5nt-ssDNA were 0.9%, 2.3%, 6.6%, 12.2%, 9.6%, 17.7%, 25% (blue) respectively. One-way ANOVA was used for the statistical analysis of the data, ns $p>0.1$ (from left, ns $p= 0.1126, 0.0513$), ****$p<0.0001$.

Conventional 5nt sticky-ends (SE) overhangs, which is a typical method used for creating origami dimers, were set at the 5'-end of edge staples to compare with the $(RF8)_2$ overhangs [82], [83], [125]. The results from these experiments showed the same pattern with the captured methods- that the degree of dimerization depends on the total number of the interactions groups. As shown in Figure 4-10, origami with $(RF8)_2$ has significant higher assembly rate compared with origami with 5-nt sticky-ends DNA. As the number of fluorous overhangs increases, so does the yield of origami assemblies, with the effect starting at 4 and plateauing at 10 fluorous groups. When compared to the same number of ssDNA overhangs, it is observed that the assembly rate of origami directed by the fluorous-effect is significantly higher, especially for the 10-$(RF8)_2$ design, which is up to 8x higher than 10-(5nt SE).

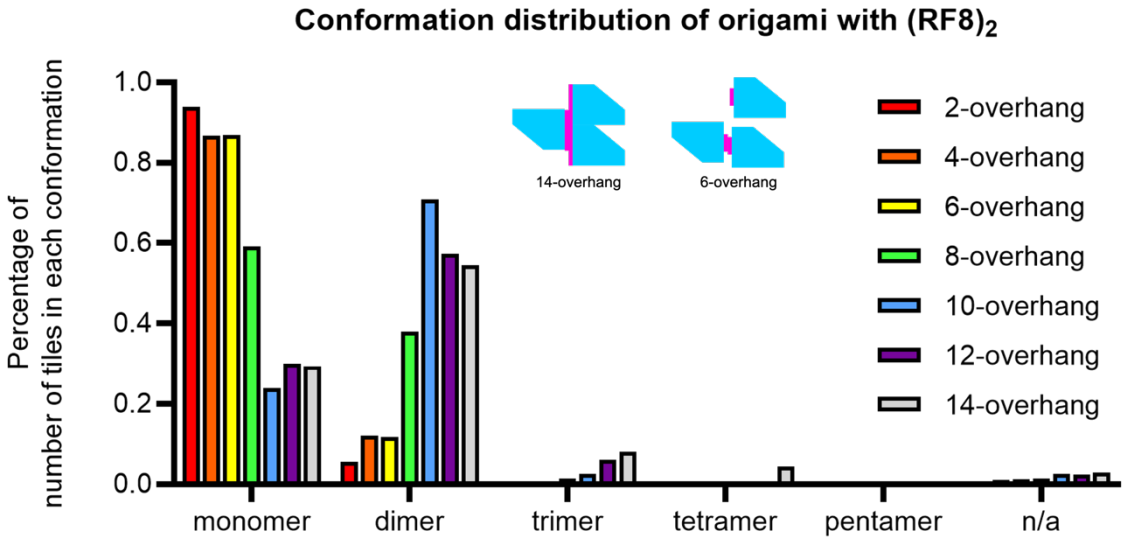

Figure 4-11 Percentages of number of $(RF8)_2$ tiles in each conformation observed via AFM. From left to right, each groups represent one conformation, which is monomer, dimer, trimer tetramer, pentamer and N/A. Each group contains overhang number of 2, 4, 6, 8, 10, 12, 14, from left to right). The yield for each conformation is: monomer (93.9%, 86.8%, 87%,59.1%, 23.9%, 30%, 29.3%); dimer (5.7%, 12.1%, 11.7%, 38%, 70.8%, 57.3%, 54.6%); trimer (0, 0, 0, 1.4%, 2.7%, 6.1%, 8%); tetramer (0, 0, 0, 0, 0, 0, 4.4%); pentamer (0, 0, 0, 0, 0, 0, 0.8%).

Due to the non-specificity of fluorous interactions, the same higher-ordered structures/ aggregations were observed with the use of 8 or more fluorous overhangs. Reducing the integrated RF-oligos is a better way of controlling the formation of aggregations. This was illustrated in Figure 4-11, as misalignment of the origami motifs with full fluorous domain exposes unbound RF, whilst origami with smaller fluorous domain, for example with 6 fluorous groups, the existence of poly-T_4 would prevent the unnecessary interactions. Moreover, from 14 to 10 fluorous overhangs, dimers become the dominant products, associated with the disappearance of higher ordered structures (trimers, tetramers and

pentamers), especially with 10-overhangs, where the dimer yield reached 70.8%, occupied about 93% of all attachment interactions. For 8-overhangs, although aggregation was well-controlled, the monomer rate firstly exceeded the dimer rate. As for 6, 4, 2-overhangs, the dimer yield reduced largely suggest they weakened the interaction between origami tiles.

4.2.3.2 Conformations of assembled structures directed by 14-(RF8)$_2$

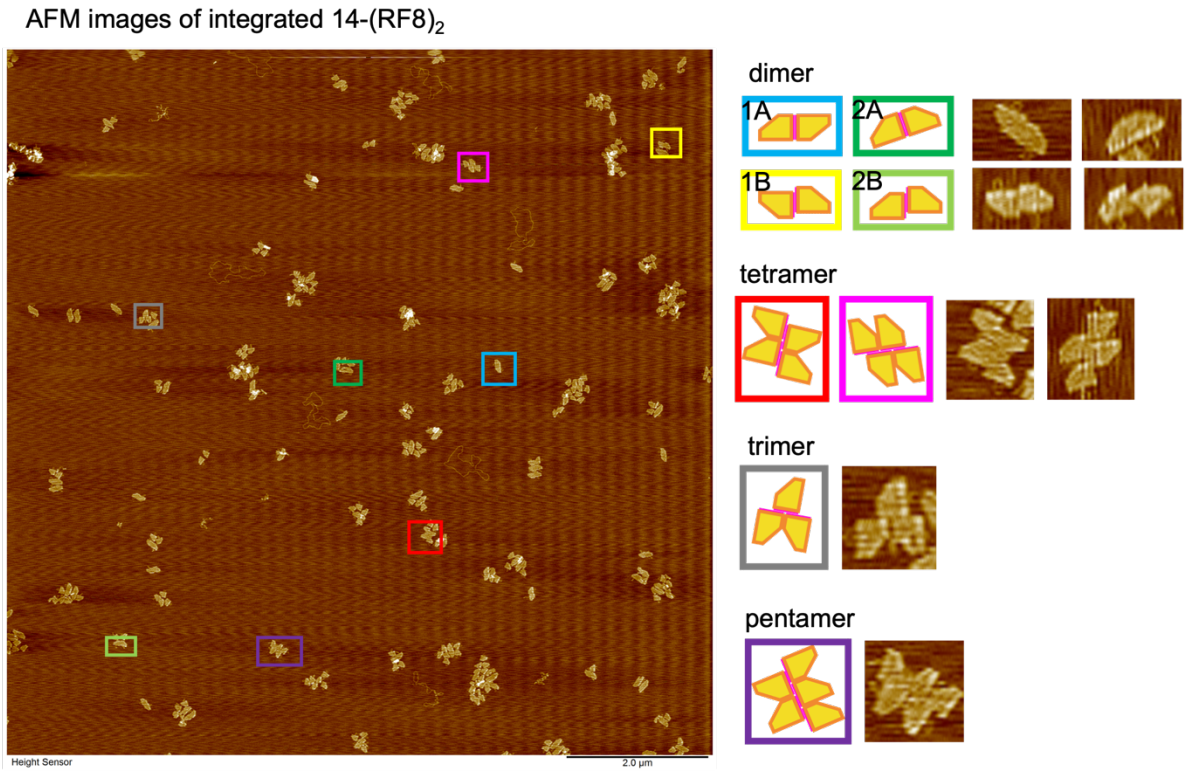

Figure 4-12 AFM images of origami with integrated 14-(RF8)$_2$ overhangs, showing the existence of dimers, trimers, tetramers and pentamers.

The AFM image presented in Figure 4-12 reveals the appearances of all the assembled structures. As previously mentioned, the formation of a more complicated structure because of the misalignment between the initial two origami tiles provides binding sites for other origami tiles close to them. This was confirmed in this AFM, as the dimers 1B and 2B can be considered intermediates of aggregations.

4.2.3.3 Dimer conformations and monomer bias

As mentioned before, square-based single-layer origami has an inherent twist because of the integer number of bases between crossovers. The Cando model shown in Figure 4-13A reveals the non-planar structure of the origami. The two faces of origami have been labelled as the A-face and B-face, where the concave face is A, and the other is B. The asymmetric design of the origami allows discriminating the orientation of monomers without face

modifications, e.g., hairpins. When deposited onto mica, the unmodified, monomeric origami motifs favoured a conformation whereby the concave A-face pointing up was observed with an approximate ratio of A-face: B-face = 64:32 (Figure 4-13B), which agrees with the results of the Cando simulation. Cando predict highly complex 3D geometries using finite-element methods, to assume the double helix is a uniform elastic rode with experimentally measured axial tensile, twisting and bending stiffness [133]–[135]. As observed in Figure 4-12, dimers were formed in different conformations. Neglecting the sliding effect, they can be separated into two major types depending on the orientation of the monomers: dimer type1 have both monomers the same face on top, and in dimer type 2 those two faces are different. As such, dimer type1, where the same faces of each monomer pointing to the same direction, inherently can have the edge fully aligned Figure 4-13C). The dimer type2 where the two faces are pointing in different directions has misaligned curvature along the edge.

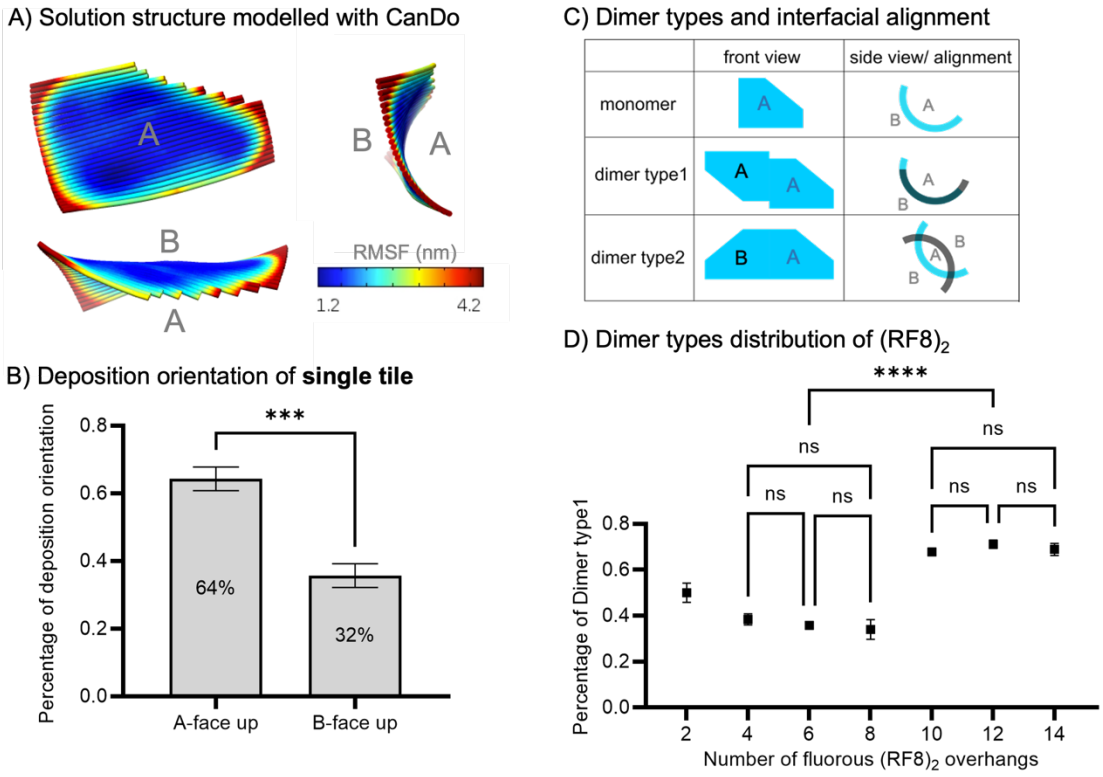

Figure 4-13 A) CanDo model of the solution structure of the asymmetric rectangle origami. B) The deposition orientation of the unmodified monomers, data obtained from AFM. T-test was used for statistical analysis, p=0.0006, ***p<0.001. C) Illustration of two dimer types and their alignment at the interface/ orientation of two tiles. A-face is the concave face. D) The distribution of dimer types, represented by the percentages of dimer type1. From left to right, the percentages of dimer type1 are 48.1%, 36.3%, 33.8%, 75.7%, 87.2%, 81.4% from 2- to 14-overhangs. One-way ANOVA was used for the statistical analysis of the data, ns p>0.1 (from left ns p= 0.947, 0.4968, 0.9828, 0.7432, 0.9983, 0.9481), ****p<0.0001.

When looking at the ratio of dimer types, it is observed that there is a correlation between the preference of dimer conformations and the number of fluorous strands. As presented in Figure 4-13D, based on the distribution of the dimer types, they can be divided into three groups. With the use of 2-overhangs, is appeared an equal amount of each dimer, showing no preference for either type. With the use of slightly more overhangs (4, 6, 8), dimer type2 became favourable as the dimer type1 rate was about 35% in three variants. When using 10, 12 and 14 RF-oligos, their average rate of dimer type1 reached 80%. It is obvious that the full coverage of RF-oligos favours the full-aligned binding of origami (thus benefiting the dimer type1 formation).

Associated with the decrease of the RF-oligos, there is an increase of poly-T_4 to prevent blunt-end stacking. With 14 to 10 RF-overhangs, the effect of ploy-T_4 can be neglected, thus origami tiles might seek a conformation that maximises the fluorous interactions. The formation of dimer type1 was supportive as the aligned curvature here provides the maximum overlap. When decreasing the number of RF-oligos to 8, the poly-T_4 domains at both ends became influential and started to interfere with the full-aligned origami interactions. Such that the formation of dimer type2 was more favourable to minimize the interference from poly-T_4. Although the data amount of the 2-overhangs was too low (N=31) to draw any conclusions, combine the data of the distribution of dimer types and the monomer bias (the orientation of origami when deposit on to mica surface), they seem to suggest that the change in dimer types can be related to the monomer bias. Because the distribution of dimers should be even if the inherent curvature doesn't play a role, suggesting the solution structure of the origami remains the same with the addition of fluorous compounds, and that the incorporation of fluorous does not significantly deform the origami structure.

4.3 Conclusion and discussions

In order to expand the toolbox for the assembly of DNA origami, this results chapter was set to determine if the fluorous effect can direct the origami dimerization. The results suggest that for the first time, the fluorous effect can be used as a linker strategy for origami dimerization. Moreover, fine control of the fluorous interaction between two origami tiles can be managed through 1) adjusting the fluorous tag with different fluorine content, e.g., the length and the number of branches of the per-fluorinated chain; 2) changing the number of RF-oligos at the interfacial domain. The former is to adjust the strength of the fluorous effect[91], [136], and the latter is based on the results of pure DNA in Chapter 3, postulating the number of RF-overhangs would affect the dismerization reaction, akin to how the sticky-ends interactions can be adjusted.

This work was first carried out through the captured method, where RF-oligos were captured by the extended complementary sequences of the edge strands. It was found that the dimerization reactions occurred with the use of RF8 and higher fluorine tags. Also, the interaction often linked more than two individual origami tiles together, leading to dimers and higher-ordered networks. A relatively weak interaction might be a better choice for better controlling this non-specific interaction. With cost of synthesis integrated $(RF8)_4$-oligos being one limiting factor, RF8 and $(RF8)_2$ were used for the integrated incorporation.

Therefore, this work was then built on through an integrated method. Strength of RF8 was not sufficient to direct origami attachment. With the use of $(RF8)_2$-oligos. Changing the number of overhangs can significantly affect the interactions and promote the formation of dimers compared with the captured method, where the aggregation structures still occurred with 2-overhangs. Here the dimer yield reached 70.8% with the use of 10-overhangs, occupying about 93% of all attachment interactions. An observation of the conformation of dimers suggests that the addition of fluorous groups does not deform the solution structure of the origami.

Overall, work presented here has demonstrate that the fluorous effect is able to induce the origami interactions. Among all species, the $(Rf8)_2$ tag has performed the optimal strength to direct origami dimerization, with the power can be controlled through adjusting the overhang numbers. Future work should continually focus on diminishing the effect from non-specificity, with the addition of specific interactions, for example sticky-ends base-pairing. The cooperation of both interactions may lead a more efficient assembly strategy.

Chapter 5 Hybrid linker system for origami dimerization

5.1 Introduction

The strict base-pairing rules that ensure the accurate assembly of origami motifs are also typically used as a connection strategy to link individual tiles together. On the one hand, the use of unique sticky-ends strictly controls the site-to-site binding and allows the precise attachment of origami tiles. On the other hand, it is limited by its simplicity, resulting from the progressive reduction of the assembly yield. The increased requirement of complex unique sequences is another concern given the range and variety of sequences used in the origami themselves. One solution is to combine non-specific interactions like blunt-end stacking which brings flexibility that can be corrected by base-pairing and at the same time strengthening the interactions between origami tiles [82].

Work presented in Chapter4 has demonstrated for the first time that origami tiles can interact and form dimers via the fluorous effect. As described previously, the fluorous effect is due to the exclusiveness of fluorous molecules which avoids the unfavourable interactions with other non-fluorine molecules. The degree of aggregation of the resulting higher-ordered structures can be tuned by using different tags or varying the number of fluorous bridging strands. The controllable non-specificity of fluorous effect and its non-covalent nature makes it an ideal auxiliary molecular recognition modality for complementing the sticky-ends strategy.

5.1.1 Context and aim of this chapter

The main purpose of work presented in this chapter is explore a hybrid system containing both fluorous tags and a relatively weak sticky-ends interaction (by choosing a short SE linker), can lead to a specificity dominated, non-specificity strengthened/ stabilised dimerization. Therefore, Therefore, the work carried out in this chapter hopes to:

1) Establish a system that can distinguish the driven effect of dimerization by using two monomeric origami designs.

2) Determine the effect of placing ssDNA onto fluorous interface on dimerization yield.

3) Balance the strength of either interaction thus allowing the base-pairing to correct the dis-assemble led by the fluorous, to obtain an optimal combination.

5.2 Results and Discussions

5.2.1 Strategy to distinguish the driven effect of dimerization

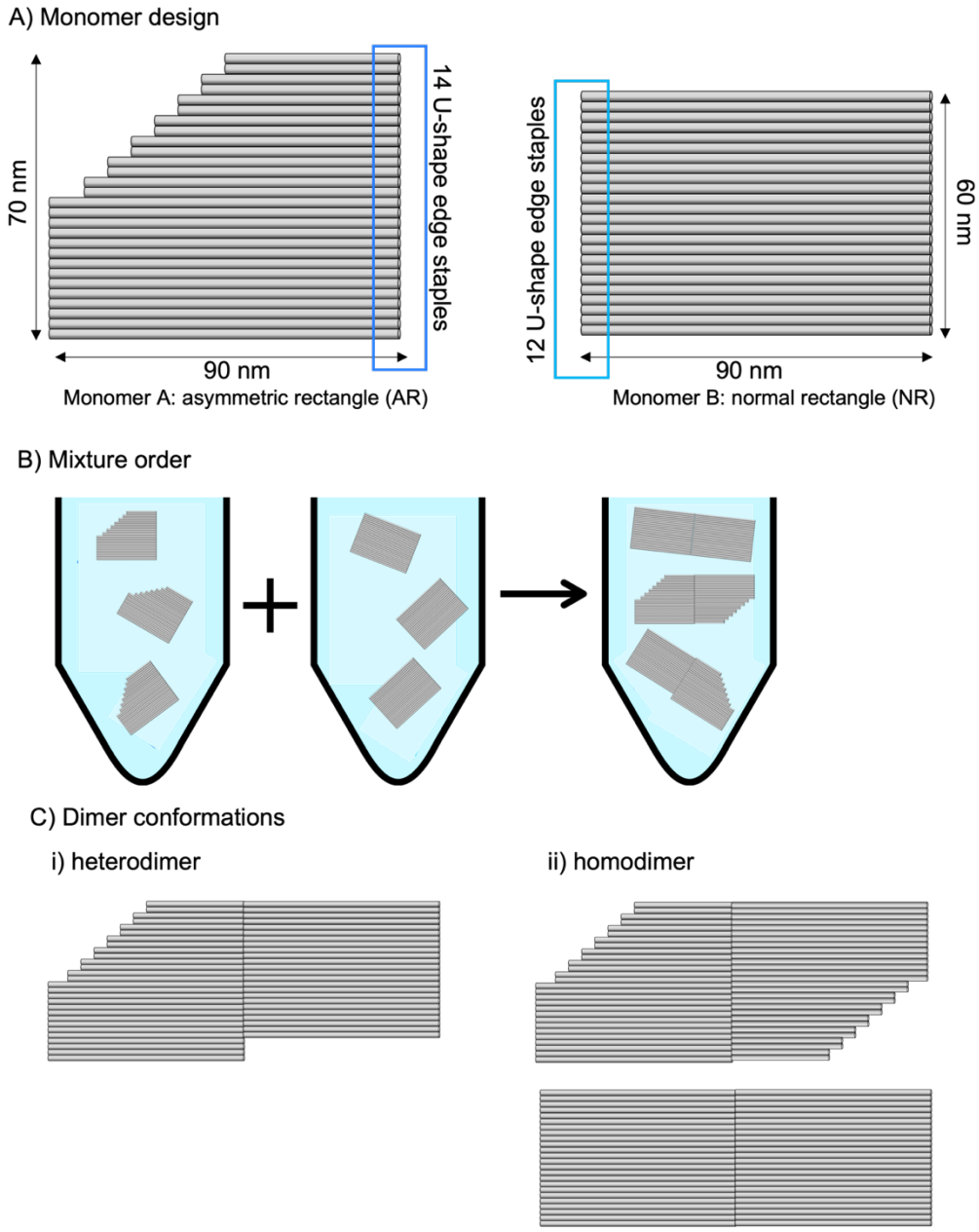

Figure 5-1 A) Two origami designs were used to compose dimer. Monomer A is the asymmetric rectangles used in previous chapters; monomer B is a normal rectangle with a shorter interface compared to the AR, it only has 12 U-shape edge staples. B) Mixture order showing that the two monomers were folded individually before being mixed. C) This "two-monomer" design allows to discriminate the formation of i) heterodimers, which contains two different monomers, and ii) homodimers, which contains two identical monomers.

To differentiate the driving forces behind dimerization, two differently shaped monomer motifs, an asymmetric rectangle (AR) used in previous chapters, and one normal rectangle (NR) in a dimension of 60 x 90 nm, were used for the creation of dimers. The monomer designs and the mixture order can be seen in Figure 5-1A&B. Here the $(RF8)_2$-oligos were

incorporated through the integrated method, same as the sticky-ends (SE) extensions. AR and NR contain 14 and 12 U-shape edge staples respectively. Thus, two edge staples in AR were not in use and they were arranged as shown in Figure 5-1C. Individual origami tiles with linker stands (of fluorous, SE, or poly-T4) were annealed and filtered before initiating dimerization reaction. Same as before, origami motifs of AR and its complementary NR were incubated equivalently for 12 hours then characterised by gel and AFM.

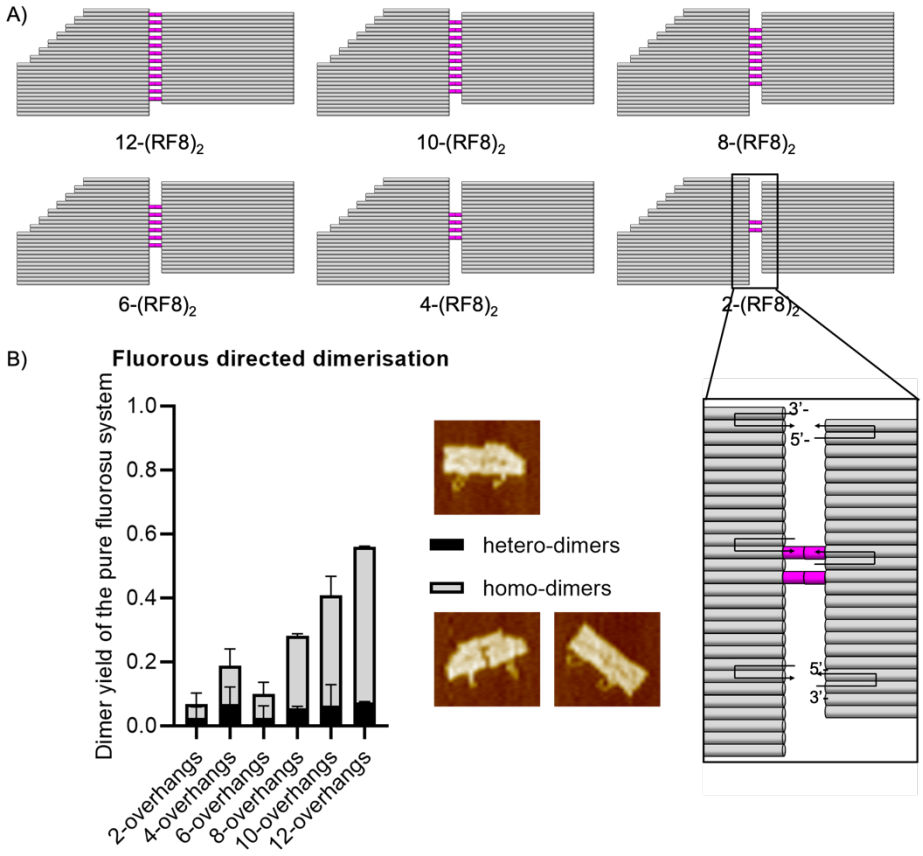

Figure 5-2 A) The arrangement of how RF-oligos were incorporated into each origami design, highlighting the orientation of two monomers. The U-shape edge staples in AR have 3'- on top and 5'- on the bottom, which is reversed in NR. B) AFM analysis of the non-specific fluorous effect directed dimerization. Both dimers were observed, and the homodimer rates were significantly higher than heterodimers. From 2 to 12 overhangs, the homodimer yields were 2.3%, 8.6%, 5.2%, 22.2%, 29.3%, 48.4% respectively, and the heterodimer yields were 0.4%, 3.5%, 0.3%, 5.0%, 2.3%, 7.2% respectively. From left to right, N= 587, 614, 836, 580, 630, 526. (N= the number of counted samples)

With the use of two different monomer designs, when specific base-pairing is dominating the interaction, as AR and NR were designed to be complementary, the major products would compose one of each monomer motif, as being the heterodimers. With the use of the RF-oligos, due to the non-specificity of the fluorous effect, there would be no preference for the heterodimer. And because of the mixture order shown in Figure 5-1B, homodimers already formed before the mixing process, the number of heterodimers should be rare. Thus,

the number of heterodimers can be used as an indicator, showing the dominating driving effect of the dimerization.

Results in Figure 5-2 are of mixtures of modified, fluorous-only AR and NR, with varying integrated fluorous strands. As before, integrated RF-oligos were incorporated onto the NR and AR origami motifs with varying amounts of RF overhangs, from 2 to 12. These samples also appeared to form more complex higher-order structures (including trimers, tetramer and pentamers) like those shown in Chapter4, however they were not presented here as the dimers are more of interest. The AFM analysis shows that, overall, the dimer yield increased as more RF-oligos were included. Among that, the homodimers were the major products, occupying above 87% of all dimers (calculated from 12-origami, 48.4% of 55.6%). This suggests that 1) the fluorous-driven dimerization reaction occurs in both fluorous modified AR and NR solutions before they were mixed; 2) the fluorous interactions are stable enough such that the dimers formed in the single-motif solutions are unlikely to dissociate with the addition of other RF-origamis. The small proportion of heterodimers observed in AFM was formed from RF-origami that was unpaired in the original single-motif solutions. This suggests that when more fluorous overhangs were used, monomeric origami can form a high percentage of homodimers before the mixture to two solutions and those interactions are too stable to be replaced. It is anticipated that origami with fewer fluorous overhangs is more ideal for the addition of sticky-ends overhangs, one is that weaker fluorous interactions are more likely to dissociate the homodimers thus promoting the heterodimer formation; another is that more sites are available for the incorporation of sticky-ends overhangs. As such, since the use of 8, 10, and 12 RF-oligos results high degree of dimerization, they are less suitable for a system containing both fluorous and DNA overhangs. Whilst origami with fewer RF-overhangs (2, 4, 6), where the fluorous-driven dimerization is less pronounced and the number of remaining attachment sites is high, are good candidates for the addition of ssDNA overhangs.

5.2.2 Hybrid linker system directed dimerization

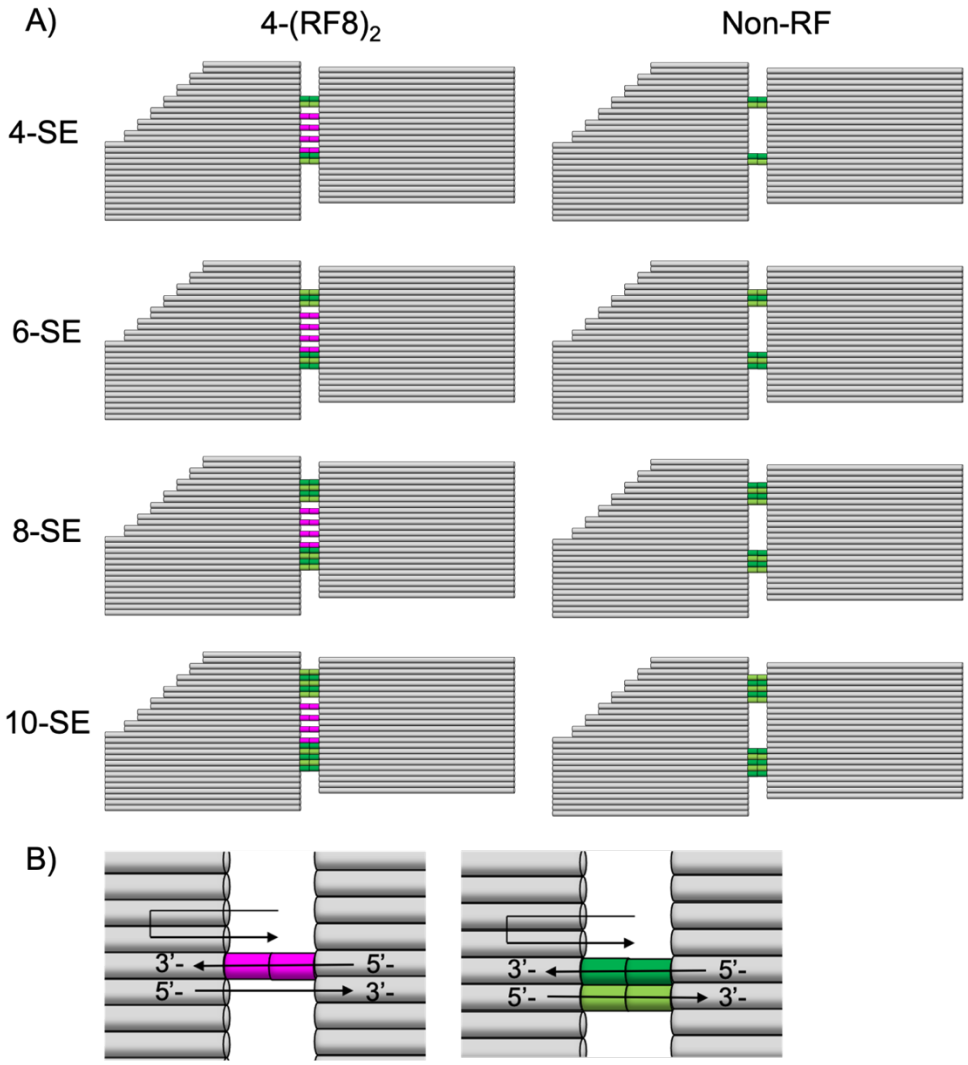

Figure 5-3 A) Schematics illustrates the position of fluorous and sticky-ends overhangs in the hybrid system. Four RF-oligos were arranged in the centre, with the sticky-end overhangs placed adjacently and on both sides of this fluorous domain. The left column is the hybrid system that contains both RF and sticky-ends overhangs, right column is the DNA-only system that contains sticky-ends only. B) Illustration of how RF-oligos and sticky-ends overhang were arranged at the interface.

The hybrid linker system contains both sticky-ends and fluorous overhangs at the interfacial domain. It contains 4 of $(RF8)_2$ overhangs as the central element, with some sticky-ends overhangs (ssDNA) placed adjacent to the fluorous domain at both sides (as shown in Figure 5-3A). Here the number of ssDNA overhangs was varied from 4, 6, 8 to 10. Again, fluorous tags were only modified at 5' -end, whilst the sticky-ends can be arranged at both ends of the U-shape staples. Here the number of linkers shows how many tags have arranged the interface, not how many of the edge staples were modified. For example, the 4-RF+8-DNA contains 12 linkers for connection: 4 staples modified with fluorous tags (at 5'- end only) and 8 sticky-ends extensions.

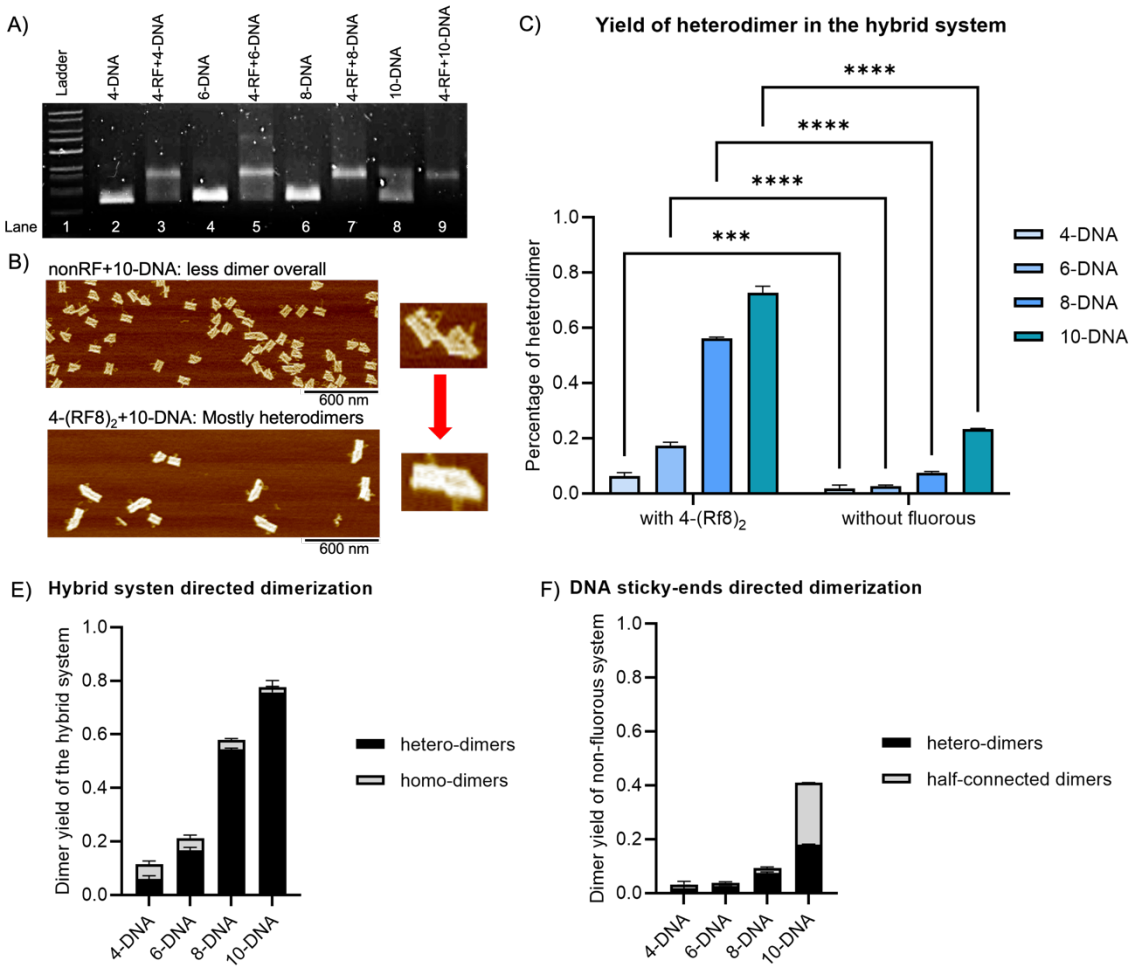

Figure 5-4 A) AGE data comparing the hybrid system and sticky-ends only system. Higher band (related to dimers) often appeared with the inclusion of the fluorous tags. B) Example AFM images showing how fluorous benefits the dimer formation, by linking two separate sticky-ends domains. C) The proportion of heterodimer observed via AFM in the hybrid system. The heterodimer yields are 1.1%, 2.5%, 7.2% and 18% for the non-RF group, and 5.3%, 16.1%, 54.4%, 76.5% for the hybrid group. From left to right, N= 538, 791, 1783, 1871 for non-RF group; N= 810, 851, 1003, 377 for RF group. N= the number of the counted samples. D) The proportion of homodimers and heterodimers in the hybrid system. The overall dimer yields were 10.1%, 20%, 57.6%, 77%. The homodimer rate was 4.8%, 3.8%, 3.2%, 0.6% from 4-SE to 10-SE; the heterodimer rate was the same as those in figure C. E) The overall dimer yields were 1.9%, 3.6%, 8.8%, 40.8%. The proportion of heterodimer was the same as those in figure D; the half-connected dimer was 0.8%, 1%, 1.6%, 22.8% from 4-SE to 10-SE. One-way ANOVA was used for the statistical analysis of the data, ***p=0.0009<0.001, ****p<0.001.

The data presented in Figure 5-4A shows that fluorous compounds act as a switch, where their inclusion significantly enhances the dimerization efficiency, evidenced by the dimer band in the gel compared to the non-fluorous groups, where the fluorous domain was replaced with poly-T_4. As for the gel of non-fluorous groups, all samples appeared to be monomeric, except for the 10-SE, which showed evidence of higher-ordered assemblies. Compared to fluorous groups, none of them can be considered as distinct dimer bands. The conformation of these dimers found in AFM has explained the phenomenon, which is that

the separated sticky-ends domains work independently as they were too far away from each other, thus the binding of one domain doesn't guarantee the binding of another, resulting in the half-connected origami tiles shown in Figure 5-4B. These half-connected dimers might dissociate during the electrophoresis process, leading to the indistinct bands in 10-SE. This also agree with the results presented in Chapter 3, where suggest that the position of bridging overhangs is one impact factor.

Compared with pure fluorous direct dimerization (Figure 5-2B), where the 4-$(RF8)_2$ had an overall dimer yield of 12.1% (3.5% of heterodimer, 8.6% of homodimer), the addition of ssDNA overhangs has improved dimer yield. The improvement was not observed with the use of 4-SE (10.1% of all dimer yield) but became significant with more ssDNA overhangs. As presented in Figure 5-4D, the addition of 6, 8, 10 ssDNA overhangs have brought up the yield to 20%, 57.6% and 77% respectively. This growth pattern was expected as it was proven in Chapter 3 that increased sticky-ends overhangs would lead to the increase of dimer yield. Moreover, with more ssDNA overhangs being used, the formation of heterodimer was more favoured. For 4-$(RF8)_2$ + 10-DNA, the proportion of heterodimer yield occupied about 99.3% of all products (76.5% of 77%), demonstrating that the non-specificity of fluorous can be corrected by the specificity of sticky-ends base-pairing.

Furthermore, if we compare the hybrid system to the DNA-only system (Figure 5-4C), the addition of fluorous overhangs to the system significantly increases the percentage of dimers. The greatest increase is seen in the 8-SE variant, where the addition of fluorous overhangs results in a 7.7x increase in dimer formation. Furthermore, the advance does not just appear at the yield increase. As described previously, there were half-connected heterodimers observed in the DNA-only system, because of the lack of co-operativity between two separated sticky-ends domains. Figure 5-4E shows the distribution of heterodimers and half-connected dimers at all variants. It is observed that the half-connected dimer rarely formed with the use below 10-SE (two of separated 5-SE). When increasing the number of ssDNA overhangs, at first there were few dimers (1.9%, 3.6%, 8.8% for 4, 6, 8-SE), until the dimer rate of origami with 10-SE has reached 40.8%. Associated with that, there is also a jump for the half-connected dimers from 1.6% to 22.8% (from 8-SE to 10-SE). The half-connected dimer here can be considered as using 5-SE as linkers only, whilst the dimer yield is significantly higher than the fully connected dimers of 6-SE (2.5% of heterodimer). This suggests that the same as the association, the dissociation of the separated sticky-ends domains were not in co-operation, but in general, the larger amount of SE overhang would improve the dimer yield, as there is an added chance that another domain can bind when one

breaks. This also suggests that those fluorous tags inserted in-between the sticky-ends domains were limiting the dissociation and promoting the association, to stabilise the dimerization overall.

5.2.3 Double extension and single extension

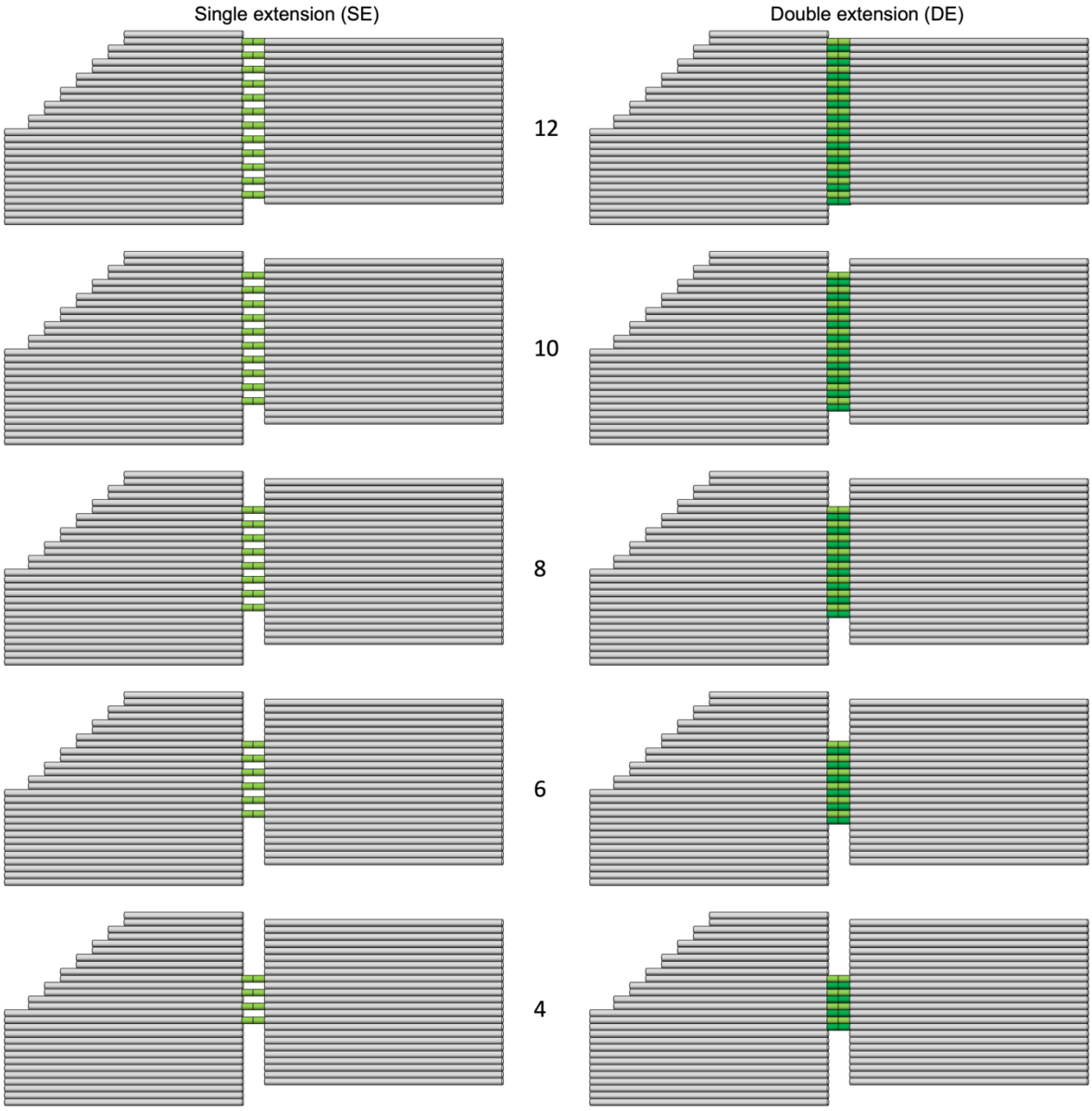

Figure 5-5 Schematics showing the arrangement of sticky-ends extension in single and double ends of the U-shape edge staples.

Attachment of fluorous compounds onto DNA oligos is less prevalent in the literature, the RF-oligos were synthesised using the automated phosphoramidite chemistry from 3'- to 5'-end, thus all RF-oligos were modified at a single extension. Although the double extension is a standard protocol in the hierarchical assembly of origami, the fluorous study was carried out to reduce the cost and time of the synthesis procedure. Therefore, the work presented in

this section was a proof-of-concept study to determine the dimerization efficiency difference of the single and double extensions with the use of 5-nt sticky-ends overhangs. Again, the AR and NR were two monomer motifs. The layout of sticky-ends overhangs is shown in Figure 5-5.

The density of the overhangs has a significant impact on the dimerization yield. As if the density induces no influence, the 8-SE and 4-DE should have the same yield as quantitatively they have the same number of sticky-ends overhangs. AFM analysis in Figure 5-6 shows that the yield of 4-DE is 4x of 8-SE, suggesting that the cooperation effect from double extensions is more efficient than single extensions.

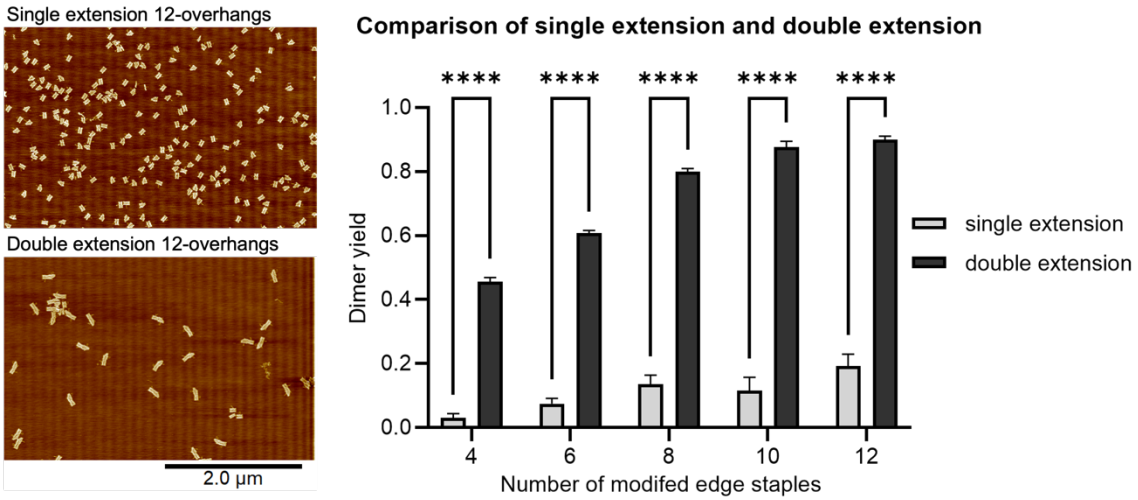

Figure 5-6 Example AFM images of origami and AFM analysis of single extended and double extended sticky-ends overhangs. The dimer yields were 2.3%, 6.6%, 12.2%, *9.6%, 17.7% from 4 to 12 overhangs for single extensions, 45.5%, 60.9%, 80.3%, 88.5%, 90.5% for double extensions. From left to right, N= 631, 500, 692, 882, 486 for single extension; N= 497, 1393, 1217, 503, 462 for double extensions.* One-way ANOVA was used for the statistical analysis of the data, ****p< 0.0001.

5.2.4 Hybrid system on the wireframe structures

The fluorous oligos was also incorporated on to the wireframe structures (the same design used in Chapter3), the incorporation of fluorous tags and their arrangement were presented in Figure 5-7 A&B. Again, fluorous tags were incorporated on to origami through integrated method, and they were only arranged on to 5'- end of the edge staples.

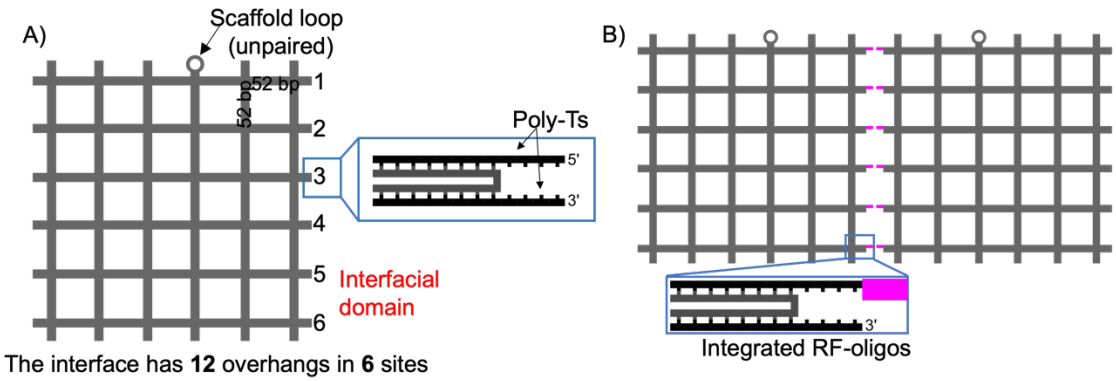

Figure 5-7 A) Schematics of the wireframe structure, labelling 6 sites at the interface that can be modified, each contains a 5'- and a 3'- end. B) Schematics of how fluorous tags were incorporated onto the wireframe origami.

Furthermore, a hybrid system was applied. Associated with the decreased number of RF-oligos from 6 to 2, there was an increase of ssDNA overhangs from 0 to 8. Figure 5-8A presents the schematics of the above variants, with non-RF groups as control (where the RF groups were replaced with poly-T_4). For example, "4-RF + 4-DNA" has four sites of fluorous overhangs that were retained, and the other two sites were replaced with double-5nt sticky-ends. The hybrid system, therefore, contains 4-$(RF8)_2$ and 4-DNA overhangs.

Results shown in Figure 5-8B&C suggest that change of ssDNA overhangs induce more effect than the change of RF-oligos. When using fluorous only, samples appeared to be monomeric, showing that the full-loaded RF-oligos (6-RF+ 0-DNA) results in no more dimer formation compared with the non-RF control. However, due to the structural limitation of the wireframe origami, here the full-loaded RF-origami contains only 6 RF oligos. Previously in an asymmetric rectangle design, origami with 6-$(RF8)_2$ has a dimer yield of 5.5%. Despite the distance between each RF-oligos in the wireframe might be too far to benefit the association (17.68 nm, 52 bps between each vertex), it is reasonable to obtain 2.9% of the dimer with the use of 6 RF-oligos. The use of 8 ssDNA-overhangs could result products with 63% dimer, and the addition of fluorous has brought the yield to 82.2% Figure 5-8C, showing the combination of 2-RF and 8-DNA is the optimal candidate.

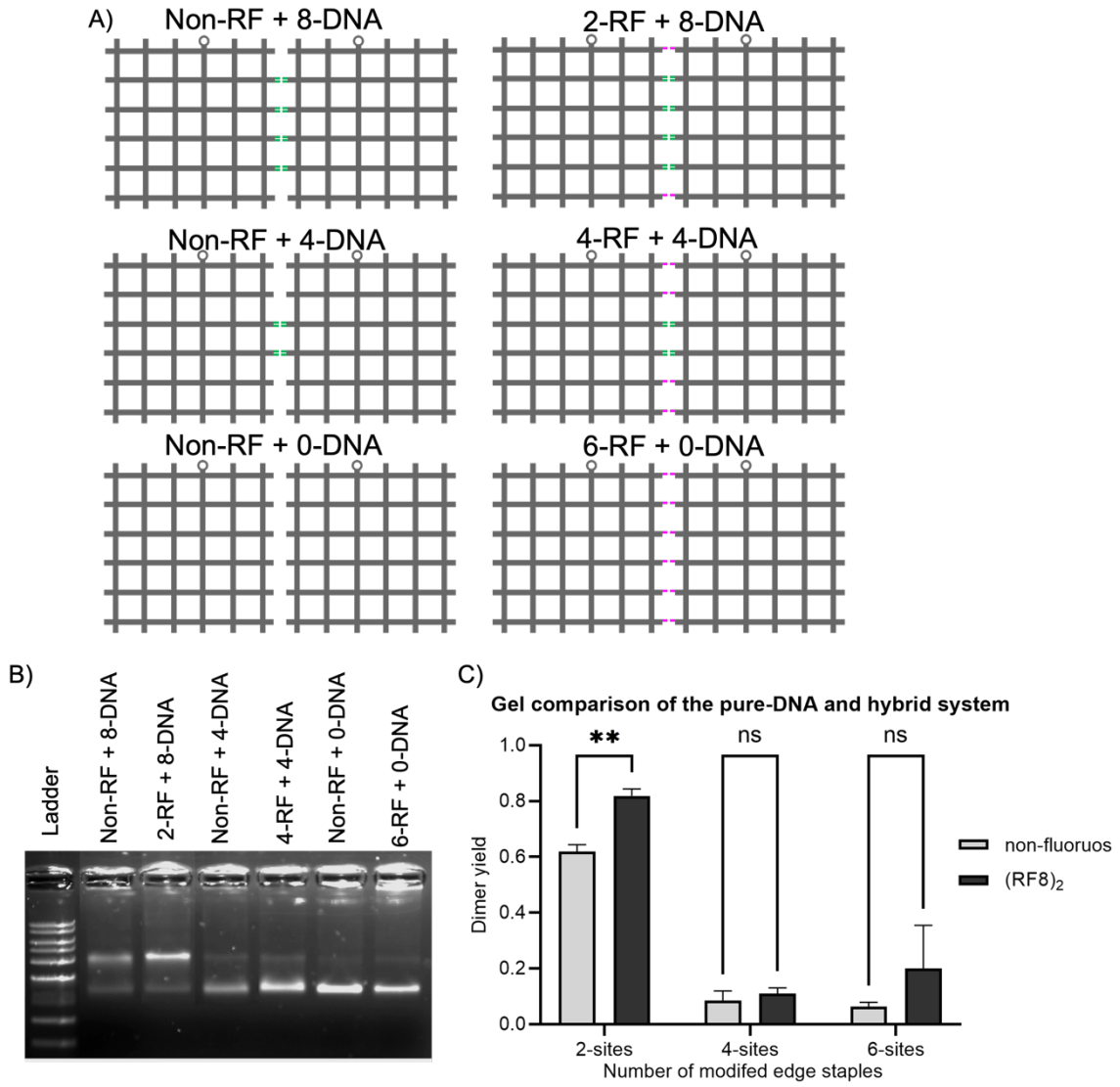

Figure 5-8 A) Schematic of the hybrid system on wireframe, with the non-RF groups as controls. B) &C) Gel image and analysis of above samples. Percentages in C) were approximate data, obtained from comparing the band density using ImageJ. From left to right, the data points are 63%, 8.5%, 5% for non-RF groups (green), 82.2%, 9%, 2.9% for RF-groups (pink). One-way ANOVA was used for the statistical analysis of the data, from left p= 0.009, 0.9593, 0.129. ns p >0.1, **p<0.01.

5.2.4.1 Position variant of 2-RF + 8-DNA

Thus, the position variants were tested, with the use of more accurate AFM analysis to compare the dimer yield. The AFM data agrees with the gel, showing the addition of fluorous results a slight dimer increase in a range of 5% to 10% (Figure 5-9A). The overall small improvement proves that the addition of the fluorous effect to the system shows significant difference, while in terms of the enhancement of the dimer yield was not quite promising. This may suggest the working of fluorous strands requires a high-density fluorous domain, as the strength presented here was less effective compared to the densely packed rectangle.

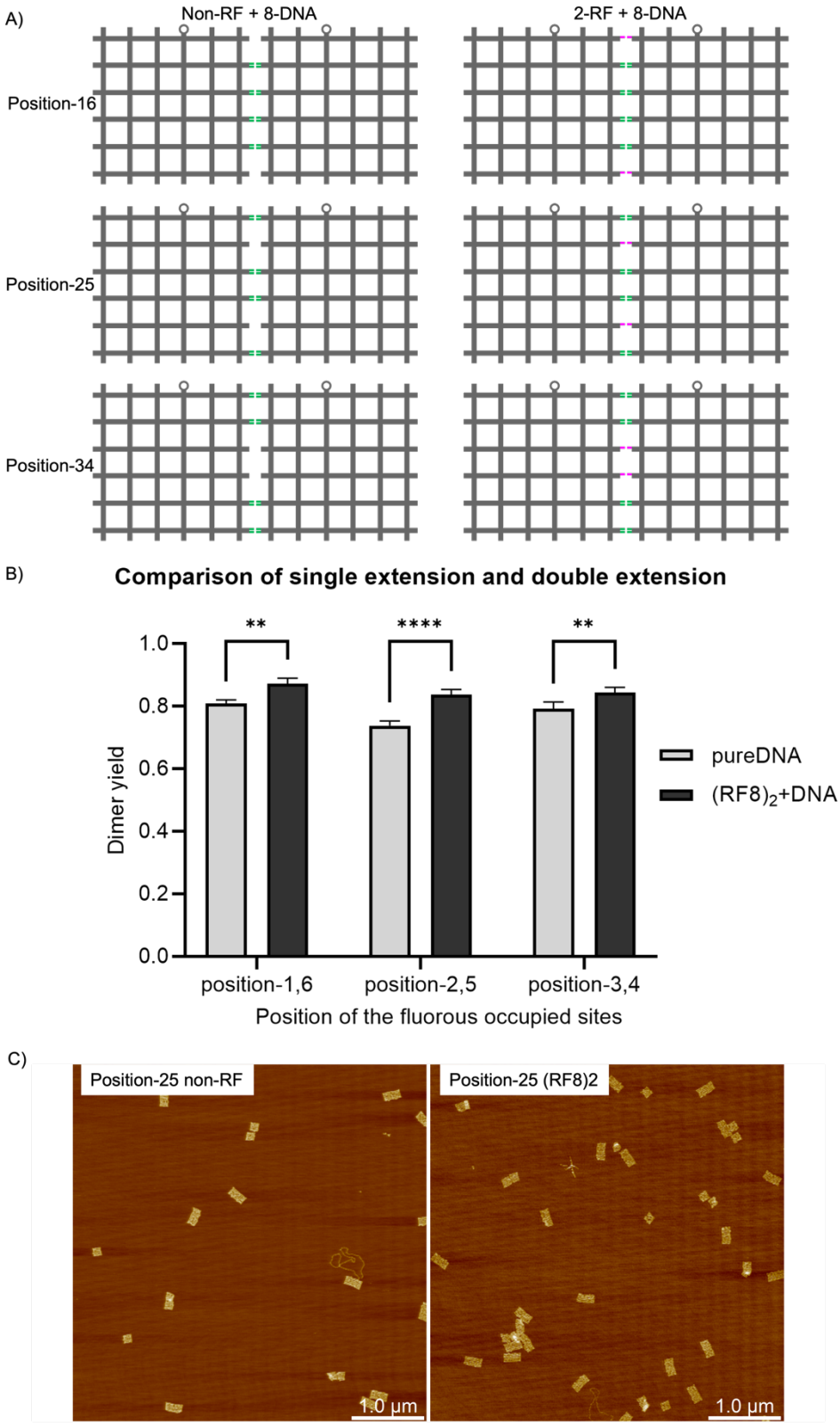

Figure 5-9 A) The layout of the hybrid linker system, each variant contains 4- (RF8)2 and 8-DNA overhangs. B) Gel images (left) and AFM analysis (right) of all samples shown in A). Data label for non-RF groups (green) from left to right were 81.7%, 75%, 80.9%; for RF groups (pink) were 88.4%, 84.9%, 85.5%. C) Example AFM images of non-RF and RF groups of position-25. One-way ANOVA was used for the statistical analysis of the data, from left p= 0.002, p<0.0001, p= 0.0091. **p<0.01, ****p<0.0001.

5.2.5 Conclusion and future work

To expand the toolbox of origami assembly and enrich the simplicity of the traditional DNA hybridisation method, non-specific chemical interactions are of interest. Results found in Chapter 4 has demonstrated that the fluorous effect can act as a linker strategy with promising impact. It suggests the fluorous effect can be an ideal auxiliary bridging method for the traditional sticky-ends hybridisation. Therefore, a hybrid linker system containing both fluorous and sticky-ends are desirable to explore. The challenge here is to balance these two interactions to achieve a specificity dominated, non-specificity stabilised dimerization.

This work was then built on a system composed of two different monomer designs. Through this strategy, conformations of dimers have used an indicator of showing the driven effect between origami tiles. A significant increase in dimer formations was observed when compares to an equivalent DNA-only system. This work proves that the inclusion of fluorous-oligos into the existing DNA nanotechnology toolkit is effective and the hybrid linker systems containing both specific and non-specific moieties can open up the traditional path for creating the larger, more stable constructs to date.

To expand the versatility of this hybrid system, it was then carried out on the wireframe design. Although not significantly, the work here also showed that the incorporation fluorous effect has a positive influence on dimer formation. Moreover, this work reveals an important impact factor - the fluorous density: the gap between every two sites on wireframe square is wider than square-based rectangle, thus the incorporation of fluorous on a wireframe is less efficient.

This work overall suggests that fluorous-modified oligos are a useful addition to the existing DNA-nanotechnology toolkit and that hybrid linker systems containing both specific and non-specific moieties may provide a route toward ordered networks of origami that are simultaneously larger, higher yielding and more stable than those that have been achieved to date. Furthermore, it showed that the double extension sticky-ends are way more efficient than the single extension. This may suggest that a more stable, and higher-yield dimer could form with the use of double-extended RF-oligos. Therefore, future work should focus on using RF-oligos with two-end modifications, which was not achieved in this work due to the cost and lengthy synthesis process.

Chapter 6 Quantum dot directed FRET on DNA origami

6.1 Introduction

The properties of luminescent quantum dots (Qdots) have exhibited potential to enable the inorganic-bioreceptor sensing materials [137]. Compared with organic dye molecules which often serve as donors/ acceptors in the FRET process, Qdots can expand the functional limitations of organic dyes such as short fluorescence lifetimes and susceptibility to photobleaching. As an alternative energy donor, Qdots have many advantages, such as their boarder excitation spectra, high emission quantum yields, narrow and tuneable photoluminescence, and resistance to photobleaching [138], [139]. For example, a Qdots-Cy3-Texas Red-Cy5 DNA tetrahedra has shown to have significant advantages in multiple-dye FRET system with there being a preferred transfer pathway, increasing the capability of harvesting energy and efficiency [140], suggesting that the DNA assisted Qdot-FRET is highly attractive. Although the assembly of Qdots onto DNA origami platform has been well-explored [141]–[145], Qdots directed FRET on DNA origami platform remains less-explored.

6.1.1 Context and aim of this chapter

This chapter focuses on the establishment of a multiple-chromophore FRET system, with Qdots as the donor and two organic fluorescent dye as subsequent acceptors. This proof-of concept work to investigate if Qdots (with high emission quantum yield) can direct the FRET with multiple acceptors on origami. Therefore, the work presented in this chapter hopes to:

1) Build Qdots-origami conjugate, which can be verified using agarose gel and AFM.

2) Determine if Qdots can achieve energy transfer to dye molecules though adjusting the arrangement.

6.2 Results and discussions

6.2.1 Incorporate FRET pairs onto DNA origami

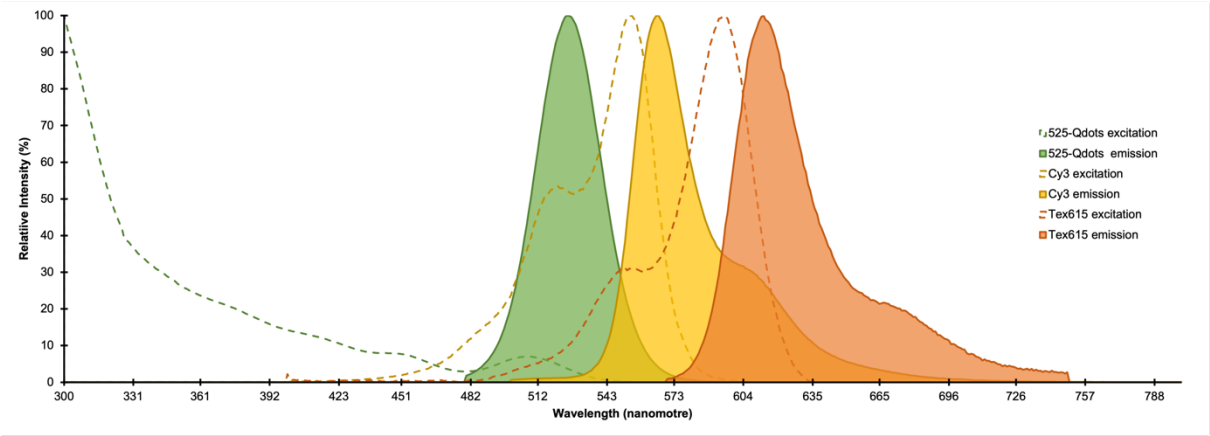

Figure 6-1 Excitation and emission spectra of selected FRET pairs. Qdot has an emission peak at 525 nm. Cy3 has an excitation peak at 554 nm, emission peak at 568 nm. Tex615 has an excitation peak at 569 nm, emission peak at 615 nm. Spectra obtained from fluorescence-spectra viewer on Thermo-Fisher website.

In order to incorporate Qdots on to DNA origami platform, 525-Qdots streptavidin conjugate (purchased from Thermo Fisher) with an emission peak at 525 nm was chosen as the primary donor of the system. According to the manufacturer, each 525-Qdots crystal has approximately 5 to 10 streptavidin, with streptavidin unit having the ability to bind four biotin molecules [146], [147]. Streptavidin is a biotin-binding protein that is commonly used to join biological and inorganic materials together. Thus, the incorporation of Qdots on to origami was achieved through interactions between the streptavidin-shell of the Qdots and the biotinylated-modified staple strands of the origami. Two fluorescent dyes, cyanine 3 (Cy3) and Tex615 were employed as acceptors. As shown Figure 6-1, the 525-Qdots can be excited along a broad range of wavelengths, and has a maximum emission at 525 nm, its emission wavelength overlaps with the excitation spectra of both Cy3 and Tex615. Cy3 has a peak emission at 568 nm which also overlaps with the Tex615 excitation wavelength.

Each chromophore was incorporated on to DNA origami structures through different linkers as shown in Table 6-1: 525-Qdots can be incorporated on DNA origami through biotin-streptavidin interaction; and dye molecules can be captured through DNA hybridisation.

Table 6-1 Modifications of staple strands to on capture sites.

Modifications on staple strands	allocated item
Biotin label	Streptavidin coated Qdots
$(CAA)_7$	Cy3-$(TTG)_7$
$(AAT)_7$	Tex616-$(ATT)_7$

The asymmetric rectangular origami was fabricated as previously stated using a M13 scaffold and 229 short staple strands, which included modified staple strands to position both the dye molecules and Qdots (Figure 6-2). Dye strands and Qdots-streptavidin were incubated subsequently after removing the excess staple strands. Dye strands were mixed with the purified, modified-DNA origami with dye capture overhangs in a 5:1 ratio (dye: dye capture) in TAE.Mg^{2+} buffer and incubated at RT for more than 12 hours to obtain sufficient binding. Qdots incubations were done after the attachment of dye molecules since the closeness of their binding sites and the relatively large scale of Qdots may be obstacles for dye binding if the Qdots are already attached. The streptavidin coated Qdots were then mixed with dye-decorated DNA origami in a ratio of 2:1 (in terms of the number of Qdots versus biotin sites) and incubated at RT for 2 hours.

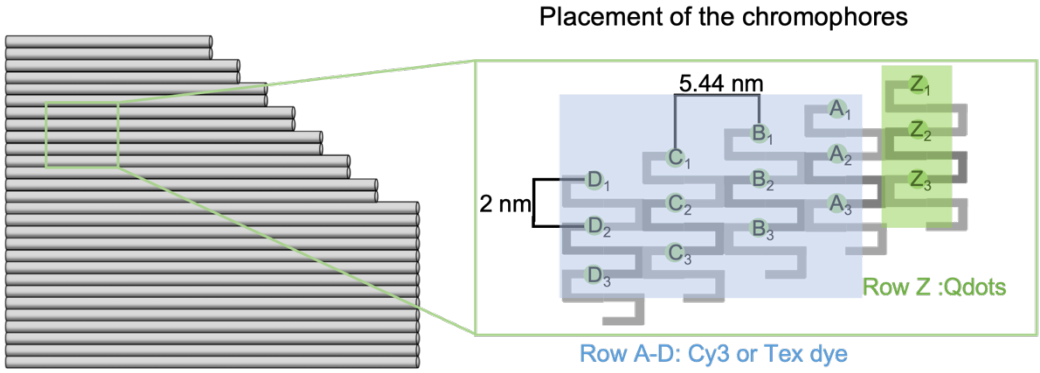

Figure 6-2 The origami platform and a 3 x 5 array for the placement of FRET pairs.

Schematics in Figure 6-2 highlights the position and layout of the capture sites. The 3 x 5 array is composed of 15 staple strands, where the strands in Z_1 to Z_3 were biotinylated and

thus used for the capture of Qdots. The remaining locations (A to D) was designed for dye capture with extended sequences. Any unused sites in the array were filled with unmodified staple strands. This way of arrangement and attachment allows for changes of dye patterns. Final origami concentration for fluorescence measurements was set to 5 nM. AFM imaging was performed in parallel to confirm their structures.

6.2.2 Trivalent-biotin sites guarantees higher Qdots occupancy compared with monovalent-

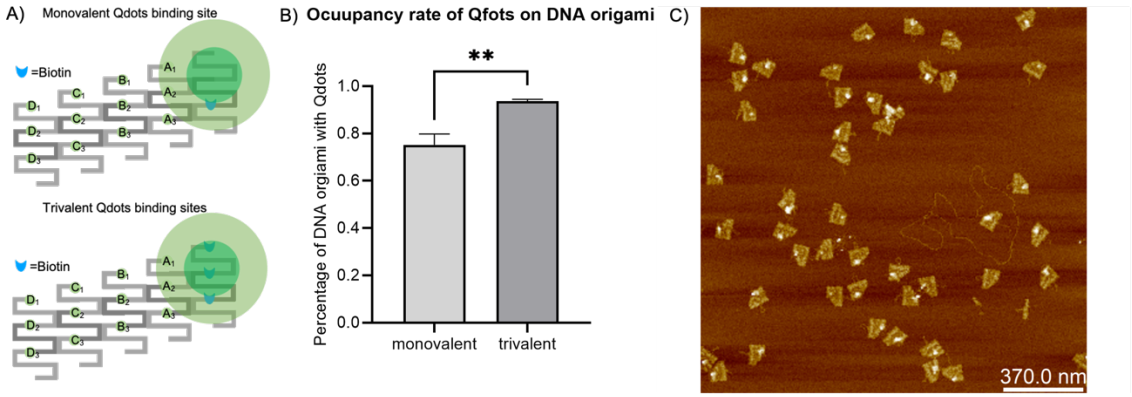

Figure 6-3 Occupancy rate of Qdots on DNA origami. A) Illustration of origami with monovalent and trivalent capture sites. B) AFM analysis of occupancy rates. monovalent: 75.2% ± 4.6%, trivalent: 93.6% ± 0.9%. t-test was used for statistical analysis, p=0.0024, **p<0.01.C) Example AFM images of origami with trivalent capture sites. Area with bright spot mean higher height as Qdots were conjugated.

It was anticipated that more biotin sites on the origami can increase the incorporation of Qdots. To verify this idea, origami with both one and three biotin binding sites were tested. As shown in Figure 6-3, due to the relative scale of the Qdots-Streptavidin and the closeness of biotin binding sites, both origamis (with monovalent and trivalent biotins) should capture no more than one Qdot. And the number of biotin sites should affect the qdots occupancy on DNA origami. The occupancy rate was assessed through AFM as shown in Figure 6-3B. It was observed that with the use of trivalent biotins, 93.6% origami tiles were incorporated with Qdots. This shows an improvement of 18.4% compared with origami with monovalent biotin binding sites, where only 75.2% origami were found to have Qdots attached. Figure 6-3C is an example AFM image of the Qdots-origami conjugates, where the white spot showing the height difference of Qdots and origami background. No origami with more than one Qdots was observed under AFM.

6.2.3 Two-chromophore system

Sample for fluorescent measurement was obtains through incubating origami tiles without further filtration, Qdots and dye strands in a 1:3:30 ratio (origami: Qdot capture strands: dye capture strands are 1:3:3). At first, the concern was the actual size of the Qdots might interfering with the energy transfer, thus patter ZA (distance = 5.79 nm) and the ZB (distance = 11. 58 nm) was applied for the two-chromophore system. According to the manufacturer's description, the streptavidin-Qdots conjugates has a core radius of 2 nm and an overall radius of 7.5 nm. Figure 6-4 shows the schematics of the 525-Qdots on DNA origami platform, and the predicted distance between Qdots and where dye will be placed on. From the core of the Qdots to row A, the distance is predicted as 9.47 nm and 13.80 nm for Qdots to row B.

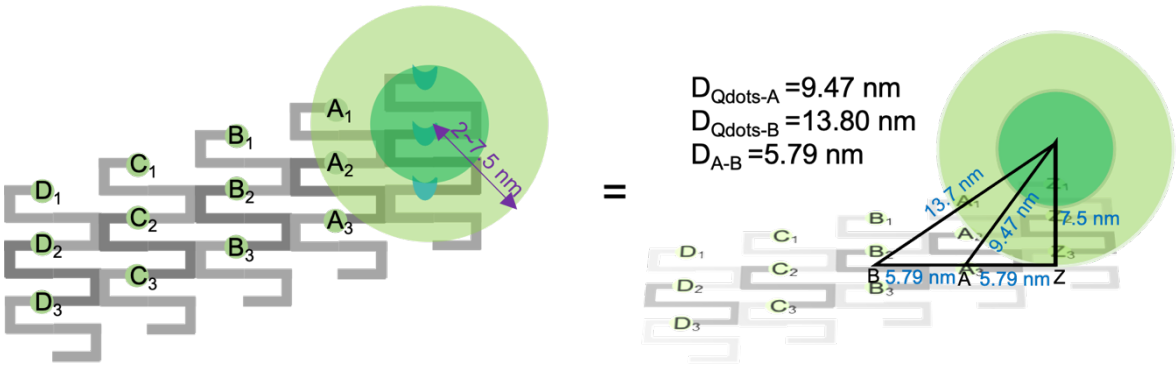

Figure 6-4 Schematics shows the distance between Qdots to dye molecules in the row-A and row-B. The radius of the Qdots core is 2 nm, the overall radius including the streptavidin shell is 7.5 nm [140].

Fluorescent measurement of samples was conducted using a microplate reader (Spark, Tecan). Data in Figure 6-5 were results of origami with two-chromophore system. When excite at 400 nm, for both Qdots-Cy3 pair (Figure 6-5A) and Qdots-Tex615 pair (Figure 6-5B), the spectra shows clearly that no FRET occurred. The fluorescence emission at ~525 nm, ~568 nm when excited the Qdots-Cy3 sample at 400 nm, 515 nm respectively, has proved the presence of the Qdots and Cy3. This suggest that the distance between these two molecules was too far to let FRET occur. As for the Cy3-Tex615 pair, the donor-acceptor distance is smaller than that in Qdots system, as there is no streptavidin in-between donor and acceptor to extend the distance. Spectra in Figure 6-5C seems to suggest the occurrence of FRET in both ZA and ZB pattern.

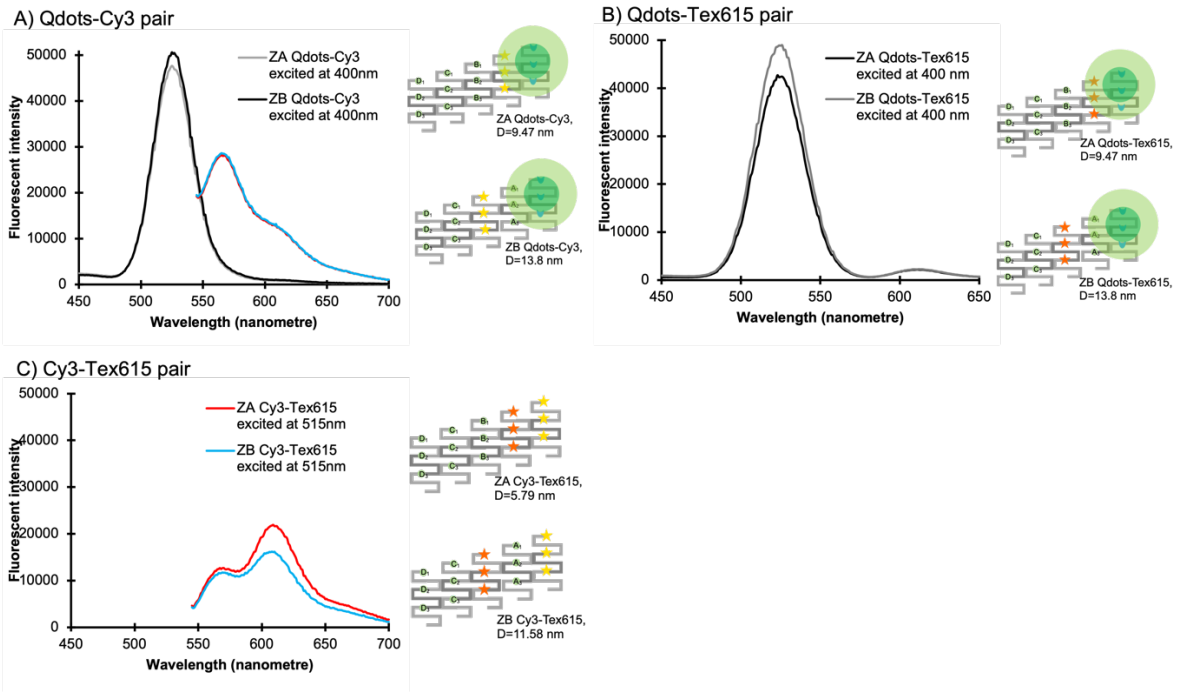

Figure 6-5 Fluorescent measurement of the emission spectra of the two-chromophore system on DNA origami with three different pairs. A), B), C) are Qdots-Cy3 pair, Qdots-Tex615 pair and Cy3-Tex615 pair respectively.

Hu et.al in 2019 has created a tetrahedral DNA-Qdots nanostructures using the similar medium [148], their system contains 525-Qdots, Cy3, Texas-red (similar to Tex615 used in this work), Cy5 and TAMRA. Their value of R_0 was used to predict the FRET efficiency in this system. The value of r and R_0 in each group was shown in Table 6-2. Thus, the FRET efficiency can be calculated follow the equation shown in Section 1.7.2. The donor-acceptor distance in pattern ZB is over 10 nm, in theory there should be no FRET occurred. One way to determine if the FRET occurred is to compare the fluorescence intensity of the donor in the absence and presence, thus this is suggested to investigate actual the actual transfer efficiency.

Table 6-2 The predicted FRET efficiency, föster distance and the donor-acceptor distance of each FRET pairs. The value of R_0 was obtained from [148].

FRET pairs	R_0 (nm)	r_{ZA} (nm)	E_{ZA}	r_{ZB} (nm)	E_{ZB}
Qdots-Cy3	6.7	9.47	11%	13.8	9%
Qdots-Tex615	5.4	9.47	3%	13.8	9%
Cy3-Tex615	5.1	5.79	32%	11.58	2%

6.2.4 Three-chromophore system

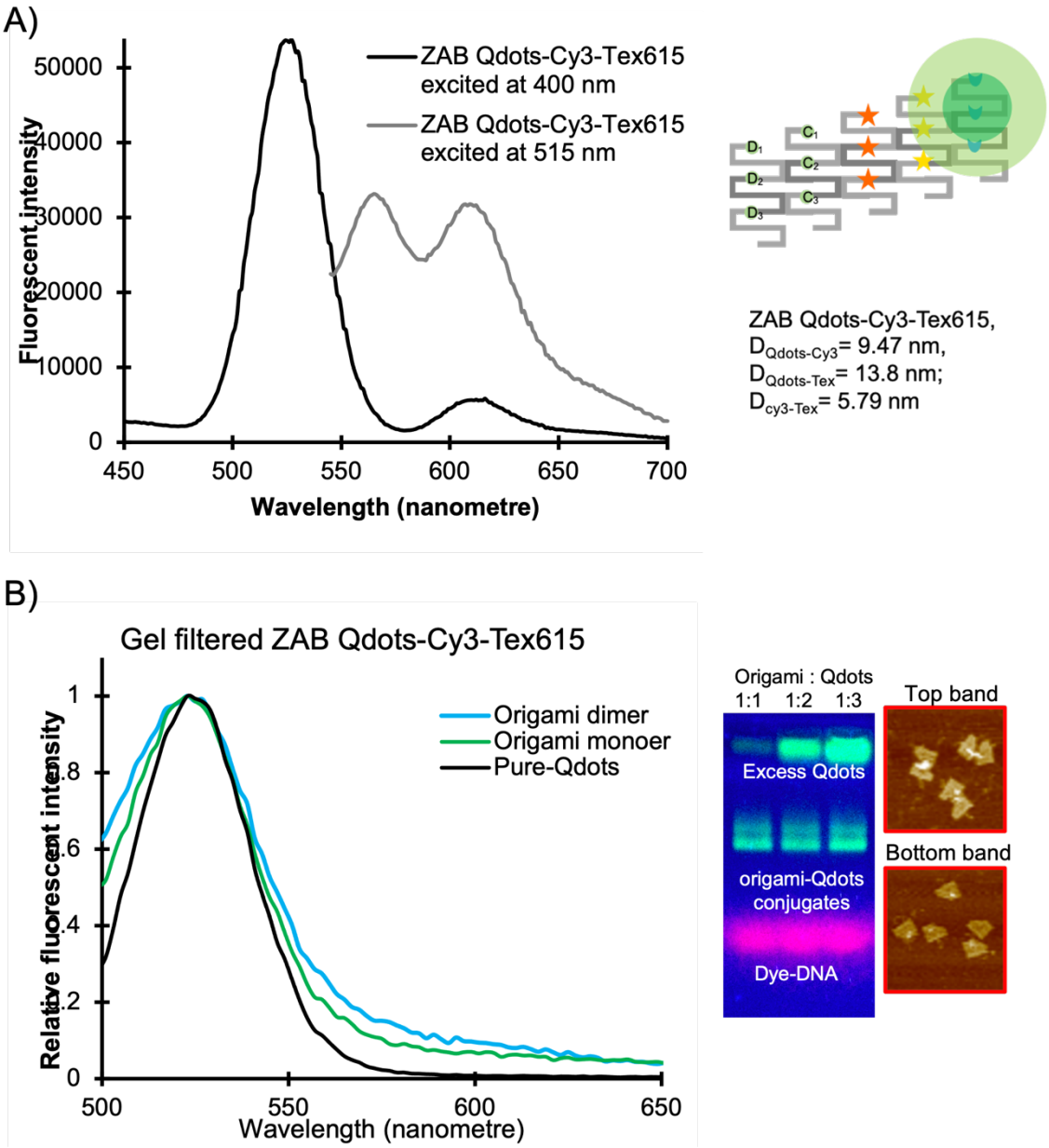

Figure 6-6 Data of the three-chromophore system. A) Qdots, Cy3 and Tex615 were arranged in ZAB pattern as shown in schematics; B) Emission spectra, agarose gel and AFM images of the three chromophores in ZAB.

Figure 6-6 shows a three-chromophore system contains 525-Qdots, Cy3 and Tex615 in a ZAB pattern. The distance between each two chromophores was labelled. When excite at 400 nm, the spectra suggest no FRET occurred (the emission peak at ~615 nm was a result of Tex615 was excited by the lamp). Again, the emission at ~568 nm and ~615nm when excite at 515 nm suggested the Cy3 and Tex615 dye molecules were presence. Figure 6-6B shows two species of the origami-Qdots conjugates. The 1% non-stained gel was run and imaged using an UV transilluminator. The final concentration of origami for gel

electrophoresis was set to 4 nM with a volume of 20 µL. As presented in Figure 6-6B, two distinct bands appeared in three samples. These two gel bands were cut, samples were extracted through the Gel extraction column following the instruction. AFM images suggested that the bottom band was monomeric Qdots-origami conjugates, and the top band was Qdots linked origami dimer, where each streptavidin has 4 binding sites that can interact with biotin on not only one origami. Sample extracted from the gel was also a cleaner system contains not excess Qdots or dye-ssDNA, and this three-chromophore system still performed no FRET signal.

6.2.4.1 Reduce the donor-acceptor distance by Qdots-Cy3 complex

As described above, the FRET efficiency is highly dependent on the acceptor-donor distance. For example, if r = 1.4 R_0, then the E_{FRET} = 11.1%; if r = 1.2 R_0, E_{FRET} =33.7%. One the other hand, placing multiple donors around one acceptor opens a light-harvesting effect funnelling the energy to acceptor, thereby enhancing the acceptors emission; while one donor surrounded by multiple acceptors, increases the pathway of energy transfer from donor and acceptors thus enhancing FRET efficiency. Hu and co-workers have constructed a tetrahedral DNA-Qdots Nanostructure, where the Cy3 emission was similar with this work, but it can afford the transfer to next dye. The system they used was multistep FRET and their ratio of Qdots to dye was 24:1, which reached the maximum coverage[148].

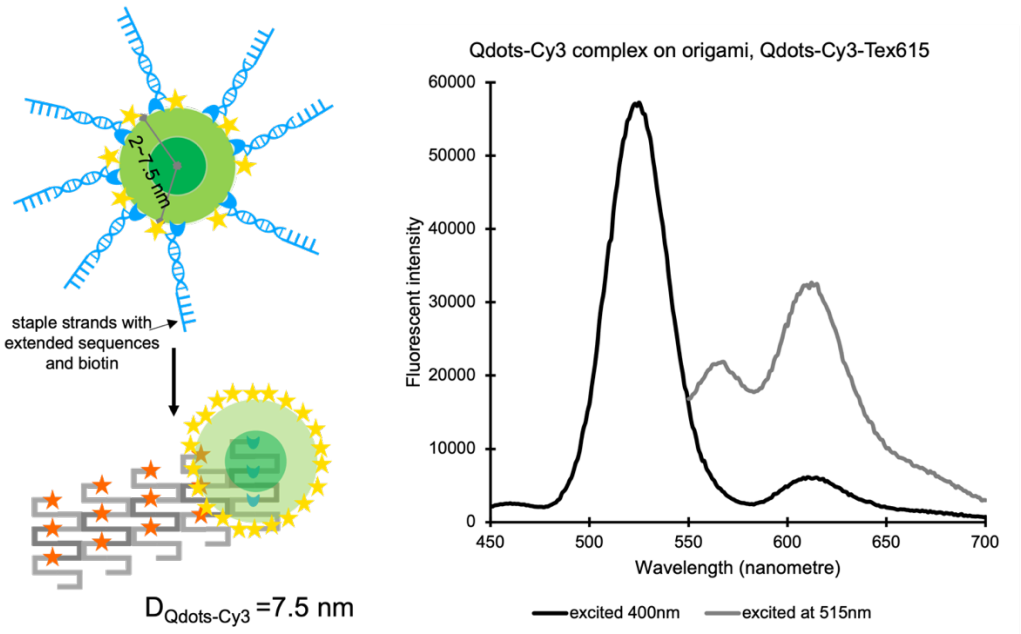

Figure 6-7 Left: illustration of Qdots-Cy3 complex and their arrangement on origami. Cy3 was directly attached on to the Qdots crystal, leaving unpaired strands segments to complement with origami. Right: FRET spectra of Qdots-Cy3 complex.

The Qdots-Cy3 crystal was designed to reduce the distance between two chromophores and at the same time enhance the ratio of donor to acceptor (Figure 6-7). To obtain the complex structure, biotinylated strands and Cy3 strands was equally hybridised, making a biotin-Cy3 duplex contains 16 nt unpair sticky-ends which then can be captured by extended sequences on origami. This duplex was then subsequently incubated with Qdots-streptavidin in a ratio of 24:1 to obtain a Qdots-Cy3 complex, and origami in a ratio of 1: 1. As illustrated in Figure 6-7, the distance between Qdots to Cy3 was 7.5 nm (r = 1.2 R_0, E_{FRET} = 33.7%). The distance between Tex615 to Cy3 was in a range from 0 to 15 (Tex615 in column A). However, the spectra still suggest no FRET occurred from Qdots to Cy3.

6.2.5 Pure Dye system in a checkerboard pattern

The streptavidin shell of the Qdots, associated with neglectable scale has impeded the energy transfer, added uncertainty to the donor-acceptor distance. A pure dye system contains only Cy3 and Tex615 molecules was used to investigate if checkboard board is a more optimal pattern than linear placement of FRET pairs.

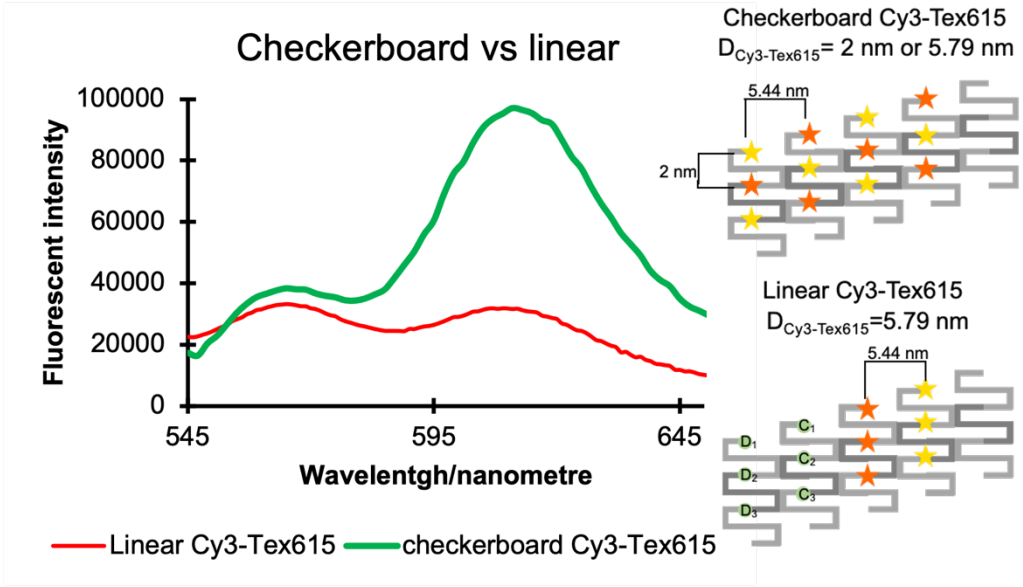

Figure 6-8 Pure dye system compares the checkerboard and linear pattern. Emission spectra was obtained by exciting at 515 nm.

As shown in Figure 6-8, a 3 x 4 checkerboard pattern composed of only two subsequent acceptors was tested in this system. In the linear pattern, the distance from Cy3 to Tex615 was fixed at 5.79 nm, leading to a FRET efficiency of 32% (Table 6-3). In the checkerboard pattern, Cy3 and Tex615 has two controlled distances of 2 nm and 5.79 nm, so the highest

FRET efficiency could reach 99.9%. It appeared in the spectra with a significant enhancement on the FRET efficiency from Cy3 to Tex615 in checkerboard pattern.

Table 6-3 The predicted FRET efficiency, föster distance and the donor-acceptor distance of Cy3 and Tex615.

Cy3-Tex615 arrangement	R_0 (nm)	r	E_{FRET}
Linear	5.1	5.79	32%
Checkerboard		2	99%
		5.79	32%

6.3 Conclusion and future work

The work carried out in this chapter was to investigate and establish a Qdots-directed FRET on DNA origami platform, through the construction of origami-based FRET system of Qdot525-Cy3-Tex615. This system uses Qdots as a donor, two fluorescent dyes as acceptors. Several dye patterns including linear, checkerboard and a Qdots-Cy3 complex were explored to optimize the energy transfer networks. However due to the streptavidin shell of the Qdots, acceptor dye molecules were always distant from the core of Qdots. This system was unable to obtain obvious FRET signal. Another discovery was when explore the pure dye system with different arrangements, the checkerboard pattern has been proven better than linear arrangement, with higher FRET efficiency.

A plan to complete this work is to obtain the absorption and the emission spectra of each chromophore to calculate its own R_0. The FRET efficiency can also be measured by compare the emission spectra of the donor with and without the presence of the acceptors. This work picked the Qdots with streptavidin shell for easy conjugation onto DNA origami construct, a preferable linker is desired if to further investigate Qdots-direct FRET sensor on DNA origami. Another direction is to explore the pure dye system with increased types of fluorescent dyes in checkerboard pattern, which has been demonstrated to improve the FRET efficiency.

Chapter 7 Conclusions & Future works

7.1 Conclusion

This thesis has focused on the fundamental research of DNA origami technology, with the aim to improve the assembly yield of origami super-structures by introducing novel connection methods. Study of dimerization reactions were carried out as these are the basic building-blocks of hierarchical assembly. Firstly, the factors which influence dimerization in DNA-only systems was explored by varying the number and the position of the sticky-end bridging overhangs. It was shown that dimer yield increases or remains steady when increasing the number of overhangs. For overhangs with equivalent base pairs, the single 10-nt resulted in stronger connections when compared to those with double 5-nt. Moreover, linker overhangs can work together when they were arranged in close proximity to one another. The impact of the layout becomes more significant with fewer bridging strands, as the minor difference could switch the dimerization reaction. It was also found that square-based origami with tightly packed helices is a better platform to study the interfacial impact factors of dimerization, as it minimizes the structural impacts.

Building on this work, the incorporation of fluorous tags on to an asymmetric rectangle was carried out. A set of systematic experiments has explored the effect of incorporation through two methods, the effect of changing the number of fluorous overhangs, and the effect of dimerization direction (edge-edge or face-face). It has found that, for the first time, the non-covalent fluorous-fluorous interaction can be used to connect origami tiles together, resulting dimers, trimers, and higher order polymers. The degree of polymerization can be tuned by the length of the fluorous tags, and the number of fluorous overhangs. Origami with higher fluorine content tends to produce higher-ordered assemblies. Among all species, the $(RF8)_2$ tag resulted in the most efficient dimerization, and with using 10-$(RF8)_2$ overhangs, the dimer rate reached to 70.8%, occupied about 93% of all attachment interactions. It was also found that the origami tends to seek a conformation that maximises the fluorous interactions when investigating the dimer distribution.

Fluorous compounds were shown to be a non-specific yet mobile linker system, which has the potential to act as an auxiliary strategy to assistant traditional sticky-ends linker strategies. Therefore, a hybrid linker system contains both sticky-ends and the fluorous effect was applied using 5-nt sticky-ends and $(RF8)_2$-tag. It is found that the specificity of the sticky-

ends can direct the proper assembly of two origami tiles, and the non-specificity of fluorous effect can strengthen the interaction, stabilising the dimer. A significant increase in formation of heterodimers was observed when compared to an equivalent DNA-only system, increasing from 18% to 76.5% with the addition of 4-$(RF8)_2$ onto 10-DNA system. The idea of using strong yet mobile interactions, combined with highly specific interactions, opens a novel avenue of creating larger, more stable origami constructs.

An origami-based sensor was also investigated. A Qdot-directed FRET system was established on an origami platform. As for the incorporation of Qdots onto origami through biotin-streptavidin interactions, trivalent biotin binding sites captured more Qdots than monovalent binding site. Utilising the crosstalk between dyes, various patterns (including linear and checkboard patterns) for demonstrating the sensitivity and versatility were explored. The construction of Qdot-Cy3 complexes on the origami maximized the FRET efficiency from Qdot to Cy3, allowed the creation of a FRET system with multiple energy transfer channels.

7.2 Future works

As the use of the fluorous effect to connect origami tiles together still in its infancy, there are many ways to expand the utility. For example, it is shown that using the same number of sticky-ends, double extensions behave much more efficiently than single extensions, indicating that the fluorous tag employed at both extensions has potential to exhibit even higher efficiencies than were achieved in this thesis. The aim is to achieve stable assembled product with high yield, with the use of fewer bridging overhangs. Another inspiration of fluorous incorporated origami is to control the deposition orientation of single-sheet origami[112]. When deposit origami with fluorous decorated on one face and functional materials on the other face, on to a fluorous functionalised surface, the affinity of fluorous has a chance to results more origami landing with the functional face towards the air. As for the exploration of FRET on origami, there was an intention to further explore the multiple dye system with different patterns combined with the strand displacement to create a finger-print sensor, which unfortunately was paused due to the lack of time.

Chapter 8 Appendices

8.1.1 Staples for wireframe square

WF5x5-2	TACCTTTTTTTTTTAATGGATTTACGAGCATTTTTGTAGAAACCACCAAG
WF5x5-3	CCCATCCTAAAACAGTACAT
WF5x5-4	AAAAATAATATAAATCAATATATGTGAGTGAACCTGAACAAG
WF5x5-5	TCAACATTTTATAGATAAGTTAACCTTGCTTTTTTCTGTAAATCGGAAAA
WF5x5-6	AGATTATTTTGAGCCGTCAAAATAAAAGGGATTTTCATTCTGGCCTAAGA
WF5x5-7	ATACGTTTTTGGCACAGACATTGAAAGGAATTTTTTGAGGAAGGTCTAAT
WF5x5-8	TATAACTTTTTATATGTAAATGAGAATCGCCTTTTATATTTAACATTCGA
WF5x5-9	TCAAGATTTTGTAATCTTGAAAAAAAAGGCTTTTTCCAAAAGGAGTTCGA
WF5x5-10	GGTGAATTTTTTTCTTAAACTGAAAGAGGACTTTTAGATGAACGGCTTCA
WF5x5-11	TTAAAGTTTTGCCGCTTTTGTCATCGCCTGATTTTTAAATTGTGTGCCGG
WF5x5-12	AGCTTGCTCCTTTAATTGTATCGTTCTGACC
WF5x5-13	TGAAAGCGAACAGAGATAGAACCCGTTTATC
WF5x5-14	AAGACAAAGAATAAAGCCAACGCTCAACAGTAATCCAATCGC
WF5x5-15	AGGGCTTAATTGCTGATGCA
WF5x5-16	GCCAGTTTTTAATAAGAGAATTATCAAAATCTTTTATAGGTCTGAGGTTA
WF5x5-17	AGAATATTTTACATAAAAACACACCCTGAACTTTTAAAGTCAGAGACATT
WF5x5-18	ACAAATTTTTTCTTACCAGTACGCGAGAAAATTTTCTTTTTCAAAATTTA
WF5x5-19	AAATATTTTTCAAACCCTCAGCGAACTGATATTTTGCCCTAAAACCAGAA
WF5x5-20	GAGGCATTACGCCAACATGTAATCGGGAGAA
WF5x5-21	TTAACTGAAGGGAAGCGCATTAGATTAGGCA
WF5x5-22	GAGTAGTTTTTAAATTGGGCTGGGATTTTGCTTTTTAAACAACTTGGAAC
WF5x5-23	AACTAATTTTAGGAATTGCGGTAACAAAGCTTTTTGCTCATTCAGAGAAC
WF5x5-24	AGAGTTTTTTGCAGCAAGCGCCTGTTTGATGTTTTGTGGT
WF5x5-25	GATAAATTTTACAGAGGTGACCACGCTGAGATTTTGCCAGCAGCAACCTC
WF5x5-26	ATGGTTTTTTTGAAATACCGATAAACACCGGTTTTAATCATAATTGTTAT
WF5x5-27	CTAAAGTTTTTTTTGTCGTCGTGAATTACCTTTTTTATGCGATTTGTTTA
WF5x5-28	ATTTTCTGTATTGAGATGGT
WF5x5-29	TTAGTAAATGATTAATTTCAACTTTAATCATTTTTCCAGACG
WF5x5-30	TAAAAATAGAGTGAGAATAGAAATCAACAGT
WF5x5-31	TTCAGCGCCGAACGAACCACCAGATCGCCAT
WF5x5-32	TTTTCACGTTGATATTCATTACCCAAATCAACAATAATAATT
WF5x5-33	AAAATCTCCACAAGAACCGG
WF5x5-34	GAAACACCTGAATAAGGCTTGCCCCCAGCAG
WF5x5-35	GCGAAAATGTCCACGCTGGTTTGCCTGACGA
WF5x5-36	TATGCAACTATTTTTAAGAA
WF5x5-37	TAGCCGAACATGTAGCTCAACATGTTTTAAAAAGTAAGCAGA
WF5x5-38	TTTTTAGAGCTTAATTGCTGTTTTAATATAATGCAAGTTACCAGATTTTAGGAA
WF5x5-39	TCGCAATTTTATGGTCAATATAAAGATTCAATTTTAAGGGTGAGACAGAG
WF5x5-40	AGCCCAAGTACGGTGTTTTTCTGGAAGTTTCATTCTTTT
WF5x5-41	TTTTCATATAACAGTTGATTTTTTCCCAATTCTGCCACA

WF5x5-42	AGAATTTTTTGAGTTAAGCCATAGCTATCTTTTTTACCGA
WF5x5-43	GAGAGATAACCGAACGAGTAGATTTAGTTTGCGCTAATATCA
WF5x5-44	ACCATTAGATGGTAATTGAG
WF5x5-45	AAATAGCACAATAATAAGAGCAAGTTTAGTA
WF5x5-46	TCATATGCACTAGAAAAAGCCTGAAACAATG
WF5x5-47	CAGTATGTAGGCGTTAAATAAGAACCGTGTG
WF5x5-48	ATAAATATAGCAAACGTAGAAAATTATTACG
WF5x5-49	GCATGATTTTTTAAGACTCCTACATACATAATTTTAGGTGGCAACAGGAA
WF5x5-50	AGCCCATTTTATAGGAACCCTACAAACTACATTTTACGCCTGTAGTAGAC
WF5x5-51	GTAAAATGTTCATTCCACAGACAGCCCTCATAGGGGGTAATA
WF5x5-52	AGTTAGCGTAGTTTTGCCAG
WF5x5-53	AAGCAAACTCCTAATAACGGAATACCCAAAAGACCAGACCGG
WF5x5-54	AACAGGTCAGGGAAACGCAA
WF5x5-55	AGTGTAGGTCGACTCTTTTTAGAGGATCCCCGGGTTTTT
WF5x5-56	TTTTACCGAGCTCGAATTCGTTTTTAATCATGGTGGAAA
WF5x5-57	GCCGGCTTTTGAACGTGGCGCGCTAGGGCGCTTTTTGGCA
WF5x5-58	CATAACCCTCTAAGAACTGGCTCATTATACCAGCAACACTAT
WF5x5-59	AGTCAGGACGGCATAGTAAG
WF5x5-60	AGCTTGACGGCATAGCTGTT
WF5x5-61	CCCCGATTTAGTCCTGTGTGAAATTGTTATCCTAAAGGGAGC
WF5x5-62	AATACACAAGCGAAAGGAGCGGGAGAAAGGA
WF5x5-63	AGGGAAGATAAAACACTCATCTTGGCAAAAG
WF5x5-64	CTGCGCGTAACGTGCCAAGCTTGCATGCCTGCAGCGGTCACG
WF5x5-65	CACCACACCCACGACGGCCA
WF5x5-66	TTTTGGTTTTCCCAGTCACGTTTTACGTTGTAAAGCCGCGCTTAATTTTTGCGC
WF5x5-67	TAACGTTTTTGCTTTCCTCGCCGATTAAAGGTTTTGATTTTAGACTGCCG
WF5x5-68	AATATATTTTATCCTGATTGAACCGTTGTAGTTTTCAATACTTCTAAGAA
WF5x5-69	CTCAAATTTTCTATCGGCCTCCAGAAGGAGCTTTTGGAATTATCATCATC
WF5x5-70	TCCGAGGCGGTTTGCGTTTTTATTGGGCGCCAGGGTTTT
WF5x5-71	TTTTTGGTTTTTCTTTTCACTTTTCAGTGAGACGCTGAG
WF5x5-72	GCCTGGCCGGCAACAGCTGATTGCCGGAACA
WF5x5-73	ACATTATTAATAAAACGAACTAACCTTCACC
WF5x5-74	AAGAAATTTTAATCTACGTTACAGGTAGAAATTTTGATTCATCAGTTGAGTTTT
WF5x5-75	TTTTCAGTCGGGAAACCTGTTTTTCGTGCCAGCTTAGCC
WF5x5-76	CGAGATTTTTAGGGTTGAGTAAAGAACGTGGTTTTACTCC
WF5x5-77	ACTACGTTTTTGAACCATCATAAAGCACTAATTTTATCGG
WF5x5-78	AACCCGCTCACAATTCTTTTCACACAACATACGAGTTTT
WF5x5-79	AACGTTTGCGTTGCGCTTTTTCACTGCCCGCTTTCTTTT
WF5x5-80	ATCAAAAGAAGCATTAATGA
WF5x5-81	ATCCCTTATAAATCGGCCAACGCGCGGGGAGAAATCGGCAAA
WF5x5-82	CCAGGCGACAAGAGTCCACTATTGTTGTTCC
WF5x5-83	AGTTTGGACATAGGCTGGCTGACTGTACAGA
WF5x5-84	ACCCTCAGCAGAAAGTACAACGGAGATTTGTACGGGATCGTC
WF5x5-85	CGAAAGACAGAGCGCGAAAC

WF5x5-86	CCCAGCTTTTGATTATACCACATCGGAACGATTTTGGGTAGCAACTTTCA
WF5x5-87	TGAGGATTTTAGTTTCCATTGCACCAACCTATTTTAAACGAAAGATGACC
WF5x5-88	AAAGACTTGGCTACAGAGGCTTTTCACTTGC
WF5x5-89	CTGAGTAGTTGATTAGTAATAACAGAGGACT
WF5x5-90	AGAGCGGTAATGCCACTACGAAGAAACGGG
WF5x5-91	TAAAATACGGAGCTAAACAGGAGGTTAGAATC
WF5x5-92	TTTGACGAGCGAAGGGCGATCGGTGCGGGCCACTATGGTTGC
WF5x5-93	TCTTCGCTATCAGGGCGCGT
WF5x5-94	GAAGGCTTTTTTATCCGGTAATCAGAAAAGCTTTTCCCAAAAACAGGAAGTTTT
WF5x5-95	AGCAAATCAGAATTTTTGTT
WF5x5-96	GCCCAATAGCAAAATCAGCTCATTTTTTAACCTCATTACCGC
WF5x5-97	CCGGTTGATATTCTAAGAAC
WF5x5-98	TCATATGTACCGCGAGGCGTTTTAGCGAACCTAGCATGTCAA
WF5x5-99	TTTTATTAATGCCGGAGAGGTTTTGTAGCTATTTAGAGC
WF5x5-100	CTAATTTTTTTGCCAGTTACAAATAAGAAACTTTTGATTT
WF5x5-101	AACGGGTTTTTATTAAACCAATGATGAAACATTTTAACATCAAGATGAAT
WF5x5-102	TAATCATTTTGTGAGGCCACTAGAACCTACCTTTTATATCAAAATTGCAT
WF5x5-103	ATCGCGTTTTCAGAGGCGAATTTTTATTTTCTTTTATCGTAGGAAAATAG
WF5x5-104	TGAGAAGTGTACTCCAGCCAGCTTTCCGGCACGCCAGAATCC
WF5x5-105	CCGCTTCTGGAGGAACGGTA
WF5x5-106	AAGCAAGCCGTTATTCATTT
WF5x5-107	TCATCGAGAACCAATTACCTGAGCAAAAGAAGAGTACCGCAC
WF5x5-108	TTATCATTATCAATAATCGGCTGTTAGTTGC
WF5x5-109	TATTTTGCAAGCCTTAAATCAAGATCTTTCC
WF5x5-110	CTTGCGTTTTGGAGGTTTTGACCCAGCTACATTTTATTTT
WF5x5-111	ATCCTGCCTGAGAGTCTTTTTGGAGCAAACAAGAGTTTT
WF5x5-112	TTTTAATCGATGAACGGTAATTTTTCGTAAAACTCCCGA
WF5x5-113	TCAGGTCATTGAATCTTACC
WF5x5-114	GCGTCTTTCCTTGAGAGATCTACAAAGGCTAAACGCTAACGA
WF5x5-115	TTTGTTGATATTCAACTTTTCGTTCTAGCTGATAATTTT
WF5x5-116	CCCAATCCAAAATAAACAGCCATAATGCAGA
WF5x5-117	TTTTAATTTTAAGTTTGAGTAGCCATTGCAATTTTCAGGAAAAACTCGTC
WF5x5-118	ACGCTCAAGCTCATGGAAATACCTTCGCTGA
WF5x5-119	AAGTTTTTGCTCCATGTTACTTACGAAATCC
WF5x5-120	TTTTCCGGAAGCATAAAGTGTTTTTAAAGCCTGGGGCCC
WF5x5-121	GCGACCTTGGGGTCGAGGTGCCGCCCAAATC
WF5x5-122	TCAGGGCGATGGTGCCTAAT
WF5x5-123	AAAACCGTCTAGAGTGAGCTAACTCACATTAACAAAGGGCGA
WF5x5-124	AACGAGTTTTGCGCAGACGGCAACAACCATCTTTTGCCCACGCATGGGAG
WF5x5-125	GGCTTGCAAACCGATATATTCGGACATTTTG
WF5x5-126	CCGACAATGATCAATCATAA
WF5x5-127	CGATAGTTGCGGGGAACCGAACTGACCAACTTAGCTTGATAC
WF5x5-128	TGAAATTTTTGGATTATTTAAGACTTTACAATTTTACAATTCGACATTAA
WF5x5-129	CATAGCTTTTGATAGCTTAGTGTCCAGACGATTTTCGACAATAAAGTTTA

WF5x5-130	ACGCGCCTCAACATGTTCAGCTATTATTTAT
WF5x5-131	AAAGTAATTCATTAAGACGC
WF5x5-132	CGACAAAAGGTTGAGAAGAGTCAATAGTGAATTATAAAGTAC
WF5x5-133	ACCATCAATATTAACGTCAA
WF5x5-134	GCAGCCTTTAAAGGCCGGAGACAGTCAAATCAAATGAAAATA
WF5x5-135	ACCACGGAATAAGCAAAGCG
WF5x5-136	AAAGATTAAGATATAAAAGAAACGCAAAGACGATTGCATCAA
WF5x5-137	TATTTTTTTTGTCACAATCACCGCCACCCTCTTTTAGAACCGCCAGAGAA
WF5x5-138	TAGGTGTTTTTATCACCGTAAGACAAAAGGGTTTTCGACATTCAAGGAAA
WF5x5-139	CCAGCGCCAACTCAGGAGGT
WF5x5-140	CATATGGTTTATTAGTACCGCCACCCTCAGAAATAGAAAATT
WF5x5-141	AGTTAATTAAGGTAAATATTGACCCGATTGA
WF5x5-142	GGGAGGGTCATCTTCTGACCTAATATATTTT
WF5x5-143	TTATTCTTTTATTAAAGGTGTGCTCAGTACCTTTTAGGCGGATAACGGAA
WF5x5-144	TAAGAGTTTTGCTGAGACTCGGAATTAGAGCTTTTCAGCAAAATCGGAAA
WF5x5-145	GAGCCATTTGCTCAAGAGAA
WF5x5-146	GTCACCGACTTGGATTAGGATTAGCGGGGTTTAATTATCACC
WF5x5-147	GCAAGGCCACCAGTAGCACCATTCCTCCGGC
WF5x5-148	TTAGGTTGGAGACTACCTTTTTAAACCATTA
WF5x5-149	CGTCACTTTTCAATGAAACCTAAACAGTTAATTTTTGCCCCCTGCAGTAT
WF5x5-150	GGTAATTTTTAAGTTTTAACGAATCAAGTTTTTTTGCCTTTAGCGTCGGT
WF5x5-151	AGTAGCGACAGGGGTCAGTG
WF5x5-152	GCACCGTAATCCCTTGAGTAACAGTGCCCGTAATCGATAGCA
WF5x5-153	CGGCATTTTCAGACTGTAGCGCGTTCCCTTA
WF5x5-154	GAATCCTTTCGCTATTAATTAATTTTTTCAT
WF5x5-155	CATAGCTTTTCCCCTTATTACTGAATTTACCTTTTGTTCCAGTAAGTACT
WF5x5-156	CACAAATTTTCAAATAAATCCGGAACCAGAGTTTTCCACCACCGGAACCG
WF5x5-157	TCAAAATCACCTCATTAAAG
WF5x5-158	TCTTTTCATAACCAGAATGGAAAGCGCAGTCTGCGTTTGCCA
WF5x5-159	ACCCTCAGAACCGCCTCCCTCAGATTTAACA
WF5x5-160	ATTTCATTAAACAAAATTAATTACAGCCGCC
WF5x5-161	CCACCCTTTTTCAGAGCCACGAGCCGCCGCCTTTTAGCATTGACAATATT
WF5x5-162	AATATACACCAGAACCACCACCACACCCTC
WF5x5-163	GATTTTTTTTCAGGTTTAACTACATCGGGAGTTTTAAACAATAACCCGTC
WF5x5-164	AGAGCCGCCAGTAACAGTACCTTTGTCAGATG
WF5x5-165	GAGTAACAACGGATTCGCCT
WF5x5-166	ATACCAAGTTTCATCAACATTAAATGTGAGCGATTGCTTTGA
WF5x5-167	TTTTCAGGGACCCCTCAAAT
WF5x5-168	TTCAGAAAACCCCTCAGAGCCACCACCCTCAGCTTTAAACAG
WF5x5-169	CAACAGTGGGCGGTCAGTATTAACGAGTTTC
WF5x5-170	GTCACCAGATGTACCGTAACACTACCGCCTG
WF5x5-171	GAGAGGGTGCATCACCTTGCTGAAATGAAAA
WF5x5-172	ATCTAAATGATATAAGTATAGCCGTGCCGTC
WF5x5-173	AAATCAACAGATATTTTTGA

WF5x5-174	GGTCAGTTGGCATGGCTATTAGTCTTTAATGCATCAATATCT
WF5x5-175	ACTAACAATATCTAAAATATCTTTATTCTGA
WF5x5-176	AACATGAACTATTTCGGAACCTATTAGGAGC
WF5x5-177	TAGAAGTATTCATTGGCAGA
WF5x5-178	ATTTGAGGATTTTCACCAGTCACACGACCAGTTAGATAATAC
WF5x5-179	CGAACGTTAACTCGTATTAAATCTTGATGAT
WF5x5-180	ACAGGAGTGCGTCATACATGGCTTCTTTGCC
WF5x5-181	AAAGAAACCATGCTGGTAAT
WF5x5-182	TTTTGCGGAACATCCAGAACAATATTACCGCCAACATTATCA
WF5x5-183	ATGGCAATTCATATTCCTGATTACAGACGAT
WF5x5-184	TGGCCTTGGGAGGTTGAGGCAGGTTCAGATG
WF5x5-185	ACTTCTGAATAAGTCTGTCCATCACGCAAATTTTTGGATTAT
WF5x5-186	ATGGAAGGGTCGAGTAAAAG
WF5x5-187	ATCGTAACCGTATTTGCACG
WF5x5-188	TAAAGAAATTCACGTTGGTGTAGATGGGCGCTAAAACAGAAA
WF5x5-189	TTTTATTGTATAAGCAAATATTTTTTTAAATTGTAAACGTTTT
WF5x5-190	TTTTTTAATATTTTGTTAAATTTTATTCGCATTAATATA
WF5x5-191	GAACGCTTTTCATCAAAAATAATTCTTTT
WF5x5-192	TTTTGCGTCTGGCCTTCCTGTTTTTAGCCAGCTTACAAA
WF5x5-193	GGATTCTTTTTCCGTGGGAACAAACTTTT
WF5x5-194	TTTTGGCGGATTGACCGTAATTTTTGGGATAGGTGCGTA
WF5x5-195	CTGCCATTTTGTTTGAGGGGACGACTTTT
WF5x5-196	TTTTGACAGTATCGGCCTCATTTTGGAAGATCGCTTTTA
WF5x5-197	GAAACCTTTTAGGCAAAGCGCCATTTTTT
WF5x5-198	TTTTCGCCATTCAGGCTGCGTTTTCAACTGTTGGACGTA
WF5x5-199	CGCTATACGCCAGCTGTTTTGCGAAAGGGGGATGTTTTT
WF5x5-200	TTTTGCTGCAAGGCGATTAATTTTGTTGGGTAACGCCAGTTTT
WF5x5-201	TTTTTTTTGATAAGAGGTCATTTTTTTTTGCGGATGGCTTTTT
WF5x5-202	ACCGAGATTAGAGAGTTTTTACCTTTAATTGCTCCTTTT
WF5x5-203	TTTTGCGTTTTAATTCGAGCTTTTTTCAAAGCGAAACTG
WF5x5-204	GCCCGATTTTAAGACTTCAAATATCTTTT
WF5x5-205	TTTTGTCTTTACCCTGACTATTTTTTATAGTCAGAAGTT
WF5x5-206	TGACCATTTTTAAATCAAAAATCAGTTTT
WF5x5-207	TTTTGAATCGTCATAAATATTTTTTCATTGAATCTAGCA
WF5x5-208	TGGATATTTTGCGTCCAATACTGCGTTTT
WF5x5-209	TTTTAATAGCGAGAGGCTTTTTTTTGCAAAAGAAACGAT
WF5x5-210	CCAGACTTTTGACGATAAAAACCAATTTT
WF5x5-211	TTTTTACATAACGCCAAAAGTTTTGAATTACGAGTTGGG
WF5x5-212	TTTTATTTAGGAATACCACATTTTTTCAACTAATGCAGATTTT

8.2 Staples for asymmetric rectangle

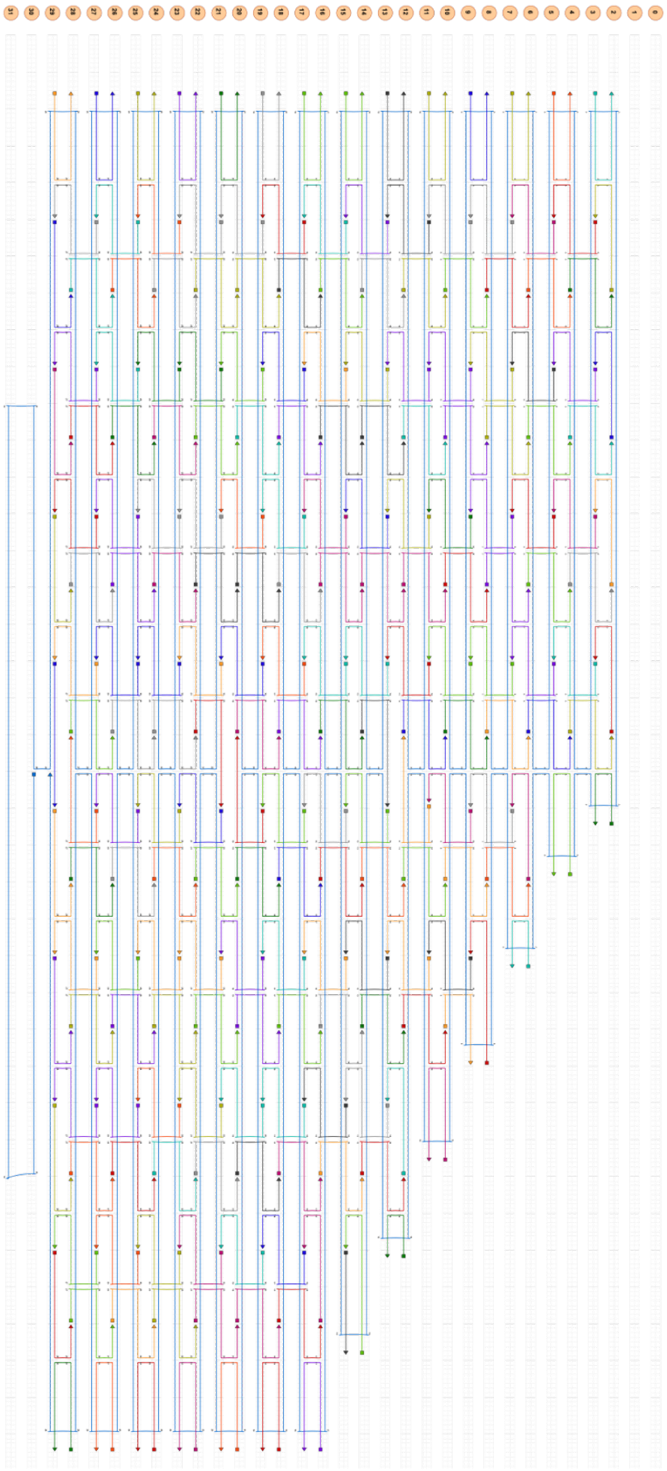

Figure 8-1 caDNAno design of the asymmetric rectangle

3[12]2[12]	TTTTATAAATCCTCATTAAATGATATTCACAAACAATTTT
5[12]4[12]	TTTTTATAAGTATAGCCCGGCCGTCGAGAGGGTTGATTTT
7[12]6[12]	TTTTAACTTTCAACAGTTTCTGGGATTTTGCTAAACTTTT
9[12]8[12]	TTTTGACAGCATCGGAACGAACCCTCAGCAGCGAAATTTT
11[12]10[12]	TTTTTCATAAGGGAACCGAAAGGCGCAGACGGTCAATTTT

13[12]12[12]	TTTTGGAAGAAAAATCTACGACCAGTCAGGACGTTGTTTT
15[12]14[12]	TTTTCATTGAATCCCCCTCAAATCGTCATAAATATTTTTT
17[12]16[12]	TTTTCTGTAGCTCAACATGTATTGCTGAATATAATGTTTT
19[12]18[12]	TTTTGGTTGTACCAAAAACAAGCATAAAGCTAAATCTTTT
21[12]20[12]	TTTTGATGAACGGTAATCGTAGCAAACAAGAGAATCTTTT
23[12]22[12]	TTTTGTAATGGGATAGGTCAAAACGGCGGATTGACCTTTT
25[12]24[12]	TTTTTGTAAAACGACGGCCATTCCCAGTCACGACGTTTTT
27[12]26[12]	TTTTCGGTTTGCGTATTGGGAACGCGCGGGGAGAGGTTTT
29[12]28[12]	TTTTCGATGGCCCACTACGTAAACCGTCTATCAGGGTTTT
3[40]5[39]	GGAAAGCGACCAGGCGGATAAGTGAATAGGTG
5[40]7[39]	TATCACCGAAATGAATTTTCTGTAAGCGGAGT
7[40]9[39]	GAGAATAGCTTTTGCGGGATCGTCGGGTAGCA
9[40]11[39]	ACGGCTACTTACTTAGCCGGAACGCTGACCAA
11[40]13[39]	CTTTGAAAAGAACTGGCTCATTATTTAATAAA
13[40]15[39]	ACGAACTAGCGTCCAATACTGCGGAATGCTTT
15[40]17[39]	AAACAGTTGATGGCTTAGAGCTTATTTAAATA
17[40]19[39]	TGCAACTAAGCAATAAAGCCTCAGTTATGACC
19[40]21[39]	CTGTAATATTGCCTGAGAGTCTGGAAAACTAG
21[40]23[39]	CATGTCAAGATTCTCCGTGGGAACCGTTGGTG
23[40]25[39]	TAGATGGGGGGTAACGCCAGGGTTGTGCCAAG
25[40]27[39]	CTTGCATGCATTAATGAATCGGCCCGCCAGGG
27[40]29[39]	TGGTTTTTAACGTCAAAGGGCGAAGAACCATC
29[40]28[56]	ACCCAAATCAAGTTTTTTGGGGTCAAAGAACG
2[55]3[39]	TGAGGCAGGTCAGACGATTGGCCTGCCAGAAT
4[55]2[56]	TGCTCAGTCAGTCTCTGAATTTACCAGGAGGT
6[55]4[56]	ACGTTAGTTACTCAGGAGGTTTAGCGGGGTTT
8[55]6[56]	AAAGGCCGAAAGGAACAACTAAAGCTTTCCAG
10[55]8[56]	GCTCCATGAGAGGCTTTGAGGACTAGGGAGTT
12[55]10[56]	CGATTTTAGAGGACAGATGAACGGCGCGACCT
14[55]12[56]	ACTGGATAACGGAACAACATTATTACCTTATG
16[55]14[56]	TTTTTGCGCAGAAAACGAGAATGAATGTTTAG
18[55]16[56]	CAAAATTAAAGTACGGTGTCTGGAAGAGGTCA
20[55]18[56]	TCAGGTCACTTTTGCGGGAGAAGCAGAATTAG
22[55]20[56]	ACCCGTCGTCATATGTACCCCGGTAAAGGCTA
24[55]22[56]	ATTAAGTTCGCATCGTAACCGTGCGAGTAACA
26[55]24[56]	GCCAGCTGCCTGCAGGTCGACTCTGCAAGGCG
28[55]26[56]	TGGACTCCCTTTTCACCAGTGAGACCTGTCGT
3[72]5[71]	TAAGCGTCGAAGGATTAGGATTAGTACCGCCA
5[72]7[71]	CCCTCAGATCTAAAGTTTTGTCGTGAATTGCG
7[72]9[71]	AATAATAAGGTCGCTGAGGCTTGCAAAGACTT
9[72]11[71]	TTTCATGAAAATTGTGTCGAAATCTGTACAGA
11[72]13[71]	CCAGGCGCTTAATCATTGTGAATTACAGGTAG

13[72]15[71]	AAAGATTCAGGGGGTAATAGTAAACCATAAAT
15[72]17[71]	CAAAAATCATTGCTCCTTTTGATAAGTTTCAT
17[72]19[71]	TCCATATACATACAGGCAAGGCAACTTTATTT
19[72]21[71]	CAACGCAATTTTTGAGAGATCTACTGATAATC
21[72]23[71]	AGAAAAGCAACATTAAATGTGAGCATCTGCCA
23[72]25[71]	GTTTGAGGGAAAGGGGGATGTGCTAGAGGATC
25[72]27[71]	CCCGGGTACTTTCCAGTCGGGAAACGGGCAAC
27[72]29[71]	AGCTGATTACAAGAGTCCACTATTGAGGTGCC
29[72]28[88]	GTAAAGCACTAAATCGGAACCCTAGTTGTTCC
2[87]3[71]	CACCAGAGCCGCCGCCAGCATTGACGTTCCAG
4[87]2[88]	CCTCAAGAATACATGGCTTTTGATAGAACCAC
6[87]4[88]	CGTAACGAACCGCCACCCTCAGAACTGAGACT
8[87]6[88]	ATATATTCTTTTTTCACGTTGAAAATAGTTAG
10[87]8[88]	CGCCTGATGGAAGTTTCCATTAAACATAACCG
12[87]10[88]	TTTCAACTATAGGCTGGCTGACCTTGTATCAT
14[87]12[88]	TTTGCCAGATCAGTTGAGATTTAGTGGTTTAA
16[87]14[88]	TACCTTTAAGGTCTTTACCCTGACAAAGAAGT
18[87]16[88]	CAATAAATACAGTTGATTCCCAATTTAGAGAG
20[87]18[88]	GGTAGCTAGGATAAAAATTTTTAGTTAACATC
22[87]20[88]	CTTTCATCCCCAAAAACAGGAAGACCGGAGAG
24[87]22[88]	CAGCTGGCGGACGACGACAGTATCGTAGCCAG
26[87]24[88]	ACTGCCCGCCGAGCTCGAATTCGTTATTACGC
28[87]26[88]	AGTTTGGAGCCCTTCACCGCCTGGTTGCGCTC
3[104]5[103]	AGTGTACTTGAAAGTATTAAGAGGCCGCCACC
5[104]7[103]	CTCAGAGCTCCACAGACAGCCCTCATCTCCAA
7[104]9[103]	AAAAAAGGACAACCATCGCCCACGCGGGTAAA
9[104]11[103]	ATACGTAAAAGTACAACGGAGATTTCATCAAG
11[104]13[103]	AGTAATCTTAAATTGGGCTTGAGAGAATACCA
13[104]15[103]	CATTCAACGCGAGAGGCTTTTGCATATTATAG
15[104]17[103]	TCAGAAGCCTCCAACAGGTCAGGATCTGCGAA
17[104]19[103]	CGAGTAGAACTAATAGTAGTAGCAAACCCTCA
19[104]21[103]	TATATTTTAGCTGATAAATTAATGTTGTATAA
21[104]23[103]	GCAAATATCGCGTCTGGCCTTCCTGGCCTCAG
23[104]25[103]	GAAGATCGGTGCGGGCCTCTTCGCAATCATGG
25[104]27[103]	TCATAGCTACTCACATTAATTGCGCCCTGAGA
27[104]29[103]	GAGTTGCACGAGATAGGGTTGAGTAAGGGAGC
29[104]28[120]	CCCCGATTTAGAGCTTGACGGGGAAATCAAAA
2[119]3[103]	GCCACCACCCTCAGAGCCGCCACCGATACAGG
4[119]2[120]	CTGAAACAGGTAATAAGTTTTAACCCCTCAGA
6[119]4[120]	TGTAGCATCACCACCCTCATTTTCCTATTATT
8[119]6[120]	CAATGACACTCCAAAAGGAGCCTTACAACGCC
10[119]8[120]	GCGAAACATGCCACTACGAAGGCATGCGCCGA

12[119]10[120]	ACGAGTAGTGACAAGAACCGGATATACCAAGC
14[119]12[120]	CCAAAATATAATGCAGATACATAAACACCAGA
16[119]14[120]	GAAGCAAAAAAGCGGATTGCATCAGATAAAAA
18[119]16[120]	TCAATTCTTTTAGTTTGACCATTACCAGACCG
20[119]18[120]	ACCGTTCTAAATGCAATGCCTGAGAGGTGGCA
22[119]20[120]	AAATAATTTTAAATTGTAAACGTTGATATTCA
24[119]22[120]	GGCGATCGCACTCCAGCCAGCTTTGCCATCAA
26[119]24[120]	GTGAGCTAGTTTCCTGTGTGAAATTTGGGAAG
28[119]26[120]	GAATAGCCGCAAGCGGTCCACGCTCCTAATGA
3[136]5[135]	TGCCTTGACTGCCTATTTCGGAACAGGGATAG
5[136]7[135]	CAAGCCCAGTCACCAGTACAAACTTAATTGTA
7[136]9[135]	TCGGTTTAGCTTGATACCGATAGTCCAACCTA
9[136]11[135]	AAACGAAATGACCCCCAGCGATTATTCATTAC
11[136]13[135]	CCAAATCACTTGCCCTGACGAGAACGCCAAAA
13[136]15[135]	GGAATTACTCGTTTACCAGACGACAAAAGATT
15[136]17[135]	AAGAGGAACGAGCTTCAAAGCGAAGATACATT
17[136]19[135]	TCGCAAATGGGGCGCGAGCTGAAATAATGTGT
19[136]21[135]	AGGTAAAGAAATCACCATCAATATAATATTTT
21[136]23[135]	GTTAAAATTTTAACCAATAGGAACCCGGCACC
23[136]25[135]	GCTTCTGGTCAGGCTGCGCAACTGTGTTATCC
25[136]27[135]	GCTCACAATGTAAAGCCTGGGGTGGGTTTGCC
27[136]29[135]	CCAGCAGGGGCAAAATCCCTTATAAAGCCGGC
29[136]29[167]	GAACGTGGCGAGAAAGGAAGGGAACAAACTAT
2[151]3[135]	GAGCCGCCACCCTCAGAACCGCCAGGGGTCAG
4[151]2[152]	AATGCCCCGTAACAGTGCCCGTATCTCCCTCA
6[151]4[152]	TGAGTTTCATAGGAACCCATGTACAAACAGTT
8[151]6[152]	CTTAAACATCAGCTTGCTTTCGAGCGTAACAC
10[151]8[152]	CTCATCTTGAGGCAAAAGAATACAGTGAATTT
12[151]10[152]	GAATAAGGACGTAACAAAGCTGCTCTAAAACA
14[151]13[167]	CATAACCCGAGGCATAGTAAGAGCGCAAGAAA
16[151]14[152]	TTTTAATTGCCCGAAAGACTTCAAAACACTAT
18[151]16[152]	TTTCATTTGGTCAATAACCTGTTTATATCGCG
20[151]18[152]	AGACAGTCATTCAAAAGGGTGAGAAGCTATAT
22[151]21[167]	GCTCATTTTCGCATTAAATTTTTGAGCTTAGA
24[151]22[152]	TTCGCCATTGCCGGAAACCAGGCATTAAATCA
26[151]24[152]	GCATAAAGTTCCACACAACATACGAAGCGCCA
28[151]26[152]	CCGAAATCCGAAAATCCTGTTTGAAGCCGGAA
7[168]9[167]	AGTTTGCCCCGTAATCAGTAGCGACACCGACT
9[168]11[167]	TGAGCCATGGTGAATTATCACCGTAAAGAAAC
11[168]12[152]	GCAAAGACAAGGTGGCAACATATACATTCAGT
13[168]15[167]	CAATGAAAAAGCCCAATAATAAGATTCCAGAG
15[168]17[167]	CCTAATTTACGCTAACGAGCGTCTAATCAATA

17[168]19[167]	ATCGGCTGCGAGCATGTAGAAACCTATCATAT
19[168]20[152]	GCGTTATAGAAAAAGCCTGTTTAGAAGGCCGG
21[168]23[167]	TTAAGACGTTGAAAACATAGCGATAACAGTAC
23[168]25[167]	CTTTTACACAGATGAATATACAGTAAACAATT
25[168]27[167]	CGACAACTAAGTATTAGACTTTACAATACCGA
27[168]28[152]	ACGAACCAAAACATCGCCATTAAATGGTGGTT
29[168]28[184]	CGGCCTTGCTGGTAATATCCAGAACGAACTGA
2[171]3[171]	TTTTGGAACCGCCCACCACCTTTT
4[182]5[182]	TTTTAAAATCACCGGAACCAGAGTTGCCATCTTTTCATAATCTTTT
6[183]7[167]	CGGTCATAGCCCCCTTATTAGCGTCAGAATCA
8[183]6[184]	TAGCAGCATTTAGCGTCAGACTGTGGCATTTT
10[183]8[184]	TCATTAAATTGGGAATTAGAGCCAACCATCGA
12[183]10[184]	CATACATAACCACGGAATAAGTTTGAAATTAT
14[183]12[184]	ATTGAGTTTAGCAATAGCTATCTTAGAAAATA
16[183]14[184]	TCTTACCAGCCAGTTACAAAATAACCACAAGA
18[183]16[184]	CTAATTTATCTTTCCTTATCATTCATCCTGAA
20[183]18[184]	AATTACTACAAATTCTTACCAGTAATCCCATC
22[183]20[184]	TAGAATCCCTGAGAAGAGTCAATAGGAATCAT
24[183]22[184]	TTTAACGTTCGGGAGAAACAATAATTTTCCCT
26[183]24[184]	GGATTTAGCGTATTAAATCCTTTGTTTTCAGG
28[183]26[184]	TAGCCCTACCAGCAGAAGATAAAAACATTTGA
9[200]11[199]	ACCAGTAGAAGGTAAATATTGACGATTTTGTC
11[200]13[199]	ACAATCAAGTATGTTAGCAAACGTACCGAAGC
13[200]15[199]	CCTTTTTAATATCAGAGAGATAACACAGCCAT
15[200]17[199]	ATTATTTAACCCAGCTACAATTTTCAAGAACG
17[200]19[199]	GGTATTAAGAACAAGAAAAATAATTAAAGCCA
19[200]21[199]	ACGCTCAAAATAAGAATAAACACCGTGAATTT
21[200]23[199]	ATCAAAATCGTCGCTATTAATTAACGGATTCG
23[200]25[199]	CCTGATTGAAAGAAATTGCGTAGACCCGAACG
25[200]27[199]	TTATTAATGCCGTCAATAGATAATCAGAGGTG
27[200]29[199]	AGGCGGTCATTAGTCTTTAATGCGCAATATTA
29[200]28[216]	CCGCCAGCCATTGCAACAGGAAAAATATTTTT
6[202]7[202]	TTTTTTTCATCAGCGCGTTTTT
10[215]9[223]	AGGGAGGGCACCATTACCATTTTT
12[215]10[216]	ATTACGCATAGAAAATTCATATGGACCGATTG
14[215]12[216]	GAGCGCTAAGAAAAGTAAGCAGATGACTCCTT
16[215]14[216]	TATTTTGCTCCCAATCCAAATAAGGGGTAATT
18[215]16[216]	TAAGTCCTACCAAGTACCGCACTCTTAGTTGC
20[215]18[216]	AGGCGTTACAGTAGGGCTTAATTGACAATAGA
22[215]20[216]	CTGTAAATCATAGGTCTGAGAGACGATAAATA
24[215]22[216]	ACAGAAATCTTTGAATACCAAGTTCCTTGCTT
26[215]24[216]	AGATTAGATTTAAAAGTTTGAGTACACGTAAA

28[215]26[216]	GAATGGCTAGTATTAACACCGCCTCAACTAAT
8[223]9[199]	TTTTTAGCAAGGCCGGAAACGTCACCAATGAAGCAAAATC
13[232]15[231]	AAAGTTACCCTGAACAAAGTCAGAAAACGATT
15[232]17[231]	TTTTGTTTAAGCCTTAAATCAAGAATCGAGAA
17[232]19[231]	CAAGCAAGACGCGCCTGTTTATCAAGAATCGC
19[232]21[231]	CATATTTAGAAATACCGACCGTGTTACCTTTT
21[232]23[231]	TAACCTCCATATGTGAGTGAATAAACAAAATC
23[232]25[231]	GCGCAGAGATATCAAAATTATTTGACATTATC
25[232]27[231]	ATTTTGCGTCTTTAGGAGCACTAAGCAACAGT
27[232]29[231]	GCCACGCTATACGTGGCACAGACAACGCTCAT
29[232]28[248]	GGAAATACCTACATTTTGACGCTCACCTGAAA
10[244]11[244]	TTTTCAAAAGGGCGACATTCATTTACCAGCGCCAAAGATTTT
12[247]13[231]	ACCCAAAAGAACTGGCATGATTAAAGCCGAAC
14[247]12[248]	CTGAACACCAGAAGGAAACCGAGGAACGGAAT
16[247]14[248]	AGGTTTTGAACGTCAAAAATGAAAAGAATTAA
18[247]16[248]	AATGCAGACCGTTTTTATTTTCATCTTGCGGG
20[247]18[248]	AATGGTTTACAACGCCAACATGTAGTTCAGCT
22[247]20[248]	AAATCAATGGCTTAGGTTGGGTTACTAAATTT
24[247]22[248]	AACCTACCGCGAATTATTCATTTCCAGTACAT
26[247]24[248]	CTAAAATAGAACAAAGAAACCACCAGGGTTAG
28[247]26[248]	GCGTAAGAGAGAGCCAGCAGCAAAAAGGTTAT
15[264]15[286]	CTTTACAGAGAGAATAACATTTT
17[264]19[263]	TCATTACCCGACAATAAACAACATATTTAGGC
19[264]21[263]	AGAGGCATAATTTCATCTTCTGACTATAACTA
21[264]23[263]	TATGTAAACCTTTTTTAATGGAAAAATTACCT
23[264]25[263]	GAGCAAAAACTTCTGAATAATGGAAGAAGGAG
25[264]27[263]	CGGAATTATTGAAAGGAATTGAGGTGAAAAAT
27[264]29[263]	CTAAAGCAAGATAGAACCCTTCTGAATCGTCT
29[264]28[280]	GAAATGGATTATTTACATTGGCAGACATTCTG
12[265]13[265]	TTTTAATAATAAACGCTTTT
16[279]17[263]	GAGGCGTTTTAGCGAACCTCCCGACGTAGGAA
18[279]16[280]	CCAGACGAGCGCCCAATAGCAAGCAAGAACGC
20[279]18[280]	TTTTAGTTTTTCGAGCCAGTAATAAATTCTGT
22[279]20[280]	TTGAATTATGCTGATGCAAATCCACAAATATA
24[279]22[280]	TGGATTATGAAGATGATGAAACAAAATTTCAT
26[279]24[280]	ATCAACAGTCATCATATTCCTGATTGATTGTT
28[279]26[280]	GCCAACAGTCACCTTGCTGAACCTGTTGGCAA
14[286]15[263]	TTTTTAAAAACAGGGAAGCGCATTAGACGGGATAGCAGC
16[307]17[307]	TTTTGCTTATCCGGTATTCTAAATCAGATATAGAAGTTTT
18[307]19[307]	TTTTCGACAAAAGGTAAAGTAGAGAATATAAAGTACTTTT
20[307]21[307]	TTTTCGCGAGAAAACTTTTTATCGCAAGACAAAGAATTTT
22[307]23[307]	TTTTATTAATTACATTTAACACATCAAGAAAACAAATTTT

24[307]25[307]	TTTTTTCATCAATATAATCCTATCAGATGATGGCAATTTT
26[307]27[307]	TTTTAATCAATATCTGGTCACAAATATCAAACCCTCTTTT
28[307]29[307]	TTTTACCAGTAATAAAAGGGATTCACCAGTCACACGTTTT

8.3 Dye strands and dye capture strands

Biotin-Z3	GCGAAACATGCCACTACGAAGGCATGCGCCGATTTTTT/3Bio/
Biotin-Z2	ACGAGTAGTGACAAGAACCGGATATACCAAGCTTTTTT/3Bio/
Biotin-Z1	CCAAAATATAATGCAGATACATAAACACCAGATTTTTT/3Bio/
Cy3-capture	CAACAACAACAACAACAACAATT/3Bio/
TEX-dye-ATT	ATTATTATTATTATTATTATT/3TEX615/
Cy3-capture-D3	ACTGGATAACGGAACAACATTATTACCTTATGTTCAACAACAACAACAACAACAA
Cy3-capture-D2	TTTTTGCGCAGAAAACGAGAATGAATGTTTAGTTCAACAACAACAACAACAACAA
Cy3-capture-D1	CAAAATTAAAGTACGGTGTCTGGAAGAGGTCATTCAACAACAACAACAACAACAA
Cy3-capture-C3	AAAGATTCAGGGGGTAATAGTAAACCATAAATTTCAACAACAACAACAACAACAA
Cy3-capture-C2	CAAAAATCATTGCTCCTTTTGATAAGTTTCATTTCAACAACAACAACAACAACAA
Cy3-capture-C1	TCCATATACATACAGGCAAGGCAACTTTATTTTTCAACAACAACAACAACAACAA
Cy3-capture-B3	TTTCAACTATAGGCTGGCTGACCTTGTATCATTTCAACAACAACAACAACAACAA
Cy3-capture-B2	TTTGCCAGATCAGTTGAGATTTAGTGGTTTAATTCAACAACAACAACAACAACAA
Cy3-capture-B1	TACCTTTAAGGTCTTTACCCTGACAAAGAAGTTTCAACAACAACAACAACAACAA
Cy3-capture-A3	AGTAATCTTAAATTGGGCTTGAGAGAATACCATTCAACAACAACAACAACAACAA
Cy3-capture-A2	CATTCAACGCGAGAGGCTTTTGCATATTATAGTTCAACAACAACAACAACAACAA
Cy3-capture-A1	TCAGAAGCCTCCAACAGGTCAGGATCTGCGAATTCAACAACAACAACAACAACAA
Tex-capture-D3	ACTGGATAACGGAACAACATTATTACCTTATGTTAATAATAATAATAATAATAAT
Tex-capture-D2	TTTTTGCGCAGAAAACGAGAATGAATGTTTAGTTAATAATAATAATAATAATAAT
Tex-capture-D1	CAAAATTAAAGTACGGTGTCTGGAAGAGGTCATTAATAATAATAATAATAATAAT
Tex-capture-C3	AAAGATTCAGGGGGTAATAGTAAACCATAAATTTAATAATAATAATAATAATAAT
Tex-capture-C2	CAAAAATCATTGCTCCTTTTGATAAGTTTCATTTAATAATAATAATAATAATAAT
Tex-capture-C1	TCCATATACATACAGGCAAGGCAACTTTATTTTTAATAATAATAATAATAATAAT
Tex-capture-B3	TTTCAACTATAGGCTGGCTGACCTTGTATCATTTAATAATAATAATAATAATAAT
Tex-capture-B2	TTTGCCAGATCAGTTGAGATTTAGTGGTTTAATTAATAATAATAATAATAATAAT
Tex-capture-B1	TACCTTTAAGGTCTTTACCCTGACAAAGAAGTTTAATAATAATAATAATAATAAT
Tex-capture-A3	AGTAATCTTAAATTGGGCTTGAGAGAATACCATTAATAATAATAATAATAATAAT
Tex-capture-A2	CATTCAACGCGAGAGGCTTTTGCATATTATAGTTAATAATAATAATAATAATAAT
Tex-capture-A1	TCAGAAGCCTCCAACAGGTCAGGATCTGCGAATTAATAATAATAATAATAATAAT

8.4 AFM images

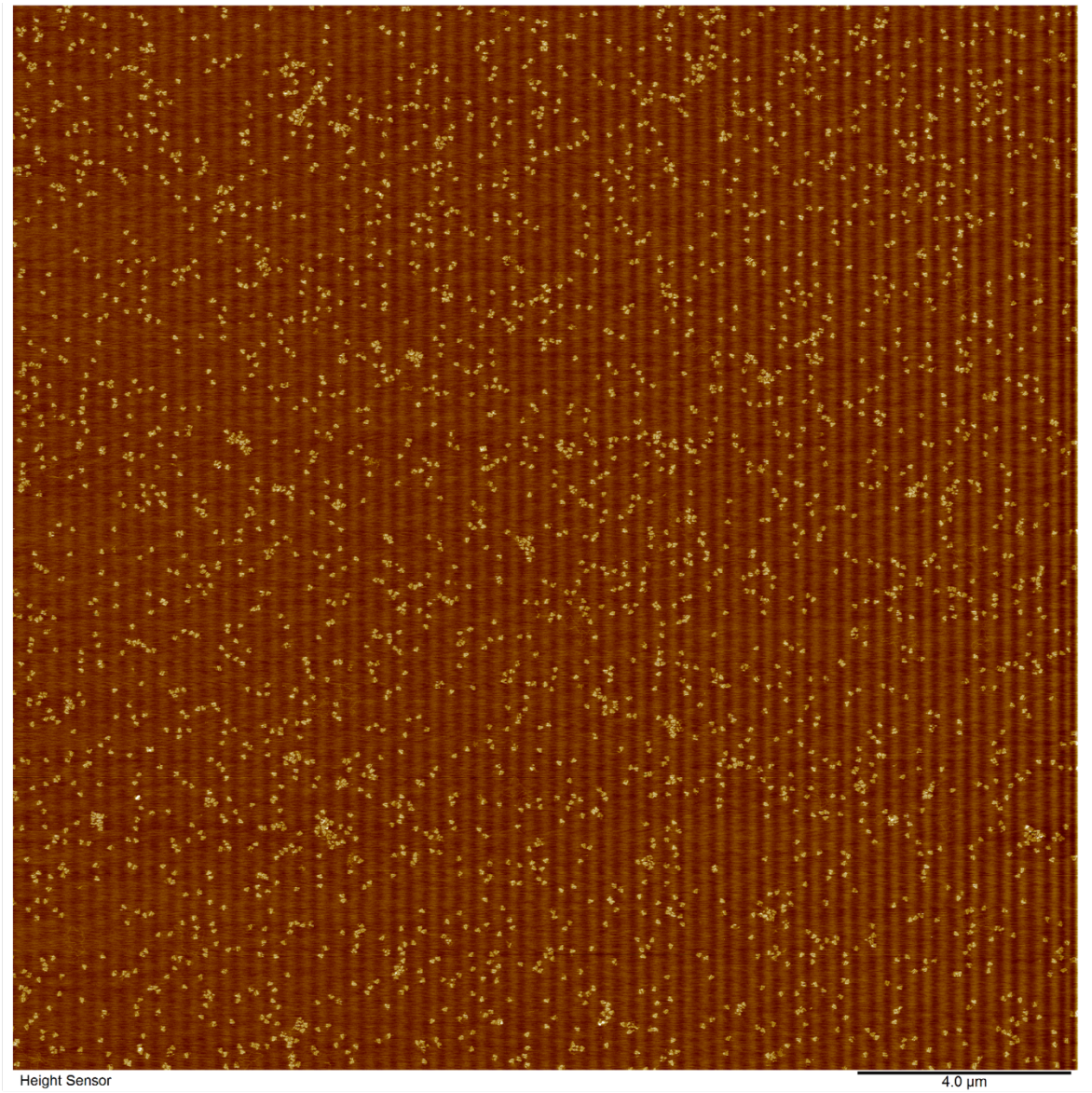

Figure 8-2 14-Alkyl through capture method.

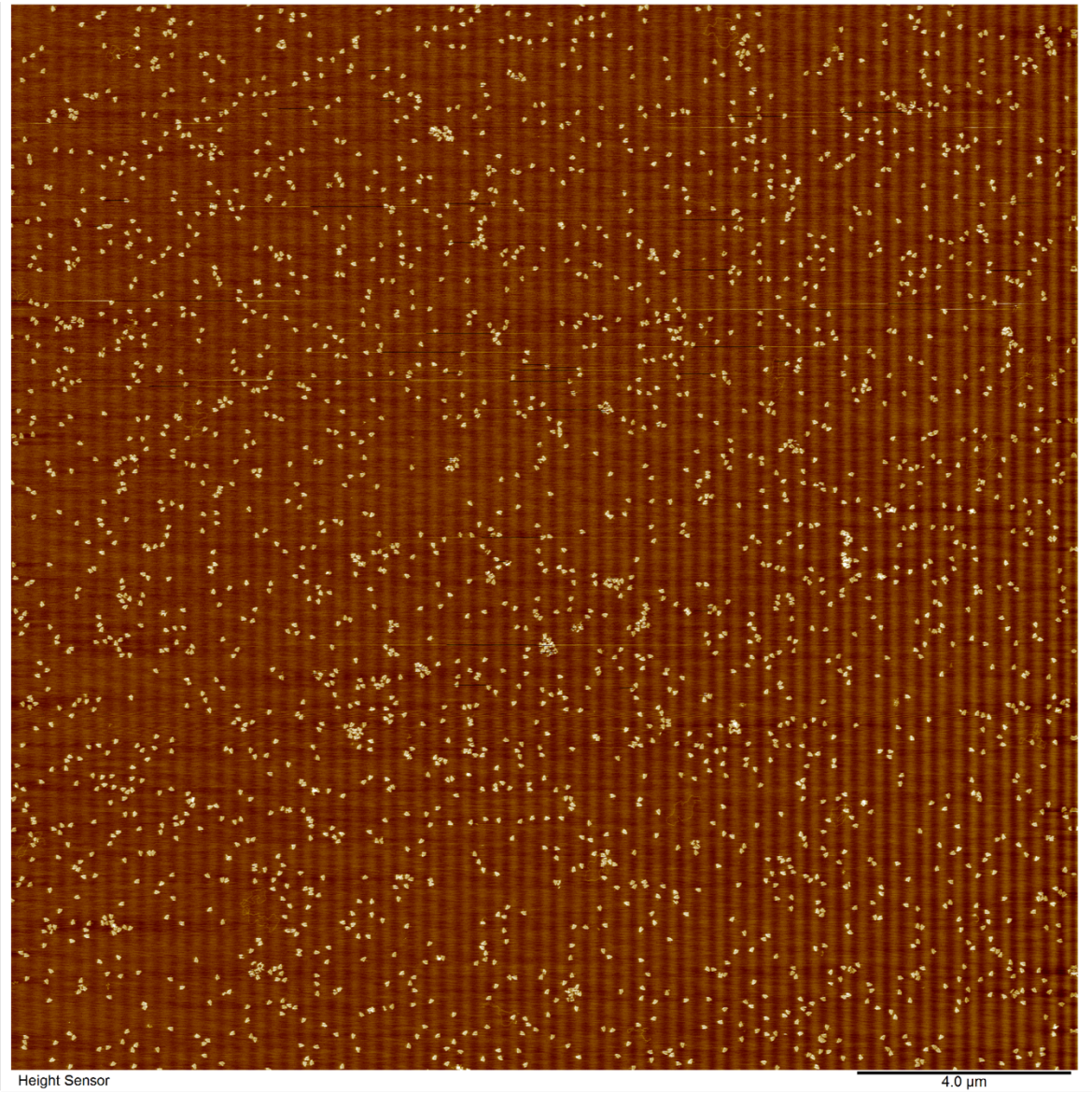

Figure 8-3 14-RF4 through capture method.

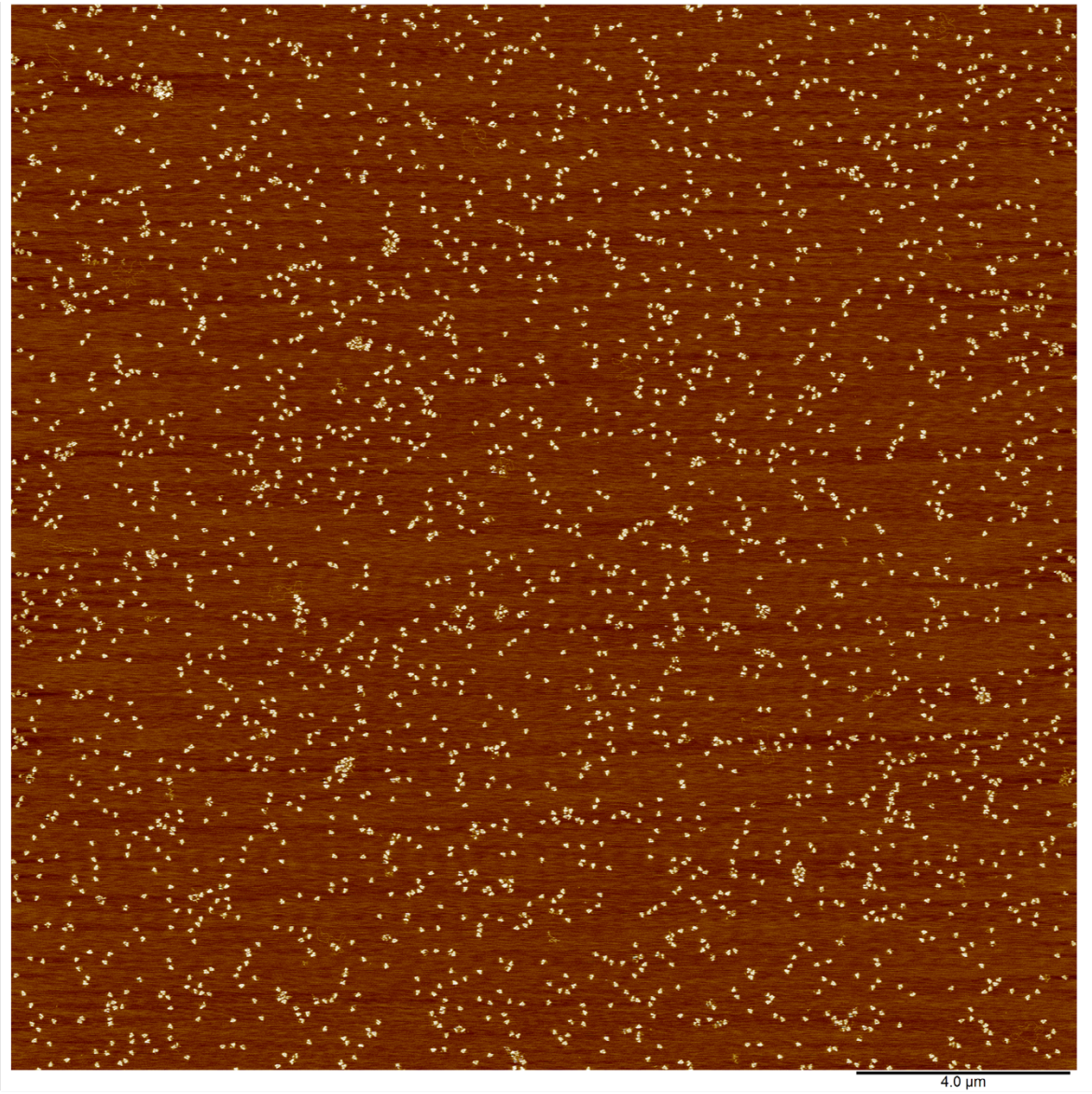

Figure 8-4 14-RF6 through capture method

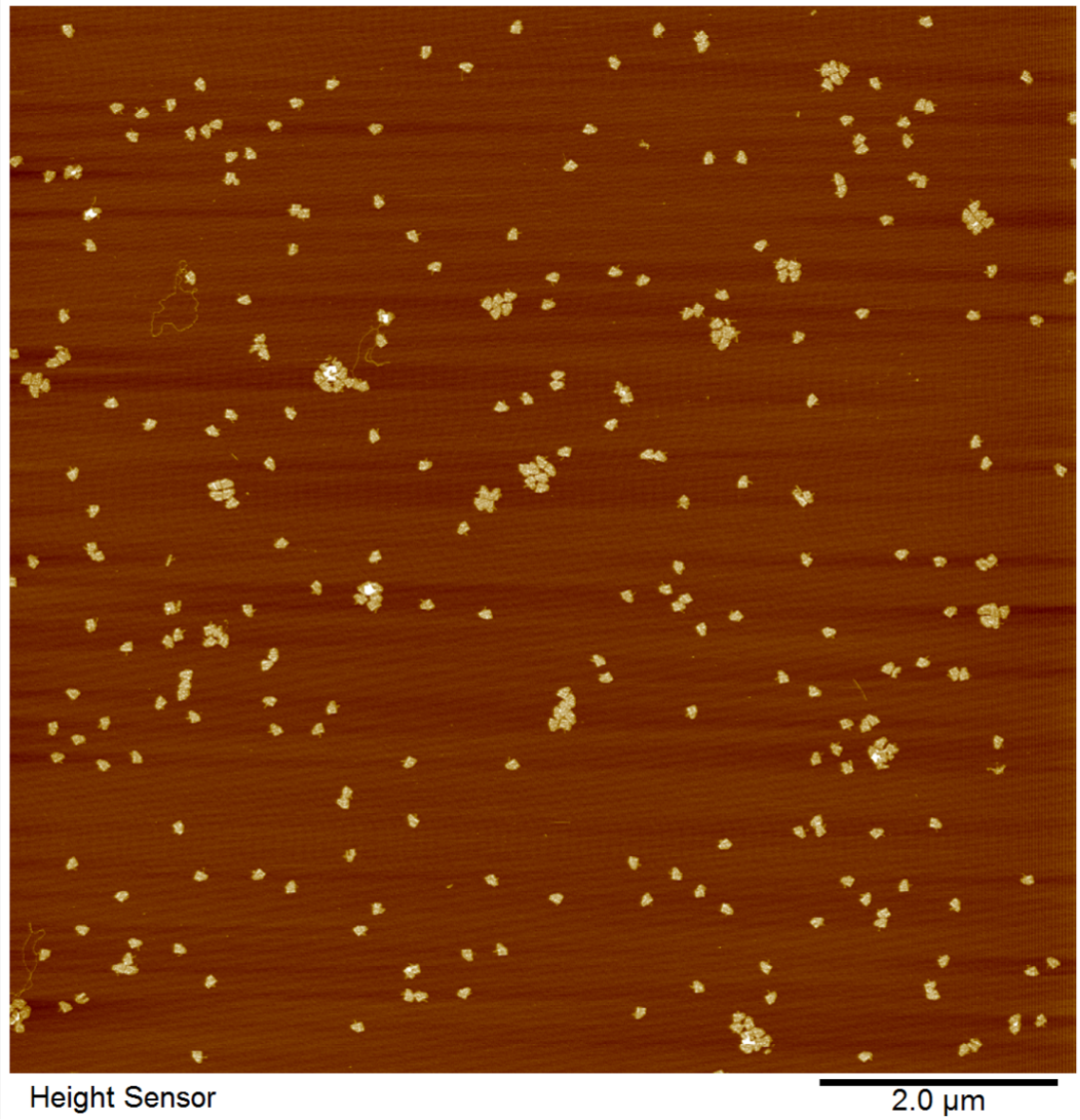

Figure 8-5 14-RF8 through capture method.

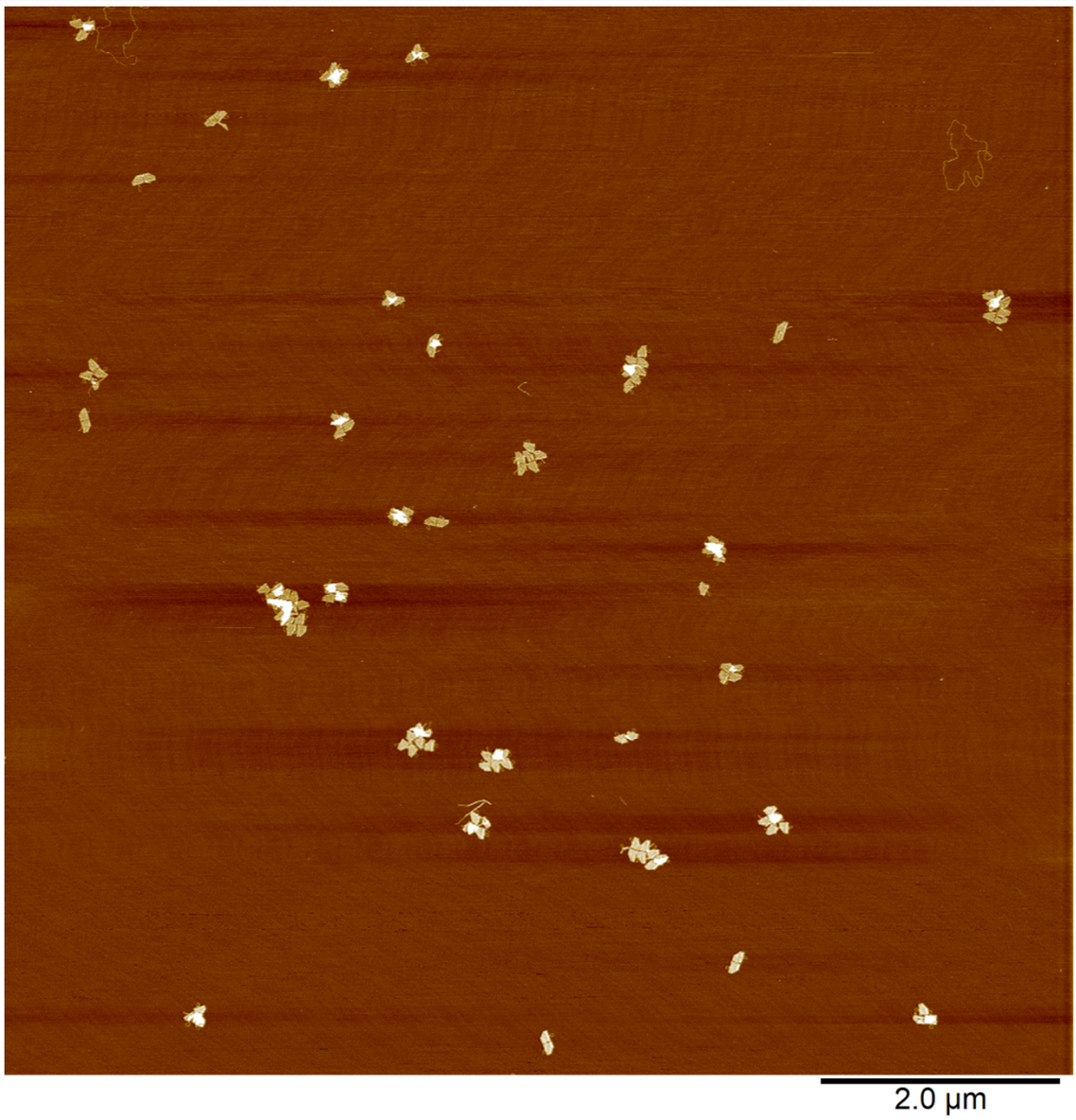

Figure 8-6 14-$(RF8)_2$ through capture method.

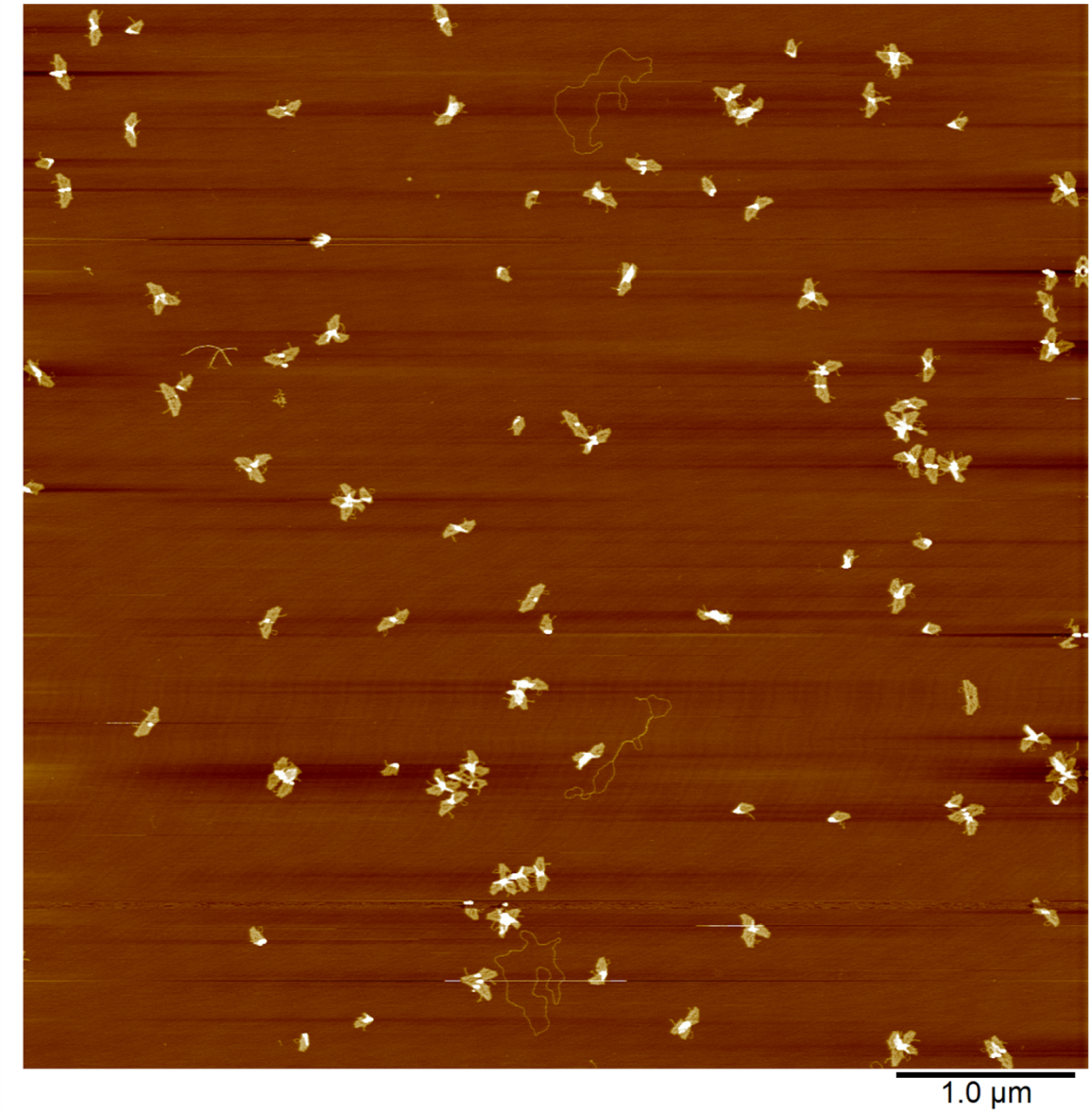

Figure 8-7 14-$(RF8)_4$ through capture method.

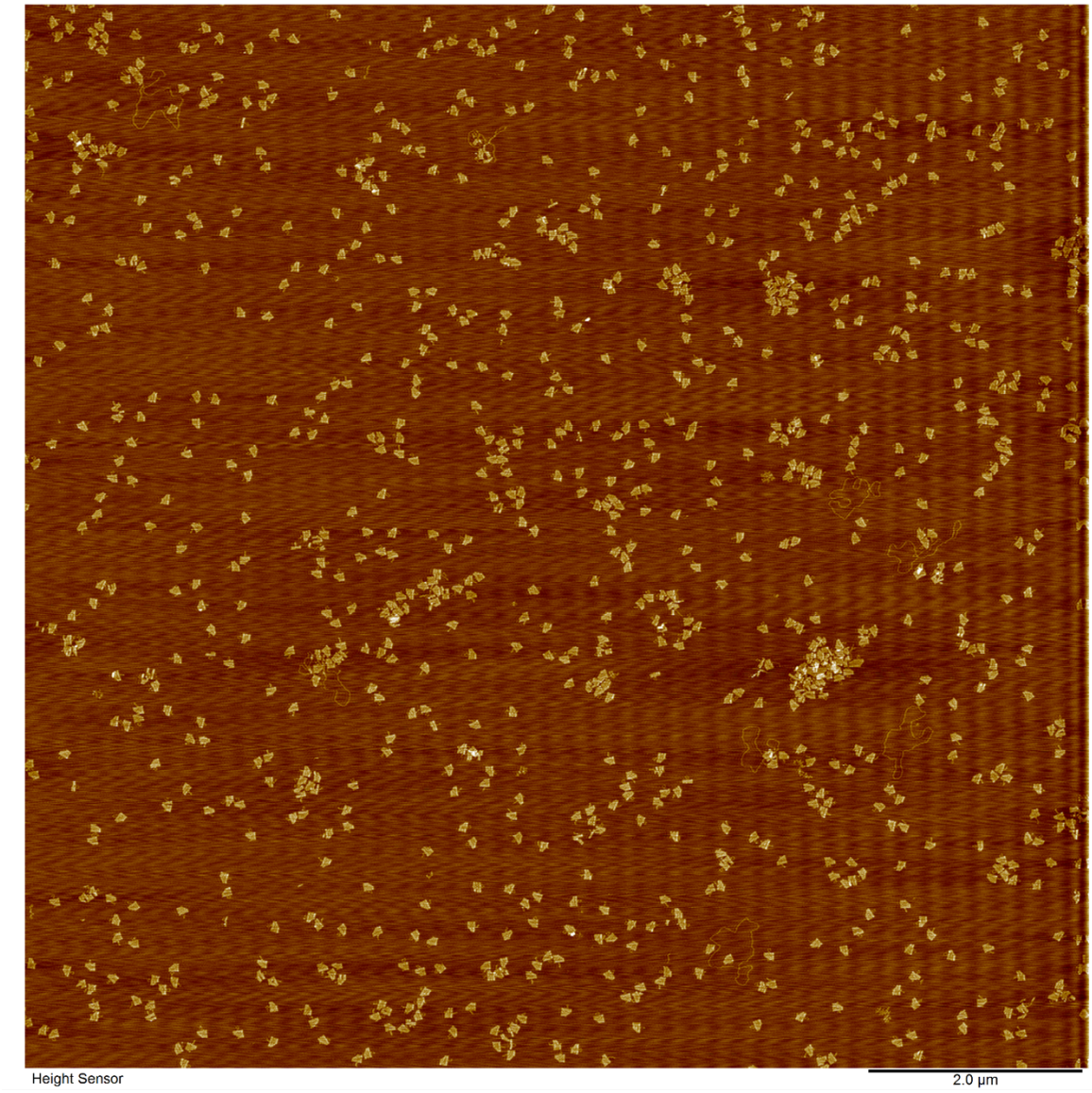

Figure 8-8 2-(RF8)2 through integrated method.

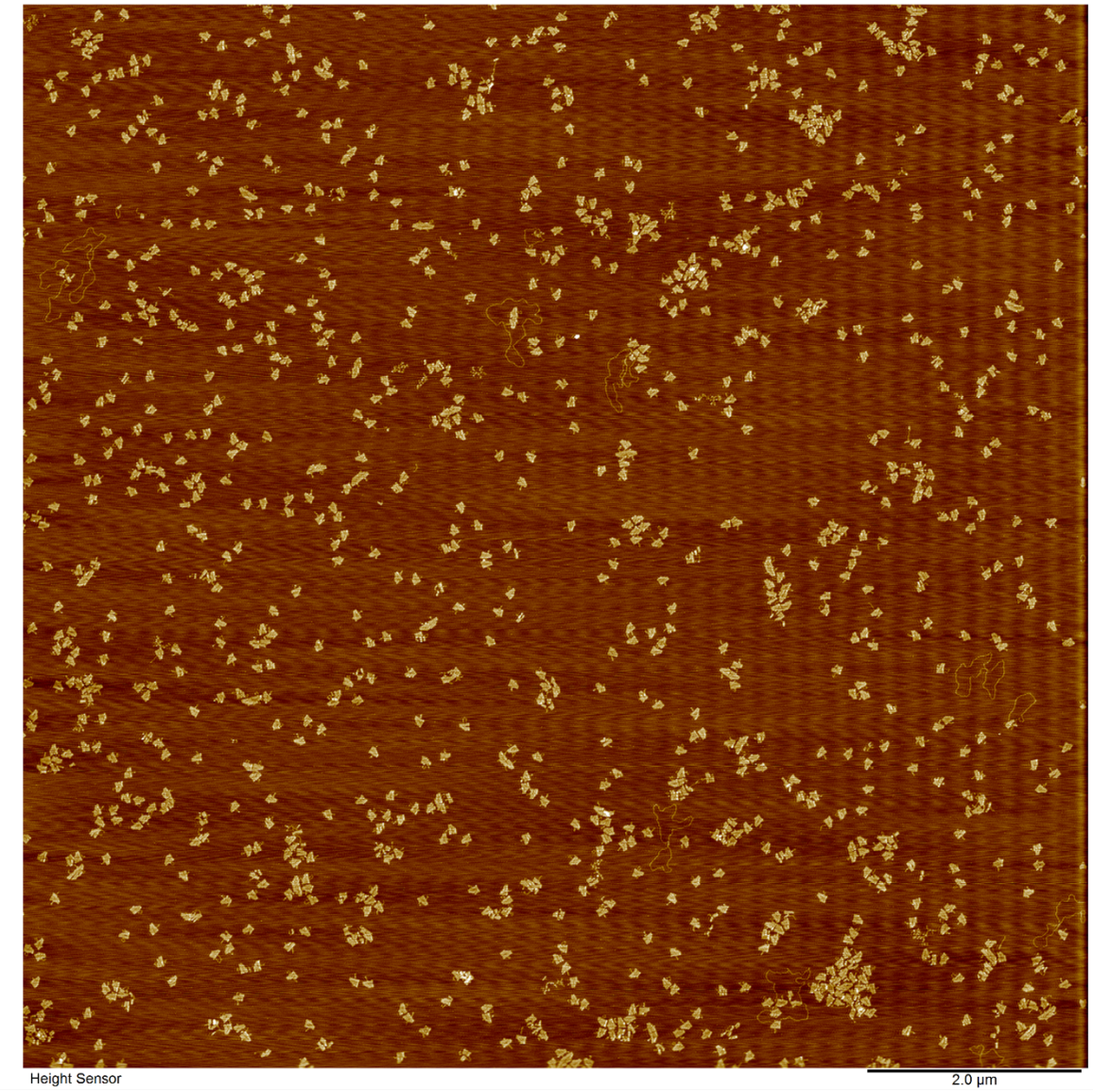

Figure 8-9 4-(RF8)2 through integrated method.

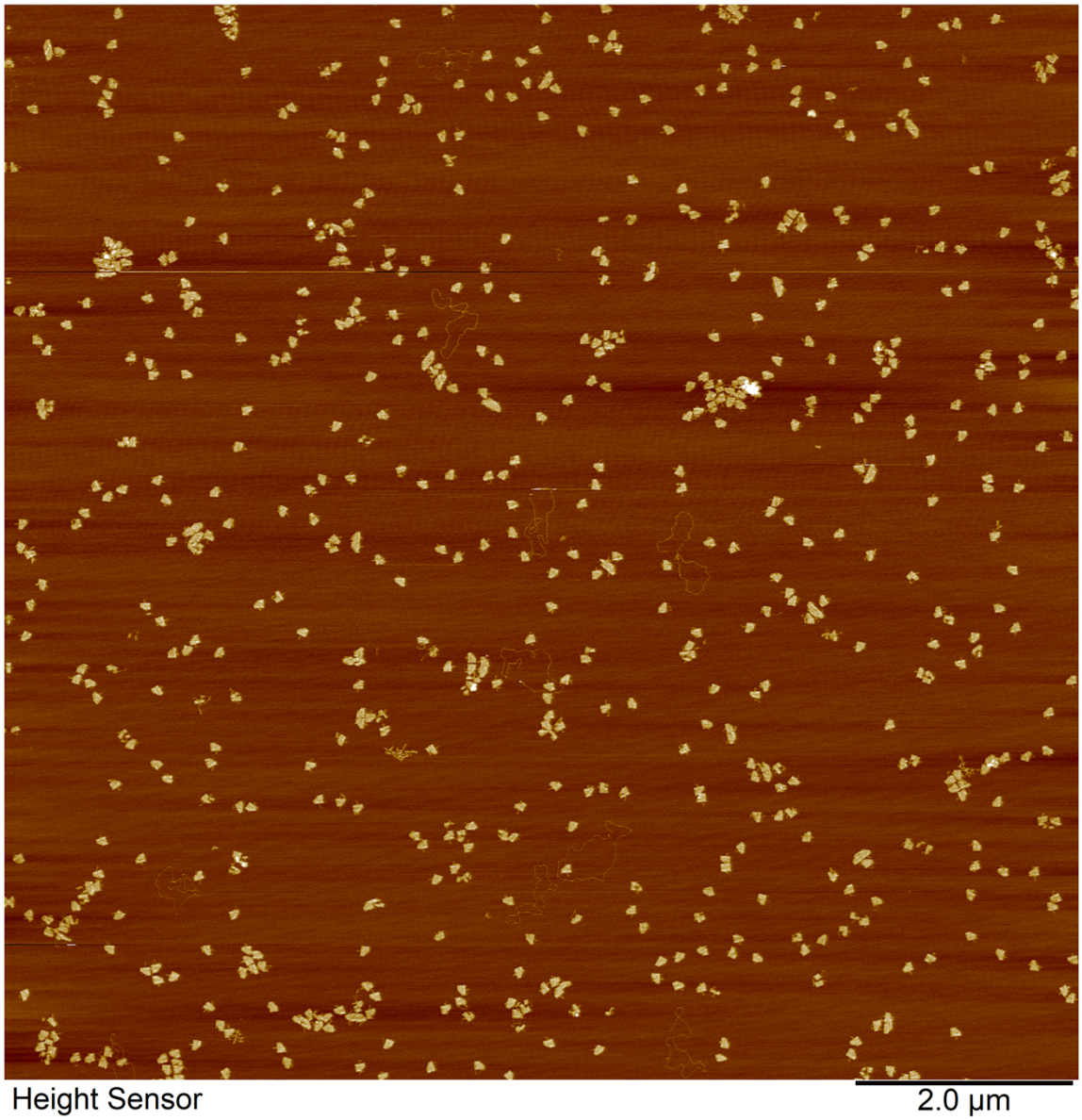

Figure 8-10 6-(RF8)2 through integrated method.

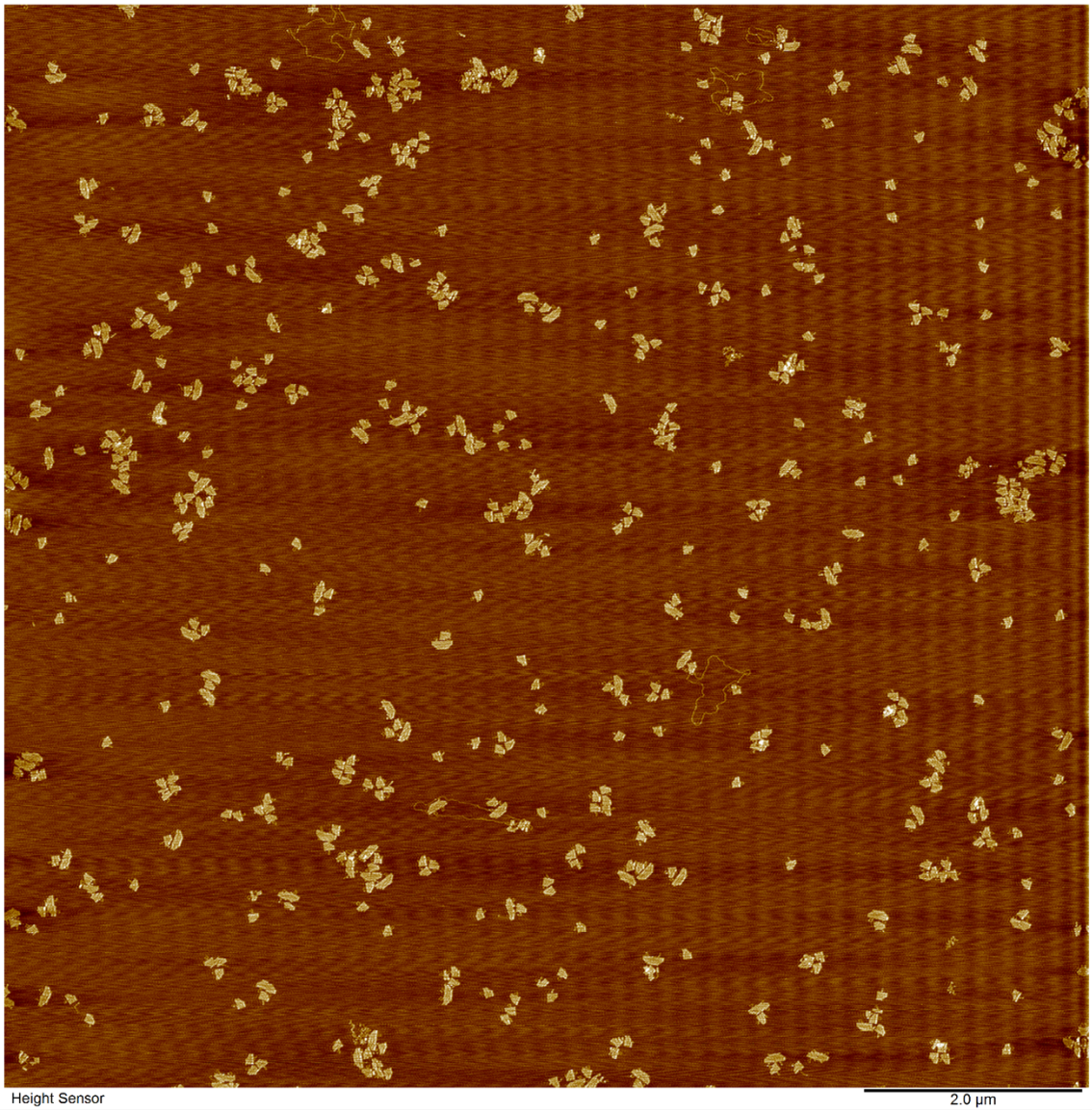

Figure 8-11 8-(RF8)2 through integrated method.

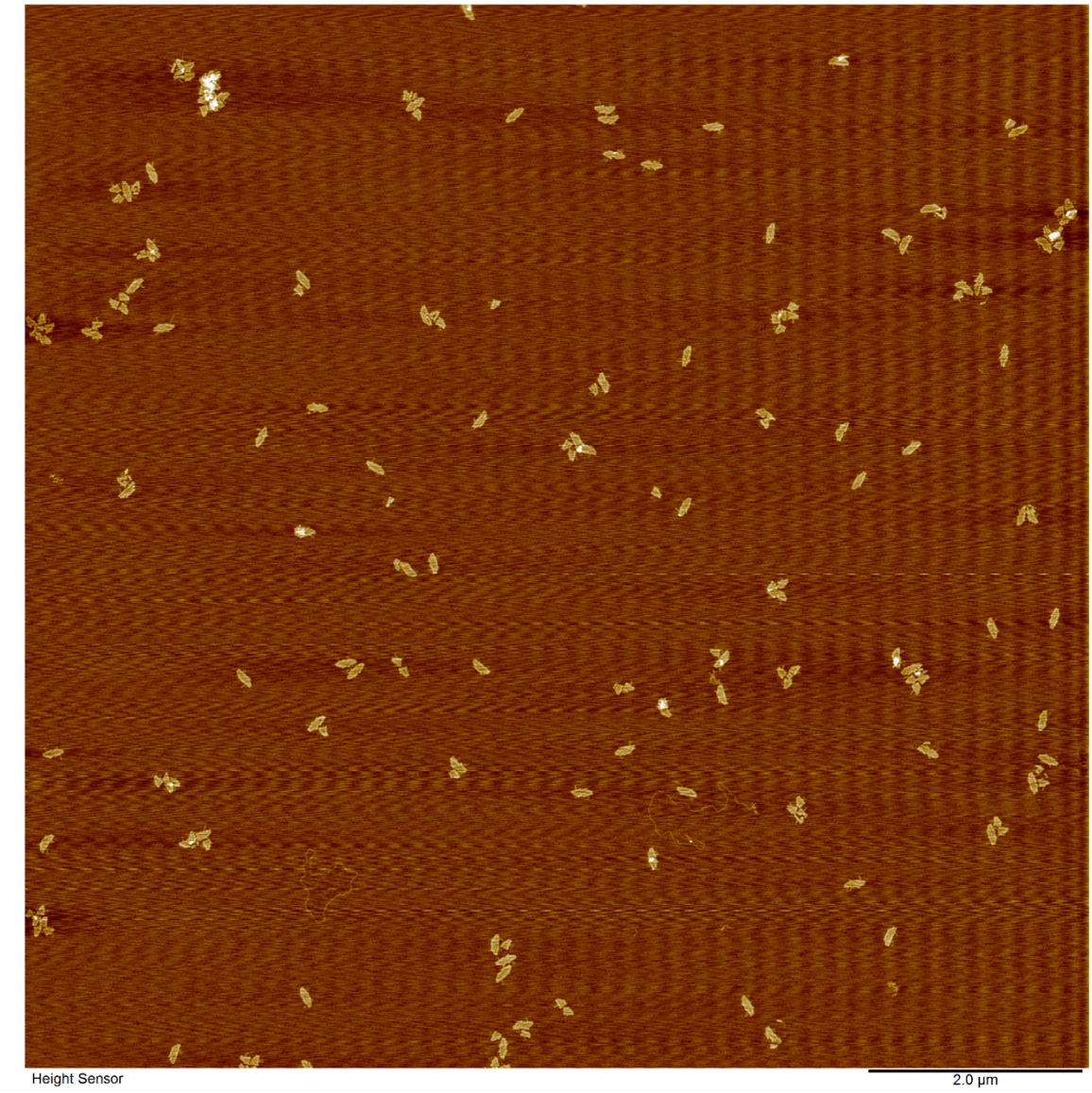

Figure 8-12 10-(RF8)2 through integrated method.

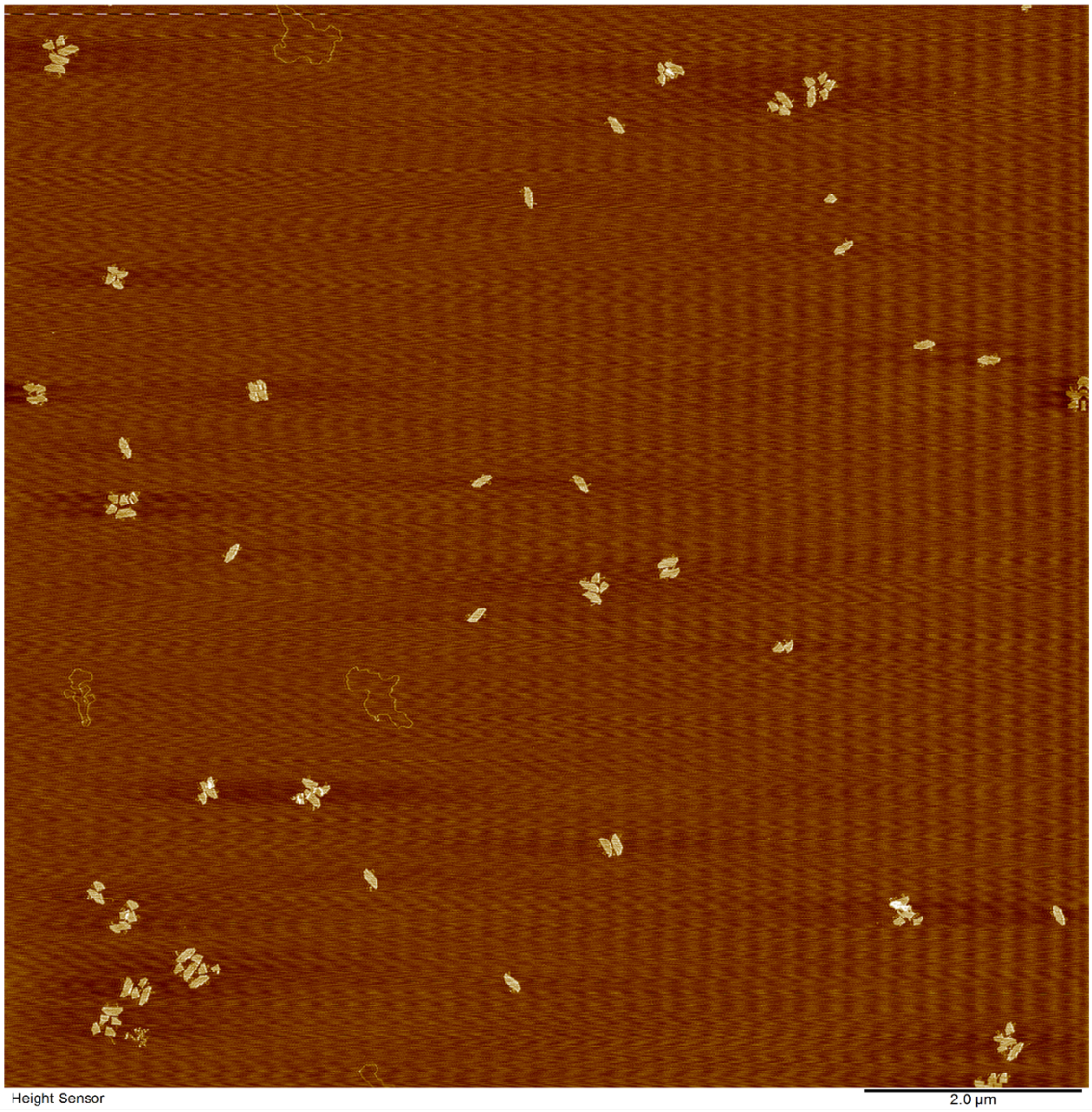

Figure 8-13 12-(RF8)2 through integrated method.

Figure 8-14 14-(RF8)2 through integrated method.

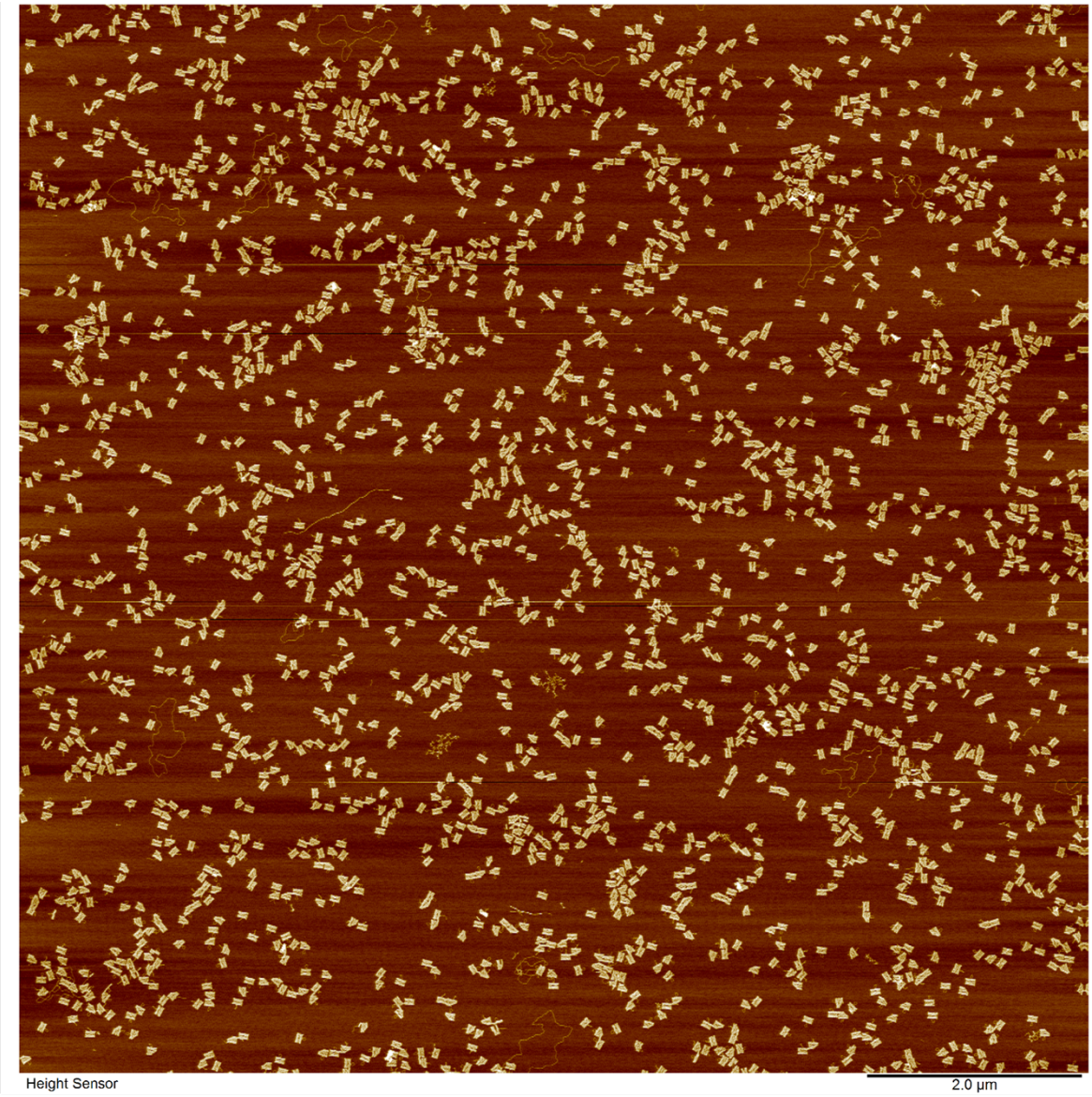

Figure 8-15 non-$(RF8)_2$ + 10-SE.

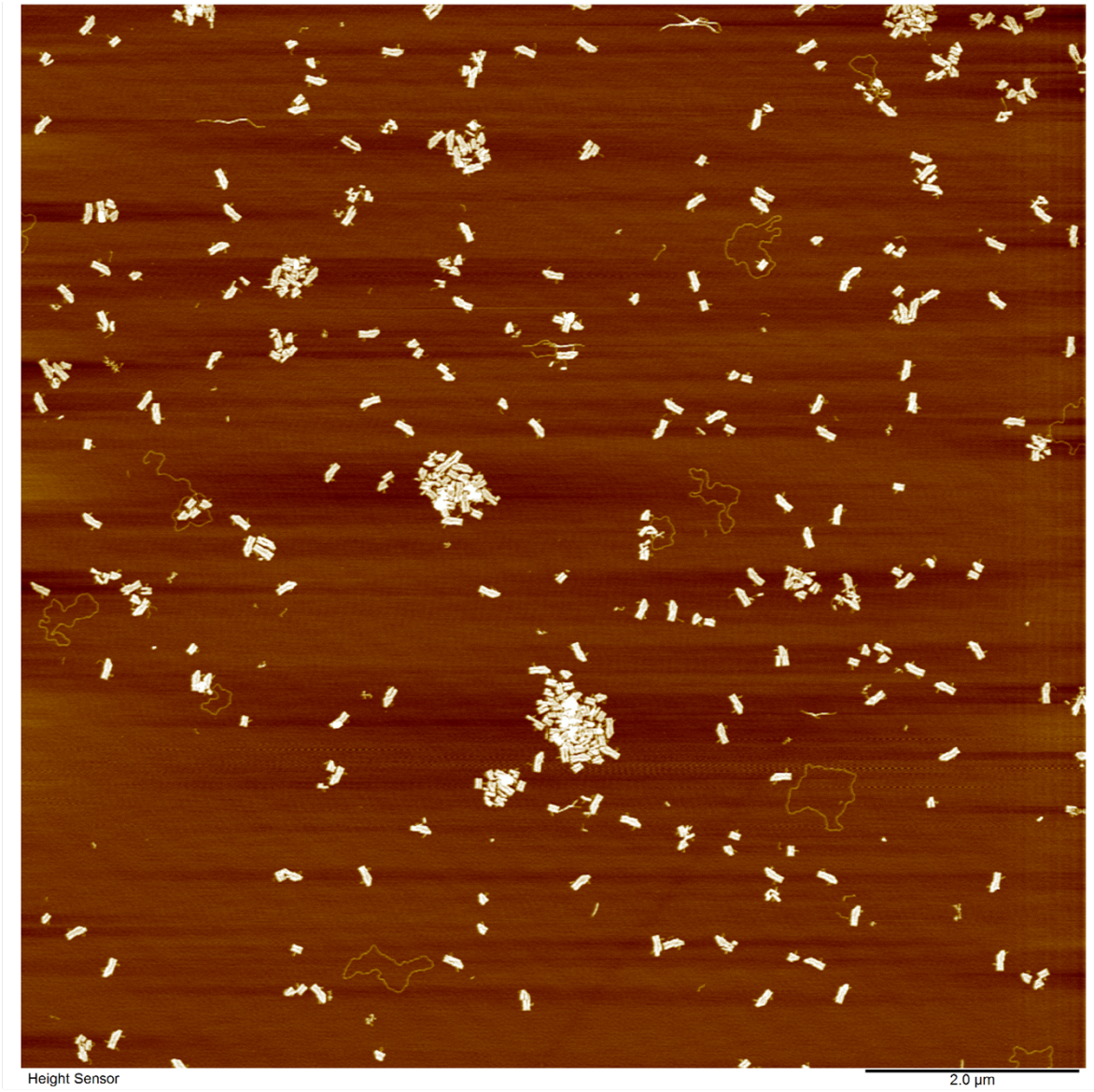

Figure 8-16 4-$(RF8)_2$ + 10-SE.

References

[1] F. CRICK, “Central Dogma of Molecular Biology,” *Nature*, vol. 227, no. 5258, pp. 561–563, 1970.

[2] R. E. FRANKLIN and R. G. GOSLING, “Molecular Configuration in Sodium Thymonucleate,” *Nature*, vol. 171, no. 4356, pp. 740–741, 1953.

[3] J. D. Watson and F. H. C. Crick, “Genetical implications of the structure of deoxyribonucleic acid,” *Nature*, vol. 171, no. 4361, pp. 964–967, 1953.

[4] W. F. H C Crick, “Molecular Struct1,1re of Deoxypentose Nucleic Acids,” *Astbury, W. T., Syrnp. Soc. Exp. Biol. 1, Nucleic Acid*, vol. 171, no. 4356, p. 192, 1953.

[5] E.-A. Raiber, R. Hardisty, P. van Delft, and S. Balasubramanian, “Mapping and elucidating the function of modified bases in DNA,” *Nat. Rev. Chem.*, vol. 1, no. 9, 2017.

[6] P. Yakovchuk, E. Protozanova, and M. D. Frank-Kamenetskii, “Base-stacking and base-pairing contributions into thermal stability of the DNA double helix,” *Nucleic Acids Res.*, vol. 34, no. 2, pp. 564–574, 2006.

[7] P. Cieplak and P. A. Kollman, “Calculation of the Free Energy of Association of Nucleic Acid Bases in Vacuo and Water Solution,” *J. Am. Chem. Soc.*, vol. 110, no. 12, pp. 3734–3739, 1988.

[8] C. A. Hunter, A. J. Kirby, and D. H. Williams, “Aromatic interactions in proteins, DNA and synthetic receptors,” *Philos. Trans. R. Soc. London. Ser. A Phys. Eng. Sci.*, vol. 345, no. 1674, pp. 77–85, Oct. 1993.

[9] M. Mandelkern, J. G. Elias, D. Eden, and D. M. Crothers, “The dimensions of DNA in solution,” *J. Mol. Biol.*, vol. 152, no. 1, pp. 153–161, 1981.

[10] M. H. F. Wilkins, A. R. Stokes, and H. R. Wilson, “Molecular structure of nucleic acids: Molecular structure of deoxypentose nucleic acids,” *Nature*, vol. 171, no. 4356, pp. 738–740, 1953.

[11] R. P. Bowater and Z. A. Waller, “DNA Structure,” *eLS*, 2014.

[12] D. W. Ussery, “DNA Structure: A-, B- and Z-DNA Helix Families,” *Encycl. Life Sci.*, no. 1998, 2002.

[13] W. Saenger, W. N. Hunter, and O. Kennard, “DNA conformation is determined by economics in the hydration of phosphate groups,” *Nature*, vol. 324, no. 6095, pp. 385–388, 1986.

[14] Y. Mitsui *et al.*, “Physical and enzymatic studies on Poly d(I-C).Poly d(I-C), an unusual double-helical DNA,” *Nature*, vol. 228, no. 5277, pp. 1166–1169, 1970.

[15] F. M. Pohl and T. M. Jovin, “Salt-induced co-operative conformational change of a synthetic DNA: Equilibrium and kinetic studies with poly(dG-dC),” *J. Mol. Biol.*, vol. 67, no. 3, pp. 375–396, 1972.

[16] J. C. García-Ramos, R. Galindo-Murillo, F. Cortés-Guzmán, and L. Ruiz-Azuara, “Metal-based drug-DNA interactions,” *J. Mex. Chem. Soc.*, vol. 57, no. 3, pp. 245–259, 2013.

[17] R. Holliday, “A mechanism for gene conversion in fungi,” *Genet. Res.*, vol. 5, no. 2, pp. 282–304, 1964.

[18] D. R. Duckett, A. I. Murchie, S. Diekmann, E. von Kitzing, B. Kemper, and D. M. Lilley, “The structure of the Holliday junction, and its resolution.,” *Cell*, vol. 55, no. 1, pp. 79–89, Oct. 1988.

[19] Z. Li, L. Wang, H. Yan, and Y. Liu, “Effect of DNA hairpin loops on the twist of planar DNA origami tiles.,” *Langmuir*, vol. 28, no. 4, pp. 1959–1965, Jan. 2012.

[20] J. Zhao, A. Bacolla, G. Wang, and K. M. Vasquez, “Non-B DNA structure-induced genetic instability and evolution,” *Cellular and Molecular Life Sciences*, vol. 67, no. 1. pp. 43–62, 2010.

[21] M. L. Bochman, K. Paeschke, and V. A. Zakian, “DNA secondary structures: Stability and function of G-quadruplex structures,” *Nat. Rev. Genet.*, vol. 13, no. 11, pp. 770–780, 2012.

[22] G. S. Manning, “The persistence length of DNA is reached from the persistence length of its null isomer through an internal electrostatic stretching force,” *Biophys. J.*, vol. 91, no. 10, pp. 3607–3616, 2006.

[23] N. C. Seeman, “Nanomaterials Based on DNA,” *Annu. Rev. Biochem.*, vol. 79, no. 1, pp. 65–87, 2010.

[24] N. C. Seeman, “DNA nanotechnology: novel DNA constructions.,” *Annu. Rev. Biophys. Biomol. Struct.*, vol. 27, pp. 225–248, 1998.

[25] N. C. Seeman, “Nucleic acid junctions and lattices,” *J. Theor. Biol.*, vol. 99, no. 2, pp. 237–247, 1982.

[26] E. Winfree, F. Liu, L. A. Wenzler, and N. C. Seeman, “Design and self-assembly of two-dimensional DNA crystals,” *Nature*, vol. 394, no. 6693, pp. 539–544, 1998.

[27] C. Lin, Y. Liu, and H. Yan, “Designer DNA Nanoarchitectures,” *Biochemistry*, vol. 48, no. 8, pp. 1663–1674, 2009.

[28] J. Chen and N. C. Seeman, “Synthesis from DNA of a molecule with the connectivity of a cube,” *Nature*, vol. 350, no. 6319, pp. 631–633, 1991.

[29] Y. Zhang and N. C. Seeman, “Construction of a DNA-Truncated Octahedron,” *J. Am. Chem. Soc.*, vol. 116, no. 5, pp. 1661–1669, 1994.

[30] B. Saccà and C. M. Niemeyer, “DNA Origami: The Art of Folding DNA,” *Angew. Chemie Int. Ed.*, vol. 51, no. 1, pp. 58–66, 2012.

[31] B. Wei, M. Dai, and P. Yin, “Complex shapes self-assembled from single-stranded DNA tiles,” *Nature*, vol. 485, no. 7400, pp. 623–626, 2012.

[32] Y. Ke, L. L. Ong, W. M. Shih, and P. Yin, “Three-dimensional structures self-assembled from DNA bricks,” *Science (80-.).*, vol. 338, no. 6111, pp. 1177–1183, 2012.

[33] H. Yan, T. H. LaBean, L. Feng, and J. H. Reif, “Directed nucleation assembly of DNA tile complexes for barcode-patterned lattices,” *Proc. Natl. Acad. Sci. U. S. A.*,

vol. 100, no. 14, pp. 8103–8108, 2003.

[34] W. M. Shih, J. D. Quispe, and G. F. Joyce, “A 1.7-kilobase single-stranded DNA that folds into a nanoscale octahedron,” *Nature*, vol. 427, no. 6975, pp. 618–621, 2004.

[35] J. Nangreave, D. Han, Y. Liu, and H. Yan, “DNA origami: A history and current perspective,” *Curr. Opin. Chem. Biol.*, vol. 14, no. 5, pp. 608–615, 2010.

[36] P. W. K. Rothemund, “Folding DNA to create nanoscale shapes and patterns,” *Nature*, vol. 440, no. 7082, pp. 297–302, 2006.

[37] M. Godonoga *et al.*, “A DNA aptamer recognising a malaria protein biomarker can function as part of a DNA origami assembly,” *Sci. Rep.*, vol. 6, no. February, pp. 1–12, 2016.

[38] A. Gietl, P. Holzmeister, D. Grohmann, and P. Tinnefeld, “DNA origami as biocompatible surface to match single-molecule and ensemble experiments,” *Nucleic Acids Res.*, vol. 40, no. 14, pp. 1–10, 2012.

[39] R. Chhabra, J. Sharma, Y. Liu, S. Rinker, and H. Yan, “DNA Self-assembly for Nanomedicine,” *Advanced Drug Delivery Reviews*, vol. 62, no. 6. pp. 617–625, 2010.

[40] A. Jahanban-Esfahlan *et al.*, “Dynamic DNA nanostructures in biomedicine: Beauty, utility and limits,” *J. Control. Release*, vol. 315, no. August, pp. 166–185, 2019.

[41] B. Ding, Z. Deng, H. Yan, S. Cabrini, R. N. Zuckermann, and J. Bokor, “Gold nanoparticle self-similar chain structure organized by DNA origami,” *J. Am. Chem. Soc.*, vol. 132, no. 10, pp. 3248–3249, 2010.

[42] J. Prinz *et al.*, “DNA origami substrates for highly sensitive surface-enhanced Raman scattering,” *J. Phys. Chem. Lett.*, vol. 4, no. 23, pp. 4140–4145, 2013.

[43] F. N. Gür, F. W. Schwarz, J. Ye, S. Diez, and T. L. Schmidt, “Toward Self-Assembled Plasmonic Devices: High-Yield Arrangement of Gold Nanoparticles on

DNA Origami Templates," *ACS Nano*, vol. 10, no. 5, pp. 5374–5382, 2016.

[44] G. Tikhomirov, P. Petersen, and L. Qian, "Programmable disorder in random DNA tilings.," *Nat. Nanotechnol.*, vol. 12, no. 3, pp. 251–259, Mar. 2017.

[45] S. M. Douglas, A. H. Marblestone, S. Teerapittayanon, A. Vazquez, G. M. Church, and W. M. Shih, "Rapid prototyping of 3D DNA-origami shapes with caDNAno," *Nucleic Acids Res.*, vol. 37, no. 15, pp. 5001–5006, 2009.

[46] S. Williams, K. Lund, C. Lin, P. Wonka, S. Lindsay, and H. Yan, "Tiamat: A Three-Dimensional Editing Tool for Complex DNA Structures," in *DNA Computing*, 2009, pp. 90–101.

[47] A. C. Stammers, "Physical Properties of Single-Sheet DNA Origami Nanotiles," University of Leeds, 2018.

[48] D. Han *et al.*, "DNA gridiron nanostructures based on four-arm junctions," *Science (80-.).*, vol. 339, no. 6126, pp. 1412–1415, 2013.

[49] F. Zhang *et al.*, "Complex wireframe DNA origami nanostructures with multi-arm junction vertices," *Nat. Nanotechnol.*, vol. 10, no. 9, pp. 779–784, 2015.

[50] R. Veneziano *et al.*, "Designer nanoscale DNA assemblies programmed from the top down," *Science (80-.).*, vol. 352, no. 6293, pp. 1534–1534, 2016.

[51] E. Benson *et al.*, "DNA rendering of polyhedral meshes at the nanoscale," *Nature*, vol. 523, no. 7561, pp. 441–444, 2015.

[52] H. Jun, X. Wang, W. P. Bricker, and M. Bathe, "Automated sequence design of 2D wireframe DNA origami with honeycomb edges," *Nat. Commun.*, vol. 10, no. 1, pp. 1–9, 2019.

[53] P. Wang, T. A. Meyer, V. Pan, P. K. Dutta, and Y. Ke, "The Beauty and Utility of DNA Origami," *Chem*, vol. 2, no. 3. Elsevier Inc., pp. 359–382, 2017.

[54] C. E. Castro *et al.*, "A primer to scaffolded DNA origami," *Nat. Methods*, vol. 8, no. 3, pp. 221–229, 2011.

[55] D. Han, S. Pal, J. Nangreave, Z. Deng, Y. Liu, and H. Yan, “DNA origami with complex curvatures in three-dimensional space,” *Science (80-.).*, vol. 332, no. 6027, pp. 342–346, 2011.

[56] T. Gerling, K. F. Wagenbauer, A. M. Neuner, and H. Dietz, “Dynamic DNA devices and assemblies formed by shape-complementary, non–base pairing 3D components,” *Science (80-.).*, vol. 347, no. 6229, pp. 1446–1452, 2015.

[57] J. Bath and A. J. Turberfield, “DNA nanomachines,” *Nat. Nanotechnol.*, vol. 2, no. 5, pp. 275–284, 2007.

[58] Y. Ke, J. Sharma, M. Liu, K. Jahn, Y. Liu, and H. Yan, “Scaffolded DNA origami of a DNA tetrahedron molecular container,” *Nano Lett.*, vol. 9, no. 6, pp. 2445–2447, 2009.

[59] F. Hong, F. Zhang, Y. Liu, and H. Yan, “DNA Origami: Scaffolds for Creating Higher Order Structures,” *Chem. Rev.*, vol. 117, no. 20, pp. 12584–12640, 2017.

[60] Y. Ke *et al.*, “Multilayer DNA origami packed on a square lattice,” *J. Am. Chem. Soc.*, vol. 131, no. 43, pp. 15903–15908, 2009.

[61] H. T. Maune *et al.*, “Self-assembly of carbon nanotubes into two-dimensional geometries using DNA origami templates,” *Nat. Nanotechnol.*, vol. 5, no. 1, pp. 61–66, 2010.

[62] Y. Ke, N. V. Voigt, K. V. Gothelf, and W. M. Shih, “Multilayer DNA origami packed on hexagonal and hybrid lattices,” *J. Am. Chem. Soc.*, vol. 134, no. 3, pp. 1770–1774, 2012.

[63] H. Dietz, S. M. Douglas, and W. M. Shih, “Folding DNA into twisted and curved nanoscale shapes,” *Science (80-.).*, vol. 325, no. 5941, pp. 725–730, 2009.

[64] H. K. K. Subramanian, B. Chakraborty, R. Sha, and N. C. Seeman, “The label-free unambiguous detection and symbolic display of single nucleotide polymorphisms on DNA origami,” *Nano Lett.*, vol. 11, no. 2, pp. 910–913, 2011.

[65] B. Saccà *et al.*, “Orthogonal protein decoration of DNA origami.,” *Angew. Chem.*

Int. Ed. Engl., vol. 49, no. 49, pp. 9378–9383, Dec. 2010.

[66] E. A. Hemmig *et al.*, "Programming Light-Harvesting Efficiency Using DNA Origami," *Nano Lett.*, vol. 16, no. 4, pp. 2369–2374, 2016.

[67] Y. Choi, L. Kotthoff, L. Olejko, U. Resch-Genger, and I. Bald, "DNA Origami Based FRET Nanoarrays and their Application as Ratiometric Sensors," *ACS Appl. Mater. Interfaces*, pp. 1–5, 2018.

[68] S. Pal, Z. Deng, H. Wang, S. Zou, Y. Liu, and H. Yan, "DNA directed self-assembly of anisotropic plasmonic nanostructures.," *J. Am. Chem. Soc.*, vol. 133, no. 44, pp. 17606–17609, Nov. 2011.

[69] R. R. F. Machinek, T. E. Ouldridge, N. E. C. Haley, J. Bath, and A. J. Turberfield, "Programmable energy landscapes for kinetic control of DNA strand displacement," *Nat. Commun.*, vol. 5, pp. 1–9, 2014.

[70] B. Yurke, A. J. Turberfield, A. P. Mills, F. C. Simmel, and J. L. Neumann, "A DNA-fuelled molecular machine made of DNA," *Nature*, vol. 406, no. 6796, pp. 605–608, 2000.

[71] S. M. Douglas, I. Bachelet, and G. M. Church, "A logic-gated nanorobot for targeted transport of molecular payloads.," *Science*, vol. 335, no. 6070, pp. 831–834, Feb. 2012.

[72] R. M. Zadegan, M. D. E. Jepsen, L. L. Hildebrandt, V. Birkedal, and J. Kjems, "Construction of a fuzzy and boolean logic gates based on DNA," *Small*, vol. 11, no. 15, pp. 1811–1817, 2015.

[73] Q. Lulu and W. Erik, "Scaling Up Digital Circuit Computation with DNA Strand Displacement Cascades," *Science (80-.).*, vol. 332, no. 6034, pp. 1196–1201, Jun. 2011.

[74] H. Zhang, J. Chao, D. Pan, H. Liu, Q. Huang, and C. Fan, "Folding super-sized DNA origami with scaffold strands from long-range PCR," *Chem. Commun.*, vol. 48, no. 51, pp. 6405–6407, 2012.

[75] A. N. Marchi, I. Saaem, B. N. Vogen, S. Brown, and T. H. Labean, “Toward larger DNA origami,” *Nano Lett.*, vol. 14, no. 10, pp. 5740–5747, 2014.

[76] B. Högberg, T. Liedl, and W. M. Shih, “Folding DNA origami from a double-stranded source of scaffold,” *J. Am. Chem. Soc.*, vol. 131, no. 26, pp. 9154–9155, 2009.

[77] M. Endo *et al.*, “Two-dimensional DNA origami assemblies using a four-way connector,” *Chem. Commun.*, vol. 47, no. 11, pp. 3213–3215, 2011.

[78] M. Endo, T. Sugita, Y. Katsuda, K. Hidaka, and H. Sugiyama, “Programmed-assembly system using DNA jigsaw pieces.,” *Chemistry*, vol. 16, no. 18, pp. 5362–5368, May 2010.

[79] W. Liu, H. Zhong, R. Wang, and N. C. Seeman, “Crystalline two-dimensional DNA-origami arrays,” *Angew. Chemie - Int. Ed.*, vol. 50, no. 1, pp. 264–267, 2011.

[80] T. C. Wu, M. Rahman, and M. L. Norton, “From nonfinite to finite 1D arrays of origami tiles.,” *Acc. Chem. Res.*, vol. 47, no. 6, pp. 1750–1758, Jun. 2014.

[81] R. Jungmann, M. Scheible, A. Kuzyk, G. Pardatscher, C. E. Castro, and F. C. Simmel, “DNA origami-based nanoribbons: assembly, length distribution, and twist.,” *Nanotechnology*, vol. 22, no. 27, p. 275301, Jul. 2011.

[82] G. Tikhomirov, P. Petersen, and L. Qian, “Fractal assembly of micrometre-scale DNA origami arrays with arbitrary patterns,” *Nature*, vol. 552, no. 7683, pp. 67–71, 2017.

[83] M. Liber *et al.*, “Study of DNA Origami Dimerization and Dimer Dissociation Dynamics and of the Factors that Limit Dimerization,” *Small*, vol. 14, no. 23, 2018.

[84] N. V Voigt *et al.*, “Single-molecule chemical reactions on DNA origami.,” *Nat. Nanotechnol.*, vol. 5, no. 3, pp. 200–203, Mar. 2010.

[85] K. Du, S. Ko, G. M. Gallatin, H. P. Yoon, J. A. Liddle, and A. J. Berglund, “Quantum dot-DNA origami binding: A single particle, 3D, real-time tracking study,” *Chem. Commun.*, vol. 49, no. 9, pp. 907–909, 2013.

[86] D. Selnihhin, S. M. Sparvath, S. Preus, V. Birkedal, and E. S. Andersen, "Multifluorophore DNA Origami Beacon as a Biosensing Platform," *ACS Nano*, vol. 12, no. 6, pp. 5699–5708, Jun. 2018.

[87] S. Loescher and A. Walther, "Supracolloidal Self-Assembly of Divalent Janus 3D DNA Origami via Programmable Multivalent Host/Guest Interactions," *Angew. Chemie - Int. Ed.*, vol. 59, no. 14, pp. 5515–5520, 2020.

[88] G. Amoako, Z. Ming, Y. Rian, P. Mensah Amoah, A. Twum, and F. Sam, "Connecting DNA origami structures using the biotin-streptavidin specific binding," *African J. Biotechnol.*, vol. 14, no. 28, pp. 2258–2264, 2015.

[89] A. Ohmann *et al.*, "Controlling aggregation of cholesterol-modified DNA nanostructures," *Nucleic Acids Res.*, vol. 47, no. 21, pp. 11441–11451, 2019.

[90] K. S. Ko, F. A. Jaipuri, and N. L. Pohl, "Fluorous-based carbohydrate microarrays," *J. Am. Chem. Soc.*, vol. 127, no. 38, pp. 13162–13163, 2005.

[91] G. E. Flynn *et al.*, "Reversible DNA micro-patterning using the fluorous effect," *Chem. Commun.*, vol. 53, no. 21, pp. 3094–3097, 2017.

[92] M. Cametti, B. Crousse, P. Metrangolo, R. Milani, and G. Resnati, "The fluorous effect in biomolecular applications," *Chem. Soc. Rev.*, vol. 41, no. 1, pp. 31–42, 2012.

[93] J. R. Lakowicz, *Principles of fluorescence spectroscopy, Springer, New York, USA, 3rd edn, 2006.* 2006.

[94] Romain Laine, "Fluorescence lifetime spectroscopy and imaging of FRET probes for the study of cell signalling," Imperial College London, 2013.

[95] G. G. Stokes, "On the change of refrangibility of light," *Philos. Trans. R. Soc. London*, vol. 142, pp. 463–562, Jan. 1852.

[96] S. A. Hussain, "An Introduction to Fluorescence Resonance Energy Transfer (FRET)," no. May, 2009.

[97] T. Förster, “Energy migration and fluorescence,” *J. Biomed. Opt.*, vol. 17, no. 1, p. 011002, 2012.

[98] H. Chen, H. L. Puhl, S. V. Koushik, S. S. Vogel, and S. R. Ikeda, “Measurement of FRET Efficiency and Ratio of Donor to Acceptor Concentration in Living Cells,” *Biophys. J.*, vol. 91, no. 5, pp. L39–L41, 2006.

[99] L. Ma, F. Yang, and J. Zheng, “Application of fluorescence resonance energy transfer in protein studies,” *J. Mol. Struct.*, vol. 1077, pp. 87–100, 2014.

[100] I. H. Stein, V. Schüller, P. Böhm, P. Tinnefeld, and T. Liedl, “Single-molecule FRET ruler based on rigid DNA origami blocks,” *ChemPhysChem*, vol. 12, no. 3, pp. 689–695, 2011.

[101] M. J. Urban *et al.*, “Gold nanocrystal-mediated sliding of doublet DNA origami filaments,” *Nat. Commun.*, vol. 9, no. 1, Dec. 2018.

[102] K. Kramm *et al.*, “DNA origami-based single-molecule force spectroscopy elucidates RNA Polymerase III pre-initiation complex stability,” *Nat. Commun.*, vol. 11, no. 1, Dec. 2020.

[103] F. Nicoli *et al.*, “Directional Photonic Wire Mediated by Homo-Förster Resonance Energy Transfer on a DNA Origami Platform,” *ACS Nano*, vol. 11, no. 11, pp. 11264–11272, Nov. 2017.

[104] N. Aissaoui, K. Moth-Poulsen, M. Käll, P. Johansson, L. M. Wilhelmsson, and B. Albinsson, “FRET enhancement close to gold nanoparticles positioned in DNA origami constructs,” *Nanoscale*, vol. 9, no. 2, pp. 673–683, Jan. 2017.

[105] S. Jäger, G. Rasched, H. Kornreich-Leshem, M. Engeser, O. Thum, and M. Famulok, “A Versatile Toolbox for Variable DNA Functionalization at High Density,” *J. Am. Chem. Soc.*, vol. 127, no. 43, pp. 15071–15082, Nov. 2005.

[106] D. A. Hiller and S. A. Strobel, “The chemical versatility of RNA,” *Philos. Trans. R. Soc. B Biol. Sci.*, vol. 366, no. 1580, pp. 2929–2935, Oct. 2011.

[107] Q. Zhang *et al.*, “DNA origami as an in vivo drug delivery vehicle for cancer

therapy," *ACS Nano*, vol. 8, no. 7, pp. 6633–6643, 2014.

[108] G. A. Knappe, E. C. Wamhoff, B. J. Read, D. J. Irvine, and M. Bathe, "In SituCovalent Functionalization of DNA Origami Virus-like Particles," *ACS Nano*, vol. 15, no. 9, pp. 14316–14322, Sep. 2021.

[109] F. T. Lee-Montiel and P. I. Imoukhuede, "Engineering quantum dot calibration standards for quantitative fluorescent profiling," *J. Mater. Chem. B*, vol. 1, no. 46, pp. 6434–6441, 2013.

[110] Y. Ito and E. Fukusaki, "DNA as a 'Nanomaterial,'" *J. Mol. Catal. B Enzym.*, vol. 28, no. 4–6, pp. 155–166, 2004.

[111] G. Tikhomirov, P. Petersen, and L. Qian, "Fractal assembly of micrometre-scale DNA origami arrays with arbitrary patterns," *Nature*, vol. 552, no. 7683, pp. 67–71, 2017.

[112] G. E. Flynn, "Immobilisation of DNA Using The Fluorous Effect," University of Glasgow, 2018.

[113] S. L. Henry *et al.*, "DNA-directed spatial assembly of photosynthetic light-harvesting proteins," *Org. Biomol. Chem.*, vol. 14, no. 4, pp. 1359–1362, 2016.

[114] Y. Ke, S. Lindsay, Y. Chang, Y. Liu, and H. Yan, "Self-assembled water-soluble nucleic acid probe tiles for label-free RNA hybridization assays," *Science (80-.).*, vol. 319, no. 5860, pp. 180–183, 2008.

[115] J. P. J. Sobczak, T. G. Martin, T. Gerling, and H. Dietz, "Rapid folding of DNA into nanoscale shapes at constant temperature," *Science (80-.).*, vol. 338, no. 6113, pp. 1458–1461, 2012.

[116] S. Vogel *et al.*, "Using DNA Origami Nanostructures to Determine Absolute Cross Sections for UV Photon-Induced DNA Strand Breakage," *J. Phys. Chem. Lett.*, vol. 6, no. 22, pp. 4589–4593, 2015.

[117] S. Gurrieri, S. B. Smith, and C. Bustamante, "Trapping of megabase-sized DNA molecules during agarose gel electrophoresis," *Proc. Natl. Acad. Sci. U. S. A.*, vol.

96, no. 2, pp. 453–458, 1999.

[118] S. Li *et al.*, “A DNA nanorobot functions as a cancer therapeutic in response to a molecular trigger in vivo,” *Nat. Biotechnol.*, vol. 36, no. 3, pp. 258–264, 2018.

[119] S. Liu and Y. Wang, “Application of AFM in microbiology: A review,” *Scanning*, vol. 32, no. 2, pp. 61–73, 2010.

[120] G. Binnig and H. Rohrer, “Scanning Tunneling Microscopy.,” *IBM J. Res. Dev.*, vol. 30, no. 4, pp. 355–369, 1986.

[121] G. Binnig, C. F. Quate, and C. Gerber, “Atomic Force Microscope,” *Phys. Rev. Lett.*, vol. 56, no. 9, pp. 930–933, Mar. 1986.

[122] G. Meyer and N. M. Amer, “Novel optical approach to atomic force microscopy,” *Appl. Phys. Lett.*, vol. 53, no. 12, pp. 1045–1047, 1988.

[123] J. Tamayo and R. García, “Deformation, contact time, and phase contrast in tapping mode scanning force microscopy,” *Langmuir*, vol. 12, no. 18, pp. 4430–4435, 1996.

[124] A. Rajendran, M. Endo, Y. Katsuda, K. Hidaka, and H. Sugiyama, “Programmed two-dimensional self-assembly of multiple DNA origami jigsaw pieces,” *ACS Nano*, vol. 5, no. 1, pp. 665–671, 2011.

[125] J. Zenk, C. Tuntivate, and R. Schulman, “Kinetics and Thermodynamics of Watson-Crick Base Pairing Driven DNA Origami Dimerization.,” *J. Am. Chem. Soc.*, vol. 138, no. 10, pp. 3346–3354, Mar. 2016.

[126] S. Jiang, H. Yan, and Y. Liu, “Kinetics of DNA tile dimerization,” *ACS Nano*, vol. 8, no. 6, pp. 5826–5832, 2014.

[127] B. E. K. Snodin, J. S. Schreck, F. Romano, A. A. Louis, and J. P. K. Doye, “Coarse-grained modelling of the structural properties of DNA origami,” *Nucleic Acids Res.*, vol. 47, no. 3, pp. 1585–1597, 2019.

[128] B. E. K. Snodin *et al.*, “Introducing improved structural properties and salt dependence into a coarse-grained model of DNA,” *J. Chem. Phys.*, vol. 142, no. 23,

p. 234901, Jun. 2015.

[129] P. Šulc, F. Romano, T. Ouldridge, L. Rovigatti, J. Doye, and A. Louis, “Sequence-dependent thermodynamics of a coarse-grained DNA model.,” *J. Chem. Phys.*, vol. 137, no. 13, p. 135101, 2016.

[130] B. Sheheade *et al.*, “Self-Assembly of DNA Origami Heterodimers in High Yields and Analysis of the Involved Mechanisms,” *Small*, vol. 15, no. 51, pp. 1–9, 2019.

[131] K. E. Dunn, F. Dannenberg, T. E. Ouldridge, M. Kwiatkowska, A. J. Turberfield, and J. Bath, “Guiding the folding pathway of DNA origami,” *Nature*, vol. 525, no. 7567, pp. 82–86, 2015.

[132] B. Y. Li, D. S. Juang, A. K. Adak, K. C. Hwang, and C. C. Lin, “Fabrication of a protein microarray by fluorous-fluorous interactions,” *Sci. Rep.*, vol. 7, no. 1, pp. 1–9, 2017.

[133] D. N. Kim, F. Kilchherr, H. Dietz, and M. Bathe, “Quantitative prediction of 3D solution shape and flexibility of nucleic acid nanostructures,” *Nucleic Acids Res.*, vol. 40, no. 7, pp. 2862–2868, 2012.

[134] J. P. Peters and L. J. Maher, *DNA curvature and flexibility in vitro and in vivo*, vol. 43, no. 1. 2010.

[135] T. Liedl, B. Högberg, J. Tytell, D. E. Ingber, and W. M. Shih, “Self-assembly of three-dimensional prestressed tensegrity structures from DNA,” *Nat. Nanotechnol.*, vol. 5, no. 7, pp. 520–524, 2010.

[136] J. A. Gladysz, D. P. Curran, and I. T. Horváth, *Fluorous chemistry: Scope and definition*. 2005.

[137] I. L. Medintz, A. R. Clapp, H. Mattoussi, E. R. Goldman, B. Fisher, and J. M. Mauro, “Self-assembled nanoscale biosensors based on quantum dot FRET donors,” *Nat. Mater.*, vol. 2, no. 9, pp. 630–638, 2003.

[138] U. Resch-Genger, M. Grabolle, S. Cavaliere-Jaricot, R. Nitschke, and T. Nann, “Quantum dots versus organic dyes as fluorescent labels,” *Nat. Methods*, vol. 5, no.

9, pp. 763–775, 2008.

[139] N. Hildebrandt *et al.*, “Energy transfer with semiconductor quantum dot bioconjugates: A versatile platform for biosensing, energy harvesting, and other developing applications,” *Chemical Reviews*, vol. 117, no. 2. pp. 536–711, 2017.

[140] J. Hu, M. H. Liu, and C. Y. Zhang, “Construction of Tetrahedral DNA-Quantum Dot Nanostructure with the Integration of Multistep Förster Resonance Energy Transfer for Multiplex Enzymes Assay,” *ACS Nano*, 2019.

[141] J. Sharma *et al.*, “DNA-tile-directed self-assembly of quantum dots into two-dimensional nanopatterns,” *Angew. Chemie - Int. Ed.*, vol. 47, no. 28, pp. 5157–5159, 2008.

[142] H. Bui *et al.*, “Programmable periodicity of quantum dot arrays with DNA origami nanotubes,” *Nano Lett.*, vol. 10, no. 9, pp. 3367–3372, 2010.

[143] Z. Deng, A. Samanta, J. Nangreave, H. Yan, and Y. Liu, “Robust DNA-Functionalized Core/Shell Quantum Dots with Fluorescent Emission Spanning from UV–vis to Near-IR and Compatible with DNA-Directed Self-Assembly,” *J. Am. Chem. Soc.*, vol. 134, no. 42, pp. 17424–17427, Oct. 2012.

[144] S. H. Ko, K. Du, and J. A. Liddle, “Quantum-dot fluorescence lifetime engineering with DNA origami constructs,” *Angew. Chemie - Int. Ed.*, vol. 52, no. 4, pp. 1193–1197, 2013.

[145] R. Schreiber *et al.*, “Hierarchical assembly of metal nanoparticles, quantum dots and organic dyes using DNA origami scaffolds,” *Nat. Nanotechnol.*, vol. 9, no. 1, pp. 74–78, 2014.

[146] O. Livnah, E. A. Bayer, M. Wilchek, and J. L. Sussman, “Three-dimensional structures of avidin and the avidin-biotin complex,” *Proc. Natl. Acad. Sci. U. S. A.*, vol. 90, no. 11, pp. 5076–5080, 1993.

[147] A.-P. Eskelinen *et al.*, “Assembly of single-walled carbon nanotubes on DNA-origami templates through streptavidin-biotin interaction.,” *Small*, vol. 7, no. 6, pp. 746–750, Mar. 2011.

[148] J. Hu, M. Liu, and C. Zhang, “Construction of Tetrahedral DNA-Quantum Dot Nanostructure with the Integration of Multistep Förster Resonance Energy Transfer for Multiplex Enzymes Assay,” *ACS Nano*, vol. 13, no. 6, pp. 7191–7201, Jun. 2019.